STOCHASTIC GEOMETRIC ANALYSIS OF COGNITIVE WIRELESS NETWORKS

SYED ALI RAZA ZAIDI

Submitted in accordance with the requirements
for the degree of Doctor of Philosophy

University of Leeds
School of Electronic & Electrical Engineering

April 2013

DECLARATION

The candidate confirms that the work submitted is his/her own, except where work which has formed part of jointly authored publications has been included. The contribution of the candidate and the other authors to this work has been explicitly indicated below. The candidate confirms that appropriate credit has been given within the thesis where reference has been made to the work of others. It is to assert that the candidate has contributed solely to the technical part of the joint publication under the guidance of his academic supervisors. Detailed breakdown of the publications and the chapters which are constituted based on these is presented in the publications section and Part I of this thesis.

Syed Ali Raza Zaidi

To the fantastic five, the beautiful ladies behind my success.

My lovely wife,
— Maryam

My beloved daughter,
— Parisa

My dearest aunt,
— Aqila

My dearest mom,
— Nusrat

&

My Loving Sister,
— Anum

ABSTRACT

The prime objective of this thesis is to study these interference management mechanisms for quantifying the potential gains of CRs in terms of spectral utility. Interference modeling is the most important aspect of this extensive evaluation. Accurate modeling of the cognitive network interference, accommodating its stochastic nature (triggered by both spatial and propagation dynamics) is therefore a central contribution of this thesis. Since the aggregate interference from CRs is a function of the access strategy, two well-known access paradigms, namely, spectrum underlay and interweave, are thoroughly analyzed.

For the spectrum underlay access mechanism, a guard-zone based interference control mechanism is examined. Specifically, CRs are obliged to maintain silence in a spatial no-talk zone of a certain radius which is centered on a primary receiver. It is shown that the radius of the guard-zone is strongly coupled with the medium access and routing strategies employed by the CRs. While the guard-zone provides a robust mechanism to protect a single primary user, it is a challenging task to achieve the same for a large scale primary network. An alternative degree of freedom, i.e., medium access probability (MAP), can easily address this issue. Furthermore, for a large CR network (CRN), significant gains can be harnessed by furnishing nodes with multiple antennas. Performance evaluation of such a network with MAP adaptation is one of the key contributions of this dissertation. It is shown that the multi-antenna paradigm results in a "win-win" situation for both primary and secondary users. In order to facilitate multi-hop communication between CRs, a quality-of-service (QoS) aware routing is also devised. We show that there exists an optimal MAP which maximizes the spectral utility of the secondary network. However, such an optimal point often lies outside the permissible operational regime dictated by the primary user's co-existence constraint. Another approach can be adopted where we exploit a different degree of freedom, i.e., the transmit power employed by the CRs. Thus CRs can extend their operational regime by adapting one degree of freedom and selecting an optimal value for another. The optimality of this adapt-and-optimize strategy is shown for a variety of networking paradigms. Finally, the performance of the primary user in the presence of the interference-channel-aware CRs is quantified.

For a CRN employing an interweave configuration, the performance of a legacy user is investigated. The impact of different network parameters is explored. It is shown that the cooperation between the CR transmitter and receiver can significantly improve the performance of the interference avoidance mechanism. Furthermore, we highlight that ignoring the self-coexistence

criteria for the secondary network leads to an over-estimation of the aggregate interference and consequently results in pessimistic design strategies. The analysis is extended to consider the performance of a large primary network. Finally, a novel modification in the analytical approach is proposed so that performance guarantees can be provided to the existing users.

Another contribution of this dissertation is to evaluate (currently very topical and very important) the energy efficiency of an ad hoc wireless network. The key motivation is to investigate the impact of the co-channel interference on the network-wide energy consumption. Both energy and spectral efficiency problems have a common origin, i.e., growing bandwidth demand. Also the design of both problems require understanding of co-channel interference management strategies.

Finally, we try to put pull together all the analysis and simulation results to look at both open problems and directions for future research in this highly topical, and strategically important research areas of enabling high speed, future wireless networks.

PUBLICATIONS

The original contributions presented in this dissertation are supported by following publications:

PAPERS

I Zaidi, S.A.R.; Ghogho, M.; McLernon, D.C.; Swami, A., "Achievable Spatial throughput in Multi-antenna Cognitive Underlay Networks with Multi-hop Relaying", IEEE Journal on Selected Areas in Communication, Special Issue on Theories and Methods for Advanced Wireless Relays, August 2013.

II Zaidi, S.A.R.**;** McLernon, D.C.; Ghogho, M., "Breaking Throughput Wall in Underlay Cognitive Radio Networks", IEEE Journal on Selected Areas in Communication, Special Issue on Cognitive Radio Networks, March 2014.

III Zaidi, S.A.R.; McLernon, D.C.; Ghogho, M., "Quantification of the Primary's Guard Zone Under Cognitive Users Routing and Medium Access", IEEE Communication Letters, March 2012.

IV Zaidi, S.A.R.; Ghogho, M.; McLernon, D.C.; Swami, A., "Outage and Transport Throughput in Spectrum Sensing Cognitive Radio Networks", IEEE Transactions on Signal Processing, April 2013 (revised).

V Zaidi, S.A.R.; Ghogho, M.; McLernon, D.C., "Comments on 'Expected Interference in Wireless Networks with Geometric Path Loss: A Closed-Form Approximation' ", IEEE Communication Letters, October 2011.

VI Zaidi, S.A.R.; McLernon, D.C.; Ghogho, M., "On Primary's Outage, Throughput and Ergodic Capacity in the Presence of Interfering Cognitive Radio Network", IEEE Transactions on Vehicular Technology, June 2013.

VII Zaidi, S.A.R.;McLernon, D.C.; Ghogho, M., "Distributed Interference Protection in Cognitive Radio Networks under Composite Shadow-Fading Channels", IEEE Communication Letters, April 2013 (revised).

VIII Zaidi, S.A.R.; McLernon, D.C.; Ghogho, M.; Swami, A.; Debbah, M., "On the Energy efficiency of Large Scale Wireless Ad hoc Networks", IEEE Transactions on Mobile Computing, April 2013 (submitted).

IX Zaidi, S.A.R.; Ghogho, M.; McLernon, D.C., “Energy Efficiency in Large Scale Interference Limited Wireless Ad hoc Networks”, IEEE Wireless Communications and Networking Conference (WCNC 2012) Workshop on Future Green Networks, Paris, France, April 2012.

X Zaidi, S.A.R.; Ghogho, M.; McLernon, D.C., “Characterizing the Node Isolation Probability in MIMO Multihop Underlay Cognitive Radio Networks”, 2nd Workshop of IC0902 on Cognitive Radio and Networking for Cooperative Coexistence of Heterogeneous Wireless Networks, Castelldefels, Barcelona, Spain, October 2011.

XI Zaidi, S.A.R.; McLernon, D.C.; Ghogho, M., “Transmission Capacity Analysis of Cognitive Radio Networks”, IEEE International Workshop on Signal Processing Advances in Wireless Communications (SPAWC) 2010, Marrakech, Morocco.

XII Zaidi, S.A.R.; McLernon, D.C.; Ghogho, M., “Characterizing Transmission Capacity of Cognitive Radio Networks”, Workshop on Spatial Network Models for Wireless Communications, Isaac Newton Institute of Mathematical Sciences, Cambridge, U.K. April 2010 (Poster)

XIII Zaidi, S.A.R.; McLernon, D.C.; Ghogho, M., “Outage Probability Analysis of Cognitive Radio Networks under Self-coexistence constraint”, IEEE Conference on Information Sciences and Systems (CISS 2010), Princeton, NJ, U.S.A, 2010.

XIV Zaidi, S.A.R.; McLernon, D.C.; Ghogho, M., “On Outage and Interference in 802.22 Cognitive Radio Networks under Deterministic Network Geometry”, ACM MobiCom 2009, Beijing, China.(Poster paper)

XV Zaidi, S.A.R.; McLernon, D.C.; Ghogho, M., “A Generalized Geometry-Inclusive Fading Model for Ad hoc Wireless Networks”, IEEE Workshop on Statistical Signal Processing 2009, Cardiff, U.K.

In the rest of this dissertation, reference to these publications is made by employing the corresponding roman numerals.

ACKNOWLEDGMENTS

First of all, I would thank Almighty Allah, for all his blessings. For whatever I achieve in life, it is due to His grace. I can recall several stages during my PhD when His help was the only hope that kept me going.

Secondly, I would like to show my appreciation to my supervisor Dr Des. C. McLernon for his guidance during the course of my study in the University of Leeds. It is due to his immense support that I have been successful in completing my thesis. He has helped me in every possible way to solve any academic or personal problem that I ever had during my stay in Leeds. It turns out that my PhD tenure was full of so many thrillers and adventures that it can be easily classified as a worst case scenario. Dr. McLernon steered me through the treacherous trajectories which I encountered during past few years. I owe a lot to my second supervisor Prof. Mounir Ghogho for helping me refine my research ideas and extending his help whenever I was in need. He was instrumental in helping me with personal and academic problems both. His tireless efforts cannot be acknowledged in words.

Along with the mentors, my colleagues have also played a vital role in my progress. They have been helpful in exchanging research ideas, meeting various challenges and contributing to a competitive environment. I would like to thank Dr. Bilal Qazi and Dr. Wanod Kumar for their moral and social support. I would also like to thank Asim Ali, Dr. Ansar Mehboob, Dr. Arif, Dr. Naveed salman, Dr. Mo Nikhar Esfahani, Dr. Samya, Dr. Sami and Dr. Omar waqar for their support and company during all these years. I would also like to express my sincere thanks for my collaborators Dr. Ananthram Swami, Prof. Merouane Debbah, Prof. Francios Baccelli and Prof. Martin Haneggi for their useful feedback on my work. Their feedback was vital in improving the quality of my work.

I would also acknowledge and appreciate the support of my family. PhD is a lengthy and challenging academic route. It is beyond any doubt that completing this degree would have been impossible without the moral and physical support of my family. I must thank my wife Maryam Hafeez, who has supported me throughout my PhD. Beyond every successful man there is a woman and Maryam has been that woman in my case.

Thank you everyone for being my wonderful mentors, companions and friends.

CONTENTS

LIST OF TABLES

FREQUENTLY USED MATHEMATICAL SYMBOLS

Π or Φ	denotes the Point process *
s	subscript s denotes secondary users
p	subscript p denotes primary users
$\mathbb{E}(.)$	is used to denote the expected value
$\Pr\{A\}$	denotes the probability of event A
r_e	is frequently used to refer to the guard-zone on primary receiver
ϵ_{ISO}	is used to denote the secondary isolation constraint
λ	is used to denote the density of the point process *
γ	is used to denote the SIR threshold **
Γ	is used to denote the received SIR**
P	is used to denote transmit power **
$\mathbb{P}_{suc}$	is used to denote the link success probability *
$\mathbb{P}_{out}$	is used to denote the link outage probability *
ζ	is used to denote forward progress in multihop network, $\bar{\zeta}$ is often used to denote the corresponding average
ϕ	is employed to denote the central angle of sector
N	is employed to refer to the number of antennas **
$\mathcal{L}_I(.)$	denotes the Laplace transform of the aggregate interference
m	is used to denote the fading severity of Nakagami-m fading channels
d	is frequently used to denote the spatial dimensions of the network
$\mathcal{T}$	is used to denote the throughput **
r	is used to denote the link distance *
α	is employed to denote the path-loss exponent

*subscripts and superscripts are used for further classification
**subscripts are used for further classification

ACRONYMS

3G	Third Generation
BS	Base Station
CGF	Cumulant Generating Function
CR	Cognitive Radio
CRN	Cognitive Radio Network
CSI	Channel State Information
D2D	Device-to-Device
DFS	Distributed Frequency Selection
DIP	Distributed Interference Protection
DSA	Dynamic Spectrum Access
ED	Energy Detector
FUE	Femto User Equipment
HPF	Half plane forwarding
HPPP	Homogenous Poisson point process
LTE	Long Term Evolution
M2M	Machine-to-Machine
MF	Matched Filter
MAC	Medium Access Control
MAP	Medium Access Probability
MGF	Moment Generating Function
MIMO	Multiple-Input-Multiple-Output
MPPP	Marked Poisson point process
MRC	Maximum Ratio Combining
MRT	Maximum Ratio Transmission

NAIP Neighborhood Aware Interference Protection

NN Nearest Neighbour

OP Outage Probability

PPP Marked Poisson point process

RSF Radian Sector forwarding

SIR Signal-to-interference-ratio

SINR Signal-to-interfernce-plus-noise-ratio

SNR Signal-to-noise-ratio

SPPP Stationary Poisson point process

UCF Unconstrained forwarding

1 INTRODUCTION

1.1 MOTIVATION

In recent times, the wireless communication industry has witnessed the sky-rocketing demand for "any time and any where" connectivity. The exponential growth in capacity requirements can be attributed to the increasing popularity of multimedia infotainment applications and the enormous penetration of smart platforms facilitating their execution. According to recent statistics [1], about $5\times$ growth is expected in the number of mobile consumers world wide by 2017. Such an unprecedented hike in bandwidth demand will be further complemented by the exponential penetration of smart-phone, tablets, cyber-physical systems, machine-to-machine (M2M) communication devices and cloud based services. Consequently, it is predicted that while the voice traffic will maintain its current trend, the data traffic will grow 15 times by the end of 2017 [1].

Design goals for the next generation wireless networks:
- *Spectrally agile;*
- *Energy smart;*

Such interminable consumer demands have acted as a double edged sword for the network designers/operators, i.e.

1. Radio spectrum has become a scarce commodity;
2. Energy costs of operating the networks are growing exponentially fast in proportion to the traffic growth.

Designing spectrally agile and energy efficient access strategies has become a vital pillar for laying down strong foundations for next generation wireless networks. This has motivated us to explore the design space of the future wireless networks with a particular focus on the two issues listed above.

1.2 SPECTRUM SCARCITY: REALITY CHECK

Key contributors to the spectrum scarcity:
- *Sky-rocketing consumer demand;*
- *Rigid spectrum allocation; and*
- *Inefficient access strategies.*

Rapid growth in consumer demands and data volumes are not the only factors contributing towards the dearth of radio spectrum. The rigid *command and control* [2] spectrum allocation policy has further exacerbated the problem. The traditional command and control approach is based on exclusive licensing of the frequency bands to authorized users by the government spectrum regulatory bodies.

A quick glance at the frequency allocation charts provided by the regulatory bodies reveals that most of the prime spectrum is assigned and the margin for accommodating the emerging wireless applications is low. Consequently, it seems natural to think of the spectrum scarcity as a real challenge

Command-and-control or Divide-and-set-aside [3]: a) Spectrum is divided into distinct bands; b) Specific communication uses are assigned to the specific bands; c) Determination of licensee with exclusive rights.

posed due to the high utilization of the Hertzian medium. However, a reality check on the usage patterns of the available spectral resources reveals that in a nutshell the spectrum scarcity is nothing but artificial. Spectrum occupancy measurements [4, 5] have revealed that these licensed bands are highly under-utilized across space and time. From 13% to 87% of the radio spectrum remains unused across spatio-temporal domains. This sporadic utilization of scarce electromagnetic spectrum creates an artificial scarcity. Regulatory bodies such as the FCC (in the USA) and Ofcom (in the UK) have already noticed that such under-utilization of the spectrum can be avoided by more flexible and dynamic spectrum access (DSA) mechanisms [6].

1.2.1 *Dynamic Spectrum Access*

Barriers to Spectrum Access [7]
- *FlexUse Barrier: Use type is fixed for the licensee;*
- *Service-Silo Barrier: Fixed services for fixed licensee;*
- *License-Scope Barrier: Large spatial and temporal scope;*
- *License-Granularity Barrier: Allocation of large chunks of bandwidth;*
- *Secondary-Usage Barrier: Opportunisim not permitted;*

Radio spectrum is a multidimensional entity, i.e., frequency is not the only dimension which characterizes the spectral opportunity. Space, time, transmission power, polarization, medium access and interference all combinely shape the radio environment . Dynamic spectrum access (DSA) mechanism employ one or more of these dimensions to break the shackles of rigidity imposed by the command and control mechanism. Fig. 1.1 highlights the taxonomy of DSA models.

1.2.1.1 *Hierarchical Spectrum Access Model*

The focus of this thesis is geared towards the Shared use/Hierarchical access model. Detailed discussion on other models can be found in [7, 8]. In hierarchical access model, users are classified into two broad classes, namely, primary/legacy and secondary users. The secondary spectrum access is subject to the interference constraint imposed by the primary user. More specifically, secondary users should operate in a manner such that the primary user remains oblivious to their presence.

1.2.1.2 *Cognitive Radio*

Cognitive radios (CRs), as the name implies, are intelligent, environment aware, agile and adaptive radios which are bestowed with pre-eminent decision making capabilities. CRs are envisaged to be a key enabling technology for DSA in future wireless networks. In the recent past, there has been a lot of effort dedicated by both academia and industry to study the DSA mechanisms for intelligent/cognitive adaptive transceivers. Several academia-industry alliances like CogNeA, PHYDYAS and ARAGON are already investigating a wide range of possibilities for making CRs commercially viable. The IEEE

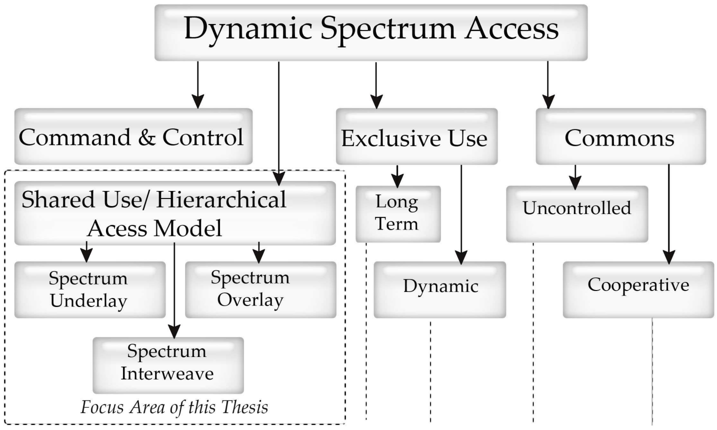

Figure 1.1: Dynamic Spectrum Access Models.

has also formed the 802.22 workgroup to develop an air interface for DSA in the TV frequency band [1].

CRs, often referred to as secondary terminals, are based on the principle of opportunistic exploitation of spectrum vacancies across space and time. These vacancies are more commonly called *spectrum holes* [9]. The fundamental *operational constraint* on CRs is to ensure that they do not cause any harmful *interference* to the primary/licensed or legacy user.

An alternative, yet eloquent view of cognition is interference management. DSA empowered by the cognitive/secondary device essentially corresponds to the way these devices co-exist with existing/legacy users by managing their interference. This can be easily put into perspective by observing the classification of hierarchical DSA schemes, i.e., underlay, overlay and interweave spectrum access mechanisms [3]. From the interference management perspective, the above-mentioned strategies translate into interference control, coordination and avoidance.

> *"Cognitive radio is an intelligent wireless communication system that is aware of its surrounding environment (i.e., outside world), and uses the methodology of understanding-by-building to learn from the environment and adapt its internal states to statistical variations in the incoming RF stimuli by making corresponding changes in certain operating parameters (e.g. transmit power, carrier frequency, and modulation strategy) in real-time with two primary objectives in mind:*
> *■ highly reliable communication whenever and whereever needed*
> *■ efficient utilization of the radio spectrum.*
> *-Simon Haykin" [10]*

1.3 COGNITIVE NETWORKING PARADIGMS & INTERFERENCE MANAGEMENT

The hierarchical DSA mechanism is further classified into three broad network paradigms: *underlay, interweave and overlay.*

1 Recommendation on installation and deployment were first published on September 28, 2012. url:http://www.ieee802.org/22/

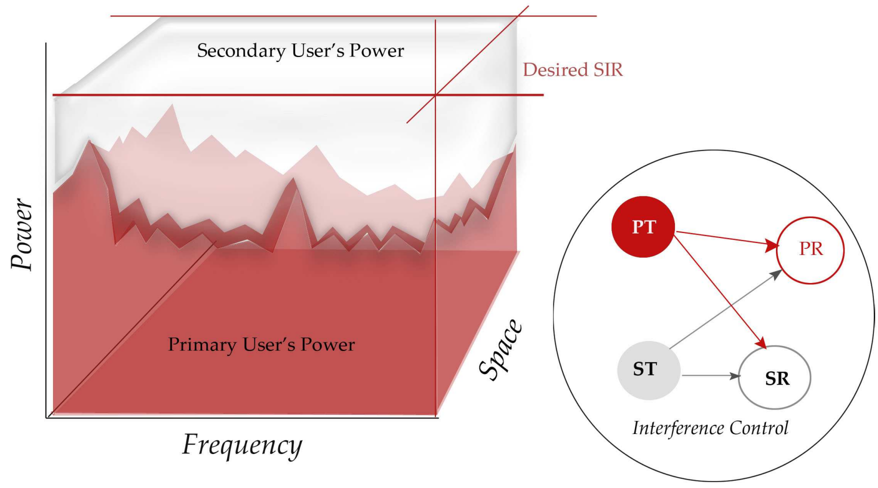

Figure 1.2: Underlay spectrum access paradigm where PT is used as a short hand for the primary transmitter, PR for the primary receiver, ST for the secondary transmitter and SR for the secondary receiver.

1.3.1 *Underlay Spectrum Access Paradigm*

Underlay paradigm leverages the transmission power as an adaptable dimension for co-existing with the legacy users. Fundamentally, the underlay paradigm is equivalent to the secondary interference control.

In 2007, the FCC abandoned the pursuit of interference temperature as a design metric for the underlay CR networks.

In an underlay mechanism, both the primary and the cognitive terminals can concurrently access the wireless medium. Secondary access is subject to the interference or quality-of-service (QoS) constraint enforced by the primary user. Specifically, secondary users are permitted to transmit provided that the primary user's performance does not deteriorate significantly, i.e., its QoS constraints are satisfied.

The interference constraint can be expressed in terms of the primary user's tolerance characterized by either peak interference power, average interference power or outage probability [11, 12]. The outage probability of a primary link is a particularly vital performance metric as it inherently accommodates the desired signal-to-interference-plus-noise-ratio (SINR). A QoS constraint expressed in the form of a required error performance or throughput threshold can be easily transformed into the SINR threshold by employing either the conditional bit-error-probability expressions [13] or Shannon's seminal theorem [14]. Figure 1.2 graphically depicts the operational principle of the underlay paradigm.

The traditional definition of the underlay spectrum access relies on the notion of interference temperature[3, 10, 15, 16]. The term *interference temperature* was introduced by the FCC's spectrum management task force in [17] as:

> "We define interference temperature as a measure of the RF power generated by undesired emitters plus noise sources that are present in a receiver system $(I + N)$ per unit of bandwidth. More specifically, it is the temperature equivalent of this power measured in units of "Kelvin" (K). The emissions from undesired transmitters could include out-of-band emissions from transmitters operating on adjacent frequencies or in adjacent frequency bands as well as from transmitters operating on the same frequency as the desired transmitter."

Consequently, interference temperature aware spectrum access requires that CR users must possess a complete knowledge of the interference inflicted on the primary receivers. More specifically, instantaneous knowledge about the interference experienced by the primary users and the channel state information regarding its own communication channel must be available to the CRs. Notice that the interference temperature estimated at the CR transmitter is not similar to the one experienced by the primary receiver. Generally, the CR transmitter and primary receiver are two different entities located at different spatial positions. Moreover, departing from a single user consideration by including the network level dynamics and interactions further complicates the state-of-affairs. This leads to:

> **Challenge 1:** Can we design an underlay CR network with the local parameter adaptation scheme in the absence of the limitations imposed by the interference temperature model?

Challenge 1 can be expanded into several important design questions? To this end, this dissertation focuses on addressing some of these issues in a comprehensive manner. A detailed discussion will follow in subsequent sections.

1.3.2 *Interweave Spectrum Access Paradigm*

The interweave spectrum access paradigm is based on the principle of opportunistic exploitation of transmission vacancies across spatial and temporal dimensions (see fig. 1.3). The opportunism is driven by the inference drawn from a spatio-temporal sensing of the frequency bands. The sensing process enables CRs to establish the presence/absence of the active primary user. Since, some of the prime spectrum is under-utilized across one of these two dimensions, the interweave paradigm aims to improve the utilization while being "invisible" to the existing users.

Interweave paradigm is a modified form of the proposal presented by Mitola et al. in [18]

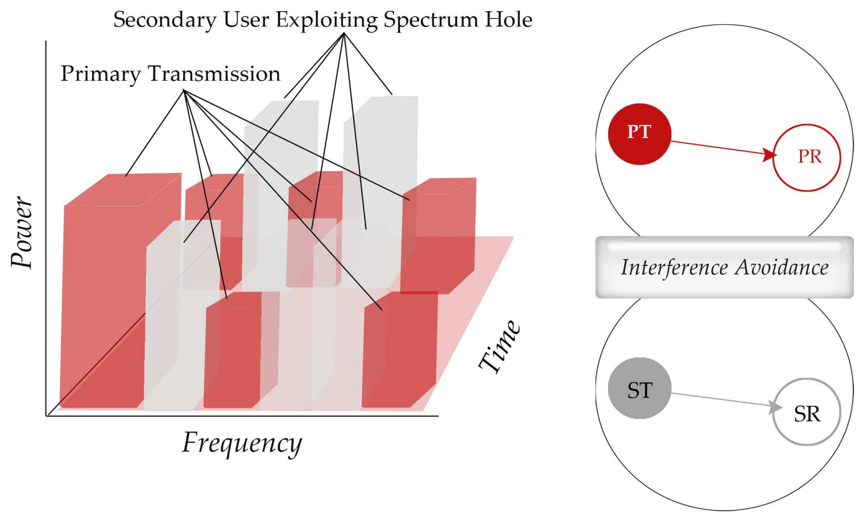

Figure 1.3: Interweave spectrum access paradigm where PT is used as a short hand for the primary transmitter, PR for the primary receiver, ST for the secondary transmitter and SR for the secondary receiver.

Spectrum Hole: A band of frequencies sporadically utilized by the primary users across the dimensions of space and time.

From the interference management perspective, the interweave mechanism corresponds to the interference avoidance. Unlike, underlay networks concurrent transmissions with the primary user only occur under a false perception of the transmission opportunity. Based on the employed sensing procedure, the interweave spectrum access mechanism can be further classified into two broad classes:

1.3.2.1 *Interweave Empowered by In-band Sensing*

The performance of the spectrum sensor is characterized by two probabilistic metrics, i.e., probability of detection and probability of false-alarm. From the primary user's perspective a higher detection probability corresponds to the better interference protection. On the other hand the secondary user desires a low false alarm probability which is vital to improve its throughput.

Under in-band spectrum sensing mechanism, CR users are obliged to periodically sense the primary channel to establish the presence of the incumbent transmission [19, 20]. Upon the positive detection of the primary signal, the CR users must vacate the frequency band in a pre-specified time. The vacation time and the sensing frequency both depend on the primary user's tolerance to the interference or its delay sensitivity. In order to realize the full potential of in-band sensing the following fundamental limitation must be addressed:

A. **Transmission Opportunity $\neq$ Detection of the primary transmitter**: The detection of the primary transmitter does not correspond to the detection of instantaneous and local transmission opportunities [21]. While the former itself is still a non trivial task, the latter requires detection of primary receivers which demands much more sophisticated sensing techniques.

B. **Large-inhibition Zone:** Since in-band sensing relies on the detection of the primary transmitter, CRs must adopt a conservative behavior in accessing the spectrum. In other words, the primary transmitter induces a large inhibition zone where an additional spatial guard zone is employed to guarantee protection of the primary receiver.

C. **Sensing-Throughput tradeoff:** Since the secondary communication is subject to the outcome of the detection process, interference avoidance needs to be traded with the attainable throughput. More specifically, as the secondary users are required to sense the channel in a periodic manner, they are left with a fixed time slot for scheduling their transmission. While CRs can sense over a longer duration (to accumulate more energy and perform robust averaging over noise process) to establish the presence of the primary this will shrink their own data transmission window [22–24].

The key advantage of in-band sensing when compared to its counterpart (out-band scheme) is that it does not require a dedicated control channel for the signaling (see 1.3.2.2). The secondary user's decision to transmit or not depends on the inference drawn from the spectrum sensing process which relies on listening to the primary user's channel.

1.3.2.2 *Interweave Empowered by Out-of-band Beacon Detection*

In out-of-band beacon enabled spectrum sharing mechanism the primary user explicitly transmits *grant* or *inhibit* beacons to indicate whether the channel is free or busy, respectively. This out-of-band sensing requires a dedicated control channel for beacon signaling. The authors in [25–27] have suggested that the dual beaconing approach can be easily integrated in legacy networks. The CR transmitters are obliged to remain silent unless a grant beacon is detected. Similarly, the CRs must vacate the spectrum band upon reception of the inhibit beacon from the legacy user. The key advantages of the out-of-band sensing as compared to in-band are as follows:

One of the key challenges associated with the out-of-band beaconing is selection of the control channel. The channel should be selected such that its propagation characteristics are highly correlated with the original data channel. At the same time, the two channels should be sufficiently separated from each other to allow the diplexing. [20]

A. **Receiver Detection:** Out-of-band beaconing (proposed by FCC in [28]) does not require a sophisticated sensing mechanism for primary receiver detection. Rather, the primary receiver explicitly transmits a grant or inhibit beacon for provisioning the spectrum sharing. Transmission of beacon can also be provisioned by installing a dedicated beaconing device with the primary receiver.

B. **Inhibition Zone:** In out-of-band sensing large inhibition zones are not required. This is mainly because the sensing process relies upon explicit beaconing from the primary receiver.

C. **Sensing-Throughput tradeoff:** The out-of-band signaling uses a dedicated control channel for beacon transmission. This allows the CRs to implement a separate radio interface which they can continuously scan for the primary inhibit beacon, while communicating simultaneously over the vacant frequency band. Consequently, unlike in-band networks the sensing-throughput tradeoff is not experienced in its primitive form.

Some of the existing studies have also proposed a hybrid interweave & underlay access paradigm. The hybrid access mechanism demands that CRs must guarantee the primary user's desired QoS requirements even under false perception of a spectral hole [29].

In brief, the interweave paradigm relies heavily on the spectrum sensing process for provisioning interference avoidance. Nevertheless a perfect interference avoidance is not feasible due to the inherent tradeoff between the probability of detection and the probability of false alarm associated with the spectrum sensor. This leads to:

Challenge 2: Can we develop an accurate statistical characterization of the aggregate interference under the varying degrees of knowledge about the beacon structure? What parameters can be tuned to counter the uncertainty inherent in the detection process? How is the primary user's performance affected in the presence of a collocated interweave CR network? How should the CRs co-exist amongst themselves?

Comprehensive analysis of challenge 2 and related design questions are the subject of Part II of this dissertation.

1.3.3 *Overlay Spectrum Access Paradigm*

In the existing literature, the term overlay spectrum access is sometimes used to actually refer to the interweave paradigm (see for instance [8] and [29]).

The overlay spectrum access mechanism is based on the premise that the CR users possess a complete knowledge about the incumbent user's codebooks and its messages [3]. The knowledge of the codebook and messages can then be exploited to perform interference cancellation, alignment or other sophisticated signal shaping techniques to coexist with the primary. The overlay paradigm can be implemented if the legacy user is operating under a uniformly standardized communication protocol. In this scenario, the CR users may already possess a complete knowledge about the codebook. An alternative solution (attained by sacrificing the obliviousness) is that the primary users should periodically broadcast their codebooks. Beside the knowledge of codebooks, a CR transmitter must possess complete knowledge of the messages before they are transmitted by the primary. Practically, this is infeasible except for the cases where the retransmission of the message occurs due to failed delivery. Implementing overlay access strategy in presence of multiple primary users becomes a formidable challenge.

In this thesis, we address design problems related to the underlay and the interweave spectrum access paradigms. Hence a detailed discussion on the overlay strategy is beyond our current scope. Interested readers are directed to [3, 30, 31] and references therein.

1.4 INTERFERENCE: AN ANCIENT CURSE

CRs provide an efficient and a streamlined approach for harnessing the throughput gains by aggressively reusing the existing spectral resources. Irrespective of the adopted access paradigm, the aggressive reuse should not be attained at the cost of excessive interference to the legacy user. Unfortunately, complete interference avoidance or control is a far-fetched dream. This can be attributed to the fundamental broadcast nature of the wireless medium. More specifically, a large scale wireless network inherently possesses several degrees of uncertainties, manifested in the forms of multi-path fading, thermal noise, path-loss, shadowing, co-channel interference, medium access frequency and routing dynamics.

Besides these channel dynamics, the spatial topology of the network adds another degree of uncertainty specially for an ad hoc wireless network. While point-to-point networks can benefit from simple link budget analysis, this is not the case with the large scale networks [32, 33]. The spatial dimension becomes an important factor as both the received signal and the co-channel interference become functions of the network geometry. Similar to the wireless fading channel, the topology of the network can assume infinite spatial configurations. Consequently, a spatial statistical model must be adopted for addressing the design and deployment issues. A complete characterization of SINR in ad hoc networks requires the following building blocks:

1. Transmission power employed for intended link;
2. Propagation channel for the desired signal;
3. Distance between the transmitter and its intended destination;
4. Set of active co-channel transmitters;
5. The transmission power and routing adapted by the co-channel transmitters;
6. Power of the additive white noise experienced at the intended receiver.

Notice that under any realistic networking paradigm these parameters presume a stochastic nature. It is obvious that an accurate characterization of SINR requires an accurate statistical model for the co-channel interference. In the past few decades, several efforts have been made towards the development of accurate interference models for large scale networks under various networking scenario [34–50]. Although interference modeling is critical in any networking paradigm, it plays a pivotal role in context of the large scale CRNs. This can be credited to the operational principle for the secondary terminals which demands adherence to the interference constraint. More specifically, secondary transmissions must be performed in a manner such that network performance can be improved rather than deteriorating it further by causing excessive interference. Interference modeling in cognitive radio networks is critical milestone which must be attained for progression on several fronts:

A. **Analyzing the primary user's performance**: An accurate statistical model for a large scale CRN under any DSA paradigm is essential for quantifying the performance degradation which legacy users may experience due to the impairments involved in a CR's observation processes.

B. **Exploring the design parameters for CRN:** Statistical modeling of the aggregate interference provides a starting point for exploring the design space of the CRNs. More specifically, the aggregate interference experienced by the primary user is related to both the node and network level parameters which can be tuned such that the primary user's QoS constraint is guaranteed. Some of these parameters can be summarized as follows:

   a) *Node level parameters*: Transmit power, spectrum sensing scheme, number of antennas, traffic etc.

   b) *Network level parameters*: Medium access strategy, frequency of transmission attempt, relaying/routing strategy, networking paradigm (multi-hop, single-hop, point-to-point, broadcast) etc.

C. **Quantifying the gains:** Throughput gains harnessed by adjusting the appropriate network and node level parameters in a CRN can only be quantified with the help of an accurate statistical model for the cognitive network interference.

D. **Efficient design of signal processing techniques:** Statistical analysis of the network interference is also critical in establishing the impact of signal processing algorithms employed by CRs for interference control or avoidance. The interference model establishes a relationship between local and network level parameters and their interactions. These interactions can then be exploited to design, improve or optimize the signal processing algorithms implemented by CRs.

E. **Exploitation vs. Mitigation:** An accurate analysis of cognitive network interference also gives insights on optimality of mitigation as compared to exploitation. In some cases, inherent uncertainties can be exploited to provide better performance and mitigating them may result in sub-optimal operation.

Interference modeling for a CRN is more challenging than ad hoc networks due to the inherent uncertainties involved in sensing and access algorithms.

Furthermore, these access and sensing processes are also coupled to the primary users communication parameters. In recent times, a few studies have worked towards establishing interference models for the CRNs [20, 29, 51–58]. However, most of these studies have their own limitations which will be discussed in due course (see Parts I, II & III).

1.5 STOCHASTIC GEOMETRIC MODELING

As discussed earlier, the definition of network interference is strongly coupled with the spatial configuration of nodes. The notion of having a link between two wireless terminals is entirely dependent upon the received SINR, which is indeed a function of inter-nodal distances. This was also conjectured by Ephermides in [59] :

> “We have all learned to draw a graph to depict a communication network, as in Fig.1. This is a useful and accurate depiction of the network topology when the nodes are interconnected with dedicated wired lines. The tendency has been to do the same when the network under consideration is a wireless one, and that has been the cause of many misconceptions and much fallacious reasoning. If there are no “hard-wired” connections between the nodes, the notion of a “link” between, say, nodes A and B is an entirely relative one. In fact, it is so relative that links in a wireless network should be thought of as “soft” entities that are almost entirely under the control of the network operator.
>
> ⋮
>
> It should be clear, then, that the existence of a wireless link is a very volatile notion. Thus, the proper way of depicting a wireless network is simply via the location of its node”

Consequently, the locations of the wireless nodes should be modeled using a point pattern. For large scale ad hoc wireless networks these point patterns can assume infinite realizations. Since it is impractical to design by considering infinite network topologies, a statistical point pattern model must be employed. Stochastic geometry is the branch of mathematics which deals with the study of random point processes [60]. Recently, stochastic geometric modeling of mobile ad hoc networks (MANET) has gained significant interest. The interested reader is directed to [33, 61, 62] and [63] for a detailed survey of the relevant literature.

In contrast to the modeling of classical networks, stochastic geometric modeling of CRNs has proven to be a more challenging task. In this thesis, we borrow well established tools from the stochastic geometry for analyzing the spatial properties of both primary and secondary networks.

1.6 RESEARCH OBJECTIVES

The primary focus of the work undertaken and presented in this thesis is:

1. To develop an accurate statistical characterization of the aggregate interference in large scale cognitive wireless networks under both interweave and underlay access mechanisms.
2. To study the impact of both the node and the network level dynamics on the aggregate interference.
3. To explore the degrees-of-freedom available for enhancing the performance of the secondary network while satisfying the co-existence constraint.
4. To investigate the end-to-end performance of a large scale CRN under multi-hop relaying strategy by developing:
    a) an appropriate metric to capture the spatial dimension for the information flow;
    b) a QoS aware forwarding mechanism.
5. To address optimal exploitation of diversity gains harnessed by adapting multiple antennas.
6. To characterize the performance of the primary user when CRs implement distributed interference protection using local channel state information.
7. To study the self-coexistence mechanism and its impact on the primary user's performance.
8. To investigate the potential of transmitter-receiver cooperation for increasing the detection reliability.
9. To characterize the performance of the secondary network under the interweave spectrum access paradigm.
10. To explore the possibility of employing CRs for provisioning energy efficient communication.

1.7 THESIS CONTRIBUTIONS & ORGANIZATION

This dissertation is organized in three distinct parts. Appendix A presents the key statistical preliminaries.The novel contributions of each part are summarized as follows:

Part I: Cognitive Underlay Networks

Part I is dedicated to address the vital design issues pertinent to cognitive underlay networks. The novel contributions presented in Part I are as follows:

Chapter 2 is based on the work published in Publication III.

A. **Dimensioning Guard-Zone for Cognitive Users:** As discussed in Section 1.3.1, the underlay cognitive radio networks can concurrently share the wireless medium with the primary user as long as the primary user's QoS requirements are guaranteed. The primary user's QoS requirements are readily expressed in terms of the link outage probability (OP). Now in order to ensure that the OP of the primary user never exceeds a specified threshold, secondary users should *remain silent* in a certain no-talk zone of spatial radius r_e. Chapter 2, investigates the dimensioning issues for the primary user's guard-zone. More specifically, we derive a closed form expression for the radius of a guard zone (r_e) required at a primary receiver. It is demonstrated that r_e is not only strongly coupled with the primary user's QoS requirement but it is also dependent upon the secondary network's connectivity, medium access, QoS and routing mechanisms.

B. **Multi-Antenna Multi-hop Underlay Cognitive Networks:** In Chapter 2, a spatial guard-zone was introduced to protect the primary user's transmission. The secondary access strategy empowered by the guard-zone based interference protection is quite effective when secondary users operate in the presence of a single primary link. However for a large scale primary network (formed by multiple active links which are distributed across space) the guard-zone based co-existence strategy is not an attractive solution. Consequently, in chapter 3, we explore an alternative degree-of-freedom, i.e., the medium access probability. In order to capture the spatial information flow in multi-hop cognitive networks, we define a new unified metric termed as *achievable spatial throughput.* We quantify the achievable spatial throughput of a multi-antenna Poisson CRN collocated with a Poisson multi-antenna primary network. CR users employ Slotted-ALOHA medium access control. The success probability (SP) of a primary link is quantified in the presence of the secondary and primary interferers. It is demonstrated that a two fold gain is experienced by employing multiple antennas at primary, i.e., (i) the fixed high desired SP threshold is met; (ii) CRs can also be accommodated without QoS deterioration. Furthermore, the maximum permissible medium access probability (MAP) for a CRN is derived from the link SP and the primary user's QoS constraint. The impact of the number of antennas and the modulation employed at the primary on the permissible MAP of the CRN is also explored. The situation where CR users employ multi-hop communication, QoS aware relaying with a radian sector forwarding area is also studied. The average forward progress (AFP) and isolation probability for a CR user with QoS based connectivity is characterized under the permissible MAP. The spatial throughput for the CRN is quantified by the analysis of the AFP and the permissible MAP. It is shown that there exists an optimal MAP which maximizes the spatial throughput of the CRN. This optimal MAP is coupled with the permissible MAP, density of users, number of antennas and modulation schemes employed in both primary and secondary networks. Lastly, a few important design questions are investigated for multi-hop MIMO underlay CRNs.

Chapter 3 is based on the work published in Publications I & X.

c. **The MAP Adaptation and the Spectral Efficiency Wall:** Chapter 4 builds on top of chapter 3. More specifically, chapter 3 leads to two interesting observations: (i) there exists an optimal MAP which maximizes the throughput performance of CRN; (ii) it is not always possible to employ the optimal MAP as an operational point due to the primary's enforced QoS constraint. This motivates us to adapt a more fundamental and comprehensive approach to explore the design parameters of a large scale cognitive underlay network. Consequently in chapter 4, we develop a comprehensive analytical framework to characterize the area spectral efficiency of a large scale Poisson cognitive underlay network. The developed framework explicitly accommodates channel, topological and medium access uncertainties. We highlight the two available degrees of freedom in cognitive underlay networks, i.e., medium access probability and transmit power. While from the primary user's perspective tuning either to control the interference is equivalent, the picture is different for the secondary network. We show the existence of an area spectral efficiency wall under both adaptation schemes. We also demonstrate that the adaptation of just one of these degrees of freedom does not lead to the optimal performance. But significant performance gains can be harnessed by jointly tuning both the medium access probability and the transmission power of the secondary networks. We explore several design parameters for both adaptation schemes. Finally, we extend our quest to more complex point-to-point and broadcast networks to demonstrate the superior performance of joint tuning policies.

Chapter 4 is based on the work published in Publication II.

Notice that in chapter 4 our primary focus is to reveal the fundamental degrees of freedom available in an cognitive underlay network. To this end, we restrict our attention to the scenario where both primary and secondary nodes are equipped with a single antenna. Extensions to the case of multiple antennas follow similar course as outlined in chapter 3.

Part II : Cognitive Interweave Networks

Part II, of this dissertation attempts to characterize the aggregate interference in large scale cognitive interweave networks. The novel contributions of this part can be summarized as follows:

A. **Modeling Aggregate Interference in Cognitive Interweave Networks:** Interference modeling for an interweave CRN is a more challenging task than the one addressed in context of underlay networks. This is because of the intricate coupling between the secondary user's aggregate interference and spectrum sensing mechanism. In chapter 5, we develop a statistical framework to model the OP, throughput and ergodic capacity of a primary/licensed user, while operating in the presence of a collocated, spectrum sensing, (Poisson) ad hoc CRN. The existing primary beacon enabled interweave spectrum sharing model is utilized for evaluating the interference at a typical primary receiver. We consider that based on the degree of knowledge about the primary user, the CRs employ either a matched filter or an energy detector for spectrum sensing. Furthermore, three different architectures for spectrum sensing based on the spatial configuration of the platform which performs the sensing are proposed. It is demonstrated that these different architectures exploit the geometric uncertainty of the link distances to provide a superior performance in terms of OP, throughput and ergodic capacity. A comprehensive study of how the OP for a primary user is coupled with different parameters of the CRN is carried out. We further investigate the optimal signal to interference ratio (SIR) threshold which maximizes the primary's throughput and an optimal medium access probability (MAP) for the secondary network which satisfies the primary's desired quality of service (QoS) constraints. Lastly, the impact of the self-coexistence constraint on both the OP and throughput of the primary is highlighted. We show that ignoring the self-coexistence constraint results in an over-estimation of the interference and the outage. So in summary, this chapter presents a comprehensive analysis of the choice of optimal design parameters for a CRN to minimize the OP or maximize the throughput and ergodic capacity of the primary while considering various detection schemes and architectures.

Chapter 5 is based on the work published in Publications VI & XIII.

B. **Transmission Capacity Analysis:** The spatial throughput of a large scale primary network can be characterized in terms of a transmission capacity metric. More specifically, the transmission capacity (TC) is defined as the number of concurrent successful transmissions occurring per unit area in the primary network, subject to some OP constraint in the presence of collocated secondary network. In chapter 6 we develop a comprehensive statistical framework to study the TC of the

Chapter 6 is based on the work published in Publications XI & XII.

primary network in the presence of a collocated CRN operating under the self-coexistence constraint. Considering a system model based on stochastic geometry and the primary beacon enabled interweave spectrum sharing model, the OP of a typical primary receiver is studied. The scaling laws for the OP of a typical primary receiver are established. With the help of simulations it is shown that the TC of the primary network decreases with an increasing number of secondary users and the degree of the self-coexistence.

Chapter 7 is based on the work published in Publication IV.

c. **Nearly Exact Laplace transform for the Aggregate Interference:** Chapter 7 revisits the problem of interference modeling introduced in chapter 5 under a more generic setup. In chapter 7 we present a novel closed-form expression for an upper bound on the OP of a primary receiver operating in the presence of a Poisson field of spectrum sensing cognitive radios (CRs). Notice that the bound is more useful than the approximations (presented in chapter 5) because the analysis based on the approximations *cannot be employed to provide* performance *guarantees* (see chapter 7 for details). In order to demonstrate the tightness of the proposed bound, we corroborate our analytical results with a Monte Carlo simulations. The upper-bound is employed to develop a more generic throughput metric for the primary link, namely, transport throughput.

Part III: Energy Efficiency

Chapter 8 is based on the work published in Publications VIII & IX.

The key motivation behind part III was to explore whether CRs can be employed to improve the energy efficiency (EE) of a large scale ad hoc wireless networks. It turns out that the quantification of energy efficiency for ad hoc networks even without any cognitive processing is an open issue. To this end, in chapter 8, we present an *analytical approach* to quantify the EE of a large scale *interference limited* wireless ad hoc network. Our quantitative investigation addresses energy consumption at *physical*, *medium access control* (MAC) and *routing* layers. Specifically, we analytically characterize the energy consumption of a large scale wireless ad hoc network, where users wish to communicate with their intended destinations under a certain *quality of service* (QoS) constraint. User/node level energy expenses are quantified by analyzing the power consumption of *communication hardware*.

Inspired by current trends in radio transceiver design, our analysis considers three popular transceiver architectures. It is assumed that nodes which defer their own transmission under Slotted ALOHA protocol, assist other nodes by acting as relays. In essence, an arbitrary source communicates with its destination via *multihop* transmission. Although, we do not consider a particular *routing* scheme, the forwarding strategy is similar to *long-hop/greedy routing* (GR). While quantifying the overall EE of the network, *the geometry of the forwarding* areas resulting from different GR type relaying strategies is also explicitly addressed. Unlike prior studies, the link model is formulated by considering: (i) the large-scale path-loss and the small-scale Rayleigh fading; (ii) the co-channel network interference; and (iii) the user's desired QoS requirements. Recognizing that the EE of a large scale ad hoc network is strongly coupled with connectivity attributes, the link and routing models are employed to establish two critical quantities, i.e., the *single hop maximum forward progress* and the *node isolation probability*. The *number of hops* required by an arbitrary source to connect with its destination is quantified from single hop maximum forward progress.

Finally, the user level hardware power consumption model, the MAC protocol, the desired QoS constraint, the single hop forward progress, the node isolation probability and the hop count statistics are all combined to establish an analytical expression for the EE of a large scale ad hoc network. Both analytical and Monte-Carlo simulations are employed to investigate the impact of several parametric variations on the connectivity attributes and the EE. Our results indicate, that several hypotheses established in the existing literature *ignore* the network interference and the fading breaks down for a large scale interference limited network. We also demonstrate that medium access probability (MAP) is a cross-layer parameter and there exists an optimum MAP which maximizes the EE

Finally, we conclude this thesis by a brief commentary on how CRs can be adapted to improve the energy and spectral efficiency and point out future directions for the research in this area.

Part I

COGNITIVE UNDERLAY NETWORKS

2

QUANTIFYING THE PRIMARY'S GUARD-ZONE UNDER COGNITIVE USER'S ROUTING AND MEDIUM ACCESS

ABSTRACT

In this chapter, we derive a closed form expression for the radius of a guard zone (r_e) required at a primary receiver operating in the presence of a cognitive radio network while ensuring the primary's desired quality of service (QoS). We demonstrate that r_e is not only strongly coupled with the primary's QoS requirement but it is also dependent upon the secondary network's connectivity, medium access, QoS and routing mechanisms.

Primary objective:
- *To dimension the guard-zone required for protecting the primary user's transmissions in presence of co-channel the secondary users.*
- *To study the impact of the secondary network's routing and medium access control strategy on dimensions of guard-zone.*

2.1 INTRODUCTION

As discussed in chapter 1, the operational interference constraint on CRs dictates that secondary users should shape their transmissions such that the primary user can still experience an acceptable QoS. The notion of shaping the transmission parameter arise from the challenge 1. Notice that challenge 1, arise due to impracticallity of implementing an interference temprature based co-existence strategy (please refer to chapter 1). Now in order to ensure that the OP of the primary user never exceeds a specified threshold, one mechanism is to design a CR network such that the secondary users should *remain silent* in a certain no-talk zone of spatial radius r_e. In [64] the authors centered such a no-talk zone on the primary transmitter and derived an expression for r_e. They termed this guard zone the *primary exclusive region* (PER).

References [65] and [66] extended [64] to study the PER under small scale Rayleigh fading and shadowing respectively, while the PER with exploitation of polarimetric dimension is investigated in [67]. However, all of these studies do not consider the actual operational details of the secondary users. More specifically, the existing studies consider neither the MAC enforced in the secondary network nor the secondary network's desired *QoS*. Consequently, the existing models can at best be extended to characterize the PER under only a *single hop* communication of the secondary users. But *multi-hop* architecture and dynamic network topology are some of the key distinguishing factors for the next generation of ad-hoc CR networks (CRNs) [68] and so in this chapter:

Key considerations:
- *Spectrum sharing enabled by employing spatial guard-zone based interference control.*
- *Single primary link operating in the presence of multiple co-channel secondary users.*
- *Secondary user's employ multi-hop transmissions.*

1. We formulate the primary's guard zone by considering an alternative definition, i.e., the primary's guard zone is defined as the disk of radius r_e centered on the *primary receiver.* This alternative definition is more generic because: (i) it allows for a straight-forward extension to the case of multiple primary users; (ii) it has a more intuitive definition since the primary receiver is the victim of the aggregate interference and not the primary transmitter; and (iii) an equivalent PER model can be constructed for the broadcast type networks as in [64].

2. We derive an explicit expression for the radius (r_e) of the guard zone, while considering the *multi-hop forwarding* strategy employed by the CRs with a certain minimum QoS requirement (expressed in terms of *SIR*). More specifically, we consider three different forwarding schemes where the CRs employ optimal relaying strategies under the slotted ALOHA MAC protocol combined with SIR threshold and geometric constraints. We study a scenario where CR transmitters tune their MAP (i.e., p) such that the *probability of isolation* (p_{ISO}) for any arbitrary CR transmitter remains below a desired threshold (ϵ_{ISO}) at a particular SIR threshold (γ_s).

Asummption I: We assume that both the primary and the secondary networks are interference limited.

Asummption II: In order to ensure analytical tractability an upper-bound on the SIR at an arbitrary secondary receiver is obtained by ignoring the interference from a single primary link (see Section 2.4).

To the best of our knowledge, no previous study has addressed the problem of quantifying the primary's guard zone while addressing both the MAC and the routing of the secondary network.

2.2 SPATIAL AND CHANNEL MODEL

2.2.1 *Primary Link and Guard Zone*

In this chapter, we consider a single primary communication link operating in the presence of an ad-hoc CRN (underlay networks with multiple primary users are studied in next two chapters). The primary link $(P_{TX} \rightarrow P_{RX})$ is formed by a primary receiver (P_{RX}) located at the origin and a primary transmitter (P_{TX}) located at a distance r_p from P_{RX}. The primary's *spatial no-talk zone* or *guard zone* is modeled by a disk of radius r_e centered on the P_{RX} .

2.2.2 *Geometry of Secondary Network*

The locations of the secondary users at any arbitrary time instant are modeled by a *stationary Poisson point process* (SPPP) [60] Π_s with intensity λ_s on $\mathbb{R}^2 \backslash b(o, r_e)$. Here $b(o, r)$ denotes a ball of radius r centered at the origin and λ_s is the number of CR nodes per unit area. More specifically, the probability of finding $k \in \mathbb{N}$ CR nodes inside an area $\mathcal{A} \subseteq \mathbb{R}^2 \backslash b(o, r_e)$ follows the Poisson law with the mean measure $\Lambda(\mathcal{A}) = \lambda_s \int_{\mathcal{A}} dx$ [60], where if $\mathcal{A}$ is a ball of radius r then $\Lambda(\mathcal{A}) = \lambda_s \pi r^2$.

2.2.3 *Channel Model*

All four type of links (i.e., primary to primary, secondary to secondary, primary to secondary and secondary to primary) are assumed to operate in a Rayleigh, flat-fading environment. The overall channel gain between transmitter and receiver separated by distance R (in both networks) is modeled as $Hl(R)$. Here, H is a unit mean exponential random variable and $l(R) = CR^{-\alpha}$ is the power-law, path-loss function. This path-loss function depends on the distance R, a frequency dependent constant C and an environment/terrain dependent path-loss exponent α. The fading channel gains are assumed to be mutually independent and identically distributed (i.i.d.) across different links.

Asummption III: Without any loss of generality, we will assume that the frequency dependent constant$C = 1$ for the rest of this discussion.

2.3 MEDIUM ACCESS AND ROUTING IN A CRN

CR transmitters which are outside the primary's guard zone employ slotted ALOHA MAC protocol to schedule their transmissions. So at an arbitrary time instant the SPPP of the CR nodes (Π_s) can be decomposed into two distinct subsets, i.e., CR transmitters and CR receivers. Let $\mathbb{1}(x)$ denote a Bernoulli indicator random variable with parameter p (independent of x), and so

$$\begin{aligned} \Pi_s^{TX} &= \{x \in \Pi_s : \mathbb{1}(x = 1)\} \text{ with } \lambda_s^{TX} = \lambda_s p, \\ \Pi_s^{RX} &= \{x \in \Pi_s : \mathbb{1}(x = 0)\} \text{ with } \lambda_s^{RX} = \lambda_s (1 - p), \end{aligned} \tag{2.1}$$

where p is the previously defined MAP. We will consider a scenario where CR transmitters want to communicate with an infinitely distant destination in a multi-hop manner. CR receivers in Π_s^{RX} serve as intermediate relays between an arbitrary CR transmitter and its destination. Each transmitted packet is routed via a secondary's QoS-aware forwarding strategy. More specifically,

Note: The assumption of infinitely far destinations can easily be relaxed (see Chapter 8). Also notice that our analysis is based on node isolation probability which is independent of the source-destination separation.

1. Any receiver $y \in \Pi_s^{RX}$ is considered as a potential relay for a CR transmitter $x \in \Pi_s^{TX}$ in an arbitrary slotted ALOHA time slot iff the SIR of the received packet at y is above a predefined, desired SIR threshold, γ_s. The set of potential relays for transmitter x that satisfy the SIR constraint can be denoted by a random set $\mathcal{R}(x)$.

2. Amongst all potential relays $\mathcal{R}(x)$, $x \in \Pi_s^{TX}$, a receiver is selected as a relay iff it provides *maximum forward progress* towards the destination.

In most practical situations $\gamma_s > 1$ [69] (for narrow-band communication) and so each relay is associated with a unique CR transmitter. Moreover, as indicated by the second condition above, the actual relay selection is strongly coupled with the geometry of the network resulting from the routing protocol. In order to maintain generality, we do not consider any specific routing protocol. Rather, we will consider three different geometric setups which result from the majority of the routing strategies.

Notice that each of these forwarding strategies corresponds to a different level of route directionality. RSF provision the best directional control between the source and its intended destination, while UCF provides the least.

A. **Radian Sector Forwarding:** Under radian sector forwarding (RSF) routing each CR transmitter only selects the relays in a sector of radius r with a central angle ϕ provided the desired SIR threshold γ_s is satisfied. Since we are considering a scenario where the destination is located at infinity ($r \rightarrow \infty$) then the RSF routing is parametrized by only ϕ. Notice that several practical routing protocols with greedy forwarding (e.g., GeRaF, GIF, GEAR[70]) result in the geometry similar to this RSF protocol [71]. Fig. 2.1a graphically illustrates the geometric setup under RSF routing mechanism.

B. **Half Plane Forwarding:** Under half plane forwarding (HPF) a CR transmitter selects the relays satisfying the SIR constraint in the left, right, top or bottom half plane depending on the location of the destination. The HPF routing protocol can be considered as a simplified version of a maximum forward progress protocol [71]. Most greedy routing schemes work under such a geometric setup. These strategies are further explored in chapter 8 in details.

C. **Unconstrained Forwarding:** Under unconstrained forwarding (UCF) a CR transmitter selects any relay that is able to decode its transmission under the SIR constraints. This type of routing protocol is considered when every node has some data for every destination in any arbitrary direction. Alternatively, a destination can be reached via different equivalent paths. Although, this type of routing protocol is idealistic, it provides an upper bound on the performance of any routing protocol.

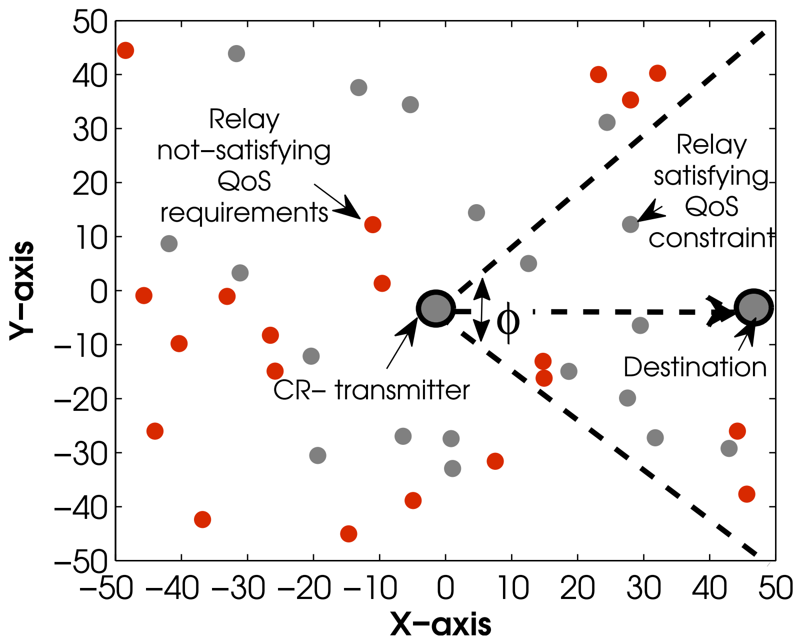

(a) QoS aware radian sector forwarding in a large scale CRN.

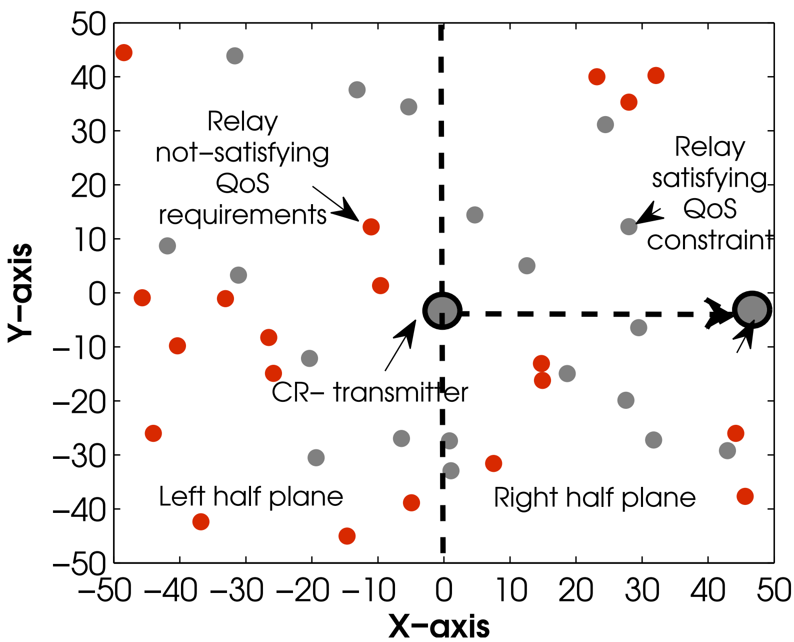

(b) Forwarding geometry under half plane forwarding. For sake of clearity, we only show top and bottom half planes.

Figure 2.1: Geometry of the forwarding region under radian sector and half plane forwarding mechanisms.

2.4 MAP FOR CRS UNDER ROUTE ISOLATION CONSTRAINT

In this section, we derive the MAP for a CR transmitter under route isolation constraint. We first characterize the route isolation probability under RSF, HPF and UCF routing strategies and then employ the isolation probability to derive the maximum permissible MAP such that a desired isolation threshold can be guaranteed.

Isolation probability of the secondary user

Theorem 2.1 *In an interference limited ad-hoc CRN the probability* (p_{ISO}) *that an arbitrary CR transmitter* ($x \in \Pi_s^{TX}$) *cannot find any suitable relay* ($y \in \Pi_s^{RX}$) *satisfying the desired SIR and routing constraints is given by*

$$p_{ISO}^{\{t\}} = \exp\left(-\kappa^t \frac{1-p}{p}\frac{\sin(\delta)}{\delta\gamma_s^{\delta/\pi}}\right), \tag{2.2}$$

where $t \in \{RSF, HPF, UCF\}$, $\kappa^{RSF} = \phi/2\pi$, $\kappa^{HPF} = 0.5$, $\kappa^{UCF} = 1$, $\delta = \frac{2\pi}{\alpha}$ *and* p *is the ALOHA MAP.*

PROOF: From (3.2) both Π_s^{RX} and Π_s^{TX} are SPPPs constructed via $p-$thinning of Π_s. Since Π_s^{TX} is stationary, by employing Silvnyak's theorem [60] a probe transmitter can be added at location z and then the network can be re-centered (appropriately at z) by translating each point of $\Pi_s \cup \{z\}$ and the primary link. The SIR with respect to probe transmitter, measured at an arbitrary CR receiver $y \in \Pi_s^{RX}$ located at distance r from the origin, is given by

Quick Reference≫ Silvnyak's Theorem: The law of the stationary Poisson point process does not change by addition of an arbitrary point.

$$\gamma(H, r, I) = \frac{HP_s l(r)}{I + I_{pc}(z, r)} \leq \frac{HP_s l(r)}{I}, \tag{2.3}$$

where, H is the channel gain between probe transmitter and a relay, P_s is the transmit power of the CR transmitter, $I = \sum_{i\in\Pi_s^{TX}\setminus\{o\}} H_i l(R_i) P_s$ is the aggregate secondary to secondary interference and $I_{pc}(z, r)$ is the interference from the primary transmitter to secondary receiver. In order to ensure analytical tractability, we utilize the upper bound on the SIR obtained by ignoring $I_{pc}(z, r)$. This upper-bound reduces to the equality when all CR receivers are capable of perfectly canceling the interference [3] from the primary user. Then the potential relays for the probe transmitter form a marked Poisson point process (Π_s^{RL}) constructed by assigning the i.i.d. fading, interference marks and a position dependent SIR constraint mark to each receiver in Π_s^{RX}. The location dependent SIR marks are defined as

$$\mathbb{1}_{\gamma_s}(\gamma(H, r, I)) = \begin{cases} 1 & \gamma(H, r, I) \geq \gamma_s \\ 0 & \gamma(H, r, I) < \gamma_s \end{cases}. \tag{2.4}$$

The mean measure of Π_s^{RL} can be computed as

$$\begin{aligned}\Lambda_s^{RL}(\mathcal{A}) &= \int_0^\infty\int_0^\infty\int_{\mathcal{A}} \lambda_s^{RX} 2\pi r \mathbb{1}_{\gamma_s}\left(\gamma(h,r,i)\right) f_H(h) f_I(i) dr dh di, \\ &= \int_0^\infty\int_0^\infty\int_{\mathcal{A}} \lambda_s^{RX} 2\pi r \mathbb{1}_{\gamma_s}\left(H > \tfrac{i\gamma_s r^\alpha}{P_s}\right) f_H(h) f_I(i) dr dh di, \\ &= \int_0^\infty \int_{\mathcal{A}} \lambda_s^{RX} 2\pi r \exp\left(-i\frac{\gamma_s r^\alpha}{P_s}\right) f_I(i) dr di, \\ &= \int_{\mathcal{A}} \lambda_s^{RX} 2\pi r \underbrace{\mathbb{E}_I\left(\exp\left(-sI\right)\right)\big|_{s=\frac{\gamma_s r^\alpha}{P_s}}}_{A_1} dr. \qquad (2.5)\end{aligned}$$

Mean measure of an inhomogenous point process formed by relays.

Notice that A_1 is the Laplace transform of the aggregate interference under the slotted ALOHA protocol which can be computed as [44]

$$A_1 = \mathbb{E}_I\left(\exp\left(-sI\right)\right)\big|_{s=\frac{\gamma_s r^\alpha}{P_s}} = \exp\left(-\frac{\lambda_s^{TX}\pi\gamma_s^{\delta/\pi}\delta}{\sin(\delta)} r^2\right). \qquad (2.6)$$

Substituting (2.6) into (2.5), then we get

$$\Lambda_s^{RL}(\mathcal{A}) = \int_{\mathcal{A}} \lambda_s^{RX} 2\pi r \exp\left(-\frac{\lambda_s^{TX}\pi\gamma_s^{\delta/\pi}\delta}{\sin(\delta)} r^2\right) dr. \qquad (2.7)$$

The UCF scheme is independent of the angle θ between the probe transmitter and the potential relays, while the other two schemes require knowledge of θ. Hence additional i.i.d. uniformly distributed marks $\theta \sim \mathcal{U}(0, 2\pi)$ are assigned to Π_s^{RL}, i.e.,

$$\Lambda_s^{RL,t}(\mathcal{A}) = \int_{\theta_1^t}^{\theta_2^t} \Lambda_s^{RL}(\mathcal{A}) f_\theta(\theta) d\theta,$$

with $\theta_1^{RSF} = -\theta_2^{RSF} = -\frac{\phi}{2}$ and $\theta_1^{HPF} = -\theta_2^{HPF} = -\frac{\pi}{2}$. The probability that a probe transmitter does not have any potential relay in $\mathcal{A}$ is the following void probability of Π_s^{RL},

$$p_{ISO}^{\{t\}} = \Pr\left\{\Pi_s^{RL}(\mathcal{A}) = \emptyset\right\} = \exp\left(-\Lambda_s^{RL,t}(\mathcal{A})\right). \qquad (2.8)$$

Finally, substituting (2.7) into (8.26) and evaluating the integral with $\mathcal{A} = [0, \infty]$, we arrive at $p_{ISO}^{\{t\}}$ in (2.2). □

An important observation from (2.2) is that the isolation probability of any $x \in \Pi_s^{TX}$ is independent of the user density (λ_s). Also notice that the CRs need to select p such that the out-degree (i.e., the average number of receivers per transmitter $(1-p)/p$) of each CR transmitter is maximized, or in other words the isolation is minimized. Consequently, CRs should intelligently tune their MAP p to tolerate a certain small amount of isolation at a desired communication rate $\log_2(1+\gamma_s)$.

Connectivity is function of desired QoS.

Maximum permissible MAP.

Corollary 2.1 *In a secondary interference limited ad-hoc CRN the maximum permissible MAP (p_{max}) which ensures that an arbitrary CR transmitter is only isolated $\epsilon_{ISO} \times 100\%$ of the time at the desired SIR γ_s under RSF, HPF or UCF routing is given by*

$$p_{max} = \min\left(\frac{\sin(\delta)\kappa^t}{\kappa^t \sin(\delta) - \delta\gamma_s^{\delta/\pi}\ln(\epsilon_{ISO})}, 1\right). \tag{2.9}$$

PROOF: The proof follows from bounding (2.2) by ϵ_{ISO}. □

2.5 PRIMARY'S GUARD ZONE UNDER SUCCESS PROBABILITY CONSTRAINT

In this section, we characterize the radius of the primary's guard zone ensuring that the primary's QoS constraint is satisfied and that the CR adapts its MAP to minimize its isolation under RSF/UCF/HPF routing strategies.

Radius of the spatial no-talk zone.

Theorem 2.2 *In an interference limited scenario, the minimum guard zone (r_e) for the primary receiver in which all CR transmitters are obliged to keep silent is given by*

$$r_e = \left[\frac{-\ln\left(s_{th}^{\{p\}}\right)(\alpha-2)\,\eta}{2\pi\lambda_s\gamma_p r_p^{\alpha}\min\left(\frac{\sin(\delta)\kappa^t}{\kappa^t\sin(\delta)-\delta\gamma_s^{\delta/\pi}\ln(\epsilon_{ISO})}, 1\right)}\right]^{\frac{1}{2-\alpha}}, \tag{2.10}$$

where, $\eta = P_p/P_s$ is the ratio of transmit powers of the primary and secondary transmitters, $s_{th}^{\{p\}}$ is the success probability threshold for the primary link , γ_p is the desired SIR threshold for the primary and r_p is the primary link distance.

PROOF: The desired QoS $(\gamma_p, s_{th}^{\{p\}})$ constraint for the primary link can be expressed as

$$\begin{aligned}
\mathbb{P}_{suc}^{\{p\}} &= \Pr\left\{ \frac{P_p H l(r_p)}{P_s \underbrace{\sum_{i\in\Pi_s^{TX}\setminus\{o\}} H_i l(R_i)}_{I_s}} \geq \gamma_p \right\}, \qquad (2.11)\\
&= \mathbb{E}_{I_s}\left(\exp\left(-\frac{\gamma_p r_p^{\alpha}}{\eta} I_s\right)\right),\\
&\underset{(a)}{\leq} \exp\left(-\frac{\gamma_p r_p^{\alpha}}{\eta}\mathbb{E}_{I_s}(I_s)\right),\\
&\underset{(b)}{=} \exp\left(-\frac{\gamma_p r_p^{\alpha}}{\eta}\frac{\lambda_s p_{max} 2\pi r_e^{2-\alpha}}{\alpha-2}\right),
\end{aligned}$$

where (a) follows from Jensen's inequality and (b) can be obtained by employing Campbell's theorem [60]. Using the fact that $\mathbb{P}_{suc}^{\{p\}} \geq s_{th}^{\{p\}}$ then solving (2.11) for r_e we obtain (2.10). □

Remark 2.1 *In deriving (2.2) and (2.10), we did not consider the impact of the large scale Log-normal shadowing. Nevertheless, by adopting the steps similar to the Publication VII, the shadowing can be incorporated into analysis in a straight forward manner. Notice that the introduction of shadowing will results in a mere rescaling of the results presented in this chapter and hence will not effect the conclusions.*

2.6 RESULTS

In the last two sections, we developed an analytical framework to quantify r_e in the presence of a collocated Poisson CRN with routing and QoS constraints. In this section, we employ simulations to study the impact of both the forwarding scheme and the user density of the secondary network on r_e. Without loss of generality we consider that the desired SIR thresholds for both the primary link and the secondary links are equal, i.e., $\gamma_s = \gamma_p$. Furthermore, we employ the SIR thresholds provided in [69] (for 802.11 networks) which corresponding to different achievable bit rates with different modulation and coding schemes (see Table II in [69]).

As is clear in Fig. 2.2a, r_e decreases with a decrease in the secondary network's isolation constraint (ϵ_{ISO}). More specifically, as $\epsilon_{ISO} \to 0$, CRs re-

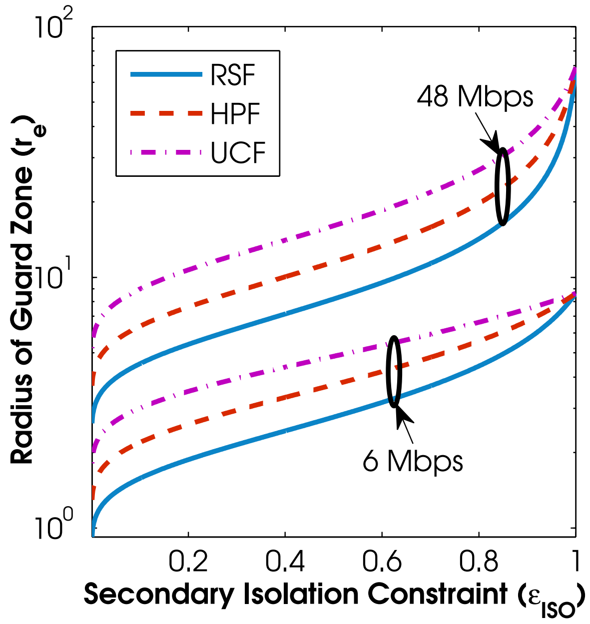

(a) Impact of the secondary's isolation constraint (ϵ_{ISO}) on the primary's guard zone (r_e).

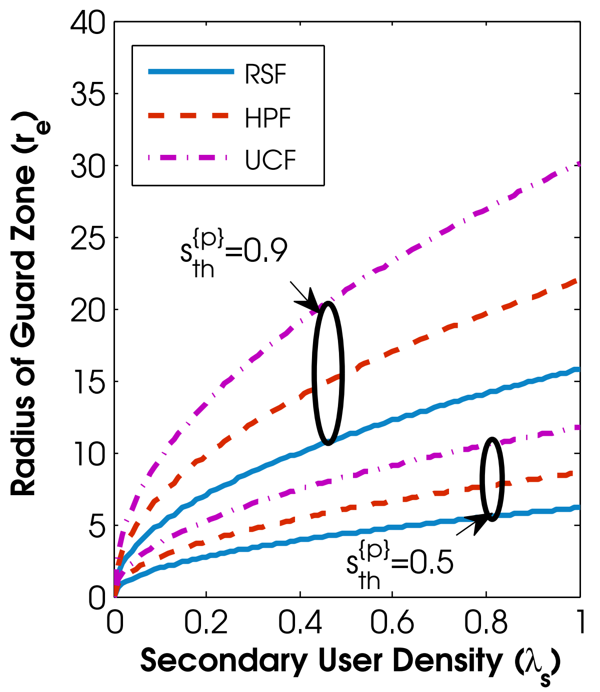

(b) Impact of the secondary user's density (λ_s) on the primary's guard zone (r_e).

Figure 2.2: Impact of the secondary network's connectivity and QoS on primary's guard zone with $\lambda_s = 10^{-3}$ (in (a)),$\phi = \pi/2$, $\eta = 1$ (in (a)) & $\eta = 10$ (in (b)), $s_{th}^{\{p\}} = 0.9$ (in (a)), $\alpha = 4$,$r_p = 5$, $\epsilon_{ISO} = 0.1$ (in (b)) and $\gamma_s = \gamma_p = 6.02$ dB (in (b)) (see 2.10)Notice that the units of r_e depends on the corresponding unit of the user density (λ_s), i.e., if λ_s is taken as number of nodes per metre square, r_e is measured in metre. Similarly, if the density is taken as per kilo metre square, r_e is measured in kilometre.

duce their MAP (p) and hence the aggregate interference experienced at P_{RX} decreases. When a constant success probability ($s_{th}^{\{p\}}$) is desired by the primary network, the decrease in the interference can be offset to decrease r_e. From Fig. 2.2a we also notice that for a fixed ϵ_{ISO} constraint, the primary's *keep-out* distance decreases with increasing directionality of the secondary's forwarding strategy. In other words, r_e for RSF is smaller than for the other two strategies. This is because, the increased directionality of routing is achieved at the cost of reducing the MAP p or by increasing the average out-degree/ number of relays. The primary's guard zone (r_e) also decreases with decrease in the desired bit-rate.

Fig. 2.2b shows that the r_e increases with an increase in the secondary user density (λ_s) for fixed SIR threshold and $s_{th}^{\{p\}}$. As noticed earlier, the maximum MAP (p_{max}) under the isolation constraint does not depend on λ_s. However, for fixed p_{max} the aggregate interference on P_{RX} increases with λ_s. So, in order to maintain constant $s_{th}^{\{p\}}$, this increase in the interference can be offset by increasing r_e.

2.7 CONCLUSION

In this chapter, we developed a statistical model to quantify the radius of the guard-zone for a primary receiver coexisting with an underlay CRN. The guard-zone empowered underlay CRN implements an interference control mechanism, i.e., simultaneous transmissions from the CRs are only provisioned outside a no-talk zone such that primary user's QoS requirements are always guaranteed. We demonstrated that such an interference control mechanism should also cater for the dynamics of the secondary network. More specifically, the co-channel interference generated by the secondary users is a function of the employed medium access control and routing strategies. Consequently, these dynamics must be appropriately addressed while dimensioning the guard-zone. Under such considerations, it is shown that high co-channel interference will not only effect the link success probability of the primary user but it is also deteriorates the QoS driven connectivity requirements of the secondary users. Moreover, when CRs adapt their transmission parameters such that their desired QoS requirements are guaranteed they also reduce the aggregate interference experienced at the primary receiver. For a certain fixed primary QoS requirements, gain in performance due to aggregate interference reduction can be translated into a smaller no-talk region, i.e., spectral efficiency can be improved by accommodating more CRs across the spatial domain.

3

ACHIEVABLE SPATIAL THROUGHPUT IN MULTI-ANTENNA COGNITIVE UNDERLAY NETWORKS WITH MULTI-HOP RELAYING

Primary objective:
- *To quantify the performance of a large scale MIMO primary network in the presence of an underlay CRN.*
- *To quantify the* bits-m/sec/Hz/m^2 *performance of the secondary network.*
- *To explore the design parameters for a multi-hop multi-antenna secondary network.*

ABSTRACT

In this chapter, we quantify the achievable spatial throughput of a multi-antenna Poisson CRN collocated with a Poisson multi-antenna primary network. CR users employ Slotted-ALOHA medium access control. The success probability (SP) of a primary link is quantified in the presence of the secondary and primary interferers. It is demonstrated that two fold gains are experienced by employing multiple antennas at primary, i.e., (i) the fixed high desired SP threshold is met; (ii) CRs can also be accommodated without QoS deterioration. Further in this chapter, the maximum permissible MAP for CRN is derived from the link SP and primary users QoS constraint. The impact of the number of antennas and modulation employed at the primary on the permissible MAP of the CRN is also explored. Assuming that CR users employ multi-hop communication, QoS aware relaying with a radian sector forwarding area is studied. The average forward progress (AFP) and isolation probability for a CR user with QoS based connectivity is characterized under the permissible MAP. The spatial throughput for the CRN is quantified by the analysis of the AFP and the permissible MAP. It is shown that there exists an optimal MAP which maximizes the spatial throughput of the CRN. This optimal MAP is coupled with the permissible MAP, density of users, number of antennas and modulation schemes employed in both primary and secondary networks. Lastly, a few important design questions are investigated for multi-hop MIMO underlay CRNs.

3.1 MOTIVATION

Why Underlay? Architectural simplicity.

In the last decade or so, underlay CRNs have gained a lot of attention from the research community [72, 73]; mainly due to the inherent architectural simplicity. As discussed in chapters 1 and 2, in an underlay paradigm, both CR and PU share the same frequency band. CR users are allowed to schedule their transmissions simultaneously with PUs as long as the QoS requirement of the PU is satisfied. In the previous chapter, we studied the spectrum sharing between a single PU link and a large scale CRN by employing a spatial guard-zone at a primary receiver. In this chapter, our analysis is mainly motivated by the fact that for a large scale primary network, implementing the guard-zone based interference protection (as introduced in chapter 2) may not be a viable solution. This is mainly because for a large scale CRNs, CRs need to localize multiple PU and estimate their relative position from them. Such a localization has to be performed in real-time which renders it infeasible from implementation perspective. Consequently, an alternative degree of freedom (such as transmit power or medium access probability) must be adapted to ensure peaceful co-existence with the primary network.

Why MIMO Underlay CRNs? Additional degree of freedom due to diversity gain.

In order to further optimize the performance of wireless networks, the multiple antenna enabled communication paradigm has become an integral part of next generation wireless standards (LTE and WiMAX [74]). This can be credited to the enormous potential which MIMO systems have demonstrated on three important fronts, i.e., (i) improving transmission reliability by harnessing diversity and coding gains [75, 76]; (ii) enhancing the throughput without bandwidth expansion using the spatial multiplexing [77] and (iii) interference mitigation by sophisticated signal processing techniques such as interference cancellation and alignment [78]. These promising performance enhancements of MIMO and the architectural simplicity of the underlay CRs, have complemented each other well [57, 79–82].

Network Uncertainities: node location,channel propagation, medium access.

Despite the growing popularity, ad-hoc underlay MIMO CRNs with multi-hop relaying have not been explored so far. The design-space and the throughput potential of such networks have not been investigated under the dynamics of geometric, channel and medium access uncertainties. The development of an appropriate metric to characterize the end-to-end performance also remains an open issue. In this chapter, we launch a preliminary investigation of these important and interesting, yet un-explored, design issues.

3.2 CONTRIBUTIONS & CHAPTER ORGANIZATION

In this chapter, we consider a primary/legacy network collocated with a CRN. The spatial properties of both networks are analyzed by borrowing well established tools from stochastic geometry [60]. The key contributions of this chapter can be summarized as follow:

1. We quantify the maximum permissible density (3.7) of the CR transmitters that can share the frequency band with the PUs under the PUs' desired QoS requirement (see 3.5). Considering that CRs schedule their transmission by employing the Slotted-ALOHA medium access control (MAC), we then characterize the maximum permissible medium access probability (MAP) for the CRN when the average number of the CR transmitters per unit area is fixed. The maximum permissible MAP for the CRN is strongly coupled with the link success probability of the PU and its desired QoS constraint. Considering a large scale legacy

network, where PUs employ maximum ratio transmission (MRT) at the transmitter and maximum ratio combining (MRC) at the receiver (combinely known as MIMO MRC [83, 84]), we quantify the link success probability of the primary in the presence of inter-network (co-channel PU) and intra-network (co-channel CR) interference. To the best of our knowledge, none of the studies in past have characterized the exact link success probability of the MIMO MRC enabled primary system in the presence of both inter-network and intra-network interference in closed form, considering both spatial and channel uncertainty. To this end, we first establish a closed form expression for the success probability of an arbitrary PU, which is then used to quantify the maximum permissible density of SUs.

2. Considering the maximum permissible density of the CR transmitters, we introduce a QoS aware multi-hop relaying strategy for a MIMO underlay ad-hoc CRN (see 3.8). The relaying model explicitly accommodates the geometry of the forwarding region and the inherent spatial and channel randomness. Unlike traditional relay selection which is solely based on the geometry of the forwarding area, we investigate an SIR based connectivity model for multi-hop secondary networks. Notice that even for traditional wireless ad-hoc networks where users are equipped with a single transmit and a single receive antenna, none of the previous studies have investigated or proposed QoS aware relaying with co-channel interference. The state of the art results in literature have considered channel-aware forwarding [85], where neither the desired QoS is taken into account nor the co-channel interference is considered.

QoS aware relaying employs only those relays which can satisfy the desired QoS (characterized by the SIR and reliabilitiy thresholds).

3. Performance analysis of the QoS aware relaying for ad-hoc MIMO CRN is performed by employing the average single hop forward progress as a key metric.. Assuming that the SUs employ MIMO MRC, we investigate the impact of the number of antennas (at both the CR transmitter and the relays) on average spatial progress. Moreover, the probability that a CR transmitter is isolated, i.e., it cannot connect to any of the relays in the desired forwarding area, is also quantified. Notice that the existing literature for traditional SISO/MIMO ad-hoc networks only considers geographical isolation [71, 86], caused by the lack of relays in the forwarding region. However, our definition of isolation also accommodates the QoS triggered isolation.

The average single hop forward progress of an arbitrary CR transmitter measures the average spatial progress of the packet from CR transmitter towards its intended destination.

4. Lastly, combining the maximum permissible MAP and the average single hop forward progress of secondary transmission under the SUs desired link SIR, we quantify the spatial throughput[1] of the underlay MIMO ad-hoc CRN under QoS aware multi-hop relaying. We then

1 The definition of spatial throughput is deferred for subsequent discussion.

demonstrate that there exists an optimal MAP probability for the CRN which maximizes its achievable spatial throughput. The existence of such an optimal MAP leads us to study some important design questions, i.e.,

a) Does the optimal MAP of the SUs depend on the density of the CRs and the number of antennas employed by the SUs?
b) Is it possible to maximize the spatial throughput of a CRN by selecting the optimal MAP under the maximum MAP constraint enforced due to PUs' desired link success probability?
c) How does the number of antennas, modulation and density of the PU effect the achievable spatial throughput of the SUs?
d) Can SUs always increase their spatial throughput by increasing the number of antennas at the CR terminal?
e) Considering the spatial throughput as a performance metric, does the choice of modulation scheme for the secondary transmitter depend upon the number of antennas at the CR user?

There exists an optimal MAP which maximizes the spatial throughput of the MIMO underlay CRN.

To the best of authors' knowledge, none of the studies in the past have addressed the above mentioned issues for multi-hop MIMO ad-hoc CRN. Hence, the available degrees of freedom a CRN designer can exploit remains un-identified. Nevertheless, for interested readers a brief survey of some literary contributions in the domain of MIMO CRN is summarized in 3.3.

3.3 RELATED LITERATURE

In [79] Scutari *et al.* have investigated the design of MIMO CRNs, using a competitive optimality approach from game theory. Under a competitive optimality criterion, every CR aims for the transmission strategy that unilaterally maximizes its achievable utility. The authors in [79], only consider a peer-to-peer communication model without addressing the spatial configuration of primary and secondary networks. In [82], the problem of transmit adaptation is explored for a single MIMO/MISO CR link operating under the constraint of opportunistic spectrum sharing. The capacity of the MIMO/MISO CR link is studied under the competing objectives of throughput maximization and interference minimization. Convex optimization framework is employed to strike an appropriate balance between the spatial multiplexing for a CR link and interference avoidance for primary receivers, when multiple antennas are employed by the SUs. The authors in [57], extended the work of Zhang et al. [82] and investigated the joint transmit-receive antenna selection for a single MIMO CR link operating under interference constraint from either multiple PUs with a single antenna or a single PU with multiple antennas. A comprehensive survey of the work on MIMO

CRNs is beyond the scope of this work. Interested readers are directed to [57] and [82] for further references. None of the above mentioned studies have addressed the dynamics induced by random topology of the CRN and the primary network. These studies also focus on peer-to-peer communication paradigm, while our focus in this chapter is to investigate MIMO CRNs employing multi-hop relaying. We employ a communication theoretic approach to explore the fundamental design space for such MIMO CRNs. Notice that contrary to past studies, we adopted a cross-layer approach for performance analysis where the network level dynamics such as medium access and routing were also considered.

We considered multiple primary and multiple secondary users where secondary communication is empowered by the multi-hop routing.

In [55, 72, 87] the authors have explored the throughput scaling of the CRN employing a single antenna for peer-to-peer communication. The authors in [52, 55, 72, 87] have utilized tools from stochastic geometry and percolation theory to derive these scaling properties. Recently, Rahul extended these studies in [81], to study the transmission capacity of a spectrum sharing ad-hoc network with multiple antennas. He considers a scenario where sophisticated signal processing can be employed at both CR transmitters and receivers such that some of the spatial transmit degrees of freedom are utilized to null the interference to the PU, while some of the receive degrees of freedom are utilized to perform interference cancellation. Like previous studies [55, 72, 87], [81] he also considers a scenario where CRs want to communicate with their receivers which are at fixed distance. Although [81] considers the spatial dynamics of a CRN, it does not consider the additional degree of uncertainty which comes with multi-hop relaying. This degree of uncertainty arises from the relay selection in the desired forwarding area. We argue that the relay selection procedure for multi-hop MIMO CRNs should also accommodate the desired QoS for the SUs. Hence, with multi-hop relaying the analysis becomes more challenging; the location of potential relays suffers from both spatial and channel dynamics. In this chapter, our focus is to take the first step towards characterizing the network level throughput for a MIMO ad-hoc underlay CRN. Consequently, optimization of the physical layer for CRs by employing sophisticated signal processing schemes such as interference cancellation and alignment is deferred for subsequent investigation. In a recent paper [80], throughput of the multi-hop MIMO CRN is studied under joint optimization of spatial multiplexing and cognitive channel assignment. The authors, consider the CRN as a fixed graph and interference is modeled by a simplified disk-model. As suggested in [59], it is more appropriate to consider wireless networks as a set of points where the notion of links is relatively soft. Moreover, it is also well known that the disk-model for interference completely ignores the stochastic nature of the fading channel and the fact that SIR is a random variable. Like previously mentioned strategies, opportunistic relay selection is also not addressed in [80]. Also

Dynamic routing adds another degree of uncertainty.

The notion of a wireless link is dependent upon the desired QoS.

notice that we are interested in network wide performance, which is often different from the link-level performance.

It is beyond the scope of this chapter to survey the existing literature on MIMO MRC with and without co-channel interference (without considering the spatial distribution of the interferers). Interested readers are directed to [83, 84, 88–91] and references therein. We will also direct the interested readers, to [92] and references therein for the analysis of diversity enabled Poisson MIMO ad-hoc networks. In brief [92] studies the success probability of an arbitrary link in the presence of a Poisson field of interferers when open loop spatial multiplexing and diversity communication is employed. Readers interested in exploring the application of stochastic geometry to wireless networks are directed to a tutorial paper [63] and references therein.

3.4 CHOICE OF PERFORMANCE METRIC

Spatial throughput unifies the well known metrics, i.e., density of forward progress, transport capacity and multi-hop information efficiency.

We have selected the spatial throughput as the performance metric for multi-hop CRNs. This metric unifies three well known metrics, namely, density of forward progress [44], transport capacity [93] and multi-hop information efficiency [94]. It can be regarded as the transport throughput per unit area. Note that contrary to the traditional definition of transport throughput, where the link distance between the transmitter and the receiver is fixed, in case of a multi-hop network we define the transport throughput as the product of the average forward progress under the relaying scheme and attainable rate at the desired SIR threshold. The transport throughput for an arbitrary CR measures the progress of each bit which is transported from a CR transmitter towards its destination each second by employing one Hertz of bandwidth. The network level spatial throughput is defined as the product of the average number of CR transmitters per unit area and their attainable transport throughput. The units of spatial throughput for CRN is bits-m/s/Hz/m^2. Like multi-hop information efficiency, the spatial throughput is also independent of the distance between source and destination. This independence assures that the design space can easily be explored without any potential bias from the source-destination distance separation. A more formal definition of the spatial throughput is presented in 3.8.

3.5 SYSTEM MODEL

3.5.1 *Network Geometry*

Notice, that a point process Π_i can also be considered as a counting measure.

We consider a primary/legacy network operating in the presence of a collocated ad-hoc CRN. The spatial distribution of both PUs and SUs is captured by two independent *homogeneous Poisson point processes* (HPPPs)-Π_p with intensity λ_p and Π_s with intensity λ_s respectively. More specifically, at any arbitrary time instant the probability of finding $n \in \mathbb{N}$ PUs/CRs inside a region $\mathcal{A} \subseteq \mathbb{R}^2$ follows the Poisson law with the mean measure $\Lambda_i(\mathcal{A}) = \lambda_i v_2(\mathcal{A}),\ \ i \in \{s, p\}$. Here $v_2(\mathcal{A}) = \int_{\mathcal{A}} \boldsymbol{dx}$ is the Lebesgue measure [60] on $\mathbb{R}^2$ and $\lambda_p(\lambda_s)$ is the average number of primary (secondary) users per unit area, where if $\mathcal{A}$ is a disc of radius r then $v_2(\mathcal{A}) = \pi r^2$.

3.5.2 *Transmission Model & Medium Access Control (MAC)*

We employ the well known *bipolar model* [44] to represent the primary's communication under a slotted medium access control (MAC). Specifically, at any arbitrary time slot the locations of the primary transmitters follow a HPPP $\Pi_{TX}^{\{p\}} \subseteq \Pi_p$ with density $\lambda_{TX}^{\{p\}} \leq \lambda_p$ and each primary transmitter communicates with its intended primary receiver located at a *fixed distance* r_p. The choice of a bipolar model facilitates abstraction in terms of the primary network architecture. In other words, it allows a unified treatment for both *ad hoc* and *infrastructure enabled* PUs. For infrastructure enabled primary such as cellular and TV-broadcasting networks, the assumption of HPPP is often made due to physical constraints and cost which prevent an optimal deployment of base stations. While for an ad hoc primary network, the inherent randomness due to unplanned deployment or mobility renders HPPP a suitable spatial model. The results obtained under the bipolar model can be easily extended to capture randomness in link distances by averaging over r_p.

Bipolar model/Dumbell model provides abstraction in terms of the primary network architecture.

CR transmitters employ the *slotted ALOHA* (S-ALOHA) MAC protocol to schedule their transmissions. In S-ALOHA, time is discretized into slots of length T_{slot}. At the beginning of a slot, a SU can independently decide either to *transmit* with a probability p_s or *defer* its transmission with a probability $1 - p_s$. It is assumed that all users always have one or more packets to transmit. This assumption is widely prevalent in the literature, mainly because it simplifies the analysis by abstracting queuing details. We also assume that both primary and secondary time-slots are identical and synchronized. The secondary nodes are assumed to be *half-duplex*, i.e., they may serve as *relays* if they defer their own transmission.

Notice that although, we focus on S-ALOHA MAC for the smiplicity of exposition, the analysis can be extended to more complicated CSMA/CA scheme by merely rescaling the MAP. As demonstrated in chapter 2, the Laplace transform of the aggregate interference for Rayleigh fading channel corresponds to the link success probability. To the best of our knowledge even for the wireless ad hoc networks, no closed form expressions are known for the Laplace transform of interference under CSMA/CA MAC. In [62] the authors demonstrated that such an ad hoc network forms Matern hardcore process of type II. In order to simplify analysis, most of the studies approximate dependent thinning of Matern's hardcore process by independent thining with retention probability $p = \frac{1-\exp(-\lambda\pi r^2)}{\lambda\pi r^2}$[61], where r is the inhibition radius between the points retained after thinning a stationary marked PPP. This implies that a rough estimate of performance for CSMA/CA can be obtained by simply adjusting the MAP to $p = \frac{1-\exp(-\lambda\pi r_c^2)}{\lambda\pi r_c^2}$. In this case, r_c is the carrier sensing range of the CSMA/CA protocol.

3.5.3 *Physical Layer Model*

Primary user employs $N_p \times N_p$ MIMO MRC.

Secondary user employs $N_s \times N_s$ MIMO MRC.

Channel Model: Rayleigh with power-law large scale path-loss function.

We consider a primary network where each user is equipped with N_p antennas. Similarly, each CR is furnished with N_s antennas. Notice that, under S-ALOHA MAC, a CR transmitter in a particular time slot, may become a receiver in another slot. Hence, it is natural to consider a symmetric MIMO MRC communication with N_s antennas for both transmission and reception. Although by virtue of the bipolar model primary transmitters and receivers can differ in terms of the number of antennas. Without loss of any generality, we consider a scenario where both possess N_p antennas. All primary transmitters use the same transmit power P_p, while all CRs transmit with the same transmit power P_s. Large scale path-loss is modeled by considering the *power law function*, i.e., $l(R) = CR^{-\alpha}$, where C is a frequency dependent constant, R is the distance between the transmitter and the receiver and $\alpha \geq 2$ is the terrain or environment dependent path-loss exponent. Although this type of path-loss model suffers from a singularity near zero, it is quite accurate in the far-field region. Both primary and secondary transmissions are subjected to Rayleigh flat-fading that is un-correlated across different antennas. An ultimate limitation on transmission in both networks is posed by co-channel interference. Without loss of any generality, we consider $C = 1$ for the rest of this chapter.

3.5.4 *Dynamic Spectrum Sharing Architecture*

Past studies have explored several potential mechanisms for dynamic spectrum sharing between the primary and the SUs. Essentially, all of these approaches can be classified into three broad classes, namely; *spectrum underlay*, *spectrum overlay* and *spectrum interweave*. In this chapter we restrict our discussion to the spectrum underlay mechanism. [3] and the references therein provide a detailed discussion on all the spectrum access mechanisms.

In the spectrum underlay mechanism, both PUs and SUs utilize the same frequency band. The achievable performance of the secondary system is dictated by the primary's desired QoS. The PU's QoS requirement can be characterized by a desired SIR threshold γ_p and a success probability threshold $s_{th}^{\{p\}}$ where

$$\mathbb{P}_{suc}^{\{p\}}\left(\lambda_s, \lambda_{TX}^{\{p\}}, \gamma_p, r_p\right) = \Pr\left\{\text{SIR} > \gamma_p\right\} \geq s_{th}^{\{p\}}. \tag{3.1}$$

SUs must adapt their transmission parameters such that (3.1) is always satisfied. This can be achieved either by a well known power adaptation technique or by more intelligent methods such as tuning the MAP, admission and topology control. In this chapter, we consider that the QoS constraint at the primary can be translated to a medium access constraint on the secondary network in terms of the MAP.

3.5.5 *Notation and Symbols*

Throughout this chapter, we use $\mathbb{E}(.)$ to denote expectation, $f_X(x)$ to denote the probability density function (PDF) and $\mathcal{F}_X(x)$ to denote the cumulative distribution function (CDF) of a random variable X. Random variables are represented by upper-case symbols, boldface symbols with lower-case (e.g. $\boldsymbol{a}$) are used to represent a vector and boldface symbols with upper-case (e.g. $\boldsymbol{H}$) are used for matrices. A circularly symmetric complex Gaussian random variable X with mean μ and variance σ^2 is denoted as $X \sim \mathcal{CN}(\mu, \sigma^2)$. Similarly, $\mathcal{E}(\mu)$ is used to represent the exponential distribution with mean μ. The symbol $\{\boldsymbol{H}\}_{i,j}$ is used to denote the $(i,j)^{th}$ entry, $\det(\boldsymbol{H})$ is the determinant and $\boldsymbol{H}^{\dagger}$ is the conjugate transpose of matrix $\boldsymbol{H}$. Finally, $\|\boldsymbol{x}\|$ is used to denote the Euclidean norm of a vector $\boldsymbol{x}$.

3.6 MACROSCOPIC PICTURE OF THE NETWORK

Consider a snapshot of the network at the beginning of an arbitrary S-ALOHA time slot. This snapshot consists of three distinct types of nodes, i.e., primary transmitters (with their associated receivers), CR transmitters and CR receivers. The HPPP of the CR nodes Π_s (Section II), can be decomposed into two distinct subsets, i.e., CR transmitters and CR receivers by employing p_s-thinning [60]. Let $\mathbb{1}(x)$ denote a Bernoulli indicator random variable with parameter p_s, and so

$$\begin{aligned} \Pi_{TX}^{\{s\}} &= \{\boldsymbol{x} \in \Pi_s : \mathbb{1}(\boldsymbol{x}=1)\} \text{ with } \lambda_{TX}^{\{s\}} = \lambda_s p_s, \\ \Pi_{RX}^{\{s\}} &= \{\boldsymbol{x} \in \Pi_s : \mathbb{1}(\boldsymbol{x}=0)\} \text{ with } \lambda_{RX}^{\{s\}} = \lambda_s (1-p_s), \end{aligned} \tag{3.2}$$

where p_s is the MAP for the secondary user.

In this chapter, we study a scenario where each transmitter $\boldsymbol{x} \in \Pi_{TX}^{\{s\}}$ wants to communicate with its desired infinitely distant destination in a

Note, that the assumption of an infinitely distant destination does not effect the generality of the analysis.

multi-hop manner. Receivers from $\Pi_{RX}^{\{s\}}$ serve as intermediate relays between transmitters and their destinations under geometric and QoS constraints. Destinations are not assumed to be a part of the point process Π_s. It is assumed that each node has a large buffer to store packets and forward them on the basis of a best-effort service.

3.7 MAXIMUM PERMISSIBLE MAP FOR CRS

Section 3.5 and 3.6, depicted a detailed sketch of the cognitive network and user level parameters critical in characterizing the permissible MAP. Based on our prior discussion, our focus in this section is:

1. To quantify the success probability (defined in (3.1)) for the PU in the presence of a collocated CRN with MIMO communication.
2. To employ the developed statistical machinery for investigating the maximum permissible MAP (p_s) for SUs under the PUs' QoS constraint.

The maximum permissible MAP for a CRN shapes the secondary network's connectivity at a certain desired QoS. Consequently, the spatial throughput of the secondary network is strongly coupled with the CR's MAP.

3.7.1 *Success Probability of the Primary User with MIMO MRC*

3.7.1.1 *Received Signal Model*

In a MIMO MRC system, each PU transmits a single data stream using N_p transmit antennas. The received signal at the corresponding primary receiver is given by

$$\begin{aligned} \boldsymbol{s}_{p,i} = & \sqrt{P_p l(r_p)}\boldsymbol{H}_i \boldsymbol{w}_{TX,i} y_i, \\ & + \sum_{\boldsymbol{x}_j \in \Pi_{TX}^{\{p\}}, i \neq j} \sqrt{P_p l(d(\boldsymbol{x}_i, \boldsymbol{x}_j))}\boldsymbol{H}_j \boldsymbol{w}_{TX,j} y_j, \\ & + \sum_{\boldsymbol{x}_k \in \Pi_{TX}^{\{s\}}} \sqrt{P_s l(d(\boldsymbol{x}_i, \boldsymbol{x}_k))}\boldsymbol{H}_k \boldsymbol{w}_{TX,k} y_k, \end{aligned} \tag{3.3}$$

Both the primary and the secondary links are assumed to operate in interference-limited regime.

where $\boldsymbol{s}_{p,i}$: $N_p \times 1$ received signal vector at the receiver associated with an arbitrary transmitter $\boldsymbol{x}_i \in \Pi_{TX}^{\{p\}}$; $\boldsymbol{H}_i$: $N_p \times N_p$ channel matrix between $\boldsymbol{x}_i$ and its intended receiver; $d(\boldsymbol{x}_i, \boldsymbol{x}_j)$ denotes the distance between the receiver of the $\boldsymbol{x}_i$ and the interfering transmitter $\boldsymbol{x}_j$; $\boldsymbol{H}_j$: $N_p \times N_p$ channel matrix between $\boldsymbol{x}_j$ and receiver of $\boldsymbol{x}_i$; $\boldsymbol{w}_{TX,i}$: $N_p \times 1$ transmission weight vector associated with the array; $\boldsymbol{w}_{TX,j}$ is the N_p dimensional transmission weight vector of inter-network interferer; $\boldsymbol{w}_{TX,k} : N_s \times 1$ is the transmission weight vector of k^{th} secondary interferer at a distance $d(\boldsymbol{x}_i, \boldsymbol{x}_k)$ from the intended receiver; $\boldsymbol{H}_k : N_p \times N_s$ channel matrix and y_i, y_j and y_k represent intended, interfering primary and interfering secondary transmitted signals respectively. In this chapter, we consider the interference limited scenario for both the primary and secondary networks. However, thermal noise can also be easily accommodated. All channel coefficients are assumed to be mutually un-correlated and $\mathcal{CN}(0,1)$.

3.7.1.2 *Probe Receiver*

In order to characterize the success probability of an arbitrary primary receiver, it is sufficient to focus on a typical transmitter-receiver pair. By employing the Silvnyak's theorem [60], we add a probe receiver at the origin with its corresponding transmitter at a distance r_p. The probe transmitter-receiver pair is not considered as a part of the HPPP $\Pi_p^{\{TX\}}$. The received signal in (3.3) can be written as $s_{p,o}$ $(i = o)$ with $d(\boldsymbol{x}_i, \boldsymbol{x}_k)$ and $d(\boldsymbol{x}_i, \boldsymbol{x}_j)$ replaced by $\|\boldsymbol{x}_k\|$ and $\|\boldsymbol{x}_j\|$ respectively. For ease of notation, we will drop the subscript o for rest of this chapter..

Quick Reference≫ Silvnyak's Theorem: The law of the stationary Poisson point process does not change by addition of an arbitrary point.

3.7.1.3 *MRC and SIR at a typical Primary*

In MIMO MRC systems the SIR of the received signal is maximized by weighing the signal both at transmitter and receiver. The optimal transmitter and receiver weights are derived in [83, 89, 90] as $\boldsymbol{w}_{TX} = \boldsymbol{u}$ and $\boldsymbol{w}_{RX} = \zeta \boldsymbol{H}\boldsymbol{u}$, where ζ is arbitrary constant; $\boldsymbol{u}$ is the unit norm (i.e., $\|\boldsymbol{u}\| = 1$) eigenvector (principal eigenvector) corresponding to the largest eigenvalue Λ_{max} of the complex Wishart matrix $\boldsymbol{R} = \boldsymbol{H}^{\dagger}\boldsymbol{H}$. Applying the receiver weights, the received signal at the probe receiver is given as

$$\hat{y} = \boldsymbol{w}_{RX}^{\dagger}\boldsymbol{s}. \tag{3.4}$$

The received SIR can be easily computed from (3.4) using the fact that $\boldsymbol{u}$ is a unit norm vector, sum of complex normal random variables is also a complex normal random variable and the maximum transmit power constraint on primary (secondary) transmitter is $P_p(P_s)$:

$$\text{SIR} = \Gamma_p = \frac{l(r_p)\Lambda_{max}}{\sum_{x_i \in \Pi_{TX}^{\{p\}}} g_i l\left(\|\boldsymbol{x}_i\|\right) + \eta \sum_{x_j \in \Pi_{TX}^{\{s\}}} g_j l\left(\|\boldsymbol{x}_j\|\right)}, \tag{3.5}$$

where $g_i \sim \mathcal{E}(1)$ and $g_j \sim \mathcal{E}(1)$ and $\eta = \frac{P_s}{P_p}$ is the ratio of transmit powers of the secondary and primary transmitters.

Distribution of maximum eigenvalue.

Lemma 3.1 *The CDF of the maximum eigenvalue (Λ_{max}) of the $N_p \times N_p$ complex central Wishart matrix is given by*

$$\mathcal{F}_{\Lambda_{max}}(z) = \Pr\{\Lambda_{max} \leq z\} = \frac{\det(\Psi_c(z))}{\left[\prod_{k=1}^{N_p}(N_p - k)!\right]^2}, \tag{3.6}$$

where $\Psi_c(z) : N_p \times N_p$ is a Hankel matrix whose elements are

$$\{\Psi_c(z)\}_{i,j} \quad = \quad \gamma(i+j-1, z), \quad i,j = 1,2,..,N_p \tag{3.7}$$

with $\gamma(a,b) = \int_0^b t^{a-1}\exp(-t)dt$ *is the lower incomplete Gamma function.*

PROOF: The proof follows from the fact that (3.6) is the special case of a well-known CDF first derived in [89] and by Kang and Alouini in [83]. □

The mathematical form of (3.6) does not permit further analysis. Motivated by [84] and [90], we derive the CDF of the maximum eigenvalue of a complex Wishart matrix as a finite linear combination of Gamma PDFs.

Alternativedistribution for maximum eigenvalue

Corollary 3.1 *The CDF of the maximum eigenvalue (Λ_{max}) can be expressed as a finite linear combination of Gamma PDFs as*

$$\mathcal{F}_{\Lambda_{max}}(z) = 1 - \sum_{i=1}^{N_p}\sum_{m=0}^{2N_p i - 2i^2}\sum_{k=0}^{m} d_{i,m}\frac{(iz)^k\exp(-iz)}{k!}, \tag{3.8}$$

where $d_{i,m}$ can be obtained from Eqs. (3.7),(3.6) and the series expansion of the lower incomplete Gamma function,

$$\gamma(a+1,b) = a!\left(1 - \sum_{k=0}^{a}\frac{\exp(-b)\,b^k}{k!}\right) \quad a \in \mathbb{Z}^+. \tag{3.9}$$

PROOF: see Appendix B . □

A simple and efficient numerical algorithm to compute the coefficients $d_{i,m}$ is proposed in [88].

Let $\mathcal{L}_I(s)$ denote the Laplace transform of the aggregate interference ($I = \sum_{\mathbf{x}_i \in \Pi_{TX}} g_i l(\|\mathbf{x}_i\|)$) experienced by a probe receiver from interfering transmitters whose locations form a HPPP Π_{TX} with intensity λ_{TX}, then the Laplace transform of the aggregate interference $\left(I_{sp} = \sum_{x_i \in \Pi_{TX}^{\{p\}}} g_i l\left(\|\boldsymbol{x}_i\|\right) + \eta \sum_{x_j \in \Pi_{TX}^{\{s\}}} g_j l\left(\|\boldsymbol{x}_j\|\right)\right)$ generated by co-channel primary and secondary interferers at the probe receiver is given by

$$\mathcal{L}_{I_{sp}}(s) = \mathcal{L}_I(s)|_{\lambda_{TX}=\lambda_{TX}^{\{p\}}+\eta^\delta \lambda_{TX}^{\{s\}}}, \tag{3.10}$$

where $\delta = \frac{2}{\alpha}$ is constant and $\mathcal{L}_I(s)$ can be obtained from [44] as

$$\mathcal{L}_I(s) = \exp\left(-\lambda_{TX}\, \underbrace{\pi \frac{\pi\delta}{\sin(\pi\delta)}}_{\kappa_1(\delta)} s^\delta\right). \tag{3.11}$$

3.7.1.4 ▶ *Success probability for the primary with $N_p = 1$*

Success probability for the SISO primary user.

The success probability for the primary link when a single antenna is employed by all primary transmitter-receiver pairs is given by

$$\begin{aligned}
\mathbb{P}_{suc}^{\{p\}}\left(\lambda_{TX}^{\{s\}}, \lambda_{TX}^{\{p\}}, \gamma_p, r_p\right) &= \Pr\left\{\mathrm{SIR} > \gamma_p\right\}, \qquad (3.12)\\
&= \mathbb{E}_{I_{sp}}\left(\Pr\left\{g > \gamma_p r_p^\alpha I_{sp}\right\}\right),\\
&= \mathcal{L}_{I_{sp}}(s)|_{s=\gamma_p r_p^\alpha},\\
&\overset{(a)}{=} \exp\left(-\left[\lambda_{TX}^{\{p\}}+\eta^\delta\lambda_{TX}^{\{s\}}\right]\kappa_1(\delta)\gamma_p^\delta r^2\right).
\end{aligned}$$

where $\kappa_1(\delta) = \frac{\pi^2\delta}{\sin(\pi\delta)}$, $\delta = \frac{2}{\alpha}$ and (a) follows from (3.10) and (3.11).

3.7.1.5 ▶ *Success probability for the primary with $N_p > 1$*

Success probability of PU employing MIMO MRC.

Theorem 3.1 *The link success probability for the primary transmitter-receiver pair equipped with N_p antennas, employing MIMO MRC communication in the presence of interference from simultaneously communicating primary and secondary users is given in*

$$\begin{aligned}
\mathbb{P}_{suc}^{\{p\}}\left(\lambda_{TX}^{\{s\}}, \lambda_{TX}^{\{p\}}, \gamma_p, r_p\right) = &\sum_{i=1}^{N_p} \sum_{m=0}^{2N_p i-2i^2} \sum_{k=0}^{m} d_{i,m} \frac{(-1)^k (i)^k}{k!} \qquad (3.13)\\
&\times \frac{\partial^k}{\partial i^k} \exp\left(-\left[\lambda_{TX}^{\{p\}} + \eta^\delta \lambda_{TX}^{\{s\}}\right] \kappa_1(\delta)\gamma_p^\delta r_p^2 i^\delta\right).
\end{aligned}$$

PROOF: The success probability of the PU employing MIMO MRC communication with N_p antennas is given by

$$\mathbb{P}_{suc}^{\{p\}}\left(\lambda_{TX}^{\{s\}},\lambda_{TX}^{\{p\}},\gamma_p,r_p\right) = \Pr\left\{\Gamma_p > \gamma_p\right\}, \quad (3.14)$$
$$= \Pr\left\{\frac{l(r_p)\Lambda_{max}}{I_{sp}} > \gamma_p\right\}.$$

Employing Corollary 1, we have

$$\mathbb{P}_{suc}^{\{p\}}\left(\lambda_{TX}^{\{s\}},\lambda_{TX}^{\{p\}},\gamma_p,r_p\right) = \mathbb{E}_{I_{sp}}\left(1-\mathcal{F}_{\Lambda_{max}}\left(\gamma_p r_p^{\alpha} I_{sp}\right)\right),$$

$$= \mathbb{E}_{I_{sp}}\left[\sum_{i=1}^{N_p}\sum_{m=0}^{2N_p i-2i^2}\sum_{k=0}^{m} d_{i,m}\frac{(i\gamma_p r_p^{\alpha} I_{sp})^k \exp\left(-i\gamma_p r_p^{\alpha} I_{sp}\right)}{k!}\right],$$

$$= \mathbb{E}_{I_{sp}}\left[\sum_{i=1}^{N_p}\sum_{m=0}^{2N_p i-2i^2}\sum_{k=0}^{m} d_{i,m}\frac{(-i)^k}{k!}\frac{\partial^k}{\partial i^k}\exp\left(-i\gamma_p r_p^{\alpha} I_{sp}\right)\right],$$

$$= \sum_{i=1}^{N_p}\sum_{m=0}^{2N_p i-2i^2}\sum_{k=0}^{m} d_{i,m}\frac{(i)^k(-1)^k}{k!}\frac{\partial^k}{\partial i^k}\mathcal{L}_{I_{sp}}(s)|_{s=i\gamma_p r_p^{\alpha}}. \quad (3.15)$$

Eq. (3.15) can be solved using (3.10). The k^{th} derivative can be easily computed using Fa'a di Bruno's formula [95]. □

Discussion:

Validation by Monte Carlo simulations

Fig. 3.1 depicts the success probability of the primary link with varying SIR threshold (γ_p). The analytical result derived in (3.13) is corroborated with the help of Monte Carlo simulations which were performed by generating 10^5 realizations of $\Pi_{TX}^{\{s\}}$, $\Pi_{TX}^{\{p\}}$ and the fading channel matrices for each SIR threshold (γ_p). As indicated by Fig. 3.1 the analytical result agrees perfectly with the Monte Carlo simulations.

PU's success probability is an increasing function of its array size N_p.

From (3.13) it is obvious that increasing the number of antennas (N_p) employed at the PU adds a positive term to the success probability of the primary. More specifically, the link success probability increases with increasing N_p. However, as depicted in Fig. 3.1 increasing N_p beyond a certain value may not bring the proportional increase in gains. From Fig. 3.1a the *'law of*

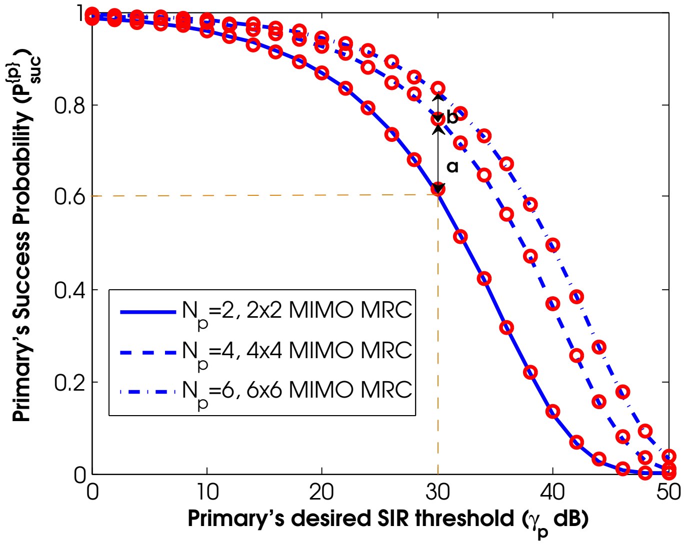

(a) PU's link success probability with the varying SIR threshold for $\eta = 1$.

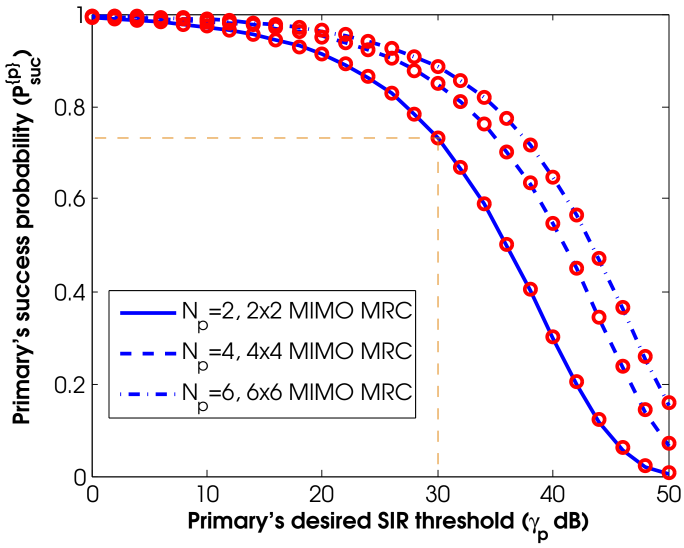

(b) PU's link success probability with varying SIR threshold for $\eta = 10^{-1}$.

Figure 3.1: Impact of desired SIR threshold (γ_p) and transmit power ratio (η) on the primary's success probability with $\lambda_{TX}^{\{s\}} = \lambda_{TX}^{\{p\}} = 10^{-3}$, $r_p = 2$, $\eta = \{10^{-1}, 1\}$, $N_p = \{2, 4, 6\}$ and $\alpha = 4$ (see (3.13)). Monte Carlo simulation results are indicated by red 'o' markers . Notice that γ_p is the primary's desired SIR threshold which is the function of its desired QoS, for instance for a certain fixed bit error probability it can be obtained by inverting the bit error rate expression of the employed modulation scheme. Alternatively for a fixed desired transmission rate it can be computed by inverting the Shannon capacity formula.

diminishing returns' comes into action as N_p is increased from 4 to 6. Both (3.13) and Fig. 3.1 indicate that the success probability is an exponentially decreasing function of γ_p, i.e., it decreases with an increase in the desired SIR threshold.

An important observation from Figs. 3.1a and 3.1b is that the success probability of the primary link is strongly coupled with the transmit power ratio (η) of the secondary and primary transmitters. Consequently, the success probability of the primary link increases when SUs employ a smaller transmit power compared to the PUs. When fixed QoS as defined in (3.1) is desired, the gain in the success probability can be harnessed by the SUs to increase their transmission opportunities either in the time domain (by using higher MAP with low transmit power) or in the power domain (by increasing the transmit power with low MAP).

3.7.2 *Maximum permissible MAP for the Secondary User*

The maximum permissible MAP for the SU is dictated by the primary's desired QoS constraint. Given the PUs' QoS constraint as in Eq. (3.1), the permissible density of the SUs can be expressed as

$$\lambda_s^{TX} = \sup \left\{ \lambda_{TX}^{\{s\}} : \mathbb{P}_{suc}^{\{p\}} \left(\lambda_{TX}^{\{s\}}, \lambda_{TX}^{\{p\}}, \gamma_p, r_p \right) \geq s_{th}^{\{p\}} \right\}. \tag{3.16}$$

The permissible MAP (p_s) for the SUs can be computed as

$$p_s = \min \left(\frac{\lambda_s^{TX}}{\lambda_s}, 1 \right). \tag{3.17}$$

Approximation for the maximum permissible MAP.

Lemma 3.2 *The permissible MAP (p_s) for the SUs such that the PU can still experience the acceptable QoS ($\gamma_p, r_p, s_{th}^{\{p\}}$) can be approximated as*

$$p_s \approx \min \left[\lambda_s^{-1} \eta^{-\delta} \left\{ s_{th}^{\{p\}} \left(\sum_{i=1}^{N_p} \sum_{m=0}^{2N_p i - 2i^2} \sum_{k=0}^{m} d_{i,m} \frac{(-1)^{k+1}}{k!} \right.\right.\right. \tag{3.18}$$
$$\left.\left.\left. \times \; \Delta(\delta, k) i^{\delta} \kappa_1(\delta) \gamma_p^{\delta} r_p^2 \right)^{-1} - \lambda_{TX}^{\{p\}} \right\}, 1 \right],$$

where

$$\Delta(\delta, k) = \delta \times (\delta - 1) \times ...(\delta - (k-1)). \tag{3.19}$$

PROOF: Using the Taylor series expansion of $\exp(-x)$ in (3.13) and evaluating the k^{th} derivative, we obtain λ_s^{TX}. The MAP p_s can be computed by employing (3.17). □

Besides approximation, precise estimates for the permissible MAP can be evaluated numerically.

3.7.2.1 *Discussion*

Relationship between the bit error probability and γ_p.

The primary's desired SIR threshold γ_p depends on the modulation and coding scheme employed by the transmitter. Considering a fixed threshold for the bit error probability (BEP) P_b^{th}, γ_p for $M-$PSK and $M-$QAM can be obtained by inverting the conditional BEP expressions presented in [96]. The PU's link success probability for $M-$ PSK ($M = \{2, 4, 8, 16, 32\}$) with increasing density of secondary transmitters ($\lambda_{TX}^{\{s\}}$) is depicted in Fig. 3.2.

As illustrated in Fig. 3.2 primary's success probability decreases with increasing density of the secondary transmitters ($\lambda_{TX}^{\{s\}}$). It can also be seen that the success probability for the fixed $\lambda_{TX}^{\{s\}}$ decreases with increasing constellation size M.

Exploiting the diversity gain for increasing transmission opportunites.

The PUs' success probability increases with increasing the number of antennas (N_p) (see Fig. 3.2). Also notice that the slope of the success probability curve changes with increasing N_p, indicating the increase in the diversity order. Figs. 3.2a, 3.2b, 3.2c, 3.2d and 3.2e can also be employed to compute the maximum permissible density of secondary transmitters (λ_s^{TX}) for some fixed success probability threshold ($s_{th}^{\{p\}}$). Employing multiple antennas at the PUs not only provides positive gains to the PUs but also increases the transmission opportunities for the SUs. Consequently, MIMO truly enables the efficient exploitation of '*white-spaces*' present in space, time and power domains for a particular frequency band. This can be better understood with the help of the following numerical example.

Example 3.1 *Consider a scenario where the primary transmitter-receiver pair has the following QoS constraint*

$$\mathbb{P}_{suc}^{\{p\}}\left(\lambda_{TX}^{\{s\}}, \lambda_{TX}^{\{p\}}, \gamma_p, r_p\right) = \Pr\left\{SIR > \gamma_p\right\} \geq 0.8. \tag{3.20}$$

From Fig.3.2a, it is obvious that PUs employing a single antenna ($N_p = 1$) cannot fulfill this constraint even in the absence of the SUs even for a BPSK modulation scheme. In this scenario, the ultimate limitation for the PUs is the inter-channel interference generated by simultaneous transmission from other PUs ($\lambda_{TX}^{\{p\}} = 10^{-3}$). However, as the number of antennas is increased from $N_p = 1$ to $N_p = 2$, the PU can satisfy this QoS constraint at least for BPSK (see Fig. 3.2b). As N_p is further increased not only the primary can satisfy the QoS constraint in (3.20) with higher modulation schemes (i.e., increase throughput) but also the number of secondary transmitters which

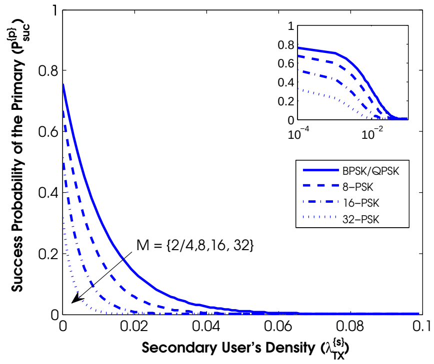

(a) Primary's success probability with varying SU density ($\lambda^{\{s\}}_{TX}$) for $N_p = 1$.

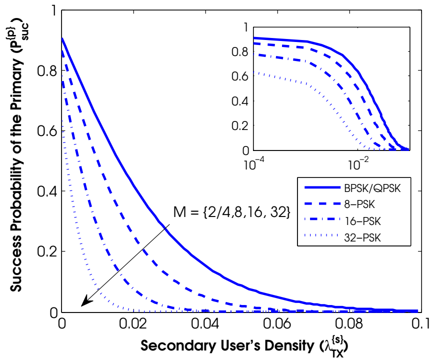

(b) Primary's success probability with varying SU density ($\lambda^{\{s\}}_{TX}$) for $N_p = 2$.

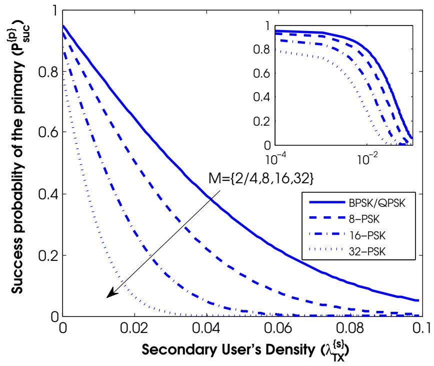

(c) Primary's success probability with varying SU density ($\lambda^{\{s\}}_{TX}$) for $N_p = 4$.

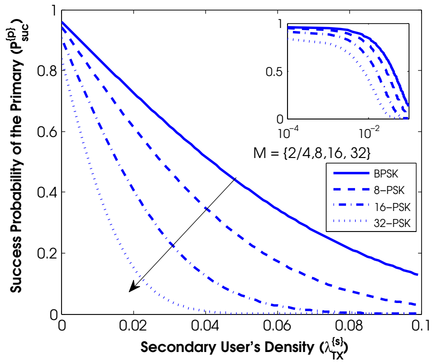

(d) Primary's success probability with varying SU density ($\lambda^{\{s\}}_{TX}$) for $N_p = 6$.

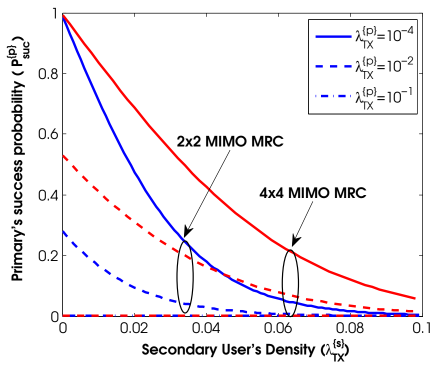

(e) Primary's success probability with varying secondary ($\lambda^{\{s\}}_{TX}$) and PU density ($\lambda^{\{p\}}_{TX}$) for BPSK/QPSK modulation.

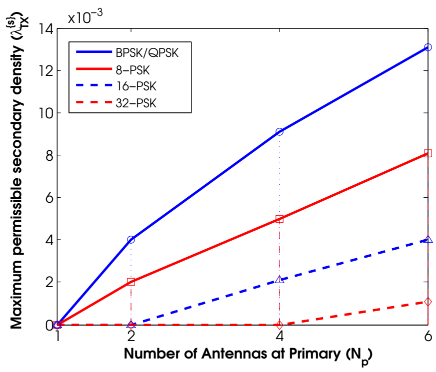

(f) Maximum permissible density for SUs (λ_s^{TX}) with varying number of antennas (N_p) at primary for BPSK/QPSK modulation.

Figure 3.2: Impact of SU density ($\lambda^{\{s\}}_{TX}$) and number of antenna at primary (N_p) on the link success probability of the primary for $\lambda^{\{p\}}_{TX} = 10^{-3}$, $\eta = 10^{-1}$, $r_p = 5$, $\alpha = 4$ and $P_b^{th} = 10^{-3}$.

λ_s	M \ N_p	2	4	6
10^{-3}	2/4	1	1	1
	8	1	1	1
	16	0	1	1
	32	0	0	1
10^{-2}	2/4	0.4	0.9	1
	8	0.2	0.5	0.8
	16	0	0.21	0.4
	32	0	0	0.1
10^{-1}	2/4	0.04	0.09	0.1
	8	0.02	0.05	0.08
	16	0	0.02	0.04
	32	0	0	0.01

Table 3.1: Maximum permissible MAP (p_s) for secondary with $s_{th}^{\{p\}} = 0.8$, $\lambda_{TX}^{\{p\}} = 10^{-3}$, $\eta = 0.1$, $r_p = 5$ and $\alpha = 4$.

can be accommodated in the network is increased (see Figs. 3.2b, 3.2c, 3.2d, 3.2e and 3.2f). Fig. 3.2f explicitly highlights the increase in the number of permissible SUs as the function of N_p for BPSK modulation scheme. Fig. 3.2e shows that increasing the number of primary transmitters can completely render the primary link useless even when multiple antennas are employed. Table 3.1 summarizes a few numerical values of p_s with different parametric configurations for $s_{th}^{\{p\}} = 0.8$.

It is worth highlighting that in the context of overlaid networks [55, 72, 81, 87], it is considered that PUs can tolerate an additional degradation of Δ_s in terms of the success probability in the presence of SUs. However, in this chapter, we do not allow such a degradation to the primary's performance. Rather, by employing MIMO, as illustrated by the previous example, positive gains are exercised in the primary's success probability and the number of SUs that can be accommodated in the network.

3.8 SPATIAL THROUGHPUT OF THE SECONDARY WITH MULTI-HOP RELAYING

In the previous section, we quantified the maximum permissible MAP (p_s) for the SU while guaranteeing the primary users QoS constraint $(\gamma_p, r_p, s_{th}^{\{p\}})$ when MIMO MRC communication with N_p antennas is employed by the PU.

In this section, we characterize the achievable spatial throughput for the SU with QoS aware multi-hop relaying and N_s antennas operating under the maximum transmission probability constraint (MTPC) p_s. To this end :

1. Firstly, we propose the QoS aware relaying employed by the CR transmitters.
2. We then define the geometry of the forwarding region in which secondary relays are selected to forward the CR transmitters' data.
3. Lastly, a statistical framework is developed to study both spatial throughput and connectivity parameters of the SUs employing MIMO MRC. Simulation results are discussed to gain further design insights for MIMO multi-hop CR underlay networks.

3.8.1 *QoS Aware Relaying*

Given a realization of a HPPP of the secondary transmitters $\Pi_{TX}^{\{s\}}$ and the receivers $\Pi_{RX}^{\{s\}}$ which serve as relays for infinitely distant destinations associated with each transmitter, SU's QoS aware relaying operates as follows:

QoS criteria for potential relays.

Condition 1: *Any receiver $\boldsymbol{x} \in \Pi_{RX}^{\{s\}}$ is considered as a potential relay for a transmitter $\boldsymbol{y} \in \Pi_{TX}^{\{s\}}$ in a particular S-ALOHA time slot, iff the SIR of the packet received from $\boldsymbol{y}$ at $\boldsymbol{x}$ is above a certain threshold γ_s.*

The threshold γ_s reflects users' desired QoS requirements. Additionally, it also dictates the number of transmitters associated with each relay. For $\gamma_s \geq 1$ at most there is *one and only one* transmitter associated with each receiver. This is intuitive since for $\gamma_s \geq 1$, the SIR constraint is only satisfied if the signal power from a certain transmitter individually exceeds the aggregate power contributed by all other transmitters. Employing the expressions of conditional BEP for M-PSK and M-QAM from [96], it is clear that γ_s is always greater than 1 for an un-coded modulation scheme and narrow-band transmissions for realistic P_b^{th}.

Progress criteria for potential relays.

Condition 2: *A receiver $\boldsymbol{x} \in \Pi_{RX}^{\{s\}}$ which fulfills the SIR requirements (Condition 1) can serve as a relay for a transmitter $\boldsymbol{y} \in \Pi_{TX}^{\{s\}}$, iff it provides maximum progress of the packet towards its desired destination. In other words if $\boldsymbol{R_y} \subseteq \Pi_{RX}^{\{s\}}$ is the random set of relays that satisfies SIR requirement for a particular transmitter $\boldsymbol{y}$ at a particular time slot, then node $\boldsymbol{x}$ is selected as a relay iff*

$$\boldsymbol{x} = \arg\max_{\boldsymbol{x}\in\boldsymbol{R_y}} \mathcal{R}\cos(\varphi), \tag{3.21}$$

where

$$\mathcal{R} = \|\boldsymbol{x} - \boldsymbol{y}\| \text{ and } \varphi = \angle\boldsymbol{x}. \tag{3.22}$$

The symbol $\angle\boldsymbol{x}$ denotes angle subtended by the vector $\mathbf{z} = \boldsymbol{x} - \boldsymbol{y}$ on the line connecting $\boldsymbol{y}$ to its infinitely far destination. It is important to highlight that the above formulation addresses both interference and QoS requirement by employing the SIR based connectivity and relaying model.

3.8.2 *Selection of Forwarding Area*

A closer look at Condition 2 reveals that even if there exists one or more relays satisfying the QoS constraint, they may not be useful unless they lie in a certain *specific region*. More specifically, only those relays which can guarantee a *positive forward progress* without sacrificing the *desired link quality* are critical in quantifying the secondary's spatial throughput. In the context of ad-hoc networks, the specific region in which existence of a relay guarantees a positive progress towards the destination is often referred to as the *forwarding area*. Different relaying protocols result in a different geometry for forwarding areas [71]. In essence, the shape of the forwarding area controls the overall directionality of the transmission. In turn, directionality of the relaying protocol quantifies the average number of hops traversed before reaching the destination. In this chapter, we consider a *decode-and-forward* type relaying strategy for SUs, where the next hop relay is selected in a radial sector with central angle ϕ around the line connecting the transmitter and its intended infinitely distant destination.

The geometry of the forwarding region characterizes the directionality of the end-to-end route.

We assume that each secondary transmitter $\boldsymbol{y} \in \Pi_{TX}^{\{s\}}$ transmits a training sequence at the beginning of each S-ALOHA time slot. This training sequence is employed by the relays to estimate the maximum eigenvalue of the channel matrix and hence the received SIR. Each relay which satisfies the SIR constraint (Condition 1) can either enter some contention based selection mechanism or alternatively, assuming that the relays are location-aware, can implement opportunistic relaying by initializing a timer according to the remaining distance from the destination. The relay whose timer expires first can transmit the principal eigenvector to the corresponding transmitter. This eigenvector is used at transmitter to perform MIMO MRT/MRC with the relay. We assume that channel state estimation and relay feed-back is error free.

3.8.3 *Forward Progress, Isolation & Spatial throughput*

The spatial throughput of the secondary network is strongly coupled with the forward progress of the transmission under QoS aware relaying. In turn, as discussed earlier, the forward progress depends on the geometry of the forwarding area and desired QoS. Effectively, the spatial throughput encapsulates the multi-hop nature of the transmission by its dependence on the forward progress. Formally, the achievable maximum forward progress is defined as follows:

Single hop forward progress.

Definition 3.1 *Consider an arbitrary CR transmitter $\boldsymbol{x} \in \Pi_{TX}^{\{s\}}$ and an associated relay $\boldsymbol{y} \in \Pi_{RX}^{\{s\}}$ such that it satisfies the QoS aware relaying conditions. Then the maximum single hop forward progress (ζ) which can be attained by transmission from $\boldsymbol{x}$ is given by*

$$\zeta = \mathcal{R}\cos(\varphi), \tag{3.23}$$

where $\mathcal{R}$ denote the distance between $\boldsymbol{x}$ and $\boldsymbol{y}$ and φ is the angle between the line connecting $\boldsymbol{x}$ to $\boldsymbol{y}$ and the line connecting $\boldsymbol{x}$ to its infinitely distant destination.

Average forward progress in an interference limited underlay MIMO CRN.

Theorem 3.2 *For an interference limited CRN which employs MIMO MRC with N_s antennas and QoS aware relaying strategy with desired SIR threshold γ_s at each CR, the average single hop forward progress attained is given by*

$$\bar{\zeta} = \Omega \int_0^\infty \left[1 - \prod_{i=1}^{N_s} \prod_{m=0}^{2N_s i - 2i^2} \prod_{k=0}^{m} \exp\left(- \frac{\lambda_s \phi (1-p_s) d_{i,m}{}^{(-i)^k / k!}}{2\kappa_2 \left(\delta, \eta, \gamma_s, \lambda_s, p_s, \lambda_{TX}^{\{p\}}\right)} \right.\right.$$
$$\left.\left. \times \frac{\partial^k}{\partial i^k} \frac{\exp\left(-i^\delta \kappa_2 \left(\delta, \eta, \gamma_s, \lambda_s, p_s, \lambda_{TX}^{\{p\}}\right) r^2\right)}{i^\delta} \right) \right] dr, \quad (3.24)$$

where

$$\kappa_2\left(\delta, \eta, \gamma_s, \lambda_s, p_s, \lambda_{TX}^{\{p\}}\right) = \left[\eta^{-\delta} \lambda_{TX}^{\{p\}} + \lambda_s p_s\right] \kappa_1(\delta) \gamma_s^\delta,$$
$$\Omega = \frac{2\sin\left(\frac{\phi}{2}\right)}{\phi}. \quad (3.25)$$

PROOF: The average forward progress can be characterized from (3.23) as

$$\bar{\zeta} = \mathbb{E}\left(\mathcal{R}\cos\left(\varphi\right)\right). \quad (3.26)$$

The angle φ is uniformly distributed between $[-\phi/2, \phi/2]$ independent from $\mathcal{R}$, so

$$\bar{\zeta} = \frac{2}{\phi} \sin\left(\frac{\phi}{2}\right) \mathbb{E}\left(\mathcal{R}\right). \quad (3.27)$$

Using the integration by parts for expressing the $\mathbb{E}\left(\mathcal{R}\right)$, we have that,

$$\bar{\zeta} = \frac{2}{\phi} \sin\left(\frac{\phi}{2}\right) \int_0^\infty \left(1 - \mathcal{F}_{\mathcal{R}}(r)\right) dr, \quad (3.28)$$

Quick Reference≫ p-thinning of HPPP: p-thinning is an operation on a HPPP which results in another HPPP such that it retains each point of original process with probability p.

Notice, that for an arbitrary transmitter $\boldsymbol{x} \in \Pi_{TX}^{\{s\}}$, $\mathcal{R}$ is the distance to the relay node $\boldsymbol{y} \in \Pi_{RX}^{\{s\}}$ in sector ϕ which satisfies its desired SIR threshold γ_s. Consider a snapshot of the network at an arbitrary time slot. From (3.2), both $\Pi_{TX}^{\{s\}}$ and $\Pi_{RX}^{\{s\}}$ are stationary HPPPs constructed by the p_s- thinning of Π_s (see Section 3.6). Hence by employing Silvnyak's theorem [60], adding a probe transmitter at say point $\boldsymbol{z}$ does not change the distribution of the point process. Furthermore, by the stationarity of the point process, the point process Π_s can be re-centered at $\boldsymbol{z}$ (such that it becomes an origin o). The potential relays for the probe transmitter can be modeled by a non-homogeneous Poisson point process (NHPPP) $\Pi_{REL}^{\{s\}} \subseteq \Pi_{RX}^{\{s\}}$. $\Pi_{REL}^{\{s\}}$ can be constructed by assigning i.i.d. marks to each CR receiver for: (i) the maximum eigenvalue of the complex central Wishart matrix; (ii) the aggregate interference from primary to secondary and (iii) the aggregate interference from secondary to secondary. The interference is i.i.d. due to the stationarity of the point process:

$$\Pi_{REL}^{\{s\}} = \left\{ [x, i_p, i_s, \lambda_{max}] : x \in \Pi_{RX}^{\{s\}} \right\}. \tag{3.29}$$

In order to accommodate the CR transmitters' QoS constraint, an additional dependent SIR mark is assigned to each receiver in $\Pi_{REL}^{\{s\}}$ as

$$\mathbb{1}_{SIR}(\Gamma_s(r)) = \begin{cases} 1 & \Gamma_s(r) \geq \gamma_s \\ 0 & \Gamma_s(r) < \gamma_s \end{cases}, \tag{3.30}$$

where the SIR $(\Gamma_s(r))$[2] with respect to probe transmitter measured at the relay located at distance r is given by

$$\begin{aligned} \Gamma_s(r) &= \frac{\lambda_{max} l(r)}{\eta^{-1} \sum_{i \in \Pi_{TX}^{\{p\}}} g_i l(r_i) + \sum_{j \in \Pi_{TX}^{\{s\}}} g_j l(r_j)}, \\ &= \frac{\lambda_{max} l(r)}{\eta^{-1} i_p + i_s}. \end{aligned} \tag{3.31}$$

The mean measure $\Lambda_{REL}^{\{s\}}(\mathcal{A})$ of the $\Pi_{REL}^{\{s\}}$ is given by

$$\begin{aligned} \Lambda_{REL}^{\{s\}}(\mathcal{A}) &= \mathbb{E}_{I_p, I_s, \Lambda_{max}} \left[\int_{\mathcal{A}} \underbrace{\lambda_s \phi (1 - p_s)}_{\vartheta_s} r \mathbb{1}_{SIR}(\Gamma_s(r)) dr \right], \ \mathcal{A} \in \mathbb{R} \\ &= \mathbb{E}_{I_p, I_s, \Lambda_{max}} \left[\int_{\mathcal{A}} \vartheta_s r \mathbb{1}_{SIR} \left(\lambda_{max} \geq \underbrace{(\eta^{-1} i_p + i_s) \gamma_s r^{\alpha}}_{\omega} \right) dr \right], \\ &= \mathbb{E}_{I_p, I_s} \left[\int_{\mathcal{A}} \vartheta_s r \Pr \left\{ \lambda_{max} \geq \omega \right\} dr \right], \\ &= \mathbb{E}_{I_p, I_s} \left[\int_{\mathcal{A}} \vartheta_s r \left\{ 1 - \mathcal{F}_{\Lambda_{max}}(\omega) \right\} dr \right], \end{aligned}$$

2 Note that the received SIR at the relay at distance r depends on i_p, i_s and λ_{max}. We have used the symbol $\Gamma_s(r)$ instead of $\Gamma_s(i_p, i_s, \lambda_{max}, r)$ for brevity.

$$
\begin{aligned}
\Lambda_{REL}^{\{s\}}(\mathcal{A}) &= \mathbb{E}_{I_p, I_s, \Lambda_{max}}\left[\int_{\mathcal{A}} \underbrace{\lambda_s \phi(1-p_s)}_{\vartheta_s} r \mathbb{1}_{SIR}(\Gamma_s(r)) dr\right], \ \mathcal{A} \in \mathbb{R} \\
&= \mathbb{E}_{I_p, I_s, \Lambda_{max}}\left[\int_{\mathcal{A}} \vartheta_s r \mathbb{1}_{SIR}\left(\lambda_{max} \geq \underbrace{(\eta^{-1} i_p + i_s)\gamma_s r^{\alpha}}_{\omega}\right) dr\right], \\
&= \mathbb{E}_{I_p, I_s}\left[\int_{\mathcal{A}} \vartheta_s r \Pr\{\lambda_{max} \geq \omega\} dr\right], \\
&= \mathbb{E}_{I_p, I_s}\left[\int_{\mathcal{A}} \vartheta_s r \{1 - \mathcal{F}_{\Lambda_{max}}(\omega)\} dr\right], \\
&= \mathbb{E}_{I_p, I_s}\left[\int_{\mathcal{A}} \vartheta_s r \sum_{i=1}^{N_s} \sum_{m=0}^{2N_s i - 2i^2} \sum_{k=0}^{m} d_{i,m}\right. \\
&\times \left.\frac{(i\omega)^k \exp(-i\omega)}{k!} dr\right], \\
&= \int_{\mathcal{A}} \vartheta_s r \sum_{i=1}^{N_s} \sum_{m=0}^{2N_s i - 2i^2} \sum_{k=0}^{m} d_{i,m} \\
&\times \frac{(-i)^k}{k!} \frac{\partial^k}{\partial i^k}\left(\mathcal{L}_{I_p}(s)|_{s=i\eta^{-1}\gamma_s r^{\alpha}} \mathcal{L}_{I_s}(s)|_{s=i\gamma_s r^{\alpha}}\right) dr, \\
&= \int_{\mathcal{A}} \vartheta_s r \sum_{i=1}^{N_s} \sum_{m=0}^{2N_s i - 2i^2} \sum_{k=0}^{m} d_{i,m} \frac{(-i)^k}{k!} \\
&\times \frac{\partial^k}{\partial i^k} \exp\left(-\left[\eta^{-\delta}\lambda_{TX}^{\{p\}} + \lambda_s p_s\right] \kappa_1(\delta) i^{\delta} \gamma_s^{\delta} r^2\right) dr. \qquad (3.32)
\end{aligned}
$$

Note that $\Pi_{REL}^{\{s\}}$ is the NHPPP of candidate relays under Condition 1. Consequently, the CDF of $\mathcal{R}$ can be expressed in terms of the void probability of $\Pi_{REL}^{\{s\}}$ as

Quick Reference≫ void probability: The void probability of the point process over a certain area $\mathcal{A}$ is defined as the probability of having no-points in $\mathcal{A}$.

$$
\begin{aligned}
\mathcal{F}_{\mathcal{R}}(r) &= \lim_{z \to \infty} \Pr\left\{\Pi_{REL}^{\{s\}}(Sec(\phi, z) \backslash Sec(\phi, r)) = \emptyset\right\}, \\
&= \exp(-\Lambda_{REL}^{\{s\}}(\mathcal{A})), \quad \mathcal{A} = (r, \infty), \qquad (3.33)
\end{aligned}
$$

where $Sec(\theta, r)$ denotes the sector with central angle θ and radius r. Notice that (3.33) provides the distance distribution of the farthest relay in $\Pi_{REL}^{\{s\}}$ and hence incorporates the Condition 2 (see (3.21)). Substituting (3.33) in (3.27) we obtain (3.24). □

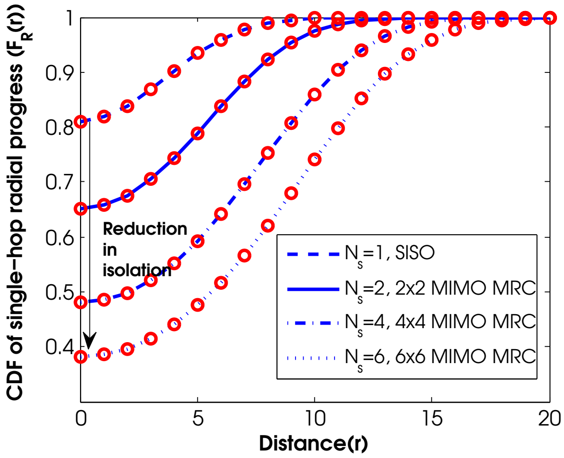

Figure 3.3: CDF of the radial progress $\mathcal{R}$ for MIMO MRC with N_s antennas with $\lambda_{TX}^{\{p\}} = 10^{-3}$,$\lambda_{TX}^{\{s\}} = 10^{-2}$,$p_s = 0.1$, $P_b^{th} = 10^{-3}$,$\eta = 10^{-1}$, $\phi = \frac{2\pi}{3}$ and $\alpha = 4$ with BPSK modulation.

Discussion

From (3.24), we observe that the average forward progress of the secondary's transmission increases with an increase in the area under the complementary CDF curve of the radial distance $\mathcal{R}$. Fig. 3.3 depicts the CDF for $\mathcal{R}$ with various MIMO MRC antenna configurations (N_s). Monte Carlo simulation results are indicated by red '○' marks and were performed by generating the empirical CDF from 10^5 realizations of $\Pi_{TX}^{\{s\}}$, $\Pi_{TX}^{\{p\}}$ and channel gain matrices for each different value of N_s. Notice that the area under the complementary CDF increases with increasing N_s. This is consistent with (3.24), where increasing N_s will increase the integrand. Hence, in brief, the average forward progress for the SU increases with the increasing number of antennas (N_s).

Average forward progress increases with an increase in the array size.

Notice that the CDF of the radial distance $\mathcal{R}$ (see Fig. 3.3) belongs to the family of extreme value distributions. More specifically, the CDF corresponds to a mixture distribution where $\Pr\{\mathcal{R} = 0\} \neq 0$. The discrete component (impulse at zero in the PDF) quantifies the isolation probability of the SU. The average forward progress of the SU becomes zero when it is completely isolated in the network. Notice, that contrary to the widely prevalent definition of isolation, this definition captures both:

Key factors contributing to the isolation of a typical node in a multi-hop ad-hoc network: > low average out degree in the desired relaying region; > stringent QoS constraint.

1. Geographical isolation: A SU may experience geographical isolation, if it is unable to find any relays in the desired forwarding region or the average out-degree of the SUs (defined as the average number of the potential relays per transmitter $\left[\frac{1-p_s}{p_s}\right]$) is too small.

2. QoS isolation: A SU may suffer from complete isolation even in the presence of a sufficient number of relays in the forwarding area, if

none of the relays can satisfy the CR's desired SIR threshold; either due to un-realistic data or bit error rate requirements or due to the high aggregate co-channel interference.

From Fig. 3.3, we observe that the isolation probability of the SU decreases with increasing the number of antennas employed (N_s). The reduction from SISO secondary to MIMO secondary with $N_s = 6$ is approximately 200%. However, the exact reduction in the isolation probability also depends on $\lambda_{TX}^{\{s\}}$, p_s and the desired directionality of the transmission. While MIMO MRC effectively combats the QoS isolation, with a very sparse network or high secondary MAP, the geographical isolation becomes the dominant contributor.

The isolation probability of a typical node is coupled with the MAP, array size, density of active transmitters and the desired QoS constraitnts.

Corollary 3.2 *The isolation probability for an arbitrary secondary transmitter under QoS aware relaying strategy with MTPC of p_s is given by*

$$p_{iso} = \prod_{i=1}^{N_s} \prod_{m=0}^{2N_s i - 2i^2} \prod_{k=0}^{m} \exp\left(- \frac{\lambda_s \phi (1-p_s) d_{i,m}{}^{\Delta_2(\delta,k) i^{-\delta}/k!}}{2\left[\eta^{-\delta}\lambda_{TX}^{\{p\}} + \lambda_s p_s\right] \kappa_1(\delta) \gamma_s^{\delta}} \right) \tag{3.34}$$

where $\Delta_2(\delta,k) = \delta \times (\delta+1) \times ... \times (\delta + (k-1))$.

PROOF: p_{iso} can be computed from Eq. (3.33) as

$$p_{iso} = \lim_{r\to 0} \lim_{z\to\infty} \Pr\left\{ \Pi_{REL}^{\{s\}} (Sec(\phi,z) \backslash Sec(\phi,r)) = \emptyset \right\}.$$

□

Closer inspection of (3.34) reveals that the isolation probability is a decreasing function of N_s, while it increases with the increase in the desired SIR threshold γ_s. The isolation probability also decreases with the increase in ϕ. However, increase in ϕ will cause a loss of directionality and thus the average forward progress towards the destination may decrease.

At this juncture, it is worth highlighting that, when CR users have their destinations located at a fixed distance r_{SD}, the average number of hops between an arbitrary CR transmitter and its destination is upper-bounded by

Quick Reference≫ Wald's identity: Let X_i $i = 1, 2, .., N$ be a sequence of i.i.d. positive random variables then $\mathbb{E}(\sum_{i=1}^{N} X_i) = \mathbb{E}(X)\mathbb{E}(N)$.

$$h \le \frac{r_{SD}}{\bar{\zeta}} + 1. \tag{3.35}$$

This result follows from Wald's identity [97]. The end-to-end throughput for an arbitrary CR with fixed destination at r_{SD} can be quantified as

$$\mathcal{T} = (1 - p_{iso})^h \, p_s \log_2(1+\gamma_s) \quad \text{(bits/s/Hz)}. \tag{3.36}$$

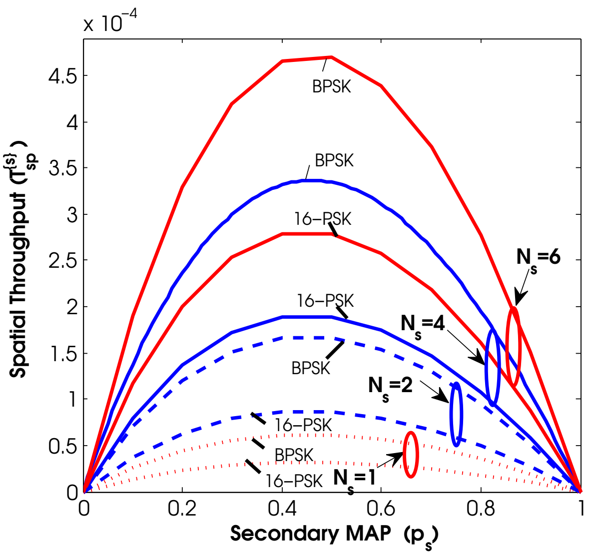

Figure 3.4: Spatial throughput (bits/s/Hz/m^2) of the Secondary transmitter with varying secondary MAP p_s for various MIMO MRC antenna configurations (N_s) and modulation schemes (BPSK and 16-PSK). Other parameters are kept constant with $\lambda_{TX}^{\{p\}} = 10^{-3}, \lambda_s = 10^{-3}, \eta = 10^{-1}, \alpha = 4$ and $\phi = \frac{2\pi}{3}$.

Notice, that the throughput depends on r_{SD}. This motivates us to employ a metric that is independent of r_{SD}, while it captures the multi-hop behavior of the transmission. Moreover, we are interested in a network wide performance metric which provides better design insights to maximize the network throughput. Both of these aspects are captured in the definition of the spatial throughput introduced in this chapter.

Definition of the spatial throughput for an ad-hoc CRN.

Definition 3.2 *The spatial throughput of the interference-limited secondary network employing the multi-hop QoS aware relaying strategy with MTPC p_s and desired SIR threshold γ_s with N_s antenna enabled MIMO MRC is*

$$T_{sp}^{\{s\}} = \lambda_s p_s \bar{\zeta} \log_2(1+\gamma_s) \ \ \textit{(bits-meter/s/Hz/m}^2\textit{)}. \tag{3.37}$$

There exists an optimal MAP which maximizes the spatial throughput of underlay CRN.

By definition, the spatial throughput of the secondary network defines the progress of each bit from the secondary transmitter towards its destination. Notice that p_s is actually a function of N_p and can be found as discussed in the previous section. Also, as discussed earlier $\bar{\zeta}$ is a decreasing function of p_s. Hence, it is intuitive to expect an optimal value of p_s, say $\bar{p}_s$, which maximizes the SUs' spatial throughput. Fig. 3.4 depicts the spatial throughput of the secondary network for BPSK modulation with varying N_s.

Fig. 3.4 confirms our hypothesis of optimal $\bar{p}_s$ and interestingly $\bar{p}_s \approx 0.5$ for the choice of simulation parameters. In general, $\bar{p}_s = 0.5$ is not always optimal, detailed discussion on the optimal MAP and its achievability under MTPC are deferred for subsequent discussions. From Fig. 3.4 it is clear that a SU can increase its spatial throughput by increasing the number of antennas employed for MIMO MRC (N_s). Also, notice that the spatial throughput of CR system with $N_s = 4$ and 16−PSK system is still higher than that of the CR system employing BPSK with $N_s = 2$. Consequently, for fixed P_b^{th} higher throughput can be supported by harvesting diversity gain. Another interesting observation from Fig. 3.4 is that the spatial throughput of the SU for $N_s = 6$ with 16−PSK is lower than that of a CR user with $N_s = 4$ and BPSK. Consequently, we conclude that the choice of modulation scheme which maximizes the spatial throughput of the SU is strongly coupled with N_s, λ_s , $\lambda_{TX}^{\{p\}}$ and N_p.

The existence of an optimal $\bar{p}_s$ leads to some interesting design questions, i.e.,

Design questions:
> Acheivability of optimal operational MAP in presence of the primary user's QoS constraint?
> Relationship between $\bar{p}_s$, N_s and N_p?

1. Is it always feasible to attain the maximum achievable spatial throughput by selecting an optimal MAP $\bar{p}_s$ under an MTPC enforced by the primary?
2. Does optimal MAP $\bar{p}_s$ depend on the number of antennas N_s employed at the CRs?
3. How does an increase in the number of antennas employed at the PU (N_p) provide gains to both primary and SUs?

In our subsequent discussion, we investigate the answers to these design questions with the help of previously developed statistical results.

1) Optimal MAP for the secondary & its achievability

As discussed earlier, the spatial throughput of the underlay CRN can be maximized by selecting an optimal MAP $\bar{p}_s$. Existence of such an optimal MAP ($\bar{p}_s$) triggers a question about its achievability under MTPC from the collocated primary network. From our previous discussion (see Section IV), we infer that the maximum permissible MAP for the CRN under PUs QoS constraint $(\gamma_p, r_p, s_{th}^{\{p\}})$ is strongly coupled with the number of antennas (N_p), modulation scheme employed at the PU and SU density (λ_s) (see Table 3.1). For a fixed set of primary parameters, the only degree of freedom available to the SU is N_s which can be increased to increase the spatial throughput by increasing the average forward progress and reducing the isolation probability.

Secondary users can employ large arrays to reduce isolation and improve the spatial progress.

Fig. 3.5 sketches the spatial throughput of the CRN with varying MAP for different SU densities for $N_s = 2$. For $\lambda_s = 10^{-3}$, the optimal MAP $\bar{p}_s$ is

0.5 (depicted by the dashed orange line). The achievable spatial throughput is illustrated in Fig. 3.5 by a superimposed red line with circular markers. Assuming that both primary and SUs employ a BPSK modulation scheme, the maximum permissible MAP for $\lambda_s = 10^{-3}$ is 1. Consequently, in this case, the SUs can employ $\bar{p}_s = 0.5$ to maximize the spatial throughput of the CRN for a fixed number of secondary antennas $N_s = 2$.

The maximum permissible MAP reduces with increasing density of the SUs for a fixed primary's QoS requirement and number of antennas (N_p), hence for $\lambda_s = 10^{-2}$ the permissible MAP reduces to 0.4. Luckily, the optimal MAP $\bar{p}_s$ is 0.3. Hence the optimum is still attainable. The maximum permissible MAP is indicated by the red solid line and the red curve with markers indicate the achievable spatial throughput. If the density of SUs further increases to $\lambda_s = 10^{-1}$, the optimal MAP $\bar{p}_s$ lies beyond the maximum permissible MAP and hence the spatial throughput cannot be maximized. Resultantly, we conclude that for a dense secondary network it is likely that an optimal MAP cannot be employed under MTPC. In such a scenario, the maximum spatial throughput which a CRN can exercise is dictated by the MTPC enforced by the primary. Moreover, SUs in dense networks should transmit with the maximum permissible MAP to maximize their spatial throughput (the spatial throughput curve is increasing before optimal MAP).

MIMO at PU aids to attain its desired QoS threshold while extending the operational region for the secondary users.

Increasing the number of antennas employed by the PU (N_p) can also facilitate the SUs to attain an optimal MAP ($\bar{p}_s$) as indicated in Fig. 3.5 for $\lambda_s = 10^{-1}$(superimposed green curve). PUs added diversity gain cannot only enable the SUs to efficiently utilize the spectrum but also facilitate the primary to satisfy the desired QoS constraint, which otherwise cannot be satisfied (see Example 1 in Section IV). For sparse networks, by increasing the N_p, the PU can increase its transmission reliability (shown by the green line), while SUs can still attain an optimal MAP $\bar{p}_s$. In brief, increasing N_p, generally leads to a win-win situation for both the primary and the CR users.

2) Optimal MAP & the size of CR array (N_s)

In the previous subsection, we studied the optimal MAP for a fixed N_s. An important question which arises from previous discussion is, does the optimal MAP ($\bar{p}_s$) for CRN depend on the size of the array employed by the CRs (N_s)?

SUs can improve their performance by adding more atennas at each node even in the presence of a restriction on the operational MAP due to primary user's QoS demands.

Fig. 3.6 shows that $\bar{p}_s$ is strongly coupled with N_s for a relatively dense CRN. In the absence of the primary network, it is obvious that a higher MAP can be supported with higher spatial throughput at the cost of added diversity and coding gain. However, when MTPC imposed on the CRN, the optimal MAP $\bar{p}_s$ may not be attainable. Nevertheless, the spatial throughput of the CRN increases with increase in N_s due to the added diversity gain. Thus,

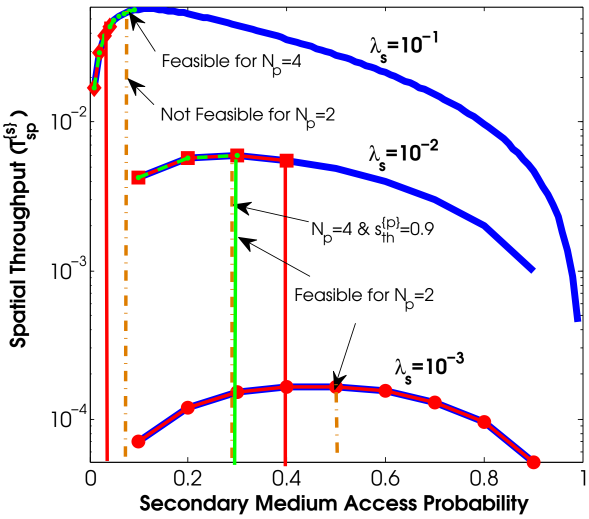

Figure 3.5: Spatial throughput (bits/s/Hz/m^2) of the CRN with varying MAP with $N_s = 2$ MIMO MRC, BPSK modulation, $\lambda_{TX}^{\{p\}} = 10^{-3}$,$\eta = 10^{-1}$,$P_b^{th} = 10^{-3}$,$\phi = \frac{2\pi}{3}$, $\alpha = 4$ and $r_p = 5$. The red lines correspond to the maximum permissible MAP which CRs can employ while guaranteeing the PU's QoS constraint. Notice that optimal MAP which maximizes the CRN throughput may exist beyond the feasible operational region. The green line indicates the extension of operation region by increasing the number of the transmit/receive antennas at the PU.

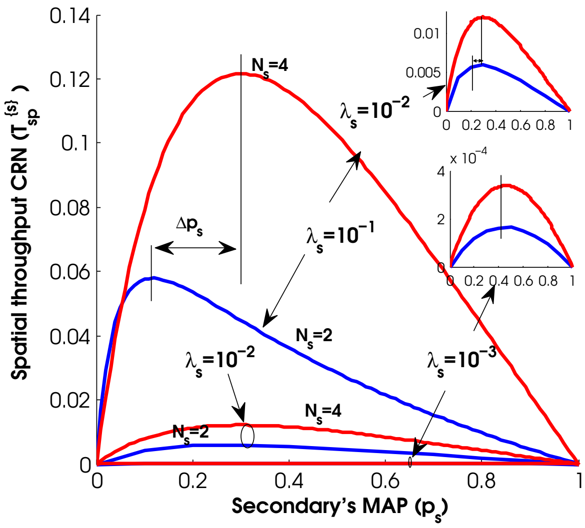

Figure 3.6: Spatial throughput (bits/s/Hz/m^2) of the CRN with varying MAP with $N_s = 2,4$ MIMO MRC, BPSK modulation, $\lambda_{TX}^{\{p\}} = 10^{-3}$,$\eta = 10^{-1}$,$P_b^{th} = 10^{-3}$, $\phi = \frac{2\pi}{3}$,$\alpha = 4$ and $r_p = 5$.

we conclude that SUs can increase their spatial throughput by increasing their array size (N_s).

3.9 CONCLUSION

In this chapter, we studied the spatial throughput of multi-hop multi-antenna ad-hoc underlay cognitive radio networks. The spatial uncertainty in both primary and secondary networks is addressed by utilizing tools from stochastic geometry. Both cognitive and primary users are assumed to employ maximum ratio transmission (MRT) and maximum ratio combining (MRC) for transmission and reception respectively. Secondary users operate under slotted-ALOHA medium access protocol and are assumed to be half-duplex. Considering, the interference from the co-channel primary and secondary users, we characterized the link success probability for the primary user. Coupled with the desired quality of service (QoS) requirement, the link success probability is then employed to quantify the maximum permissible medium access probability (MAP) for secondary users under slotted-ALOHA protocol. It is shown that contrary to existing studies on overlaid networks (where primary users sacrifice their QoS to accommodate secondary users), two-fold gains can be harnessed by employing multiple antennas at the primary user. More specifically, primary users can meet high desired QoS requirements while accommodating some secondary transmitters without performance degradation. A QoS aware relaying strategy is proposed for multi-hop relaying in a secondary network. The average forward progress of CR transmission towards its destination and the node isolation probability are characterized with a signal-to-interference ratio (SIR) based connectivity model under a geometry of forwarding area. The geometry of forwarding area controls the overall directionality of transmission from the CR transmitter to its destination. Both, the average forward progress and the maximum permissible MAP are employed to quantify the spatial throughput of the secondary network. It is shown that:

1. There exists an optimal MAP for a CRN which maximizes its spatial throughput.

2. The optimal MAP for the CRN depends on the number of antennas employed at CRs specially for the dense secondary networks.

3. The choice of modulation scheme for the CRN is also coupled with the number of antennas employed at the secondary user and the density of the CRs.

4. The achievability of optimal MAP which maximizes the spatial throughput is dependent upon the number of antennas employed and modulation scheme employed at primary user.

5. Secondary users can increase the overall spatial throughput by increasing the number of antennas at individual nodes even when optimal MAP can not be attained due to maximum permissible MAP constraint.

6. With increasing number of antennas at primary user, secondary user may attain optimal MAP even for dense CRN. For relatively less dense secondary networks, primary users can increase their QoS by exploiting added diversity and coding gains. Hence, increase in array size of primary results in a win-win situation for both networks.

7. About 200% reduction in node isolation is possible by increasing the number of antennas employed at secondary users.

4

BREAKING THE AREA SPECTRAL EFFICIENCY WALL IN COGNITIVE UNDERLAY NETWORKS

Primary objective:
- *To develop a comprehensive statistical framework for interference modeling in cognitive underlay networks.*
- *To explore the available degrees of freedom in an underlay cognitive radio network.*
- *To characterize the performance of both the primary and the secondary networks.*
- *To extend the operational region of secondary users for harnessing the throughput gains.*

ABSTRACT

In this chapter, we develop a comprehensive analytical framework to characterize the area spectral efficiency of a large scale Poisson cognitive underlay network. The developed framework explicitly accommodates channel, topological and medium access uncertainties. The main objective of this study is to launch a preliminary investigation into the design considerations of underlay cognitive networks. To this end, we highlight two available degrees of freedom, i.e., shaping medium access or transmit power. While from the primary user's perspective tuning either to control the interference is equivalent, the picture is different for the secondary network. We show the existence of an area spectral efficiency wall under both adaptation schemes. We also demonstrate that the adaptation of just one of these degrees of freedom does not lead to the optimal performance. But significant performance gains can be harnessed by jointly tuning both the medium access probability and the transmission power of the secondary networks. We explore several design parameters for both adaptation schemes. Finally, we extend our quest to more complex point-to-point and broadcast networks to demonstrate the superior performance of joint tuning policies.

4.1 MOTIVATION

The underlay CRNs will play a vital role in future communication networks on several fronts, i.e.:

1. They will enable practical realization of small-cell networks where interference management between the femto user equipment (FUE) and the macro base station (BS) is the key challenge [98].The small-cell networks promise high capacity gains with highly reliable connectivity at low energy costs. For small-cell networks, the underlay approach outranks the arch-rival interweave approach because of several practical reasons. The simplest example of the interference avoidance based access strategy is carrier sense multiple access with collision avoidance (CSMA/CA) whose weakness are well known in the literature.

Even with the most advanced signal processing techniques perfect interference avoidance cannot be attained. This can be attributed to the inherent trade off between the probability of false alarm and the probability of detection of the employed detector. Hence, establishing performance guarantees for the user associated with the macro BS in the presence of interweave empowered FUEs is not trivial. On the other hand, the underlay approach presents a simple alternative with quantifiable performance assurance.

2. They will provision short range transmissions in next generation M2M [99] or device-to-device (D2D) [100] communication networks. It is envisioned that M2M and D2D communication networks will operate in an underlay manner with the existing 3G and upcoming 4G cellular services[100, 101]. M2M communication is the key propeller for smart living spaces and will also facilitate bi-directional smart grid communications. In D2D communication paradigm cellular BS's will coordinate with the the devices so that they can shape their transmission parameters for controlling the aggregate interference.

Link level dynamics correspond to the uncertainty experienced due to multi-path propagation and topological randomness, while the network level dynamics are shaped by medium access control, user density etc.

In summary, underlay CRNs will be central to next generation wireless networks. Despite their prime importance, as noted in the previous chapter the design space of the cognitive underlay networks remains an un-charted territory. To the best of our knowledge, the available degrees of freedom for the design of such networks in presence of both the link and network level dynamics remains un-explored. Furthermore, the throughput potential of such networks is also not quantified in existing literature. In the previous chapter, we launched a preliminary study to explore the design parameters of large scale MIMO multi-hop underlay CRN. Chapter 3 leads to two important observations: (i) there exists an optimal MAP which maximizes the throughput performance of CRN; (ii) it is not always possible to employ the optimal MAP as an operational point due to the primary's enforced QoS constraint. This motivated us to adapt a more fundamental and alternative approach in this chapter for investigating the design parameters of a large scale cognitive underlay network. More specifically, we seek to answer the important design question: Can we break the so called 'spectral efficiency wall' which is imposed due to primary user's QoS constraint?

4.2 CONTRIBUTIONS & ORGANIZATION

For a more sophisticated MAC protocol such as CSMA/CA, the ALOHA MAP adaptation can be replaced by adaptation of the radius of the carrier sensing region.

In this chapter, we consider a legacy ad-hoc network collocated with an ad-hoc CRN. The spatial properties of both networks are analyzed by borrowing well established tools from stochastic geometry [43]. The key contributions of this chapter can be summarized as follow:

1. Considering that both the primary and secondary users employ a Slotted-ALOHA medium access control (MAC) protocol (see Section 4.4), it is demonstrated that in order to satisfy the primary user's desired QoS requirements (see Section 4.5), secondary users have two degrees of freedom which they can adapt for performing interference control, i.e. (i) MAP adaptation; and (ii) transmit power adaptation.

2. It is shown that from the primary user's perspective both the power and the MAP adaptation are equivalent, as long as the desired QoS requirements are fulfilled (see Section 4.5). However, the achievable performance of the secondary networks under these schemes differs significantly (see Section 4.5). In this chapter, we employ the area spectral efficiency [32] as the performance metric for underlay CRNs. We show that under the adaptation schemes introduced there exists a spectral efficiency wall beyond which the operation of the CRN is infeasible. The optimal operating point which maximizes the spectral performance of the CRN often lies beyond this wall and hence cannot be attained. It is shown that under transmit power (MAP) adaptation scheme there exists an optimal MAP (transmit power) which maximizes the bits/s/Hz/m^2 performance of the network. Furthermore, it is demonstrated that mere adaptation of either the MAP or the transmission power results in a sub-optimal performance. Superior performance can be attained by employing the coupling of these adaptation schemes (for one degree of freedom) with the optimization of the remaining degree of freedom. In other words, network-wide performance is optimized by either (i) adapting MAP in conjunction with optimal transmission power selection; or (ii) adapting the transmission power in conjunction with optimal MAP selection.

The location of the area spectral efficiency wall is dictated by the primary user's desired QoS constraint.

Adapt and optimize strategy!

3. The optimal MAP and SIR threshold for CRs is quantified under a transmission power adaptation scheme. It is shown that the optimal MAP decreases as an inverse-function of the secondary user density. The secondary link success probability (with power adaptation and optimal MAP) converges to e^{-1}. Moreover, the optimal MAP must decay in a square law manner to cater for an increase in link distance while decay with SIR threshold depends on the path-loss exponent (see Section 4.7). It is shown that optimal MAP is independent of the transmit power employed by the primary user.

Properties of an optimal MAP

4. It is shown that transmit power adaptation with optimal MAP selection breaks the area spectral efficiency wall for a more complex underlay networking scenario. More specifically, characterization of the area spectral efficiency for the point-to-point and broadcast scenario is pursued with the same objectives. For point-to-point transmission, two receiver association models are considered, i.e., (i) nearest neighbor; (ii) n^{th} neighbor in a sector. These two scenarios can be visualized as a snap shot of the multi-hop relaying strategy at an arbitrary time slot. The first strategy corresponds to short hop transmissions while the second provides the flexibility of selecting the hop length. Under both strategies the receivers which defer their transmission under the slotted-ALOHA protocol are selected as a single hop destination (see Section 4.8). The optimal MAP under transmit power adaptation is characterized for both point-to-point scenarios. It is shown that optimal MAP is independent from the user density and depends on the average out-degree (see Section 4.8).

Adapt and optimize is the best strategy, irrespective of the networking paradigm.

5. The definition of area spectral efficiency for a broadcast underlay network is presented (see Section 4.8). The performance of a broadcast underlay network is studied and it is shown that transmit power adaptation with MAP selection outperforms a mere adaptation scheme.

To the best of authors' knowledge, none of the studies in the past have addressed the above mentioned issues for a large scale underlay CRNs. The available degrees of freedom and there optimal exploitation remains an open-issue. Nevertheless, for the interested readers a brief survey of some literary contributions in the domain is summarized in Section 4.3.

4.2.1 *Notations*

Throughout this chapter, we use $\mathbb{E}_Z(.)$ to denote the expectation with respect to the random variable Z. A particular realization of a random variable Z is denoted by the corresponding lower-case symbol z. The probability density function (PDF) of the random variable Z is denoted by $f_Z(z)$ and its corresponding cumulative distribution function by $\mathcal{F}_Z(z)$. The symbol $\prod_{i\in S}$ denotes the product when i is replaced by the elements of the set S. For instance, if $S = \{s, p\}$ then $\prod_{i\in S} g_i(.)$ coressponds to the product $g_p(.)g_s(.)$. The bold-face lower case letters (e.g., $\boldsymbol{x}$) are employed to denote a vector in $\mathbb{R}^2$. The symbol $\setminus$ denotes the set subtraction and the symbol $\|\boldsymbol{x}\|$ denotes the Euclidean norm of vector $\boldsymbol{x}$. The symbol $b(x, r)$ denotes the ball of radius r centered at point $\boldsymbol{x}$.

4.3 RELATED WORK

In [102] Chen et al. studied the performance of multi-path routing with end-to-end QoS provisioning in cognitive underlay networks. The authors consider large scale cognitive underlay networks where the secondary users control their MAP for peaceful co-existence with the primary network. As MAP control is equivalent to transmission density control, the authors in [103] explore the phase transition phenomenon experienced in cognitive underlay networks. More specifically, the authors study the relationship between latency, connectivity, interference and other system parameters. Percolation theoretic analysis of cognitive underlay networks is also pursued in [104, 105]. In [106] the authors explore the achievable capacity of cognitive mesh network when different MAC protocols are employed. They compared the throughput potential of Slotted ALOHA, CSMA/CA and TDMA schemes. Co-existence between the secondary and the primary networks based on the Slotted-ALOHA protocol is also explored in [107]. In [108] authors studied the performance of a multi-hop multi-antenna underlay cognitive ad hoc networks in presence of the co-channel interference. The authors demonstrated that the inherent diversity gains due to multiple antennas provide performance gains for both the primary and the secondary users.

All of the above mentioned studies intrinsically rely on the optimality of MAP/density adaptation. However, in this chapter, we show that both the MAP and power adaptations by themselves are sub-optimal. Furthermore, due to the QoS constraint enforced by the primary user, the performance of these adaptation schemes is bounded by the area spectral efficiency wall. Notice that the simulation results in [106] (Fig 3-5) also depict the manifestation of the throughput wall in terms of power ratio and threshold SIR. In this chapter, we demonstrate that this wall can be broken by exploiting the optimizing the remaining degree-of-freedom. To the best of our knowledge, none of the studies in past has presented a generic and a comprehensive statistical framework for quantifying the performance of the large scale underlay CRNs. This motivate us to develop a generic framework considering link and network dynamics while addressing the important design questions. We also present the extensions of our analytical framework to more generic point-to-point and broadcast underlay networks whose performance remains un-explored in the existing literature.

4.4 NETWORK MODEL

4.4.1 *Geometry of the Network*

We consider a primary/legacy network operating in the presence of a collocated ad-hoc CRN. The spatial distribution of both primary and secondary users is captured by two independent *homogenous Poisson point processes* (HPPPs) $\Pi_p(\lambda_p)$ and $\Pi_s(\lambda_s)$ respectively. More specifically, at any arbitrary time instant the probability of finding $n \in \mathbb{N}$ primary/secondary users inside a region $\mathcal{A} \subseteq \mathbb{R}^2$ is given by

$$\mathbb{P}\left(\Pi_i(\mathcal{A}) = n\right) = \frac{(\lambda_i v_2(\mathcal{A}))^n}{n!} \exp\left(-\lambda_i v_2(\mathcal{A})\right), \quad i \in \{s, p\} \tag{4.1}$$

Notice that Π_i is also a counting measure on $\mathbb{R}^2$.

where, $v_2(\mathcal{A}) = \int_{\mathcal{A}} d\boldsymbol{x}$ is the Lebesgue measure on $\mathbb{R}^2$[109] and $\lambda_p(\lambda_s)$ is the average number of primary (secondary) users per unit area. If $\mathcal{A}$ is a disc of radius r then $v_2(\mathcal{A}) = \pi r^2$.

4.4.2 *Transmission Model & Medium Access Control (MAC)*

In this chapter, we assume that both primary and secondary users employ Slotted ALOHA MAC protocol to schedule their transmissions over a shared medium. More specifically, at an arbitrary time instant both the primary and the secondary users can be classified into two distinct groups, i.e., nodes which are granted with the medium access and those whose transmissions are deferred. If p_i denotes the MAP for an arbitrary user $\boldsymbol{x} \in \Pi_i$[1], then the set of active users under a Slotted ALOHA MAC also forms a HPPP

$$\begin{aligned} \Pi_i^{\{TX\}} &= \{\boldsymbol{x} \in \Pi_i : \mathbb{1}(\boldsymbol{x}) = 1\} \text{ with density } \lambda_i p_i \\ & \quad \text{where } i \in \{s, p\}. \end{aligned} \tag{4.2}$$

where $\mathbb{1}(\boldsymbol{x})$ denotes a Bernoulli random variable and that is independent of Π_i and $i \in \{s, p\}$ is the shorthand for $\{$secondary, primary$\}$. We employ the famous bipolar model [43] to capture the spatial distribution of the primary and the secondary receivers. Specifically, each primary transmitter has its intended receiver at a fixed distance r_p in a random direction. Similarly, each secondary receiver is located at distance r_s from its corresponding transmitter. The bipolar/dumbbell model can be generalized to more realistic models. These receiver association models are strongly tied with the considered networking scenario. In Section 4.8, we will introduce more general models for quantifying the performance of a large scale CRN.

We also assume that both the primary and the secondary time-slots are identical and synchronized.

1 With a slight abuse of notation, $\boldsymbol{x} \in \mathbb{R}^2$ is employed to refer to the node's location as well as the node itself.

It is assumed that all active transmitters have one or more packets to transmit. This assumption is widely prevalent in the literature, mainly because it simplifies the analysis by abstracting the queuing details.

4.4.3 *Physical Layer Model*

In current chapter, we assume that all four types of links, i.e., primary-to-primary communication; secondary-to-primary interference; primary-to-secondary interference and secondary-to-secondary communication links experience Nakagami-m flat fading channel. The fading severity of the Nakagami-m channel is captured by parameter m_s for all links originating from the secondary transmitters, while the fading severity of the primary communication and interference links is captured by employing the parameter m_p. The overall channel gain between a transmitter and a receiver separated by the distance r is modeled as $Hl(r)^2$. Here, H is a Gamma random variable and $l(r) = Kr^{-\alpha}$ is the power-law path-loss exponent. The path-loss function depends on the distance r, a frequency dependent constant K and an environment/terrain dependent path-loss exponent $\alpha \geq 2$. The fading channel gains are assumed to be mutually independent and identically distributed (i.i.d.). It is assumed that the communication is interference limited and hence thermal noise is negligible. Notice that the choice of the Nakagami-m fading model is motivated by the generality of the model, but our main interest lies in studying the performance for the worst case scenario of Rayleigh fading (which is obtained as a special case by setting $m = 1$).

Without any loss of generality, we will assume $K = 1$ for the rest of the discussion.

4.5 AREA SPECTRAL EFFICIENCY OF COGNITIVE UNDERLAY NETWORK

The area spectral efficiency of the cognitive underlay network is strongly coupled with the transmit power and the MAP adopted by the secondary users. However, secondary users are obliged to tune either or both of these parameters (i.e., transmit power or MAP) such that the primary user's QoS requirement is always satisfied. In this section, we first derive a condition for the transmit power and MAP such that the CR users can peacefully coexist with the legacy network. This condition is then employed to quantify the achievable area spectral efficiency for the cognitive underlay network.

4.5.1 *Primary user's QoS constraint*

Consider an arbitrary primary transmitter $\boldsymbol{x} \in \Pi_p$ and its associated receiver at distance r_p. Employing the stationarity property of the point process Π_p, each node can be translated such that the receiver corresponding

Quick Reference≫ Silvnyak's Theorem: The law of the stationary Poisson point process does not change by addition of an arbitrary point.

2 We also employ symbol G instead of H to denote the fading channel gain from the secondary transmitter.

to the primary transmitter $\boldsymbol{x}$ lies at the origin. Alternatively, we can employ the Silvnyak's theorem [109], which states that adding a probe point to the HPPP at an arbitrary location does not effect the law of the point process. Consequently, the received SIR at the primary receiver can be quantified as

$$\begin{aligned} \mathrm{SIR} = \Gamma_p &= \frac{h_p l(r_p)}{\sum_{i \in \Pi_p^{\{TX\}} \setminus \{x\}} h_i l\left(\|\boldsymbol{x}_i\|\right) + \sum_{j \in \Pi_s^{\{TX\}}} \eta g_j l\left(\|\boldsymbol{x}_j\|\right)}, \\ &= \frac{h_p l(r_p)}{I_p + \eta I_s} = \frac{h_p l(r_p)}{I_{tot}}. \end{aligned} \tag{4.3}$$

where $I_s = \sum_{j \in \Pi_s^{\{TX\}}} g_j l\left(\|\boldsymbol{x}_j\|\right)$ is the co-channel interference caused by the secondary transmitters, $I_p = \sum_{i \in \Pi_p^{\{TX\}} \setminus \{x\}} h_i l\left(\|\boldsymbol{x}_i\|\right)$ is the interference experienced due to simultaneous transmissions from other primary users and $\eta = \frac{P_s}{P_p}$ is the ratio of the transmit powers of the secondary and the primary transmitters.

Operational constraint for secondary underlay network.

The primary user's QoS constraint can be expressed in terms of the desired SIR threshold $\gamma_{th}^{\{p\}}$ and an outage probability threshold

$$\mathbb{P}_{out}^{\{p\}}\left(P_s, p_s\right) = \Pr\left\{\Gamma_p \leq \gamma_{th}^{\{p\}}\right\} \leq \rho_{out}^{\{p\}}. \tag{4.4}$$

Notice that the primary user's outage probability is coupled with the aggregate interference generated by the secondary network. Consequently, secondary access is limited subject to the constraint in Eq. (4.4).

4.5.2 *Secondary User's Permissible MAP and Transmit Power*

Laplace transform of the aggregate interference experienced by the primary receiver.

Lemma 4.1 *The Laplace transform $\left(\mathcal{L}_{I_{tot}}(s)\right)$ of the aggregate interference $\left(I_{tot}\right)$ experienced at the primary receiver, caused by both the co-channel primary and the secondary, when the primary interfering link suffers from the Nakagami$-m_p$ fading and the secondary interference link experiences the Nakagami $-m_s$ fading, can be quantified as in Eq.(4.5) with $\delta = 2/\alpha$.*

$$\begin{aligned} \mathcal{L}_{I_{tot}}(s) &= \exp\left[-\pi\left(\lambda_p p_p \frac{\Gamma(m_p+\delta)}{\Gamma(m_p) m_p^{\delta}} + \eta^{\delta} \lambda_s p_s\right.\right. \\ &\times \left.\left.\frac{\Gamma(m_s+\delta)}{\Gamma(m_s) m_s^{\delta}}\right) \Gamma\left(1-\delta\right) s^{\delta}\right]. \end{aligned} \tag{4.5}$$

PROOF: Consider a HPPP Π with intensity λ then the aggregate interference experienced at the probe receiver is given as

$$I = \sum_{\boldsymbol{x}_i \in \Pi} h_i l(\|\boldsymbol{x}_i\|). \tag{4.6}$$

The Laplace transform of I is given by

$$\begin{aligned} \mathcal{L}_I(s) &= \mathbb{E}\left(\exp\left(-sI\right)\right), \\ &= \mathbb{E}\left(\prod_{\boldsymbol{x}_i \in \Pi} \mathbb{E}_H\left(\exp\left(-shl(\|\boldsymbol{x}_i\|)\right)\right)\right). \end{aligned} \tag{4.7}$$

Using the definition of the Generating functional of HPPP in [109]

Quick Reference≫ Generating functional of HPPP: Let Φ be a Poisson process of intenstity measure Λ then the generating functional is given by $\mathcal{G}(f(x)) = \mathbb{E}\left(\prod_{i\in\Phi} f(x)\right) = \exp\left(-\int(1-f(x))\Lambda(dx)\right)$.

$$\mathcal{L}_I(s) = \exp\left(\int \left[1 - \mathbb{E}_H\left(\exp\left(-shl(r)\right)\right)\right] \lambda 2\pi r dr\right). \tag{4.8}$$

This can be solved to obtain

$$\mathcal{L}_I(s) = \exp\left(-\lambda\pi\mathbb{E}(h^\delta)\Gamma\left(1-\delta\right)s^\delta\right), \tag{4.9}$$

where, $\delta = \frac{2}{\alpha}$ is a constant. The aggregate interference experienced by the probe receiver from both the primary and the secondary users is given by

$$I_{tot} = \underbrace{\sum_{i \in \Pi_p^{\{TX\}} \setminus \{x\}} h_i l(\|\boldsymbol{x}_i\|)}_{I_p} + \eta \underbrace{\sum_{j \in \Pi_s^{\{TX\}}} g_j l(\|\boldsymbol{x}_j\|)}_{I_s}. \tag{4.10}$$

From Eq. (4.10) it can be easily shown that $\mathcal{L}_{I_{tot}}(s) = \mathcal{L}_{I_p}(s)\mathcal{L}_{I_s}(s)$. Moreover, employing Eq. (4.9)

$$\begin{aligned} \mathcal{L}_{I_{tot}}(s) &= \exp\left(-\pi\left[\lambda_p p_p \mathbb{E}_H\left(h^\delta\right) + \eta^\delta \mathbb{E}\left(g^\delta\right)\lambda_s p_s\right]\right. \\ &\times \left.\Gamma\left(1-\delta\right)s^\delta\right). \end{aligned} \tag{4.11}$$

The δ^{th} moment of the interfering channel gain for Nakagami$-m_p$ and Naka-gami$-m_s$ fading can be computed as

$$\mathbb{E}_H\left(h^{\delta}\right)=\frac{\Gamma(m_p+\delta)}{\Gamma(m_p)m_p^{\delta}} \text{ and } \mathbb{E}_G\left(g^{\delta}\right)=\frac{\Gamma(m_s+\delta)}{\Gamma(m_s)m_s^{\delta}}. \tag{4.12}$$

Substituting Eq.(4.12) into Eq. (4.11), we obtain Eq. (4.5). □

Lemma 4.1 indicates that the Laplace transform of the aggregate interference is a decreasing function of both the secondary user's MAP (p_s) and the transmit power $(P_s$ through $\eta)$. However, the rate at which it decreases is not similar. Notice that the difference between the fading conditions experienced by the primary and the secondary interfering links also plays a vital role.

Coexistence condition for secondary network.

Theorem 4.1 *Consider a primary QoS constraint expressed in terms of desired SIR threshold ($\gamma_{th}^{\{p\}}$) and the desired outage probability threshold $\rho_{out}^{\{p\}}$, then the co-located secondary network with density λ_s must adapt its transmit power and/or MAP such that the condition in Eq. (4.13) is satisfied.*

$$\begin{aligned} P_s^{\delta}p_s \;\leq\; \max & \left(\frac{\ln\left(\frac{1}{1-\rho_{out}^{\{p\}}}\right)\Gamma(m_p)\Gamma(m_s)}{\pi\lambda_s r_p^2\Gamma(m_p-\delta)\Gamma(m_s+\delta)}\left(\frac{m_sP_p}{m_p\gamma_{th}^{\{p\}}}\right)^{\delta}\right. \\ & \left. -\;\frac{\lambda_p}{\lambda_s}p_p\frac{\Gamma(m_s)}{\Gamma(m_p)}\frac{\Gamma(m_p+\delta)}{\Gamma(m_s+\delta)}\left(\frac{m_sP_p}{m_p}\right)^{\delta},0\right). \end{aligned} \tag{4.13}$$

PROOF: From Eqs. (4.4) and (4.3), we have

$$\begin{aligned} \mathbb{P}_{out}^{\{p\}}(P_s,p_s) &= \Pr\left\{\Gamma_p \leq \gamma_{th}^{\{p\}}\right\}, \\ &= \mathbb{E}_H\left[1-\Pr\left\{I \leq \underbrace{\frac{P_ph_pl(r_p)}{\gamma_{th}^{\{p\}}}}_{z}\right\}\right], \\ &= \mathbb{E}_H\left[1-\underbrace{\Pr\left\{I_p\leq z\right\}\Pr\left\{I_s\leq z\right\}}_{A_1}\right], \end{aligned} \tag{4.14}$$

where with a slight abuse of the introduced notation, we define $I=I_p+I_s$; $I_p=\sum_{i\in\Pi_p^{\{TX\}}}P_ph_il(r_i)$ and $I_s=\sum_{i\in\Pi_s^{\{TX\}}}P_sg_jl(r_j)$. Notice that Eq. (4.14) can be evaluated equivalently by employing the distribution of H_p (which admits the closed-form expression) and taking the expectation with respect to the interference. But the interference distribution cannot be expressed in a closed form. However, the approach based on the distribution of H_p leads to a solution which requires evaluation of an infinite summation and composite derivative of the Laplace transform (requiring application of the Faa di Bruno's formula [95]) for an arbitrary m_p. Moreover, the resulting expression cannot be inverted to quantify the permissible MAP and the transmit power. Hence motivated by [46], we propose an alternative method. Let $\Pi_p^{\{TX\},\{dom\}} = \left\{\boldsymbol{x}_i \in \Pi_p^{\{TX\}} : P_p h_i l\left(\|\boldsymbol{x}_i\|\right) > z\right\}$, $\Pi_s^{\{TX\},\{dom\}} = \left\{\boldsymbol{x}_j \in \Pi_s^{\{TX\}} : P_s g_j l\left(\|\boldsymbol{x}_j\|\right) > z\right\}$ and $I_k = I_{\Pi_k^{\{TX\},\{dom\}}} + I_{\Pi_k^{\{TX\}} \setminus \Pi_i^{\{TX\},\{dom\}}} - k \in \{s,p\}$ where $\Pi_k^{\{TX\},\{dom\}}$ reperesents the dominant interferers, then A_1 can be bounded as

$$\begin{aligned}
A_1 &\leq \Pr\left\{I_{\Pi_p^{\{TX\},\{dom\}}} \leq z\right\} \Pr\left\{I_{\Pi_s^{\{TX\},\{dom\}}} \leq z\right\}, \\
&\leq \Pr\left\{\Pi_p^{\{TX\},\{dom\}} = \emptyset\right\} \Pr\left\{\Pi_s^{\{TX\},\{dom\}} = \emptyset\right\}, \\
&\leq \prod_{i\in\{s,p\}} \exp\left(-\mathbb{E}_H\left(2\pi\lambda_i p_i \int_0^\infty r\right.\right. \\
&\times \left.\left. \mathbb{1}\left(\frac{P_i h_i}{r^\alpha} > z\right) dr\right)\right), \qquad (4.15) \\
&\leq \prod_{i\in\{s,p\}} \exp\left(-\pi\lambda_i p_i z^{-\delta} P_i^\delta \frac{\Gamma(m_i+\delta)}{\Gamma(m_i) m_i^\delta}\right).
\end{aligned}$$

By employing the upper-bound on A_1, the lower-bound on the primary user's outage probability can be quantified as

$$\begin{aligned}
\mathbb{P}_{out}^{\{p\}}\left(P_s, p_s\right) &\geq \mathbb{E}_H\left[1 - \exp\left(-\pi\left\{\lambda_p p_p \frac{\Gamma(m_p+\delta)}{\Gamma(m_p) m_p^\delta}\right.\right.\right. \\
&+ \left.\left.\left. \lambda_s p_s \eta^\delta \frac{\Gamma(m_s+\delta)}{\Gamma(m_s) m_s^\delta}\right\} \gamma_{th}^{\{p\}\delta} h^{-\delta} r_p^2\right)\right], \\
&\overset{(a)}{\geq} 1 - \mathcal{L}_{I_{tot}}(s)\Big|_{s=\frac{\gamma_{th}^{\{p\}} r_p^\alpha \mathbb{E}(H^{-\delta})}{\Gamma(1+\delta)^{1/\delta}}}, \qquad (4.16)
\end{aligned}$$

where (a) is obtained by employing Jensen's inequality and Eq. (4.5). The derived lower bound is very tight (especially for $\mathbb{P}_{out}^{\{p\}}\left(P_s, p_s\right) \leq 0.1$). As a matter of fact for $m_p = 1$ (Rayleigh fading), the inequality can be replaced with an equality. The tightness for an arbitrary m_p can be easily verified by Monte-Carlo simulation (see Fig. 4.1). Bounding (4.16) by the desired outage constraint $\rho_{out}^{\{p\}}$ from above then with several mathematical manipulations

Quick Reference≫
Jensen's inequality:
For a concave function $f(x)$
$\mathbb{E}(f(x)) \geq f(\mathbb{E}(X))$.

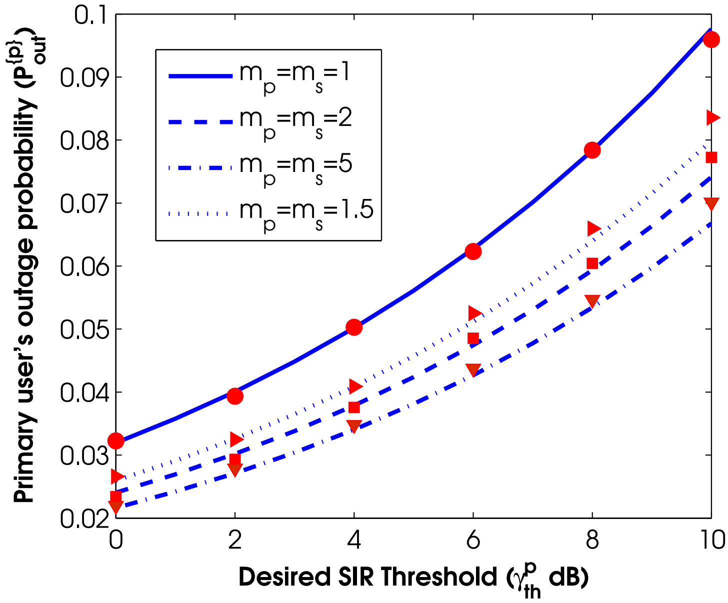

Figure 4.1: Primary user's outage probability with varying desired SIR threshold for $\lambda_p = \lambda_s = 10^{-3}$, $p_p = p_s = 0.2$, $\eta = 10^{-1}$, $\alpha = 4$ and $r_p = 5$. The markers correspond to the results obtained from Monte-Carlo simulation of the network with 10^5 trials for each SIR threshold.

we get Eq. (4.13). □

Remarks

1. An immediate observation from Eq. (4.13) is that from the primary user's perspective both the secondary user's power control and/or the MAP control are equivalent. Hence as long as the constraint in Eq. (4.13) is satisfied, it does not matter whether this is attained by the MAP or the power control.

For a dense cognitive network, either CRs should transmit seldom or adapt a low transmission power. This will significantly limit the distance over which a link can be established while satisfying the desired QoS requirements.

2. For certain fixed p_s, the maximum permissible transmit power ($\bar{P}_s$) for a secondary user can be easily obtained from Eq. (4.13) as $\bar{P}_s = \sup\left\{P_s : \mathbb{P}_{out}^{\{p\}}\left(P_s, p_s\right) \leq \rho_{out}^{\{p\}}\right\}$. Similarly, the maximum permissible MAP ($\bar{p}_s$) when the secondarys transmit with a certain power P_s can also be obtained from Eq. (4.13) as $\bar{p}_s = \sup\left\{p_s : \mathbb{P}_{out}^{\{p\}}\left(P_s, p_s\right) \leq \rho_{out}^{\{p\}}, \, p_s \leq 1\right\}$. The former is referred as the secondary transmit power control based underlay access, while the later is refereed as the secondary MAP control based underlay.

3. Notice that either the transmit power or the MAP must reduce to cater for the increasing secondary user density, i.e., with an increase in secondary nodes per unit area either the frequency of transmission should be reduced or the nodes should transmit with a lower power to ensure that the primary user's desired QoS constraint is satisfied. Also notice (from Eq. (4.13)) that the decay in the transmission frequency of the primary user increases the opportunity for the secondary transmission.

4.5.3 *Area Spectral Efficiency of the Secondary Network*

The area spectral efficiency of the secondary underlay network is defined as the number of bits per unit time per Hertz of bandwidth that are successfully exchanged between active secondary transmitter-receiver pairs per unit area. The probability of success for the secondary network is strongly coupled with the transmit power and the MAP, as the former shapes the signal strength and the later characterizes the co-channel interference. In a previous sub-section, we quantified these parameters in terms of the condition enforced under the primary's required QoS constraint. In this sub-section, we derive a closed-form expression for the area spectral efficiency of the secondary network.

Area spectral efficiency.

Definition 4.1 *The area spectral efficiency of the secondary underlay network in the presence of the legacy network when the transmit power adaptation is employed by the users to ensure primary's QoS constraint, can be characterized as*

$$\mathcal{T}_{\mathcal{P}_s} = \lambda_s p_s \log_2\left(1+\gamma_{th}^{\{s\}}\right) \mathbb{P}_{suc}^{\{s\}}\left(\bar{P}_s, p_s\right), \quad \text{bits/s/Hz/m}^2 \qquad (4.17)$$

where $\bar{P}_s$ is the maximum permissible transmit power for an arbitrary secondary user at a particular MAP p_s, which is obtained from Eq. (4.13) and $\mathbb{P}_{suc}^{\{s\}}\left(\bar{P}_s, p_s\right)$ is the success probability of an arbitrary secondary link.

Link success probability for a secondary user.

Theorem 4.2 *Consider a secondary transmitter $x \in \Pi_s^{\{TX\}}$ with the transmit power P_s, while attempting to access the medium with probability p_s, then the probability of success $\mathbb{P}_{suc}^{\{s\}}$ for the link between x and its desired secondary receiver (separated by distance r_s) can be upper-bounded as given in Eq. (4.18).*

$$\begin{aligned}\mathbb{P}_{suc}^{\{s\}}(P_s, p_s) \leq\ & \exp - \Bigg\{\pi \Bigg(\lambda_p p_p \left(\frac{P_p}{P_s}\right)^{\delta} \frac{\Gamma(m_p+\delta)}{\Gamma(m_p) m_p^{\delta}} \\ & + \lambda_s p_s \frac{\Gamma(m_s+\delta)}{\Gamma(m_s) m_s^{\delta}}\Bigg) \frac{\Gamma(m_s-\delta)}{\Gamma(m_s)} \left(\gamma_{th}^{\{s\}} m_s\right)^{\delta} r_s^2 \Bigg\}.\end{aligned} \tag{4.18}$$

PROOF: The proof follows similar steps as for Propositions 1 & 2. □

Similar to the transmit power adaptation case the area spectral efficiency of the secondary underlay network with MAP adaptation is given by

$$\mathcal{T}_{p_s} = \lambda_s \bar{p}_s \log_2\left(1+\gamma_{th}^{\{s\}}\right) \mathbb{P}_{suc}^{\{s\}}(P_s, \bar{p}_s), \quad \text{bits/s/Hz/m}^2 \tag{4.19}$$

where $\bar{p}_s$ is the maximum permissible MAP at the transmission power P_s obtained from (4.13). Notice that under MAP adaptation the number of concurrent transmission sessions is also bounded due to the upper-bound on the secondary MAP.

4.6 DISCUSSION

Recall that m_p and m_s correspond to the fading severity of the communication and the interference channels from the primary and secondary user respectively (Section 4.4).

Figs. 4.2 and 4.3, depict the area spectral efficiency of the cognitive underlay network under the transmit power adaptation scheme. As shown in the Fig. 4.2, the area spectral efficiency is strongly coupled with the fading severity of the propagation channel. The fading severity for a Nakagami-m channel decreases with an increase in m. For $m_p = m_s = 1$, the area spectral efficiency corresponds to the case when both the primary interference and the secondary communication channel suffers from Rayleigh fading. As shown in Fig. 4.2 for a CRN more densely deployed than the primary network ($\lambda_s > \lambda_p$), the fading severity m_s plays a more important role than that of the m_p. Hence, the attainable spectral efficiency is dramatically reduced when the fading severity of secondary-to-secondary communication and secondary-to-primary interference channel is reduced (see $m_s = m_p = 2$ and $m_s = 1$, $m_p = 2$ in Fig. 4.2). In other words, a reduction in fading severity results in a more restrictive power adaptation which outweighs the gain obtained due to better propagation condition for the communication link.

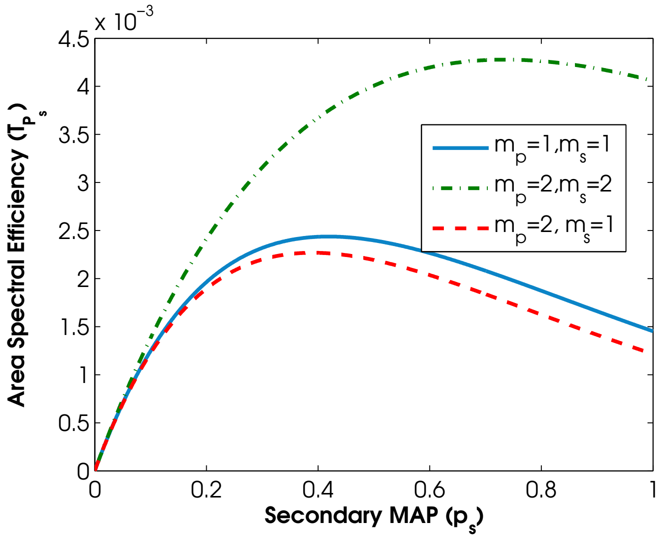

Figure 4.2: Area spectral efficiency (bits/s/Hz/m^2) of a cognitive underlay network with transmit power adaptation $\lambda_s = 10^{-2}$, $\lambda_p = 10^{-3}$, $P_p = 1$, $\alpha = 4$, $r_p = r_s = 4$, $\rho_{out}^{\{p\}} = 0.1$, $p_p = 0.4$, $\gamma_{th}^{\{p\}} = 5$ dB and $\gamma_{th}^{\{s\}} = 3$ dB (see Eq. (4.17)).

Fig. 4.3 shows the area spectral efficiency of the CRN under the transmit power adaptation scheme for the Rayleigh fading channel. The solid part of the curve corresponds to the operational regime for the CRN where the primary user's desired QoS constraint is guaranteed. Moreover, the dashed part corresponds to the values of the transmit power which cannot be selected due to the bound enforced by the primary network. An interesting observation here is that there exists a so called "area spectral efficiency wall" beyond which the operation is not feasible. Hence the area spectral efficiency obtained under transmit power adaptation is limited by this wall. The existence of the wall can be better understood with the help of Eq. 4.18. From Eq. 4.18 it follows that for an arbitrary but fixed MAP, the success probability of the secondary link increases with an increase in P_s[3]. However, the maximum permissible transmit power ($\bar{P}_s = \sup\left\{P_s : \mathbb{P}_{out}^{\{p\}}\left(P_s, p_s\right) \leq \rho_{out}^{\{p\}}\right\}$) is bounded due to the primary user's QoS constraint. Consequently, the area spectral efficiency is also bounded.

An important and interesting observation which follows from Figs. 4.2 and Fig. 4.3 is regarding the existence of an optimal MAP (i.e., p_s^*) which maximizes the network wide area spectral efficiency. Intuitively, increas-

3 Notice that an increase in P_s effectively translates into an increase in the signal power. Since, secondary transmitters employ the same transmit power, an increase in P_s does not reduce the co-channel interference due to CR transmitters. However it increases the signal power relative to the co-channel interference inflicted by the primary transmitters. Consequently, it is beneficial for secondary users to increase the transmit power to improve their link success probability.

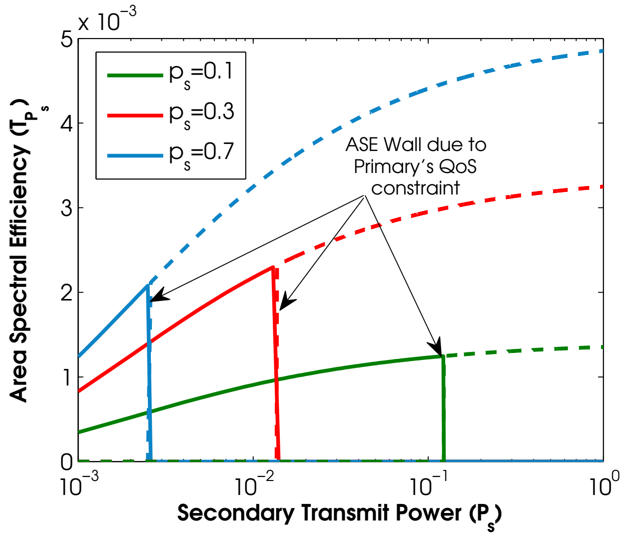

Figure 4.3: Area spectral efficiency (bits/s/Hz/m^2) of a cognitive underlay network with transmit power adaptation $\lambda_s = 10^{-2}$, $\lambda_p = 10^{-3}$, $P_p = 1$, $\alpha = 4$, $r_p = r_s = 4$, $\rho_{out}^{\{p\}} = 0.1$, $p_p = 0.4$, $m_p = m_s = 1$, $\gamma_{th}^{\{p\}} = 5$ dB and $\gamma_{th}^{\{s\}} = 3$ dB (see Eq. (4.17)).

ing the secondary MAP should increase the effective number of concurrent transmission sessions and hence the area spectral efficiency[4]. However, as indicated by Fig. 4.3, this is not necessarily the case. The maximum attainable area spectral efficiency for $p_s = 0.7$ is less than the efficiency obtained by employing $p_s = 0.3$. This validates that there exists an optimal operational MAP which when employed in conjunction with the transmit power adaptation maximizes the area spectral efficiency attained by the CRN. The detailed analytical characterization of p_s^* will be deferred until subsequent discussion.

Fig. 4.4 plots the area spectral efficiency of the CRN under the MAP adaptation scheme. As discussed earlier under this scheme, the maximum permissible density of the active secondary transmitter is bounded due to the primary user's QoS constraint (see Eq. (4.19)). Fig. 4.4 further consolidates this observation. Notice that the bound on the permissible MAP translates into an "area spectral efficiency wall". As demonstrated in Fig. 4.4 the location of the area spectral efficiency wall is strongly coupled with the channel

4 Nevertheless, an increase in the operational MAP will also translate into a higher co-channel interference to the primary user and hence a more stringent operational constraint by a reduction in the maximum permissible transmission power. The reduction in maximum permissible power will result in the reduction of the link success probability. Hence the gain obtained due to an increase in the simultaneous transmissions may vanish because of the reduction in the success probabilities of the individual links. This indicates that there may exist an optimal operational point where the reduction in the link success can be balanced by increasing the number of concurrent transmissions.

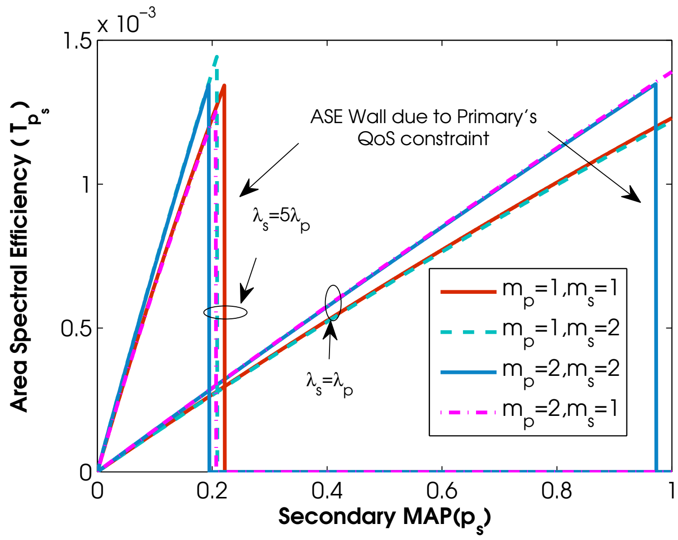

Figure 4.4: Area spectral efficiency (bits/s/Hz/m^2) of a cognitive underlay network under MAP adaptation with $\lambda_p = 10^{-3}$, $P_p = 1$, $P_s = 10^{-1}$, $\alpha = 4$, $r_p = r_s = 4$, $\rho_{out}^{\{p\}} = 0.1$, $p_p = 0.4$, $\gamma_{th}^{\{p\}} = 5$ dB and $\gamma_{th}^{\{s\}} = 3$ dB (see Eq. (4.19)).

propagation conditions, primary/secondary user density and the transmit power employed by the primary network.

The parameters m_p and m_s play a dual role, i.e., for instance m_p not only characterizes the fading severity of the channel between an arbitrary primary transmitter and receiver but also shapes the interference environment in which the CRN must operate. A small m_p reduces the link reliability of the primary user, which in turn enforces more stringent constraints on the secondary access. However, it also reduces the aggregate interference experienced by the secondary receivers. The area spectral efficiency of the CRN is jointly dependent on the density of users and the propagation conditions. When both the primary and the secondary networks are equally dense, the impact of the fading severity m_p dominates the performance as compared to m_s. This can be attributed to the higher transmit power employed by the primary users which bounds the CRN performance by primary inflicted interference (see Fig. 4.4). For a CRN with higher density than the collocated primary network, the dominant fading severity parameter is reversed. In other words, the performance is now dictated by m_s. This is as expected because the increased density limits the secondary network's performance by its own co-channel interference (see Fig. 4.4).

The primary to secondary transmit power ratio (η) is an important design parameter. Secondary users employing low transmit power result in a low aggregate interference and hence increase their chances of co-existing with the primary network. Fig. 4.5 plots the area spectral efficiency for several

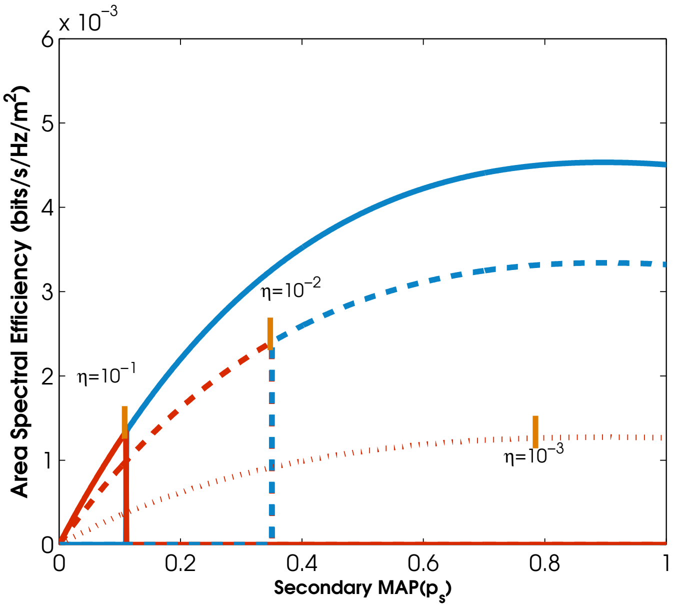

Figure 4.5: Area spectral efficiency (bits/s/Hz/m^2) under the MAP adaptation scheme for various value of η with $\lambda_s = 10^{-2}$, $\lambda_p = 10^{-3}$, $m_p = m_s = 1$, $\alpha = 4$, $r_p = r_s = 4$, $\rho_{out}^{\{p\}} = 0.1$, $p_p = 0.4$, $\gamma_{th}^{\{p\}} = 5$ dB and $\gamma_{th}^{\{s\}} = 3$ dB (see Eqs. (4.17) & (4.19)).

different values of η against the MAP. Reducing η: (i) pushes the spectral efficiency wall to the right along secondary MAP axis; and (ii) reduces the overall spectral efficiency. The former occurs due to the reduced interference caused to the primary users[5], while the later occurs due to a reduction in the received signal power at the CR receiver. Consequently, although a smaller η may push the conceivability boundary on the MAP spectral efficiency curve the attained performance may deteriorate due to the reduction in the overall spectral efficiency. This indicates that their may exist an optimal value of η where the reduction in the signal strength can be balanced by increasing the density of concurrent secondary transmissions. Note that for a fixed primary transmit power P_p, the optimal η^* reflects the existence of an optimal secondary transmit power say P_s^*.

The existence of an area spectral efficiency wall under the adaptation of either degree-of-freedom (MAP/transmit power) and optimal operating points for the remaining degree of freedom (transmit power/MAP) triggers two important design questions:

1. In terms of maximizing the secondary network throughput what is the optimal strategy? In other words, can secondary users maximize the

5 The reduction in co-channel interference at the primary receiver can be traded to increase the effective number of concurrent secondary transmissions.

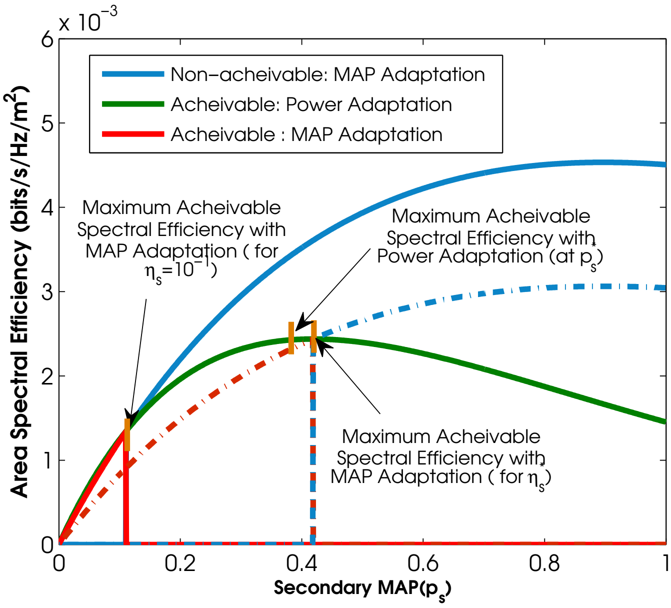

Figure 4.6: Area spectral efficiency (bits/s/Hz/m^2) comparison for the MAP and the transmit power adaptation with $\lambda_s = 10^{-2}$, $\lambda_p = 10^{-3}$, $m_p = m_s = 1$, $\alpha = 4$, $r_p = r_s = 4$, $\rho_{out}^{\{p\}} = 0.1$, $p_p = 0.4$, $\gamma_{th}^{\{p\}} = 5$ dB and $\gamma_{th}^{\{s\}} = 3$ dB (see Eqs. (4.17) & (4.19)).

attainable area spectral efficiency by exploiting one of these two degrees of freedom? The answer to this question is critical from the secondary network's perspective as adaptation of either parameter will satisfy the co-existence requirements imposed by the primary. However, the secondary spectral efficiency may differ.

2. How does the power adaptation scheme coupled with an optimal MAP selection compares to the MAP adaptation scheme with an optimal transmit power selection? Will both schemes provide comparable performance?

Fig. 4.6 seeks answers to these design questions by comparing the performance of the MAP and the transmit power adaptation schemes. As illustrated in the figure, the maximum spectral efficiency (for a certain arbitrary but fixed transmit power ratio, in this case $\eta = 10^{-1}$) under the MAP adaptation scheme is much higher than the one attained with the power adaptation. However, the maximum throughput under MAP adaptation cannot be attained due to the wall imposed by the primary user's QoS constraint. By contrast, if the secondary user selects p_s^* as a MAP and employs transmit power adaptation the area spectral efficiency far exceeds that for MAP adaptation. In brief, the power adaptation scheme coupled with optimal MAP selection outperforms the simple MAP adaptation scheme. The conceivability boundary of the MAP adaptation scheme can be pushed further by employing optimal transmit power ratio η^*. The maximum attainable spectral efficiency under MAP adaptation in conjunction with η^* is similar to the one obtained by employing transmit power adaptation at p_s^*. From these observations, it is obvious that sole adaptation of a single degree of freedom with an arbitrary selection of the other results in a sub-optimal performance in terms of spectral efficiency. The best strategy is to adapt one degree of freedom, while optimizing over the other. Moreover, in terms of performance it is immaterial that which degree is adapted and which one is optimized as long as the "adapat-and-optimize" rule is followed.

Key observations

1. In an underlay CRN, there exist two degrees of freedom, i.e., the transmit power and the MAP. In a large scale CRN adapting one of these parameters while keeping the other fixed, the attainable area spectral efficiency is bounded by a wall due to the primary user's QoS requirements. This wall can be broken, i.e. the area spectral efficiency can be increased by optimizing the fixed parameter. More specifically, the secondary user must adapt one design parameter and optimize the other to realise the maximum attainable performance. In brief, neither degree of freedom by itself is capable of unleashing the true potential of the network.

2. The CRN's throughput is jointly coupled with the propagation conditions, user density and the transmit power.

3. Both the transmit power and the MAP adaptations are identical from the primary users' perspective. Nevertheless, the secondary attainable throughput may differ depending on the selected operational point (MAP (p_s) or the transmission power (P_s)).

4. The area spectral efficiency of CRN can be maximized by selecting an optimal operational point. The optimal operational point is obtained by adapting either degree-of-freedom (MAP or transmit power) while optimizing over the remaining degree (transmit power or MAP). Fig. 4.7 depicts the optimal operational points under both adaptation schemes. Notice that the optimal operating point under both schemes is same. However, the area spectral efficiency performance for an arbitrary operational point may differ under both schemes[6].

6 From Eq. (4.18), it follows that the success probability of an arbitrary secondary link scales differently with respect to the transmit power and the MAP. The scaling with the transmit power is further coupled with the path-loss exponent which is not the case for the MAP. Consequently, the area spectral efficiency of a secondary network scales differently under

In order to avoid the redundancy, we will only characterize the optimal parameters under the power adaptation scheme. A similar characterization for the MAP adaptation scheme can be carried out in a straightforward manner.

A Note on Practical Implementation

In this article, we do not propose any specific protocol for implementation of the discussed adapt-and-optimize strategy. Our prime focus is in quantifying the attainable performance without restricting our analysis to a particular implementation. Nevertheless it is worth highlighting that the practical implementation can be realized in a straightforward manner. From Eq. (4.13) it is obvious that in order to adapt either degrees-of-freedom, the secondary network requires the knowledge of the following primary network parameters:

1. Primary user's desired QoS constraint expressed in terms of SIR threshold ($\gamma_{th}^{\{p\}}$) and the outage probability threshold $\rho_{out}^{\{p\}}$;
2. Average number of primary transmitters per unit area (λ_p);
3. Primary user's MAP (p_p) and the fading severity of its communication link (m_p);
4. Primary user's link distance (r_p) or average link distance if r_p is random variable.

With the precise knowledge of these parameters along with the knowledge of the CRN parameters allows robust implementation of the adaptat-and-optimize strategy. Consequently, the practical implementation of the protocol is closely coupled with the ways of obtaining such knowledge. Since the knowledge of these parameters can be obtained in either an online or offline mode, both dynamic and fixed implementations are possible. In other words, the adaptation and the optimization parameter can be computed prior to the deployment and CRs can use them to access the spectrum. Alternatively, CRs can compute these parameters in operational mode. The computation can either be based on the

- Explicit exchange of the parameters between the primary and the secondary users.
- Estimation of these parameters indirectly by learning and observing the radio environment.

The explicit exchange can be provisioned by employing a dedicated control channel, while the estimation can be based on the signal strength, retransmission frequency etc.

---

both schemes. This can be verified from Fig. 4.4 which can be considered as a two dimensional slice of Fig. 4.7.

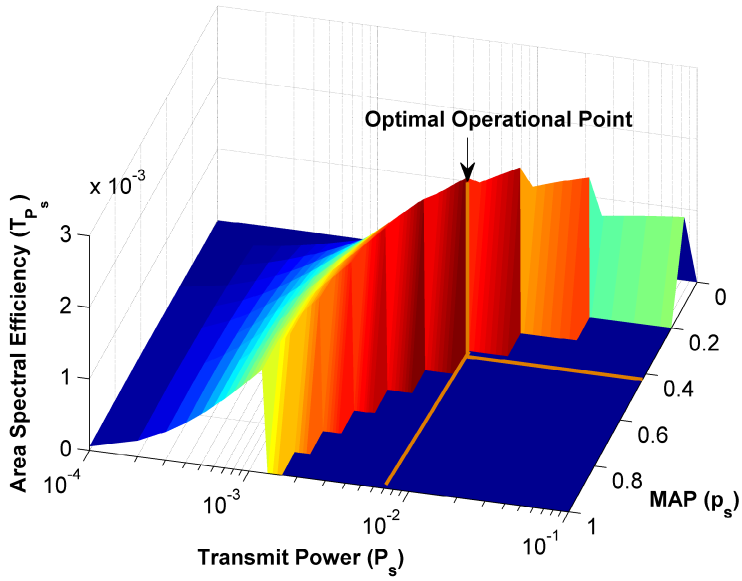

(a) Area spectral efficiency of underlay CRN under the transmit power adaptation scheme. Notice the spectral efficiency walls and existence of the optimal MAP.

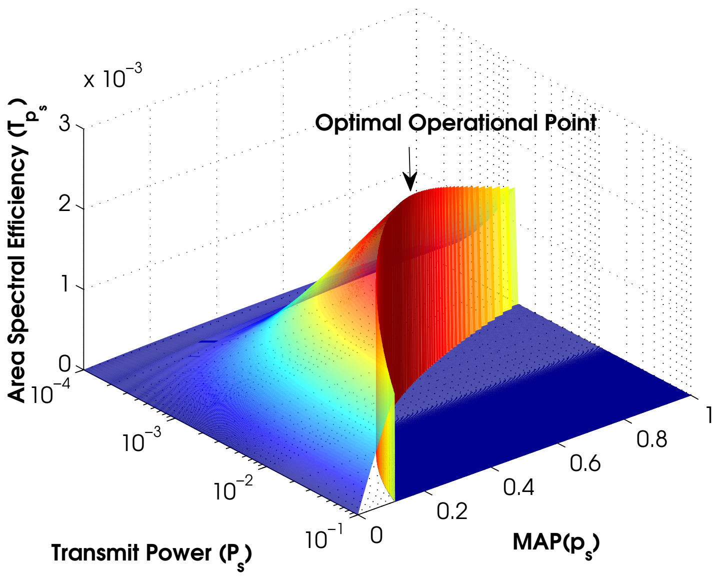

(b) Area spectral efficiency of underlay CRN under the MAP adaptation scheme. Notice the spectral efficiency walls and the existence of the optimal transmit power.

Figure 4.7: Optimal operating points under transmit power and MAP adaptation schemes for $\lambda_s = 10^{-2}$, $\lambda_p = 10^{-3}$, $P_p = 1$, $\alpha = 4$, $r_p = r_s = 4$, $\rho_{out}^{\{p\}} = 0.1$, $p_p = 0.4$, $m_p = m_s = 1$, $\gamma_{th}^{\{p\}} = 5$ dB and $\gamma_{th}^{\{s\}} = 3$ dB.

4.7 OPTIMIZATION UNDER TRANSMIT POWER CONTROL

Optimal MAP under transmit power control.

As illustrated in the previous section, there exists an optimal MAP (p_s^*) which maximizes the bits/s/Hz performance in a unit area. Also from Eq. (4.17), we notice that there exists an optimal SIR threshold $\gamma_{th}^{\{s\}*}$ for the secondary user at which its throughput performance is maximized. To this end, in this section we quantify these optimal operating points.

4.7.1 *Optimal MAP for Secondary Users*

As depicted in Fig. 4.2, there exists an optimal operating MAP which can be employed by secondary users to maximize their achievable spatial throughput. The existence of this optimal throughput can be credited to the fact that the link success probability of the secondary user is a decreasing function of its MAP (p_s) under the transmission power control scheme. However, the effective transmission density ($\lambda_s p_s$) increases with an increase in MAP (p_s). Hence, this opposing behavior suggests existence of an optimal operating point.

Relationship between the link SP and secondary user's employed MAP under transmit power adaptation scheme.

Lemma 4.2 *The link success probability of the secondary user is a decreasing function of its employed MAP (p_s) when CRs employ transmit power adaptation.*

PROOF: From Eq. (4.13), the maximum transmit power P_s can be quantified as

$$P_s \leq \left[\frac{\kappa_1 \left(\rho_{out}^{\{p\}}, m_p, m_s, \alpha, \lambda_p, p_p, \gamma_{th}^{\{p\}}, r_p^2, P_p \right)}{\lambda_s p_s} \right]^{\frac{1}{\delta}}, \tag{4.20}$$

where $\kappa_1(.)$ is obtained by taking $\lambda_s p_s$ as a common factor from the denominator of Eq. (4.13). For the sake of simplicity, we will denote $\kappa_1(.)$ simply by κ_1. Then employing Eq. (4.18) we have that

$$\mathbb{P}_{suc}^{\{s\}}(p_s) \leq \exp\left\{ -\pi \lambda_s p_s \frac{\Gamma(m_s+\delta)}{\Gamma(m_s)} \kappa_2 \right\}, \tag{4.21}$$

where κ_2 is given by

$$\kappa_2 = \left(1 - \frac{\lambda_p p_p \Gamma\left(m_p+\delta\right) \pi \Gamma(m_p-\delta) r_p^2 \left(\gamma_{th}^{\{p\}}\right)^{\delta}}{\Gamma(m_p)^2 \ln\left(\frac{1}{1-\rho_{out}^{\{p\}}}\right)}\right)^{-1} \times \frac{\Gamma\left(m_s-\delta\right)}{\Gamma(m_s)}\left(\gamma_{th}^{\{s\}}\right)^{\delta} r_s^2. \tag{4.22}$$

Proposition 5 follows from the Eq. (4.21) . □

Notice that the secondary user's link success probability is independent of the transmit power employed by the primary user. This indeed follows from the adaptation rule where secondary users compensate for the primary users' transmit power when selecting their own operating point (see Eq. (4.13)).

Optimal MAP for CRN under transmit power adaptation.

Theorem 4.3 *The optimal MAP (p_s^*) which maximizes the maximum attainable area spatial efficiency for secondary network under the transmit power control scheme subject to a Nakagami-m fading environment is given by*

$$p_s^* = \frac{\Gamma(m_s+\delta)}{\pi\lambda_s\kappa_2\Gamma(m_s)}. \tag{4.23}$$

PROOF: From Eqs. (4.17) and (4.21), we can write for the area spectral efficiency of the secondary underlay network

$$\mathcal{T}_{\mathcal{P}_s} \leq \bar{\mathcal{T}}_{\mathcal{P}_s} = \lambda_s p_s \log_2\left(1+\gamma_{th}^{\{s\}}\right) \times \exp\left\{-p_s \underbrace{\pi\lambda_s \frac{\Gamma(m_s+\delta)}{\Gamma(m_s)}\kappa_2}_{\kappa_3}\right\}, \tag{4.24}$$

Then the optimal MAP (p_s^*) is the solution of

$$\frac{\partial\bar{\mathcal{T}}_{\mathcal{P}_s}}{\partial p_s} = 0. \tag{4.25}$$

So from Eq. (4.24), we obtain

$$\frac{\partial\bar{\mathcal{T}}_{\mathcal{P}_s}}{\partial p_s} = \lambda_s \log_2\left(1+\gamma_{th}^{\{s\}}\right) \exp\left\{-p_s\kappa_3\right\}\left[1-\kappa_3 p_s\right]. \tag{4.26}$$

Finally, from Eq. (4.26) and Eq. (4.25) we obtain Eq. (4.23). □

Remarks

Impact of secondary user density.

1. The optimal MAP (p_s^*) is inversely related to the number of secondary users per unit area (λ_s). Notice that in the context of a classical analysis of Slotted ALOHA protocol, a similar result is obtained by Markovian/Queuing theoretic analysis [110]. Fig. 4.8 confirms this inverse relation. Notice that the area spectral efficiency curve follows a similar trend for all values of λ_s. However, the rate of variation (increase and decrease) with respect to the MAP significantly differs with the change in CR density. Moreover, the maximum attainable spectral efficiency remains same when an optimal MAP (p_s^*) is employed by the CRN. This is due to the inverse proportionality of the MAP with density. So, the area spectral efficiency while employing optimal throughput can be quantified as

$$\mathcal{T}_{ps}^* = \frac{e^{-1}\Gamma(m_s+\delta)\log_2\left(1+\gamma_{th}^{\{s\}}\right)}{\pi\kappa_2\Gamma(m_s)}, \tag{4.27}$$

where $e \approxeq 0.277$.

Impact of link distance and desired SIR threshold.

2. From Eq. (4.23) and (4.22), it follows that p_s^* must decay in a square root manner to cater for the increase in the link distance r_s. However, the decay with respect to the desired SIR threshold is coupled with the large scale propagation conditions. Fig. 4.8 shows the impact of distance variation on the area spectral efficiency. Similar to p_s^*, the square root decay is experienced in the maximum attainable area spectral efficiency (see Eqs. (4.23) and (4.27)). The impact of path-loss exponent and the desired SIR threshold on bits/sec/Hz/m^2 performance of underlay CRN is depicted in Fig. 4.9.

3. As stated earlier Eq. (4.22) is independent on the primary user's transmission power (P_p). Hence the choice of p_s^* is also independent of P_p.

4.7.2 *Optimal SIR threshold for Secondary User*

In this sub-section, we characterize the optimal SIR threshold for the cognitive underlay network. More specifically, we want to optimize the achievable area spectral efficiency of the secondary network when CRs employ optimal MAP, p_s^*.

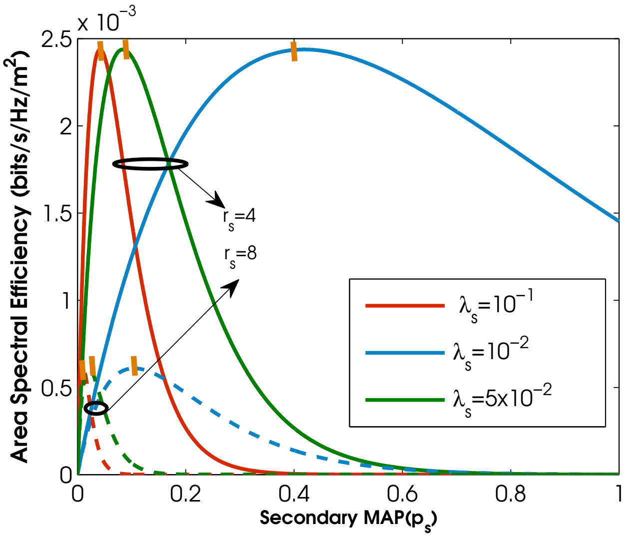

Figure 4.8: Impact of secondary user density and the link distance on the area spectral efficiency of the cognitive underlay network with $\lambda_p = 10^{-3}$, $m_p = m_s = 1$, $\alpha = 4$, $r_p = 4$, $\rho_{out}^{\{p\}} = 0.1$, $p_p = 0.4$, $\gamma_{th}^{\{p\}} = 5$ dB and $\gamma_{th}^{\{s\}} = 3$ dB (see Eq. (4.17)).

Optimal SIR threshold under power adaptation scheme.

Proposition 4.1 *The optimal SIR threshold ($\gamma_{th}^{\{s\}*}$) which maximizes the secondary user's attainable spectral efficiency in the presence of a col-located primary network under the transmit power adaptation scheme, when secondary links suffer Rayleigh fading, is given by*

$$\gamma_{th}^{\{s\}*} = \exp\left(-\mathcal{W}\left(-\delta\exp(-\delta)\right) + \delta\right) - 1, \tag{4.28}$$

where $\mathcal{W}(.)$ is the principal branch of the Lambert W function.

PROOF: The proof follows similar steps as in [111] (Proposition 6). □

Remark

The optimal SIR threshold $\gamma_{th}^{\{s\}*}$ only depends on the path-loss exponent. Moreover, $\gamma_{th}^{\{s\}*}$ is function of the modulation and coding scheme selected by the secondary user. For instance, given a certain fixed desired bit error rate threshold (say $\bar{P}_b$) the conditional bit error probability expressions for a certain constellation size can be inverted to obtain $\gamma_{th}^{\{s\}*}$. Hence, the optimal

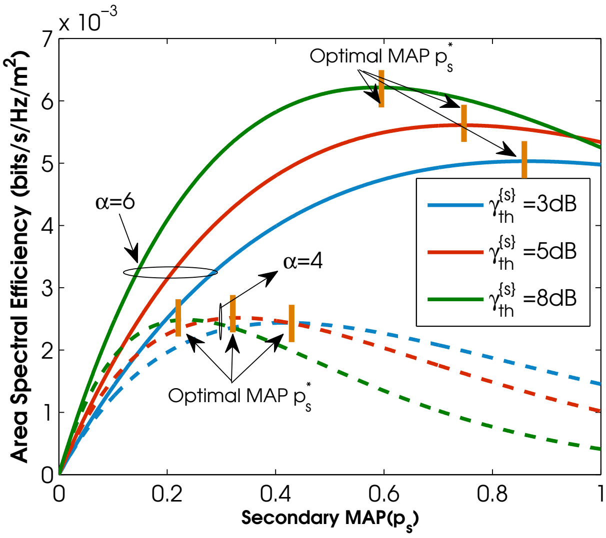

Figure 4.9: Impact of secondary user desired SIR threshold and the path-loss exponent on the area spectral efficiency of the cognitive underlay network-with $\lambda_s = 10^{-2}$, $\lambda_p = 10^{-3}$, $m_p = m_s = 1$, $r_p = r_s = 4$, $\rho_{out}^{\{p\}} = 0.1$, $p_p = 0.4$ and $\gamma_{th}^{\{p\}} = 5$ dB. (see Eq. (4.17)).

constellation size is only a function of the path-loss exponent and does not depend on the secondary and primary network parameters.

4.8 POINT-TO-POINT & BROADCAST UNDERLAY CRN

In the previous sections, we derived closed form expressions for the maximum attainable area spectral efficiency of a cognitive underlay network under transmit power and MAP adaptation. In this section, we extend the already developed analytical framework to different networking scenarios. More specifically, we extend the bipolar spatial model to more generic configurations, i.e.,

Nearest neighbor transmission is of a particular importance in dense networks where permissible transmission power is quite low.

1. Point-to-Point Underlay Networks: We study two different point-to-point communication scenarios: (i) Point-to-point nearest receiver transmission; (ii) Point-to-point n^{th} receiver transmission. These two scenarios are representative of a multi-hop transmission strategy which may result under certain classes of routing protocols.

2. Broadcast Underlay Networks: We extend the secondary spatial model for the broadcast networks where the transmission is intended for multiple receivers. The broadcast networks are of practical importance for robust information dissemination.

4.8.1 *Point-to-Point Underlay Networks*

In point-to-point cognitive underlay networks, each CR transmitter communicates with a single destination. The bipolar MANET model, used in Section 4.2, is indeed an example of such point-to-point communication networks. As discussed before, the bipolar model assumes that under the Slotted ALOHA protocol, each CR transmitter has its corresponding receiver at a fixed distance r_s. From a practical perspective, it is of more importance to extend this simple model to a more sophisticated scenario. For instance, consider the case where each CR transmitter wants to communicate with a particular CR node that has deferred its transmission for a given time slot. The criteria for selection of a particular CR node depends on a networking scenario. Notice, that such a receiver association model can also be visualized as a snapshot of a multi hop relaying strategy at an arbitrary time slot. In this chapter, we study two different receiver selection models for point-to-point cognitive underlay networks.

4.8.1.1 *Underlay Networks with Nearest Neighbor Transmission*

As implied by the name, in point-to-point underlay networks with nearest neighbor transmission, an arbitrary CR transmitter $\boldsymbol{x} \in \Pi_s^{\{TX\}}$ intends to communicate with its nearest neighbor which has deferred its transmission in a given time slot.

ASE of a CRN under NN transmission.

Theorem 4.4 *The area spectral efficiency of a large scale point-to-point nearest neighbor underlay cognitive networks can be quantified as in Eq. (4.29).*

$$\mathcal{T}_{p2p}^{nn} \leq \left[\frac{\lambda_s p_s \log_2\left(1+\gamma_{th}^{\{s\}}\right)}{1 + \frac{\left(\lambda_p p_p \left(\frac{P_p}{P_s}\right)^{\delta} \frac{\Gamma(m_p+\delta)}{\Gamma(m_p) m_p^{\delta}} + \lambda_s p_s \frac{\Gamma(m_s+\delta)}{\Gamma(m_s) m_s^{\delta}}\right) \frac{\Gamma(m_S-\delta)}{\Gamma(m_s)} \left(\gamma_{th}^{\{s\}} m_s\right)^{\delta}}{\lambda_s(1-p_s)}} \right]. \tag{4.29}$$

PROOF: Let R_s denote the distance separating a CR transmitter $\boldsymbol{x} \in \Pi_s^{\{TX\}}$ from the nearest node which has deferred its transmission. Then the CDF of the random variable R_s follows the Poisson law as follows:

$$\begin{aligned} \mathcal{F}_{R_s}(r_s) &= 1 - \Pr\{\Pi_s \backslash \Pi_s^{\{TX\}} (b(x, r_s)) = \emptyset\}, \\ &= 1 - \exp\left(-\lambda_s(1-p_s)\pi r_s^2\right). \end{aligned} \tag{4.30}$$

Here $b(x, r)$ denotes a ball/disc of radius r centered at point x. The PDF of the random variable R_s can easily be obtained as

$$f_{R_s}(r_s) = \lambda_s(1-p_s)2\pi r_s \exp\left(-\lambda_s(1-p_s)\pi r_s^2\right).$$

Notice that the expression of success probability derived in Eq. (4.18) in the current scenario plays the role of conditional success probability given a certain distance r_s. Then applying the expectation with respect to the random link distance R_s on Eq. (4.18), we obtain Eq. (4.31).

$$\mathbb{P}_{suc}^{\{s\}}(P_s, p_s) \quad \leq \quad \mathbb{E}_{R_s}\left[\exp\left\{-\pi\zeta r_s^2\right\}\right], \tag{4.31}$$

where

$$\begin{aligned}\zeta \quad &= \quad \left(\lambda_p p_p \left(\frac{P_p}{P_s}\right)^{\delta} \frac{\Gamma(m_p+\delta)}{\Gamma(m_p)m_p^{\delta}} + \lambda_s p_s \frac{\Gamma(m_s+\delta)}{\Gamma(m_s)m_s^{\delta}}\right) \\ &\times \quad \frac{\Gamma(m_s-\delta)}{\Gamma(m_s)}\left(\gamma_{th}^{\{s\}} m_s\right)^{\delta}.\end{aligned} \tag{4.32}$$

So, the success probability of the secondary link can be computed as

$$\begin{aligned}\mathbb{P}_{suc}^{\{s\}}(P_s, p_s) \quad &= \quad \int_0^{\infty} \lambda_s(1-p_s)2\pi r_s \exp\left\{-\pi\zeta r_s^2\right\} \\ &\times \quad \exp\left\{-\lambda_s(1-p_s)\pi r_s^2\right\} dr_s, \\ &= \quad \lambda_s(1-p_s)2\pi \int_0^{\infty} r_s \exp\left\{-\pi\right. \\ &\times \quad \left.(\zeta + \lambda_s(1-p_s))\, r_s^2\right\} dr_s, \\ &= \quad \frac{1}{\frac{\zeta}{\lambda_s(1-p_s)}+1}.\end{aligned} \tag{4.33}$$

□

Independence of the link SP from secondary user density.

Corollary 4.1 *Under a transmit power control scheme the link success probability of the cognitive underlay network is independent of the density of the secondary network (λ_s).*

PROOF: Let $\bar{\kappa}_2 = \kappa_2|_{r_S=1}$, then from Eq. (4.21), we have

$$\mathbb{P}_{suc}^{\{s\}}\left(p_s|_{R_s=r_s}\right) \leq \exp\left\{-\pi\lambda_s p_s \frac{\Gamma(m_s+\delta)}{\Gamma(m_s)} \bar{\kappa}_2 r_s^2\right\}.$$

Employing the expectation as in the proof of Theorem 4.4, the un-conditional $\mathbb{P}_{suc}^{\{s\}}$ is obtained as

$$\mathbb{P}_{suc}^{\{s\}}(p_s) \leq \left[\frac{1}{1 + \frac{p_s}{(1-p_s)} \frac{\Gamma(m_{s+\delta})}{\Gamma(m_s)} \bar{\kappa}_2}\right]. \tag{4.34}$$

Hence, the link success probability is independent of the secondary network density and only depends on the ratio of the deferring and transmitting nodes per unit area. □

From 4.1, it follows that the area spectral efficiency of the point-to-point underlay network with nearest neighbor transmission is not influenced by the secondary user density. Intuitively, this can be explained by considering the interference which increases with an increase in node density (for a given MAP) while the distance between the nearest neighbor and its corresponding CR transmitter decreases at the same rate. Hence the density of the secondary nodes does not affect the link success probability.

Optimal MAP for the NN point-to-point underlay CRN.

Theorem 4.5 *The optimal MAP (p_s^*) which maximizes the area spectral efficiency for the nearest neighbor point-to-point underlay network under a Rayleigh fading environment is given as the solution of following quadratic equation:*

$$(\Omega - 1)\, p_s^2 - 2\Omega p_s + \Omega = 0. \tag{4.35}$$

where $\Omega = \frac{\Gamma(m_s)}{\Gamma(m_s+\delta)\bar{\kappa}_2}$. *Since* $0 \leq p_s \leq 1$ *then the only allowable solution (verified by evaluating p_s^*) is*

$$p_s^* = \frac{1}{1 + \sqrt{\frac{\Gamma(m_s+\delta)\bar{\kappa}_2}{\Gamma(m_s)}}}. \tag{4.36}$$

PROOF: The proof follows maximization of area spectral efficiency in Eq. (4.29).

□

Remarks

1. The optimal MAP (p_s^*) is independent of the secondary user density λ_s. This follows from the fact that under the transmit power adaptation scheme, the success probability of a secondary user is independent from the secondary user density. Rather it only depends on the average number of receivers per transmitter present in secondary network, i.e.,

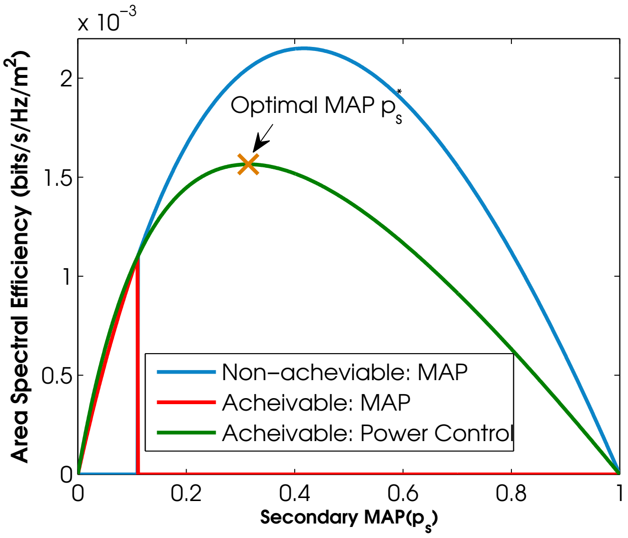

Figure 4.10: Area spectral efficiency of a cognitive underlay network employing the nearest neighbour transmission with $\lambda_s = 10^{-2}$, $\lambda_p = 10^{-3}$, $m_p = m_s = 1$, $\alpha = 4$, $r_p = 4$, $\rho_{out}^{\{p\}} = 0.1$, $p_p = 0.4$, $\gamma_{th}^{\{p\}} = 5$ dB and $\gamma_{th}^{\{s\}} = 3$ dB (see Eqs. (4.29) & (4.36)).

$\frac{1-p_s}{p_s}$. Notice that the impact of the density is hidden in the average number of receivers per transmitters as for the fixed p_s increasing the density impacts both the number of transmitters and the relays proportionally.

2. The optimal MAP (p_s^*) depends on the propagation characteristics of both the secondary communication and the primary interference channel.

3. A transmit power adaptation scheme with optimal MAP (p_s^*) is more efficient than a MAP adaptation mechanism for point-to-point underlay networks employing nearest neighbor transmission. Fig. 4.10 compares the performance of the MAP and the power adaptation schemes in terms of their area spectral efficiency. The optimal MAP obtained from Eq. (4.36) is also plotted in Fig. 4.10.

4. Notice that the area spectral efficiency curve for the nearest receiver model differs from the one obtained under the bipolar model. More specifically, with the nearest neighbor transmission and the MAP adaptation, there exists an optimal MAP which will maximize the overall area spectral efficiency. However, such an optimal choice may not be present in case of the bipolar networks. Nevertheless, as shown in Fig. 4.10 such an operating point may lie beyond the acheivability wall and hence the CRN must optimize its transmit power to extend its operational range. In brief, similar to the bipolar case, the nearest neighbor

CRN underlay network also requires tuning of both degrees of freedom (i.e., MAP and transmission power).

4.8.1.2 *Point-to-point Underlay Networks with n^{th} Neighbor Transmission*

Notice that for $n = 1$, the point-to-point underlay network reduces to a nearest neighbor transmission model.

In n^{th} neighbor based cognitive underlay networks, each CR transmitter transmits to the n^{th}-distant node which has deferred its transmission inside a sector with a central angle ϕ. This scenario can be considered as a single snapshot of the multi-hop forwarding protocols where n is selected such that the desired reliability of the link is attained while satisfying the energy constraints. More specifically, for a small value of n, the routing policy utilizes small hops on which a high reliability can be attained while requiring the least number of re-transmissions. However, the progress of the packet towards its intended destination requires a large number of small hops which will increase the energy penalty. By contrast, if a large value of n is employed the a large number of retransmissions must be incurred for attaining a high link reliability. Hence the energy consumption due to retransmission will increase at the cost of decreasing the energy required to traverse small paths. Detailed discussion on energy efficiency and relaying for underlay CRNs is beyond scope of this chapter. The central angle ϕ controls the overall directionality of the transmission.

ASE for n^{th} neighbor underlay CRN.

Theorem 4.6 *The area spectral efficiency of the n^{th} neighbor underlay cognitive radio networks can be quantified as in Eq. (4.37).*

$$\mathcal{T}_{p2p}^{nth} \leq \left[\frac{\lambda_s p_s \log_2\left(1+\gamma_{th}^{\{s\}}\right)}{\left(\frac{2\pi\left(\lambda_p p_p \left(\frac{P_p}{P_s}\right)^{\delta} \frac{\Gamma(m_p+\delta)}{\Gamma(m_p) m_p^{\delta}} + \lambda_s p_s \frac{\Gamma(m_s+\delta)}{\Gamma(m_s) m_s^{\delta}}\right) \frac{\Gamma(m_s-\delta)}{\Gamma(m_s)} \left(\gamma_{th}^{\{s\}} m_s\right)^{\delta}}{\lambda_s(1-p_s)\phi} + 1\right)^n} \right]. \tag{4.37}$$

PROOF: Consider the link success probability of a secondary user conditional on the link distance r, as given in Eq. (4.31). The distance distribution to the n^{th} neighbor within the sector with central angle ϕ is given by

$$\begin{aligned} \mathcal{F}_{R_n}(r) &= 1 - \Pr\{\Pi_s \backslash \Pi_s^{\{TX\}} \left(Sec(o,r,\phi)\right) = n-1\}, \qquad (4.38) \\ &= 1 - \sum_{i=0}^{n-1} \frac{\left(\frac{\lambda_s(1-p_s)\phi}{2}\right)^i}{i!} \exp\left(-\frac{\lambda_s(1-p_s)\phi}{2} r^2\right), \end{aligned}$$

where $Sec(o, r, \phi)$ denotes a sector of radius r centered at origin with central angle ϕ. Selection of the origin follows from the Slivnyak's theorem. The PDF of the random link distance (R_n) can be derived as

$$f_{R_n}(r) = \frac{2}{\Gamma(n)} \left(\frac{\lambda_s(1-p_s)\phi}{2} \right)^n r^{2n-1} \exp\left(-\frac{\lambda_s(1-p_s)\phi}{2} r^2 \right). \quad (4.39)$$

Utilizing Eqs. (4.31) and (4.39) we obtain

$$\begin{aligned} \mathbb{P}_{suc}^{\{s\}}(P_s, p_s) \leq= & \int_0^\infty \frac{2}{\Gamma(n)} \left(\frac{\lambda_s(1-p_s)\phi}{2} \right)^n r^{2n-1} \quad (4.40) \\ \times & \exp\{-\pi\zeta r^2\} \exp\left(-\frac{\lambda_s(1-p_s)\phi}{2} r^2 \right) dr, \\ = & \frac{2}{\Gamma(n)} \left(\frac{\lambda_s(1-p_s)\phi}{2} \right)^n \int_0^\infty r^{2n-1} \\ \times & \exp\left\{ - \underbrace{\left(\pi\zeta + \frac{\lambda_s(1-p_s)\phi}{2} \right) r^2}_{u} \right\} dr, \\ = & \frac{\left(\frac{\lambda_s(1-p_s)\phi}{2} \right)^n \int_0^\infty u^{n-1} \exp\{-u\} du}{\Gamma(n) \left(\pi\zeta + \frac{\lambda_s(1-p_s)\phi}{2} \right)^n}. \\ = & \left[\frac{1}{\frac{2\pi\zeta}{\lambda_s(1-p_s)\phi} + 1} \right]^n. \end{aligned}$$

Finally, Eq. (4.37) can be obtained by employing the definition of area spectral efficiency. □

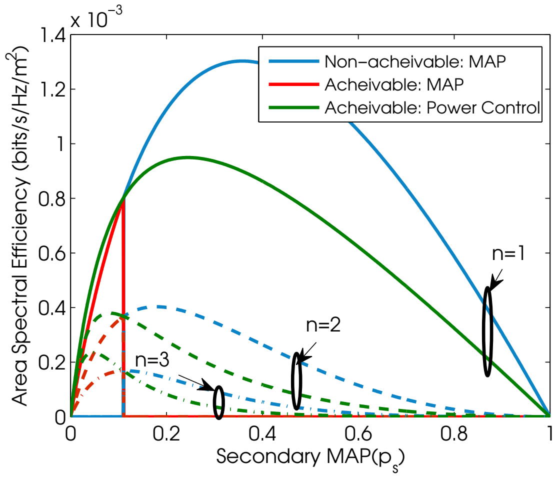

Figure 4.11: Area spectral efficiency of a cognitive underlay network employing the n^{th} neighbour transmission with $\phi = \pi$, $\lambda_s = 10^{-2}$, $\lambda_p = 10^{-3}$, $m_p = m_s = 1$, $\alpha = 4$, $r_p = 4$, $\rho_{out}^{\{p\}} = 0.1$, $p_p = 0.4$, $\gamma_{th}^{\{p\}} = 5$ dB and $\gamma_{th}^{\{s\}} = 3$ dB (see Eq. (4.37)).

Optimal MAP for n^{th} neighbor CRN under transmit power control.

Theorem 4.7 *The optimal secondary MAP under transmit power control when both the interference and the communication channels suffers Rayleigh fading and each secondary transmitter communicates to n^{th} secondary user, can be characterized as in Eq. (4.41):*

$$p_s^* = \frac{-\omega_1 + \sqrt{\omega_1^2 + 4\omega_2}}{2\omega_2}, \tag{4.41}$$

where $\omega_1 = \kappa_3(n-1) + 2$, $\omega_2 = \kappa_3 - 1$ *and* $\kappa_3 = \frac{2\pi}{\phi} \frac{\Gamma(m_s+\delta)}{\Gamma(m_s)} \bar{\kappa}_2$.

Remarks

Optimal MAP is a cross layer parameter.

1. The optimal MAP for transmit power adaptation is strongly coupled with the relaying scheme, i.e., the MAP is a cross layer parameter which can be tuned to maximize the area spectral efficiency. Fig. 4.11 confirms this observation. The figure also depicts an exponential decrease in the spectral efficiency with an increase in the index of the intended receiver. Moreover, the optimal MAP (p_s^*) decreases exponentially with the decrease in the central angle ϕ. Hence the increase in MAP is attained at the cost of reduced directionality of transmission.

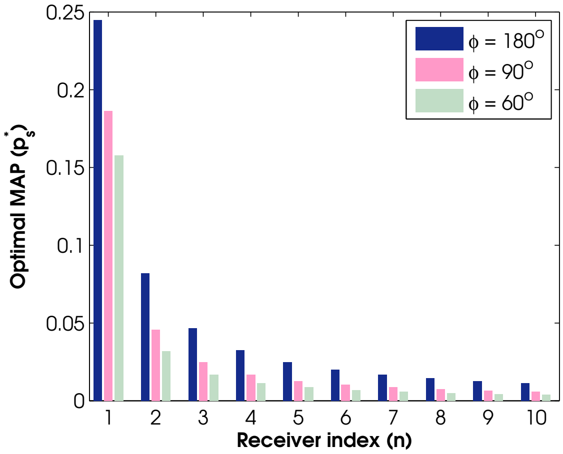

Figure 4.12: Optimal MAP vs. the receiver index n for varying central angle ϕ with $\lambda_s = 10^{-2}$, $\lambda_p = 10^{-3}$, $m_p = m_s = 1$, $\alpha = 4$, $r_p = 4$, $\rho_{out}^{\{p\}} = 0.1$, $p_p = 0.4$, $\gamma_{th}^{\{p\}} = 5$ dB and $\gamma_{th}^{\{s\}} = 3$ dB (see Eq. (4.41)).

2. The maximum feasible MAP under the transmit probability adaptation scheme does not depend on the secondary transmitter receiver separation and hence is independent from the receiver index n (see Fig. 4.11).

Maximum permissible MAP does not change with receiver index n

3. While the area spectral efficiency decreases with increasing n, considering the multi-hop scenario the effective progress of the packet towards its destination increases. Hence a CR can attain a high spectral efficiency by communicating with the nearest neighbor but at the cost of high end-to-end delay because of the increased number of hops. By contrast CRs can reduce the delay by using long hops (i.e., high values of n) but at the cost of decreased spectral efficiency. Hence there exists a tradeoff between the delay and the spectral efficiency.

4.8.2 *Broadcast Underlay Cognitive Radio Networks*

In this section, we employ the statistical machinery developed in previous subsections to characterize the information flow per unit area in a cognitive broadcast underlay network. In cognitive broadcast networks each secondary transmitter $\boldsymbol{x} \in \Pi_s^{\{TX\}}$ has a broadcast cluster of radius r_{BS}. The transmission from a secondary user $\boldsymbol{x}$ is intended for all nodes which defer their transmission and lie inside its corresponding broadcast cluster. The broadcast messages from different secondary transmitters is not necessarily the same. Such a scenario corresponds to an infra-structured cognitive underlay network where the spatial randomness is inevitable due to uncoordinated deployment. Notice that the optimal deployment in a regular manner in a regular lattice structure is often not feasible due to environment and cost.

No. of successful broadcast transmission receipents.

Definition 4.2 *Let the point process of intended broadcast receivers be denoted as* $\Pi_s^{\{RX\}} = \Pi_s \backslash \Pi_s^{\{TX\}}$. *Furthermore, in order to accommodate the flat fading channel, consider the Marked Poisson Process* $\bar{\Pi}_s^{\{RX\}}$ *constructed by assigning i.i.d. fading marks to each broadcast receiver with respect to the probe broadcast transmission. Then the number of secondary receivers which can successfully decode the broadcast message from a typical secondary transmitter within each cluster is given by*

$$\Lambda_{BC} = \mathbb{E}\left(\sum_{\boldsymbol{y} \in b(o, r_{BS}) \cap \Pi_s^{\{RX\}}} \mathbb{1}\left(\mathrm{SIR}(h_{\boldsymbol{y}}, \|\boldsymbol{y}\|) \geq \gamma_{th}^{\{s\}} \right) \right), \tag{4.42}$$

where $\mathrm{SIR}(h_{\boldsymbol{y}}, \|\boldsymbol{y}\|)$ *is the received SIR at the cognitive broadcast receiver* $\boldsymbol{y}$ *located at a distance* $\|\boldsymbol{y}\|$ *from the origin and experiencing small scale fading channel,* $h_{\boldsymbol{y}}$. *Here, without any loss of generality, we center the typical cognitive transmitter at the origin. The definition is not affected by the positioning of the transmitter since the point process of broadcast receivers is stationary.*

Broadcast ASE of underlay CRN.

Definition 4.3 *The broadcast area spectral efficiency of the cognitive underlay networks is defined as*

$$\begin{aligned} \mathcal{T}_i^{BC} &= \lambda_s p_s \Lambda_{BC} \log_2\left(1 + \gamma_{th}^{\{s\}}\right) \\ &\quad \textit{with } i = \{\mathcal{P}_s, p_s\}. \end{aligned} \tag{4.43}$$

The broadcast area spectral efficiency is the number of bits transmitted times the number of successful recipients within each cluster weighed by the number of concurrent transmissions. Notice that the broadcast clusters may overlap with each other. However, for most of the practical modulation schemes $\gamma_{th}^{\{s\}} \geq 1$ and this implies that each broadcast receiver is associated with a maximum of one broadcast cluster. Moreover, the broadcast efficiency can be treated as a probability of success for each cluster. Hence the definition is consistent with the point-to-point case.

Cardinality of the successful broadcast cluster.

Theorem 4.8 *The average number of secondary receivers which can successfully decode a transmission in a typical cognitive underlay broadcast cluster can be quantified as*

$$\Lambda_{BC} \leq \lambda_s(1-p_s)\left[\frac{1-\exp\left\{-\pi\zeta r_{BS}^2\right\}}{\zeta}\right], \tag{4.44}$$

where ζ is defined in Eq. (4.31).

PROOF: Consider the polar transformation of the intensity of the HPPP $\Pi_s^{\{RX\}}$ given by

$$\lambda_s(r) = \lambda_s(1-p_s)2\pi r. \tag{4.45}$$

Employing Silvnyak's theorem [109], consider a typical cognitive broadcast transmitter located at the origin. The HPPP of broadcast receivers $\Pi_s^{\{RX\}}$ can be modified to accommodate the flat fading propagation environment by constructing a Marked Poisson Process $\bar{\Pi}_s^{\{RX\}}$:

$$\bar{\Pi}_s^{\{RX\}} = \left\{[\boldsymbol{x}, h_{\boldsymbol{x}}] : \boldsymbol{x} \in \Pi_s^{\{RX\}}\right\}. \tag{4.46}$$

In order to cater for the required QoS of each broadcast transmitter, additional marks are introduced which depend upon the location, the channel gains and i.i.d. interference experienced from both co-channel primary and secondary users. That is:

$$\tilde{\Pi}_s^{\{RX\}} = \left\{[\boldsymbol{x}, h_{\boldsymbol{x}}, \mathbb{1}(\gamma(\boldsymbol{x}, h_{\boldsymbol{x}})), I_p, I_s] : \forall [\boldsymbol{x}, h_{\boldsymbol{x}}] \in \bar{\Pi}_s^{\{RX\}}\right\}, \tag{4.47}$$

where the SIR at an arbitrary receiver $\boldsymbol{x}$ is given by

$$\gamma(\boldsymbol{x}, h_{\boldsymbol{x}}) = \frac{P_p h_{\boldsymbol{x}} l(\|\boldsymbol{x}_i\|)}{\underbrace{\sum_{i\in\Pi_p^{\{TX\}}} P_p h_i l(\|\boldsymbol{x}_i\|)}_{I_p} + \underbrace{\sum_{j\in\Pi_s^{\{TX\}}} P_s g_j l(\|\boldsymbol{x}_j\|)}_{I_s}}. \tag{4.48}$$

The inhomogenous Poisson process $\tilde{\Pi}_s^{\{RX\}}$ effectively corresponds to the broadcast receivers that can decode transmissions from the probe broadcast transmitter. Considering an arbitrary area say $\mathcal{A} \in \mathbb{R}^2$ the average num-

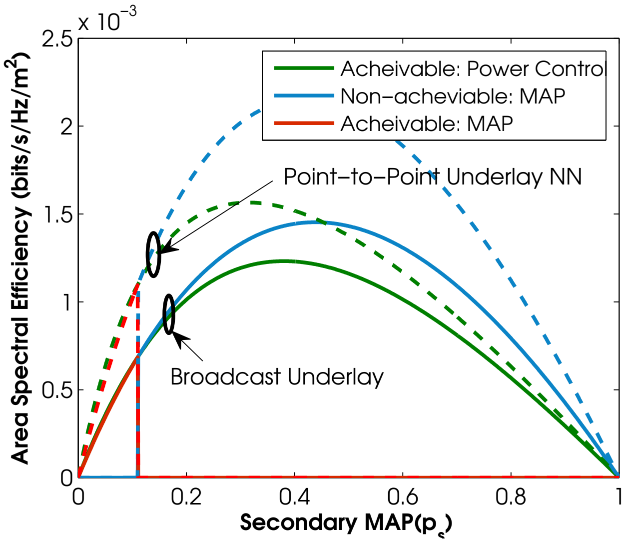

Figure 4.13: Spectral efficiency of the broadcast underlay network vs. the point-to-point network with nearest neighbour (NN) transmission with $\lambda_s = 10^{-2}$, $\lambda_p = 10^{-3}$, $m_p = m_s = 1$, $\alpha = 4$, $r_p = r_{BS} = 4$, $\rho_{out}^{\{p\}} = 0.1$, $p_p = 0.4$, $\gamma_{th}^{\{p\}} = 5$ dB, $\gamma_{th}^{\{s\}} = 3$ dB (see Eqs. (4.43) & (4.44)).

ber of broadcast receivers in this area can be characterized using the mean measure of the point process $\tilde{\Pi}_s^{\{RX\}}$ as follows

$$\begin{aligned}\Lambda_{BS} &= \mathbb{E}_{H,I_p,I_s}\left(\int_{\mathcal{A}} \lambda_s(r)\mathbb{1}(\gamma(\boldsymbol{x},h_{\boldsymbol{x}}))]f_H(h)dr\right),\\ &= \mathbb{E}_{I_p,I_s}\left(\int_{\mathcal{A}} \lambda_s(r)\Pr\left\{I \leq \frac{P_p h}{\gamma_{th}^{\{s\}} r^{\alpha}}\right\} dr\right),\\ &\overset{(a)}{\leq} \lambda_s(1-p_s)2\pi \int_{\mathcal{A}} r\exp\left(-\pi\zeta r_s^2\right) dr, \qquad (4.49)\end{aligned}$$

where (a) is obtained by taking expectation with respect to the i.i.d. interference random variables. Consider the geometry of the broadcast cluster, i.e., a disc of radius r_{BS} centered at the probe transmitter and then $\mathcal{A} = b(o, r_{BS}^2)$

$$\begin{aligned}\Lambda_{BS} &\leq \lambda_s(1-p_s)2\pi\int_0^{r_{BS}} r\exp\left(-\pi\zeta r_s^2\right) dr, \qquad (4.50)\\ &\leq \lambda_s(1-p_s)\left[\frac{1-\exp\left(-\pi\zeta r_{BS}^2\right)}{\zeta}\right].\end{aligned}$$

□

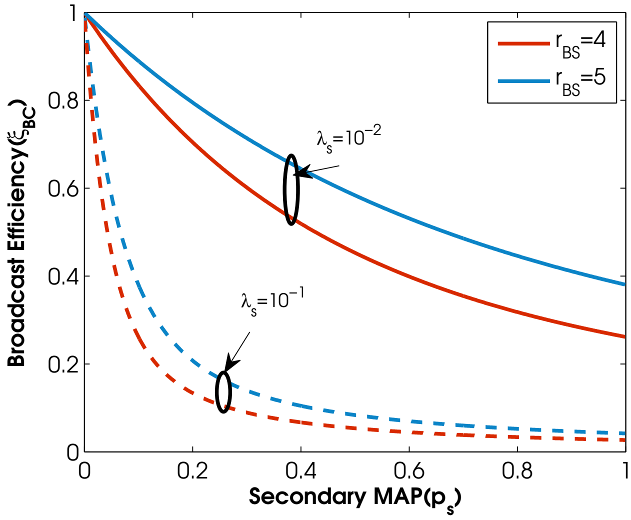

Figure 4.14: Broadcast efficiency of the cognitive underlay network with varying secondary user density and broadcast cluster size for $\lambda_p = 10^{-3}$, $m_p = m_s = 1$, $\alpha = 4$, $r_p = 4$, $\rho_{out}^{\{p\}} = 0.1$, $p_p = 0.4$, $\gamma_{th}^{\{p\}} = 5$ dB and $\gamma_{th}^{\{s\}} = 3$ dB .

Remarks

Impact of the dimensions of broadcast cluster.

1. The broadcast area spectral efficiency depends on the the size of the broadcast cluster. As the size of the broadcast cluster grows the probability that more nodes can decode the transmission increases exponentially, hence the broadcast spectral efficiency also increases.

2. Like point-to-point networks, there exists an optimal MAP (p_s^*) for the broadcast CRN. But this optimal MAP (p_s^*) for the broadcast case differs from the point-to-point case.

Broadcast efficiency.

3. The broadcast efficiency is defined as the

$$\xi_{BC} = \frac{\Lambda_{BC}}{\lambda_s(1 - p_s)\pi r_{BS}^2}.$$

It can be interpreted as a probability that an arbitrary receiver inside a broadcast cluster can decode its intended transmission at the desired QoS constraint. Fig. 4.14 depicts the broadcast efficiency of an underlay CRN. Notice that the broadcast efficiency is coupled with the density of secondary users only through the average broadcast out-degree. As shown in the Fig. 4.14 the broadcast efficiency increases with an increase in broadcast cluster size.

4. Similar to the point-to-point networks, the achievable throughput of the broadcast network can be optimized by employing the MAP adaptation in conjunction with optimal transmit power. Without proper selection of the transmission power, significant throughput loss may be incurred. This loss can be attributed to both the co-channel interference environment created between the secondary users themselves and the stringent constraint on the MAP enforced by the primary user due to the sub-optimal operating point.

4.9 CONCLUSIONS

In this chapter, we developed a comprehensive statistical framework for characterizing the area spectral efficiency of Poisson cognitive underlay networks. We explored the two degrees-of-freedom that are available to network designers in the form of secondary medium access probability (MAP) and transmit power. The developed statistical machinery is employed to show that primary user is oblivious to the adaptation as long as its desired quality of service (QoS) can be guaranteed. In other words, secondary users can tune either of these two parameters to satisfy the imposed QoS requirement. However, secondary user's area spectral efficiency under both schemes differ significantly. It is shown that there exists a spectral efficiency wall for CRs, irrespective of the adaptation scheme. The location of the wall is coupled with the primary user's desired QoS requirement. This wall limits the performance of the secondary communication links. However, this wall can be broken and better performance can be obtained by adapting one degree of freedom and optimizing the another one. We show that there exists an optimal MAP which maximizes the spectral efficiency under transmission power adaptation scheme. Equivalently, there exists an optimal transmission power under a MAP adaptation scheme. Several important properties of the optimal the MAP are explored in details. We then extend our analytical framework to more complicated networking scenarios of point-to-point and broadcast underlay CRNs. It is demonstrated that irrespective of the networking scenario, a simple adaptation of MAP (or transmit power) with arbitrary selection of the transmit power (or MAP) is sub-optimal. Hence both degrees of freedom should be jointly tuned to maximize the throughput potential of the network.

Part II

COGNITIVE INTERWEAVE NETWORKS

5

ON PRIMAY USER'S OUTAGE, THROUGHPUT AND ERGODIC CAPACITY IN THE PRESENCE OF INTERFERING COGNITIVE RADIO NETWORKS

In this chapter, we develop a statistical framework to model the OP, throughput and ergodic capacity of a primary/licensed user, while operating in the presence of a collocated, spectrum sensing, (Poisson) ad hoc CRN. The existing primary beacon enabled interweave spectrum sharing [3] model is utilized for evaluating the interference at a typical primary receiver. We consider that based on the degree of knowledge about the primary user, the CRs employ either matched filter or energy detector for spectrum sensing. Furthermore, three different architectures for spectrum sensing based on the spatial configuration of the platform which performs the sensing are proposed. It is demonstrated that these different architectures exploit the geometric uncertainty of the link distances to provide a superior performance in terms of OP, throughput and ergodic capacity. A comprehensive study of how the OP for a primary user is coupled with different parameters of the CRN is carried out. We further investigate the optimal SIR threshold which maximizes the primary's throughput and an optimal MAP for the secondary network which satisfies the primary's desired QoS constraints. Lastly, the impact of the self-coexistence constraint on both the OP and throughput of the primary is highlighted. We show that ignoring the self-coexistence constraint results in an over-estimation of the interference and the outage. So in summary, this chapter presents a comprehensive analysis of the choice of optimal design parameters for a CRN to minimize the OP or maximize the throughput and ergodic capacity of the primary while considering various detection schemes and architectures.

Primary objective:
- *To characterize the aggregate interference experienced by the primary receiver in the presence of spectrum sensing CRN.*
- *To highlight the importance of self-coexistence mechanism.*

5.1 INTRODUCTION

5.1.1 *Motivation*

In Part I, we presented a comprehensive statistical framework for analyzing the performance of cognitive underlay networks. The aim of this part is to attain similar objective for a large scale CRN coexisting with the primary user under interweave spectrum access paradigm.

In interweave spectrum access paradigm secondary terminals opportunistically exploit transmission vacancies across space and time. These vacancies are more commonly called *white-spaces* or *spectrum holes* [9]. The fundamental *operational constraint* on CRs is to ensure that they do not cause any harmful *interference* to the primary/licensed or legacy user. In order to avoid harmful interference to the primary network, CRs usually employ a detection mechanism to determine the primary's presence. This detection mechanism indeed enables CRs to realize transmission opportunities. Unfortunately, none of these spectrum access mechanisms can guarantee interference-free operation of primary users in the presence of a cognitive radio network (CRN). This in fact is essence of the several uncertainties involved in the spectrum sensing/detection process, i.e.,

1) Uncertainty in terms of distances: In an ad hoc CRN, the detection performance of a CR is tightly coupled with its distance from the primary user. CRs which are located very far away from the primary user may receive a very weak signal from the primary mainly due to the path-loss attenuation. It is difficult to detect such a weak signal, especially when it is buried in thermal noise. Even if a mis-detecting CR transmits with a low power, accumulation of power from different CRs may significantly deteriorate the primary's performance.

2) Uncertainty in terms of channel: Multipath propagation and shadowing pose an additional challenge in detecting a primary user. These conditions may preclude a possibility of detecting a nearby primary user. Consequently, CRs perceiving the false transmission opportunities may cause significant interference to the primary users.

The impact of these uncertainties for different detection mechanisms may differ significantly. Consequently, the *degree of sensitivity* to these uncertainties for a particular detector is also critical in characterizing the interference at the primary receiver. In brief, it is not possible for a CRN to completely avoid the interference with the primary user in the presence of these uncertainties. This dilemma has warranted studies in the domain of statistical characterization of the outage encountered at a primary receiver in the presence of secondary nodes.

5.1.2 *Contributions and Organization*

In this chapter, we develop a statistical framework for characterizing the primary user's performance in presence of spectrum sensing CRs. Our analysis is motivated by the following intriguing design questions:

1. Is it more appropriate that the secondary receiver (RX) should assume the responsibility of deciding about the channel status or should the secondary transmitters (TX) render this task? Does spectrum sensing at the CR transmitter (TX) always guarantee *minimum* outage prob-

ability (OP) for the primary user or is it possible to reduce the OP of primary by delegating the spectrum sensing task to the CR receiver (RX)?

CR TX and RXs may possess different sensing capabilites due to the heterogenity in the network.

2. When CR TXs and CR RXs possess different spectrum sensing capabilities, i.e. a different level of *sensitivity to spatial and channel variations*, is it always optimal[1] to assign the task of spectrum sensing to the device with better capabilities? When does the spatial configuration of a better device outrank its capability gains?

How to combine the inferences obtained at RX and TX to reduce the OP of the primary link.

3. When both CR TX and CR RX cooperate to detect the legacy user, whose decision takes precedence? What factors are critical to establish the precedence criterion? What if CR users become greedy, i.e., biased while establishing primary's presence, will this deteriorate the primary's performance significantly?

4. What is the achievable throughput of a primary user in the presence of a collocated ad hoc CRN? Can the primary get any potential gains by sharing some signaling information with the secondary users? Can primary tune some communication parameters to optimize its throughput?

Self coexistence refers to the peaceful co-existence of secondary user's amongst themselves.

5. How does the *self-coexistence* constraint affects the primary's outage probability? Is there an optimal non-zero MAP for CRs which can guarantee a desired QoS for the primary user, while ensuring the usefulness of the CRN? How does the spectrum sensing mechanism impact the MAP of the CR users?

To the best of our knowledge, these questions remain unanswered. In this work, we try to provide answers to some of these questions while establishing the fundamental statistical framework for the modeling of such a network. We hope that this will provoke more interest in the research community towards such questions which indeed form the foundations for an optimal CRN design. A brief road map for the rest of the chapter is as follows:

1. We consider a network model (Section 5.2) where the spatial distribution of the secondary nodes is characterized by a Poisson point process. We formalize a stochastic geometry based network model and the notion of self-coexistence for CRNs in terms of its MAC (Section 5.2). The process of spectrum sensing/primary's detection at a CR is accomplished by considering two well-established detectors, i.e., the matched filter (MF) and the energy detector (ED) (Section 5.3). We further introduce three different spectrum sensing architectures (Section 5.3), namely, (i) transmitter (TX) based detection; (ii) receiver (RX)

1 By optimal, we mean the strategy which minimizes the primary's OP.

based detection and (iii) TX-RX joint detection. Two particular decision fusion strategies, i.e., *greedy transmitter* and *content transmitter* strategy are also introduced. Both of these strategies are studied for four different combinations of detectors based upon their location (TX,RX), i.e. (MF,MF), (ED,ED), (ED,MF) and (MF,ED). The main motivation besides considering these different architectures is to exploit the geometric uncertainty. In brief, Section 5.3 is dedicated to answer aforementioned design questions, 1-3.

We characterize the OP performance of primary link for all possible combinations of detectors employed at CR TX & RX. However, it is worth highlighting that from practical perspective combination where both TX and RX have same type of detector are perferable. One key motivation beside considering the different detectors across TX & RX is to provide an outlook towards hybrid detection algorithms.

2. A comprehensive statistical framework for modeling the OP of the primary receiver in the presence of a Poisson field of secondary interferers employing the spectrum sensing architectures as introduced in Section 5.3 is established in Section5.4. The impact of several important parametric variations of the secondary network on the OP of the primary user is also addressed. These parametric variations include the secondary user density, the primary's exclusion region, the primary's link distance, transmit power ratio of primary to secondary transmitter, the secondary MAP, the signal to noise ratio (SNR) of the beacon channel and the signal to interference ratio (SIR) threshold of the primary channel.

3. We then develop an analytical framework for studying the throughput of the primary network in the presence of interfering CRs (Section 5.5). We also investigate the optimum SIR threshold that maximizes the primary user's throughput.

4. Based on the analytical machinery introduced in Section 5.4, we present closed-form expressions for the ergodic capacity of the primary user (Section 5.6).

5. Lastly, we study the optimal MAP for the secondary network that satisfies the given QoS parameters of the primary user (Section 5.7) while considering the spectrum sensing process. We highlight the importance of the self-coexistence constraint and the gains in terms of the throughput and the OP which can be exercised by enforcing the self-coexistence constraint. We will also briefly discuss the conditions necessary for the validity of the Gaussian approximation for the interference distribution at the primary receiver with derivations in the Appendix.

5.1.3 *Related Work*

Essentially, the modeling of interference encountered at the primary receiver in the presence of a Poisson field of CRs is a more intricate problem than its ad hoc counterpart. The main reason behind this is the strong coupling of the spectrum sensing process employed at the CRs with several attributes of the primary system. The problem of interference modeling in the context of spectrum sensing CRs was first studied by Ghasemi and Sousa in [20]. The authors employed beacon enabled spectrum sharing between the primary and secondary users. Reference [20] only considered the scenario where the Poisson field of CR transmitters which fail to detect the primary's beacon by employing ED contribute towards the aggregate interference at the primary receiver. By contrast, in this chapter we investigate OP, throughput and ergodic capacity of the primary link when different detection and medium access mechanisms are employed by the secondary users (see Section 5.2). Moreover, notice that [20] characterizes the probability of interference and not the distribution of SIR. The former is more intricate to characterize and more useful for a performance analysis. The Shifted Lognormal or Lognormal [20] approximation does not admit closed form expression for the moment generating function (MGF). Hence quantifying the performance of the primary link using these distributions is intricate. Contrary to [20] our focus in this work is not only to quantify the interference but also to explore the several degrees of freedom intrinsically available to reduce the interference at a primary receiver.

In [51], Vu et al. developed an interference model for the CRN in the presence of primary beaconing. The authors in [51] only study the average interference and do not consider the explicit detection mechanism. The authors in [51] employ a Gaussian assumption for the interference distribution in deriving the OP of the primary which is generally not valid, see [63]. Hong et al. [112] utilized an alpha stable distribution for modeling interference in CRNs. However, in [112] the authors do not consider any spectrum sensing mechanism, which reduces the case to traditional ad hoc network interference modeling. Moreover, expressions obtained for the characteristic function of the interference in [112] cannot be established in closed-form. Consequently, further analysis is intricate. Like [51], authors in [53] do not consider any explicit sensing mechanism. Moreover, the analysis is geared towards quantifying distribution of interference and not the distribution of SIR.

Recently, the authors in [113], [55] and [114] studied the transmission capacity (TC) for Poisson distributed interfering CRs. The TC of an ad hoc network characterizes the average number of simultaneous transmissions per unit area subject to an OP constraint [114]. The capacity of the primary network in the low SNR regime (considering a single secondary interferer with geometric uncertainty) was recently studied in [115]. However, none of these works consider explicit detection mechanisms and architectures. Moreover, all of these works ignore the fundamental self-coexistence constraint for CRs. To the best of our knowledge, none of these studies explored a choice of different mechanisms and architectures for spectrum sensing as we have proposed in this chapter. Ergodic capacity and throughput of the pri-

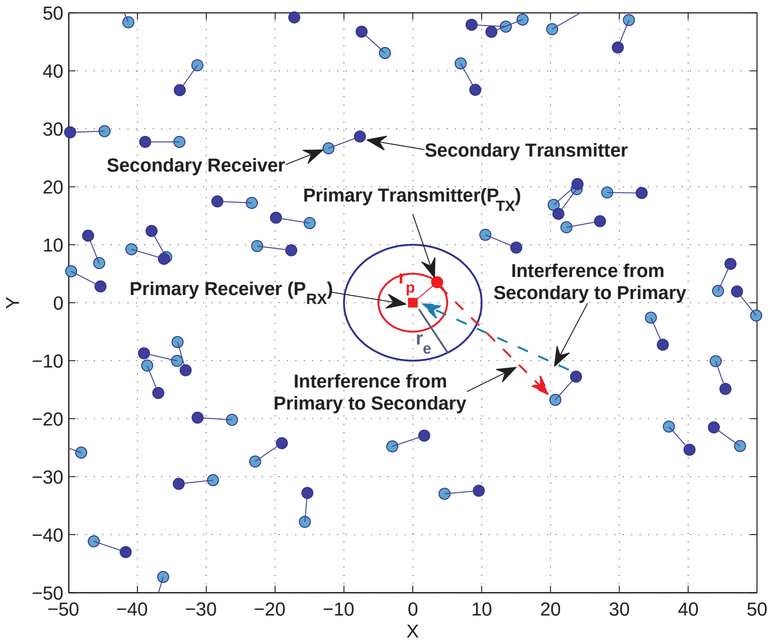

Figure 5.1: Primary Link in the presence of Poisson distributed secondary interferers with density $\lambda_s^{TX} = 5 \times 10^{-3}$, distance between primary transmitter and receiver $r_p = 5$; distance between secondary transmitter and receiver $r_s = 3$ and radius of the primary exclusive region $r_e = r_o + r_s + 2$.

mary in the presence of secondary interferers and optimal selection of the MAP and the SIR threshold for secondary network based on the primary's QoS constraints, also remain unaddressed.

5.2 SYSTEM MODEL AND ASSUMPTIONS

In this section, we introduce the system model and some fundamental results from stochastic geometry. This discussion serves as an essential building block for our subsequent analysis.

5.2.1 *Spatial Configuration of Primary and Secondary Network*

We consider a single primary link operating in the presence of a Poisson field of secondary interferers (see Fig.5.1). The primary communication link (P_{RX},P_{TX}) is formed by a primary receiver (P_{RX}) located at the origin and a primary transmitter (P_{TX}) at a distance r_p from P_{RX}. The *primary's exclusive region* is modeled by a disk of radius r_e centered at the origin. In order to ensure stable operation of the primary link, secondary transmitters located inside this region are obliged to maintain silence. The radius of the primary's exclusive region should be typically larger than the distance between P_{TX} and P_{RX}. This is achieved by introducing an additional *guard-band* of width Δ which ensures that the primary link is well protected. Mathematically, $r_e = r_p + \Delta$.

Detailed discussion on selection of Δ is beyond current scope, interested readers are directed to [64] and [116].

The locations of the secondary transmitters at any arbitrary time instant is modeled by a homogeneous Poisson point process (HPPP) [60] Φ_s^{TX} on $\mathbb{R}^d \backslash b(o, r_e)$ with intensity λ_s^{TX}. Here $b(o, r_e)$ denotes a $d-$dimensional ball of radius r_e centered at the origin and λ_s^{TX} quantifies the number of secondary users per unit area/volume[2].It is assumed that each secondary transmitter has an intended receiver at a fixed distance r_s. We assume (as was done in [44] and [117]) that the receivers do not belong to the point process.

Considering $\Phi_s^{TX}(B)$ as a counting process defined over a bounded (Borel set) subset of the secondary network area B, the number of nodes (i.e., points of Φ_s^{TX} in B) have a Poisson distribution with a finite mean $\lambda_s^{TX} v_d(B)$ for some constant λ_S^{TX}. $v_d(B)$ is the Lebesgue measure defined on the measurable space $[\mathbb{R}^d, B^d]$. In other words, $v_d(B)$ is the volume of a $d-$dimensional bounded Borel set B . If B is a $d-$dimensional sphere then $v_d(B) = b_d r^d$, where r is the radius of the sphere and b_d is the volume of the unit sphere in $\mathbb{R}^d$, with $b_d = \sqrt{\pi^d}/\Gamma(1+d/2)$ and $\Gamma(a) = \int_0^\infty x^{a-1} \exp(-x) dx$.

5.2.2 *Channel Model*

The large-scale path-loss between any arbitrary transmitter $y_t \in \mathbb{R}^d$ and receiver $y_r \in \mathbb{R}^d$ is given by $l(\|y_t - y_r\|)$, where, $l(.)$ is a distance dependent path-loss function and $\|.\|$ corresponds to the Euclidean norm. Generally, path-loss is modeled by considering the power law function, i.e., $l(R) = CR^{-\alpha} \quad R \geq 1$, where C is the frequency dependent constant, R is the distance between the transmitter and the receiver and $\alpha > 2$ is the terrain or environment dependent path-loss exponent. The path-loss between P_{TX} and P_{RX} is given by $l(r_p)$. However, when considering the path-loss between an arbitrary secondary transmitter ($y_t \in \Phi_s^{TX}$) and primary receiver (P_{RX}) this path-loss function needs a minor modification, i.e., $\tilde{l}(R) = CR^{-\alpha} \quad R \geq r_e \geq 1$. This modification is required to cater for the primary's exclusive region, as previously described. Note that although catering for the primary's exclusive region increases the analytical complexity, it provides an inherent advantage of precluding the singularity in the path-loss model for $R \leq 1$, iff $r_e > 1$.

Without loss of generalization we will assume $C = 1$ for the rest of the discussion.

The channel effects due to the multipath impairment process between any arbitrary transmitter $y_t \in \mathbb{R}^d$ and $y_r \in \mathbb{R}^d$ receiver can be modeled using a random variable H (a realization is denoted by h) with the probability

2 Note that although we are interested in a 2-D network on $\mathbb{R}^2$, we retain a generalized notion of $d-$dimensions for establishing a generic statistical framework.

distribution function (PDF) $f_H(.)$, cumulative distribution function (CDF) $F_H(.)$ and mean $\mu = E(H)$. We also consider that fading channel gains are independent and identically distributed (i.i.d.) in the spatial domain. The overall impact of the communication channel is modeled using a random variable $G(H, R) = Hl(R)$ which represents a flat-fading channel gain.

5.2.3 *Spectrum Sharing Model and Primary Detection*

Beacon enabled out-of-band interweave spectrum access.

We consider an interweave spectrum access approach, where secondary transmitters are allowed to opportunistically exploit transmission vacancies. This opportunism is derived by the spatio-temporal sensing of the frequency bands [3]. Hence the secondary's decision to transmit or not depends on the inference drawn from the spectrum sensing process. Such a spectrum sensing process requires the secondary transmitters to detect not only the primary transmitter in the vicinity of its intended receiver but also the primary receivers in its own vicinity. Notice that the detection of the primary transmitter does not correspond to the detection of instantaneous and local transmission opportunities [21]. While the former itself is still a non trivial task (considering the inherent randomness of the wireless channel) the latter requires much more sophisticated and demanding techniques. In order to circumvent these limitations, we consider an out-of-band beacon enabled spectrum sharing mechanism as proposed by the FCC [28]. This out-of-band sensing requires a dedicated control channel for beacon signaling. The primary user explicitly transmits *grant* or *inhibit* beacons to indicate whether the channel is free or busy respectively due to the activity of the primary itself.

Several detection mechanisms have been proposed in order to ensure reliable detection of the primary's beacon. The sophistication of the detection process employed at the CR depends on its knowledge about the primary. Based on the degree of knowledge about the primary, the task of spectrum sensing can be achieved by simple matched filtering [118] or (in contrast) by a complicated feature detector [118]. In this study, we consider two detection mechanisms for detecting beacons, i.e., the matched filter and the energy detector. We will also consider that these detectors can be used in three different configurations. We will delay the discussion on these configurations until Section 5.2.1.

5.2.4 *Self-Coexistence and Medium Access Control for the Secondary Network*

Existing studies [51, 112] have developed the theoretical framework for modeling the aggregate interference at the primary receiver. Nevertheless, these studies neither explicitly address the detection process employed by the CRs nor do they address the fundamental *'self-coexistence constraint'* [119] enforced on CRs in the secondary network. In particular, even if every secondary transmitter *always* has data to transmit to its intended secondary receiver, *not all* of them can transmit at the same time. This constraint stems from the fact that, if all the secondary transmitters transmit data all the time, none of them will be successful in its transmission. In practice, this is dealt with the MAC mechanism employed at the secondary transmitter.

We consider a modified form of *Slotted ALOHA* MAC for the CRN; we call it a cognitive slotted ALOHA (CSA). The choice of Slotted ALOHA is made due to the simplicity and tractability of the analysis. The CSA protocol is simply the traditional Slotted ALOHA with spectrum sensing capabilities. In CSA, time is discretized into fixed transmission intervals called slots. Each secondary transmitter which has either detected the 'grant' beacon from the primary receiver or mis-detected the 'inhibit' beacon, transmits in a given slot with a probability p or defers its transmission with probability $1 - p$. We assume that the primary and CR transmitters always have some data to transmit. In other words, we do not consider the packet arrival and the queuing procedures.

Note that the statistical framework developed here is generic enough to accommodate certain modifications of Slotted ALOHA such as Opportunistic ALOHA and CSMA/CA.

5.3 SPECTRUM SENSING DETECTORS AND ARCHITECTURES

In this section, we present a brief account of the spectrum sensing detectors and architectures considered in this chapter. We consider explicit beaconing from the primary receiver to notify CRs about the channel status. We use the term beacon in a generic sense. In practice, it may be a simple sinusoidal tone or a training sequence embedded in the packet header.

5.3.1 *Spectrum Sensing Detectors*

In order to develop a generic framework, we consider *two extreme* cases, i.e., the CRs possess *exact knowledge* about the primary's beacon or alternatively the CRs have *no knowledge* about the precise beacon structure. In the first case, the optimal choice for detection is the well known matched filter [120], while in the later case, the energy detector [120] forms a natural choice. All three performance metrics (outage, throughput and ergodic capacity of the primary operating in the presence of a CRN) are coupled with the interference encountered at the primary receiver. This interference, in turn depends on the detection performance and the MAC employed by the secondary network. This motivates us to provide a quick recap of the detection performances of both the matched filter and the energy detector.

Detection performance for an MF.

Proposition 5.1 *(See [120]) The probability of successfully detecting the primary beacon (when it is present) by employing the matched filter at a CR is,*

$$P_D^{MF} = Q\left(Q^{-1}\left(P_{FA}^{MF}\right) - \sqrt{2\gamma(h,r)\tau}\right), \tag{5.1}$$

where $Q(x) = \frac{1}{\sqrt{2\pi}}\int_x^\infty \exp(-\frac{y^2}{2})dy$, P_{FA}^{MF} *is the probability of false alarm (i.e., the probability of detecting the primary beacon when it is not present),* τ *is the time-bandwidth product for the beacon signal and* $\gamma(h,r) = \frac{P_b h l(r)}{\sigma^2}$ *is the SNR (where the beacon transmit power is* P_b *and* σ^2 *is the noise variance) of the beacon channel.*

Detection performance for an ED.

Proposition 5.2 *(See [120]) The probability of successful beacon detection when an energy detector is employed at a CR is*

$$P_D^{ED} = Q\left(\frac{Q^{-1}(P_{FA}^{ED}) - \sqrt{\tau}\gamma(h,r)}{\sqrt{1+2\gamma(h,r)}}\right), \tag{5.2}$$

where $Q(x) = \frac{1}{\sqrt{2\pi}}\int_x^\infty \exp(-\frac{y^2}{2})dy$, P_{FA}^{ED} *is the probability of false alarm (i.e., the probability of detecting the primary beacon when it is not present),* τ *is the time-bandwidth product for beacon signal and* $\gamma(h,r) = \frac{P_b h l(r)}{\sigma^2}$ *is the SNR of the beacon channel.*

Discussion

τ is also known as signal processing gain.

Fig. 5.2a provides a comparison between the performance of the MF and the ED for $P_{FA}^t = 10^{-1}(t \epsilon \{MF, ED\})^3$. For a constant γ, τ and equal false alarm probability $P_{FA}^{MF} = P_{FA}^{ED}$, P_D^{MF} is higher than the P_D^{ED}. In other words, the MF can attain the same detection performance as that of the ED with all other parameters being equal at a much lower SNR than required for ED. Of course, the superior detection performance of the MF is exercised due to the complete knowledge of the signal and the channel state information (CSI).

Notice that with increasing SNR (see Fig.5.2), the detection performance of both the ED and the MF improves. Moreover, as illustrated in Fig. 7.1, beyond a certain SNR threshold both the ED and the MF can detect the primary's beacon with probability 1 while operating under constant probability of false alarm. This indeed has motivated [20], and [121] to propose a simplified analytical model for the detection in terms of an indicator func-

3 We use notation P_{FA}^t and P_D^t with $t \epsilon \{MF, ED\}$ to avoid repetition, when both MF and ED can be treated in same context

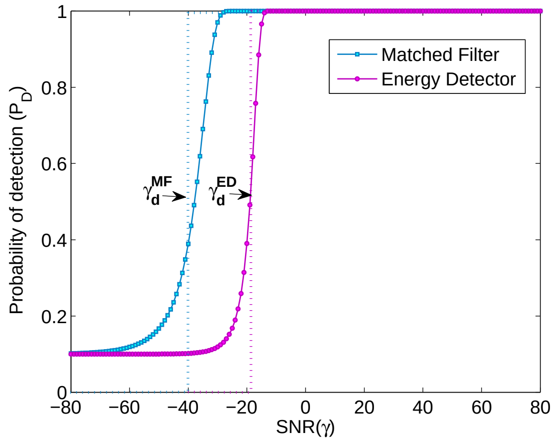

(a) Detection performance of MF vs. ED. Solid line represents P_D as a function of γ for constant $P_{FA} = 10^{-1}$ and $\tau = 10^4$. The dotted line step function represents a simplified analytical model for P_D as a function of γ (see Eqs. (7.2), (7.3) and (5.3)).

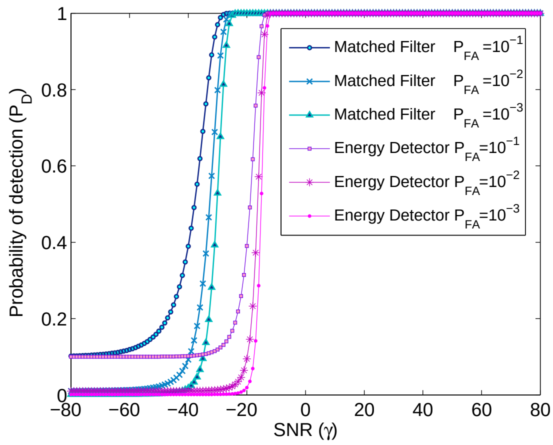

(b) Detection performance of MF vs. ED for varying P_{FA} and γ with constant $\tau = 10^4$ (see Eqs. (7.2) and (7.3)).

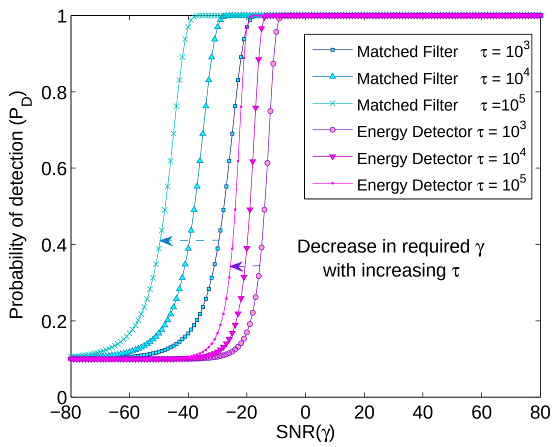

(c) Performance of MF vs. ED for varying signal processing gain τ and constant $P_{FA} = 10^{-1}$(see Eqs. (7.2) and (7.3)).

Figure 5.2: Impact of parametric variations on performance of MF and ED.

tion, since considering the exact expressions for the probability of detection makes further analysis intricate. We will adopt this simplification to make the analysis tractable. Since our prime interest is obviously in the probability of mis-detection, rather than detection, we represent mis-detection as the following indicator random variable

Threshold model for detection.

$$\mathbb{1}^{t}_{MD}(\gamma(h,r)) = \begin{cases} 1 & \gamma(h,r) \leq \gamma^{t}_{th} \\ 0 & \gamma(h,r) > \gamma^{t}_{th} \end{cases}. \tag{5.3}$$

The threshold SNR γ^{t}_{th} is selected such that the probability of detection/mis-detection becomes 50% [121]. Also notice that the SNR threshold is different for the ED and the MF. Solving (7.2) and (7.3), we get

$$\gamma^{MF}_{th} = \frac{Q^{-1}(P^{MF}_{FA})^2}{2\tau}. \tag{5.4}$$

$$\gamma^{ED}_{th} = \frac{Q^{-1}(P^{ED}_{FA})}{\sqrt{\tau}}. \tag{5.5}$$

Note that γ^{t}_{th} depends on both probability of false alarm and time-bandwidth product. Also as discussed earlier, it is clear from (5.4) and (5.5) that the threshold SNR for the ED is of the order of the square of the threshold SNR for MF, which indicates the superior performance of the MF. Notice that the threshold SNR for the ED does not change significantly as compared tothat of the MF when subjected to a similar change in the desired P_{FA} (see Figs. 5.2b-5.2c).

5.3.2 *Spectrum Sensing Architecture*

In this chapter, we consider three different architectures for spectrum sensing based on the type and location of the detector, i.e.,

1. *TX based detection:* Secondary transmitters perform detection using either a MF or an ED and decide to transmit with probability p (or refrain from it with probability $(1-p)$) based on the inference drawn from the spectrum sensing procedure.

2. *RX based detection:* Secondary receivers perform detection using either a MF or an ED and inform secondary transmitters about the status of the channel on an error free communication link [4]. Secondary transmitters then decide whether to transmit with probability p over the channel (or not). We further consider two extreme cases according to the spatial configuration of receiver: *(a) best case:* when all secondary

4 CR receivers provide a single bit feed-back to the CR transmitters. Hence assuming the error free feed-back channel does not affect the generality of analysis.

receivers are arranged in the *best* possible topological configuration (see Section 5.4); *(b) worst case:* when all secondary receivers presume the *worst* spatial configuration (see Section 5.4).

Transmitter receiver cooperation over beacon channel.

3. *TX-RX joint detection:* Both secondary transmitters and receivers perform detection using either the same detector, i.e, (ED,ED) and (MF,MF) or operate in a heterogeneous mode by using (ED,MF) and (MF,ED). For the sake of simplicity, we consider the best and the worst case configuration of receivers for all four combinations. Moreover, the decision of transmission is derived by using two different strategies: *(a) Greedy TX strategy:* The secondary transmitter employs a greedy rule to decide whether to transmit with probability p or not, i.e., it transmits with probability p if either the secondary receiver or the secondary transmitter itself fail to establish the presence of primary; *(b) Content TX strategy*: The secondary transmitter employs a content rule for deciding whether to transmit with probability p or defer the transmission to the next slot with probability $1-p$, i.e., it only transmits with probability p if both the secondary transmitter and the secondary receiver fail to detect the primary user.

Assumptions

Most of these assumptions are required for analytical tractability.

Following assumptions are employed throughout the chapter:

1. The communication channel between the secondary transmitter and receiver is error-free.
2. All secondary transmitter employ fixed transmission power for communication.
3. Secondary devices are aware of their relative position with respect to the primary receiver.
4. Cognitive users can adapt their transmission parameters such as MAP, so that the QoS constraint of the primary user and self-coexistence constraint of the secondary user can be satisfied.

5.4 OUTAGE AND INTERFERENCE INCURRED AT THE PRIMARY RECEIVER

In this section, we derive the closed form expressions for the outage probability of the primary receiver operating in the presence of a Poisson field of secondary interferers.

Considering the primary receiver P_{RX} located at the origin, the probability of successful (P_{suc}) transmission for the primary link is given by,

$$P_{suc} = \Pr\{\text{SIR} > \gamma_p\} = \Pr\left\{\frac{P_p h_p l(r_p)}{\sum_{i\epsilon\Phi_{INT}} P_s h_i \tilde{l}(r_i)} > \gamma_p\right\}, \quad (5.6)$$

where P_p and P_s are the transmit powers of the primary and secondary transmitters respectively, h_p is the channel gain between P_{TX} and P_{RX}, h_i is the channel gain between the secondary interferer i and the P_{RX}, r_p is the distance between P_{TX} and P_{RX}, R_i is the distance between the secondary interferer i and the P_{RX}, γ_p is the primary SIR threshold which corresponds to the desired primary quality of service (QoS), $l(.)$ and $\tilde{l}(.)$ are the previously defined path loss functions and Φ_{INT} is the set of interferers.

Note that in this chapter while we assume that the primary channel is interference limited, we can consider noise in the same framework, with a minor modification. Moreover, we consider that the primary channel suffers from small scale Rayleigh flat-fading. Without loss of generality, considering the Rayleigh fading with zero mean and unit variance, the H_p follows an exponential distribution with unit mean. Hence (5.6) becomes,

The aggregate interference generated by secondary users is strongly dependent upon the sensing mechanism. Moreover, the detection performance of the spectrum sensor and its contribution to aggregate interference are both coupled through the distance between primary receiver and secondary spectrum sensing platform.

$$P_{suc} = \Pr\left\{h_p > \frac{r_p^\alpha \gamma_p I}{\eta}\right\} = \mathbb{E}_I\left(\exp\left(-\frac{r_p^\alpha \gamma_p I}{\eta}\right)\right) = M_I\left(-\frac{r_p^\alpha \gamma_p}{\eta}\right) \quad (5.7)$$

where η is the power ratio of primary transmit power to the secondary transmit power, $I = \sum_{i\epsilon\Phi_{INT}} h_i \tilde{l}(r_i)$ and $M_I(s)$ is moment generating function (MGF) for the interference. We assume that the secondary nodes transmit with a constant power P_s. Notice that P_{suc} can be completely characterized by the evaluation of the MGF of the interference generated by the secondary users. Hence in those cases, where the probability density function (PDF) of the interference cannot be computed, it is still possible to characterize metrices like outage, throughput, bit error rate and ergodic capacity. At this juncture, it is worth registering that not all the secondary transmitters will contribute towards the aggregate interference, i.e., Φ_{INT} depends on the *spectrum sensing architecture* and *medium access protocol.*

Consider that Φ_{INT} is an inhomogeneous Poisson point process constructed by the thinning of Φ_s^{TX} based on the spectrum sensing architecture and the MAC mechanism employed by the CRN. Further, assume that $\lambda_{INT}(h,r)$ is the density of the point process Φ_{INT}, then the MGF for the interference (shot noise) random field is given by

$$\begin{aligned} M_I(s) &= \mathbb{E}_{\Phi,H}\left(\exp\left(s\sum_{i\epsilon\Phi_{INT}} h_i\tilde{l}(r_i)\right)\right) = \mathbb{E}_I\left(\exp\left(sI\right)\right), \quad (5.8) \\ &= \mathbb{E}_{\Phi}\left[\prod_{i\epsilon\Phi_{INT}} \mathbb{E}_H\left(\exp\left(sh_i\tilde{l}(r_i)\right)\right)\right]. \end{aligned}$$

Using the definition of the Generating functional [60] for the Poisson point process, $\mathcal{G}(f(x)) = \exp\left(-\int_{\mathbb{R}^d}(1-f(x))\lambda(dx)\right)$, then the MGF for the interference can be written as,

$$M_I(s) = \exp\left[-\mathbb{E}_H\left\{\int_{\mathbb{R}^d\backslash b(0,r_e)}(1-\exp(sh\tilde{l}(r)))\lambda_{INT}(h,r)dr\right\}\right]. \tag{5.9}$$

In general, (5.9) does not have a closed form expression even for the simplest spectrum sensing architecture. Hence we focus on deriving the cumulants (κ_n) for the interference. Once the cumulants are obtained in closed form, the MGF or the distribution of the interference can be approximated in a variety of ways which will be discussed later. So,

Notice that characterizing success probability of the primary link requires computation of MGF.

$$K_I(s) = \ln M_I(s) = -\mathbb{E}_H\left\{\int_{\mathbb{R}^d\backslash b(0,r_e)}(1-\exp(sh\tilde{l}(r)))\lambda_{INT}(h,r)dr\right\}. \tag{5.10}$$

$$\kappa_n = \left.\frac{d^nK_I(s)}{ds^n}\right|_{s=0} = \mathbb{E}_H\left\{\int_{\mathbb{R}^d\backslash b(0,r_e)}(h\tilde{l}(r))^n\lambda_{INT}(h,r)dr\right\} \tag{5.11}$$

We now consider a specific spectrum sensing architecture introduced in Section III and derive closed form expressions for the cumulants.

5.4.1 *TX based detection*

When CSA is employed with the secondary transmitter based detection, only those secondary transmitters which satisfy the following two conditions will qualify as potential contributors towards Φ_{INT} :

Condition 1: Only the secondary transmitters outside the exclusion region of a primary receiver can potentially transmit and cause harmful interference (the effect of the exclusion region is incorporated into the path-loss model).

Condition 2: Condition 1, is not sufficient to characterize the secondary transmitter as a potential interferer, rather only those secondary transmitters that lie outside the exclusion region and cannot detect the inhibit beacon from the primary will transmit with a medium access probability p and cause interference to the primary receiver.

Condition 2 can be accommodated by the two step thinning [60] of the HPPP of secondary transmitters Φ_s^{TX}:

Please refer to Appendix A for definitons.

1. Mis-detection introduced in (5.3), can be incorporated by the location dependent thinning of Φ_s^{TX}. In other words, only those secondary nodes which fail to detect the primary's beacon are retained in the set of potential interferers $\bar{\Phi}_{INT}$.

2. Medium access control in form of Slotted ALOHA is incorporated by independent p-thinning of $\bar{\Phi}_{INT}$. More specifically, each secondary node in $\bar{\Phi}_{INT}$ is retained with probability p independent of the others to form Φ_{INT}. Here, p is the MAP for ALOHA protocol.

For the following analysis, it is convenient to express the density of the HPPP Φ_{INT} in polar coordinates. Hence, using the Mapping theorem [60], the intensity of the inhomogenous Poisson point process Φ_{INT} is given as,

$$\lambda_{INT}(h,r) \quad = \quad p\lambda_s^{TX} d r^{d-1} b_d \mathbb{1}_{MD}^t(\gamma(h,r)). \tag{5.12}$$

Note that our objective is to obtain closed form expressions for the cumulants of the interference from the CRN employing CSA with detection at the secondary receiver. For exact descriptions of Φ_{INT} and $\lambda_{INT}(h,r)$ at our disposal, (5.11) can be evaluated as,

$$\begin{aligned} \kappa_n &= \int_0^\infty \int_{\mathbb{R}^d \backslash b(0,r_e)} (h\tilde{l}(r))^n \lambda_{INT}(h,r) dr f_H(h) dh, \qquad (5.13)\\ &\overset{(a)}{=} \frac{p\lambda_s^{TX} d b_d}{\alpha n - d}\left[\gamma_l\left(\mu_1, \frac{\gamma_{th}^t r_e^\alpha}{\gamma_b}\right) r_e^{d-\alpha n} + \Gamma\left(\mu_2, \frac{\gamma_{th}^t r_e^\alpha}{\gamma_b}\right)\left(\frac{\gamma_{th}^t}{\gamma_b}\right)^{n-\frac{d}{\alpha}}\right]. \end{aligned}$$

The detail derivation for computing (a) is provided in Appendix D

where, $\gamma_b = \frac{P_b}{\sigma^2}$ is the SNR of the beacon channel in the absence of path-loss and fading when P_{RX} transmits a beacon with power P_b, $\gamma_l(a,b) = \int_0^b x^{a-1}\exp(-x)dx$ is the lower incomplete Gamma function, $\mu_1 = n+1$ and $\mu_2 = \frac{d}{\alpha} + 1$. Note that γ_{th}^t is one of the important parameters that characterize κ_n in (5.13). In order to highlight this dependence and also to accommodate the fact that (5.13) refers to the cumulant for the interference when the secondary transmitter based detection scheme is employed, we will slightly modify the notation, i.e., we will use $\kappa_n^{t,TX}$ instead of κ_n.

5.4.2 *RX based detection*

Consider a case where CR transmitters delegate the task of beacon detection to the associated CR receiver. Due to the inherent randomness in both channel and geometry of the network, some secondary receivers can detect the beacon sent by the primary receiver while their associated transmitter might not detect the beacon. Conversely, it is also possible that the receiver may not detect the beacon while its corresponding transmitter does. This form of spatial diversity can be exploited to reduce the primary's OP when secondary devices are location and channel aware. Since it is difficult to obtain the instantaneous channel state information (CSI) at CR transmitters, we study a case where CR transmitter delegate the spectrum sensing task based on the relative distance from the primary receiver. This is effectively same as designating the spectrum sensing task based on the knowledge of average CSI.

Consider a typical secondary receiver located at a distance r_s from its transmitter. The distance between P_{RX} and this secondary receiver can be easily found from,

$$\tilde{r} = \sqrt{r^2 + r_s^2 - 2rr_s\cos(\psi)}, \tag{5.14}$$

where, ψ is the angle between r and r_s which is distributed as $\mathcal{U}(0, 2\pi)$ and r is the distance between P_{RX} and the secondary transmitter. Note that (5.14) can be simplified by considering two extreme case.

1. *Worst case*: In the worst case topological arrangement of the secondary receiver, $\cos(\psi) = -1$, consequently $\tilde{r}$ is maximized. This occurs for $\psi = \pi$ and implies that the secondary receiver is more distant from P_{RX} when compared to the secondary transmitter. In this case,

$$\tilde{r} \;=\; r + r_s \leq c_W r \quad 1 \leq c_W \leq \infty. \tag{5.15}$$

Best case: The best case spatial configuration of secondary receiver minimizes the distance $\tilde{r}$. This occurs when $\cos(\psi) = 1$, or $\psi = 0$. Moreover the best possible case occurs when $r = r_e$. Note that this also implies that the guard band should satisfy the constraint $\Delta \geq r_s$. Considering these two facts,

$$\tilde{r} \;=\; r - r_s \leq c_B r, \quad \epsilon_1 \leq c_B \leq 1. \tag{5.16}$$

where, $\epsilon_1 = \left(1 - \frac{1}{r_e/r_s}\right)$, for the special case when $r_p = r_s = \Delta$,$\epsilon_1 = 0.5$.

The Best and the worst case topological configurations provides upper and lower bounds on beacon channel SNR.

Using these two cases and condition 1, the cumulants for the interference when the secondary network employs CSA and receiver based detection can be evaluated as follows,

$$\begin{aligned}\kappa_n^{t,RX} &= \int_o^{\infty}\int_{\mathbb{R}^d\setminus b(0,r_e)} (h\tilde{l}(r))^n \lambda_{INT}(h,r) dr f_H(h) dh, \\ &= p\lambda_s^{TX} db_d \int_o^{\infty}\int_{r_e}^{\infty} h^n r^{d-\alpha n-1} \mathbb{1}_{MD}^t(\gamma(h,\tilde{r})) dr f_H(h) dh, \\ &= p\lambda_s^{TX} db_d \int_o^{\infty}\int_{r_e}^{\infty} h^n r^{d-\alpha n-1} \mathbb{1}_{MD}^t(\gamma(h,cr)) dr f_H(h) dh,\end{aligned} \tag{5.17}$$

where, $c = c_B$ for the best case and $c = c_W$ for the worst case. Now $\kappa_n^{t,RX}$ can be obtained by using a similar procedure as outlined for $\kappa_n^{t,TX}$ in the Appendix D:

$$\kappa_n^{t,RX(best)} = \frac{p\lambda_s^{TX} db_d}{\alpha n - d}\left[\frac{\gamma_l\left(\mu_1, \frac{\gamma_{th}^t r_e^{\alpha} c_B^{\alpha}}{\gamma_b}\right)}{r_e^{\alpha n-d}} + \frac{\Gamma\left(\mu_2, \frac{\gamma_{th}^t r_e^{\alpha} c_B^{\alpha}}{\gamma_b}\right)}{\left(\gamma_{th}^t c_B^{\alpha}/\gamma_b\right)^{\frac{d}{\alpha}-n}}\right], \tag{5.18}$$

$$\kappa_n^{t,RX(worst)} = \frac{p\lambda_s^{TX} db_d}{\alpha n - d}\left[\frac{\gamma_l\left(\mu_1, \frac{\gamma_{th}^t r_e^{\alpha} c_W^{\alpha}}{\gamma_b}\right)}{r_e^{\alpha n-d}} + \frac{\Gamma\left(\mu_2, \frac{\gamma_{th}^t r_e^{\alpha} c_W^{\alpha}}{\gamma_b}\right)}{\left(\gamma_{th}^t c_W^{\alpha}/\gamma_b\right)^{\frac{d}{\alpha}-n}}\right]. \tag{5.19}$$

where, $\gamma_b = \frac{P_b}{\sigma^2}$ is the SNR of the beacon channel in the absence of path-loss and fading when P_{RX} transmits a beacon with power P_b, $\gamma_l(a,b) = \int_0^b x^{a-1}\exp(-x)dx$ is the lower incomplete Gamma function, $\mu_1 = n+1$ and $\mu_2 = \frac{d}{\alpha} + 1$.

The coupling between the primary's success probability and the secondary's MAP is explored in Section 5.7.

Remark 5.1 *For a large scale CRN it is just as likely to have a secondary receiver in a worst case spatial configuration as in a best case. Hence, it is of key importance to delegate task of spectrum sensing to only those receivers which are in best spatial configuration or are equipped with superior detection capabilities. By such a delegation, the overall success probability for primary link can be increased and in turn MAP of secondary network itself can be increased.*

Exact characterization for cumulants.

Remark 5.2 *In deriving (5.18) and (5.19), it was assumed that the fading channel gains between P_{RX} and both the CR transmitter and the receiver are the same. It is also possible to relax this assumption, by considering that for a given distance r, both the CR transmitter and the CR receiver experience identical but independent fading conditions. Consider the Marked point process (MPP) $\tilde{\Phi}_s^{TX}$ constructed by assigning i.i.d. fading marks T in the mark space $\mathbb{R}^+$, $\tilde{\Phi}_s^{TX} = \{x_i, t_i : x_i \epsilon \Phi_s^{TX} \text{ and } t_i \sim f_T(.)\}$, then the intensity measure of MPP $\tilde{\Phi}_s^{TX}$ is given by $\tilde{\lambda}_s^{TX}(t,r) = \lambda_s^{TX} f_T(t) db_d r^{d-1}$. These marks represent the fading channel gain between the CR receiver and the primary receiver. Additional dependent marks can be introduced to cater for the detection process as in the case of transmitter based sensing. We will skip the detailed derivation for brevity. The final result for the cumulants is:*

$$\kappa_n^{t,RX} = \frac{p\lambda_s^{TX} db_d \Gamma(n+1)}{\alpha n - d} \left[\left\{ 1 - \exp\left(-\frac{\gamma_{th}^t r_e^\alpha c^\alpha}{\gamma_b} \right) \right\} r_e^{d-\alpha n} \right. \tag{5.20}$$
$$\left. + \; E_{n-\frac{d}{\alpha}} \left(\frac{\gamma_{th}^t r_e^\alpha c^\alpha}{\gamma_b} \right) \left(\frac{\gamma_{th}^t c^\alpha r_e^{\alpha+d-\alpha n}}{\gamma_b} \right) \right].$$

Here $c \,\epsilon\, \{c_b, c_w\}$ for 'best' and 'worst' cases and $E_n(x) = \int_1^\infty t^{-n} \exp(-xt) dt$ is the generalized exponential integral [122]. Simulation results indicate that the detection performance of the secondary is pre-dominantly determined by spatial randomness, rather than channel randomness. Hence both (5.20) and (5.18) result in similar outage probability of the primary link. Due to analytical simplicity, we employ (5.18) for further analysis.

5.4.3 *TX-RX joint detection*

Both transmitter and receiver based schemes introduced in the previous subsections only exploit a single degree of freedom. However, with a random topological configuration of the CRN, we actually have an added degree of freedom, i.e., the CR transmitter and receiver lie at different distances from P_{RX}. This may enable one to perform better than the other. This sort of spatial diversity is best exploited by combining the decisions drawn from the spectrum sensing process executed at both the CR transmitter and receiver. In this chapter, we study two particular cases:

5.4.3.1 *Greedy TX strategy*

Aggressive/Optimistic transmission policy.

In terms of greedy transmitter strategy the set of potential interferers is characterized by the following condition:

Condition 3: All secondary transmitters which are located outside the exclusive region of the primary and their associated receivers perform spectrum sensing by employing either a MF or an ED. Based on the inference drawn from the spectrum sensing procedure, all secondary receivers notify their associated secondary transmitters about their decision by using an error free communication channel. A greedy CR transmitter transmits with probability p, if either its own or the associated receiver's decision indicates absence of the primary user. Consequently, those CR transmitter-receiver pairs which mis-detect primary's beacon, contribute towards the aggregate interference experienced at the primary receiver.

Note that the CR receiver can assume either worst or best spatial configuration relative to the CR transmitter as discussed in the previous subsection. Exact computation of cumulants for greedy strategy is very difficult, if not impossible. In order to simplify analysis, we can approximately assume that the two channels, i.e., between P_{RX}-CR transmitter and between P_{RX}-CR receiver are identical. In other words, the differences between the inferences established by the spectrum sensing on the CR transmitter and receiver result only from the network geometry. This indeed leads to the worst case analysis while considering sensing diversity. Note, that to the best of our knowledge even for the point-to-point case with known distance between CR transmitter and receiver, heterogeneous detectors (i.e., one of them employs MF while the other uses ED) have not been investigated. It is complex to obtain closed form expressions without making appropriate simplifications when considering the geometry of the network.

At large spatial distances the impact of path-loss is more pronounced than the fading. This can be demonstrated by plotting the probability $\Pr\{H > r^{\alpha}\}$, which is exponentially decreasing with respect to r.

Consider the output of the spectrum sensing at the CR transmitter and receiver $O = \{(\text{MD,MD}),(\text{MD,DET}),(\text{DET,MD}),(\text{DET,DET})\}$, where, DET refers to detection of beacon and MD refers to mis-detection of beacon. Also consider the following two events: $A_1 =$ CR transmitter mis-detects, and $A_2 =$ CR receiver misdetects, then the output of the greedy transmitter strategy is given by,

$$\begin{aligned} P_{MD}^{Greedy}(\gamma(R,H)) &\leq \Pr\{A_1\} + \Pr\{A_2\}, \\ &\leq \mathbb{1}_{MD}^{t}(\gamma(R,H)) + \mathbb{1}_{MD}^{t}(\gamma(cR,H)). \end{aligned} \tag{5.21}$$

The upper-bound in (5.21) follows from the probabilistic argument by approximating dependent events as independent. Under these assumptions cumulants of a greedy approach can be obtained as,

$$\kappa_{n,(t_1,t_2)}^{greedy,best} = \kappa_n^{t_1,TX} + \kappa_n^{t_2,RX(best)}. \tag{5.22}$$

$$\kappa_{n,(t_1,t_2)}^{greedy,worst} = \kappa_n^{t_1,TX} + \kappa_n^{t_2,RX(worst)}. \tag{5.23}$$

Note that there are four possible combinations of the detectors (t_1, t_2) which can be employed, i.e., both the CR transmitter and receiver use the same detectors ((MF,MF) and (ED,ED)) or alternatively, the CR transmitter and receiver both employ different detectors ((MF,ED) and (ED,MF)).

5.4.3.2 *Content TX strategy*

In the content secondary transmitter strategy:
Condition 4: All secondary transmitters which are located outside the exclusive region of the primary and their associated receivers perform spectrum sensing by employing either a MF or an ED. Assuming an error free communication channel between secondary transmitter and secondary receiver each CR transmitter only transmits if both CR transmitter and CR receiver have detected the channel as idle, i.e., CR transmitter transmits with probability p if both CR transmitter and receiver fail to detect the beacon.

Considering the same assumptions as employed in the greedy transmitter strategy,

$$\begin{aligned} P_{MD}^{Content}(\gamma(R,H)) &= \Pr\{\text{mis-detection}\} = \Pr\{A_1 \cap A_2\}, \quad (5.24) \\ &\leq \mathbb{1}_{MD}^{t}(\gamma(R,H))\mathbb{1}_{MD}^{t}(\gamma(cR,H)). \end{aligned}$$

The cumulants for the interference can now be derived as,

The detail derivation for computing (b) is provided in Appendix D

$$\kappa_{n,(t_1,t_2)}^{content} \overset{(b)}{=} \mathbb{E}_H\left[p\lambda_s^{TX} d b_d \int_{\max\left(r_e, \max(\eta_1,\eta_2) h^{\frac{1}{\alpha}}\right)}^{\infty} h^n r^{d-\alpha n-1} dr\right] \quad (5.25)$$

where, $\eta_1 = \left(\frac{\gamma_b}{\gamma_{th}^{t_1}}\right)^{\frac{1}{\alpha}}$ and $\eta_2 = \left(\frac{\gamma_b}{c^\alpha \gamma_{th}^{t_2}}\right)^{\frac{1}{\alpha}}$. The function $\max(\eta_1, \eta_2)$ depends on the combination of the detectors. Moreover, the spatial configuration of the receiver can assume two states, i.e., the worst and best.

With the help of Tables (5.1) and (5.2), (5.25) can be solved to obtain a closed form solution for the cumulants of interference under content transmitter strategy. Since we have already solved (5.25) for different CR transmitter and receiver configurations, cumulants obtained for previous cases can be utilized as shown in Table (5.3).

Although we formulated Table (5.3) based on a pure analytical approach several results follow intuition. It is obvious that when the CR receiver is in its best spatial configuration and both the CR transmitter and receiver use the same type of detector, the cumulant of interference corresponds to the receiver based sensing scheme. This in turn illustrates that the overall behavior is dictated by the CR receiver. Note that although we employed a probabilistic argument of independence to simplify our analysis, the results obtained are rather more generic. This can be easily observed by a closer inspection of the cumulants, since the detection of both transmitter and receiver is highly correlated and the only difference is in terms of geometry. If the CR receiver which is in best configuration mis-detects the beacon, the CR transmitter

TX \ RX	MF	ED
MF	$\eta_2 = c_B^{-1}\eta_1$ $\eta_2 \geq \eta_1$.	$\eta_1 = c_B\zeta^{\frac{1}{\alpha}}\eta_2$, $\eta_2 \geq \eta_1 \quad c_B \leq \frac{1}{\zeta^{\frac{1}{\alpha}}}$, $\eta_2 < \eta_1 \quad c_B > \frac{1}{\zeta^{\frac{1}{\alpha}}}$.
ED	$\eta_2 = \frac{\zeta^{\frac{1}{\alpha}}}{c_B}\eta_1$, $\eta_2 \geq \eta_1 \quad c_B \leq \zeta^{\frac{1}{\alpha}}$, $\eta_2 < \eta_1 \quad c_B > \zeta^{\frac{1}{\alpha}}$.	$\eta_2 = c_B^{-1}\eta_1$ $\eta_2 \geq \eta_1$.

Table 5.1: Best case configuration of the secondary receiver where we define $\zeta = \frac{2\sqrt{\tau}}{Q^{-1}(P_{FA})}$.

TX \ RX	MF	ED
MF	$\eta_1 = c_W\eta_2$ $\eta_1 \geq \eta_2$.	$\eta_1 = c_W\zeta^{\frac{1}{\alpha}}\eta_2$, $\eta_1 \geq \eta_2 \quad c_W \geq \frac{1}{\zeta^{\frac{1}{\alpha}}}$, $\eta_1 < \eta_2 \quad c_W < \frac{1}{\zeta^{\frac{1}{\alpha}}}$.
ED	$\eta_2 = \frac{\zeta^{\frac{1}{\alpha}}}{c_W}\eta_1$, $\eta_1 \geq \eta_2 \quad c_W \geq \zeta^{\frac{1}{\alpha}}$, $\eta_1 < \eta_2 \quad c_W < \zeta^{\frac{1}{\alpha}}$.	$\eta_1 = c_W\eta_2$ $\eta_1 \geq \eta_2$.

Table 5.2: Worst case configuration of the secondary receiver where we define $\zeta = \frac{2\sqrt{\tau}}{Q^{-1}(P_{FA})}$.

will also mis-detect the beacon with a high probability. Hence, the overall behavior is dictated by a receiver-based spectrum sensing process. Similar results are obtained for the worst case scenario. It is intuitive that when both the CR transmitter and receiver employ the same kind of detector, if the CR transmitter does not detect the beacon, the CR receiver stands little chance to detect it. Consequently, the overall behavior of interference is governed by the detection performance employed at the transmitter. While, for a similar pair of detectors intuitive explanations can easily be provided, the same is not true for the heterogeneous detection scenario. We will provide some insights on heterogeneous detection by utilizing extensive simulations in our later discussion.

5.4.4 *Approximation of Outage Probability from Cumulants*

Besides the approaches highlighted in this section, approximation using Saddle point methods can also be employed.

In this subsection our main objective is to derive P_{suc} and consequently the outage probability (OP) $P_{out} = 1 - P_{suc}$ for the primary link. Since we have

CR RX configuration	TX \ RX	MF	ED
Best case	MF	$\kappa_n^{MF,RX(best)}$	$\kappa_n^{ED,RX(best)}$ $c_B \leq \zeta^{-\frac{1}{\alpha}}$, $\kappa_n^{MF,TX}$ $c_B > \zeta^{-\frac{1}{\alpha}}$.
	ED	$\kappa_n^{MF,RX(best)}$ $c_B \leq \zeta^{\frac{1}{\alpha}}$, $\kappa_n^{ED,TX}$ $c_B > \zeta^{\frac{1}{\alpha}}$.	$\kappa_n^{ED,RX(best)}$
Worst case	MF	$\kappa_n^{MF,TX}$	$\kappa_n^{MF,TX}$ $c_W \geq \zeta^{-\frac{1}{\alpha}}$, $\kappa_n^{ED,RX(worst)}$ $c_W < \zeta^{-\frac{1}{\alpha}}$.
	ED	$\kappa_n^{ED,TX}$ $c_W \geq \zeta^{\frac{1}{\alpha}}$, $\kappa_n^{MF,RX(worst)}$ $c_W < \zeta^{\frac{1}{\alpha}}$.	$\kappa_n^{ED,TX}$

Table 5.3: Cumulants for the interference $\kappa_{n,(t_1,t_2)}^{content}$ when the secondary transmitter adopts content strategy, here $\zeta = \frac{2\sqrt{\tau}}{Q^{-1}(P_{FA})}$ and $t_i \in \{MF, ED\}$.

established the cumulants for the interference caused by the secondary for different spectrum sensing architectures in the last subsection, we will now utilize these results for the statistical characterization of OP. From now on we will use the notation κ_n for the cumulants of interference to avoid repetition. However, depending upon the spectrum sensing scenario, corresponding expressions derived in the last subsection for cumulants are used for $\kappa_n \in \left\{\kappa_n^{t,TX}, \kappa_n^{t,RX(best)}, \kappa_n^{t,RX(worst)}, \kappa_{n,(t_1,t_2)}^{greedy,best}, \kappa_{n,(t_1,t_2)}^{greedy,worst}, \kappa_{n,(t_1,t_2)}^{content}\right\}$.

Several approximation methods can be employed to approximate OP for the primary link. Here we will outline two such methods,

5.4.4.1 *Approximation using the Cumulant Generating Function (CGF)*

Considering (5.7) in order to evaluate success probability, the MGF of the interference is required. By definition the CGF is natural logarithm of the MGF,

$$K_I(s) = \ln(\mathbb{E}(\exp(sI))) = \sum_{n=1}^{\infty} \frac{\kappa_n s^n}{n!}, \tag{5.26}$$

$$M_I(s) = \exp(K_I(s)) = \exp\left(\sum_{n=1}^{\infty} \frac{\kappa_n s^n}{n!}\right). \tag{5.27}$$

Now from (5.7) ,

$$P_{suc} = M_I(-\frac{r_p^{\alpha}\gamma_p}{\eta}) = \exp\left(\sum_{n=1}^{\infty} \frac{(-1)^n \kappa_n r_p^{\alpha n}\gamma_p^n}{n!\eta^n}\right). \tag{5.28}$$

Considering only the first cumulant,

$$P_{suc} \leq \exp\left(-\frac{\kappa_1 r_p^{\alpha}\gamma_p}{\eta}\right), \tag{5.29}$$

$$P_{out} \geq 1 - \exp\left(-\frac{\kappa_1 r_p^{\alpha}\gamma_p}{\eta}\right). \tag{5.30}$$

Note that this is indeed consistent with Jensen's inequality, i.e., $\mathbb{E}(\exp(-sI)) \leq \exp(-s\mathbb{E}(I)) = \exp(-s\kappa_1)$. At this juncture, it is worth highlighting that although (5.29) gives an upperbound on the P_{suc}, it is quite useful in further analysis due to its exponential form. Simulation results indicate that the lower bound is quite tight over a wide range of parameters.

5.4.4.2 *Approximation by the Moment Matching Method*

Approximation by Gamma distribution.

The PDF of the aggregate interference can be obtained from the cumulants using the Method of Moments. Authors in [20] have employed a similar approach in the context of transmitter based sensing to model the interference by the Log normal or shifted Log normal distribution. Note that it is well established in the literature that the Gaussian approximation is not valid for interference [20, 34, 36, 123] due to its skewed and fat-tailed behavior (for certain parameters) [20]. The discussion on the validity of the Gaussian approximation can be found in Appendix, where we have explicitly questioned the validity of the Gaussian assumption and the conditions required for such an assumption. The main problem with Log normal, Log logistic, Inverse Gamma and Shifted Log normal distributions is that although they closely fit in the body, they do not fit accurately in the tail for all parameters (see Figure 5.3). Moreover, the expressions for matching such moments (see [20]) are quite complex. After conducting several experiments and goodness of fit testing, we found that the Gamma distribution [123] is the best fit for the interference distribution (see Fig. 5.3). An added advantage with the Gamma distribution is that moment matching expressions lend themselves into a very simple form. So for the interference we say $I \sim \mathcal{G}amma(k, \theta)$ where k is the shape parameter and θ is the scale parameter with $k = \frac{\kappa_1^2}{\kappa_2}$ and $\theta = \frac{\kappa_2}{\kappa_1}$.

Since the PDF of interference is known in closed form, we can easily establish success and outage probabilites in terms of the MGF which is simply the Laplace transform of the PDF (with change of sign for s).

$$M_I(s) = \frac{1}{(1-\theta s)^k} \Rightarrow P_{out} = 1 - \frac{1}{\left(1 + \frac{\theta r_p^\alpha \gamma_p}{\eta}\right)^k}. \tag{5.31}$$

This indeed provides a very close approximation and so does the upper bound established by using the first cumulant in the CGF based approach.

5.4.5 *Discussion*

5.4.5.1 *Impact of parametric variations on the OP for TX based spectrum sensing*

In the previous subsections, we established a comprehensive statistical characterization of the OP for the primary link in the presence of a Poisson field of secondary interferers. Although analytical expressions provide some hints on how OP scales with different network parameters, simulation of these expressions demystify some important design aspects.

a) Impact of QoS requirement and detector: Fig. 5.4a illustrates how OP of the primary link is coupled with primary's desired QoS. The QoS of the primary is partially dictated by the required SIR threshold (γ_p) for successful communication over the primary link. Consequently, the OP of the primary link decreases with an increase in γ_p.

Sensitivity of detector to change in desired probability of false alarm.

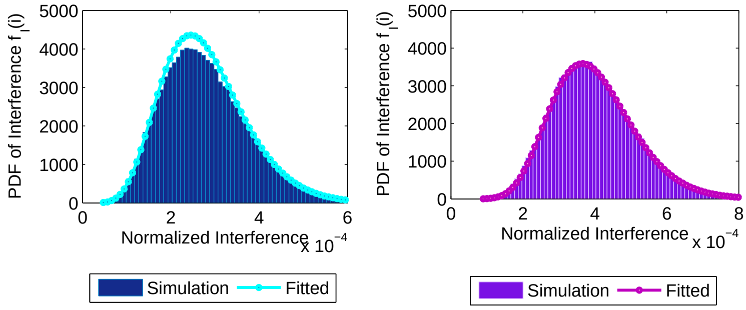

(a) PDF of interference $f_I(.)$ considering the Rayleigh fading (blue/right) and Log normal shadowing (purple/left) channels, with $p = 1$, $\lambda_s^{TX} = 0.01$, $\alpha = 4$, $\eta = 1$, $r_e = 2$).

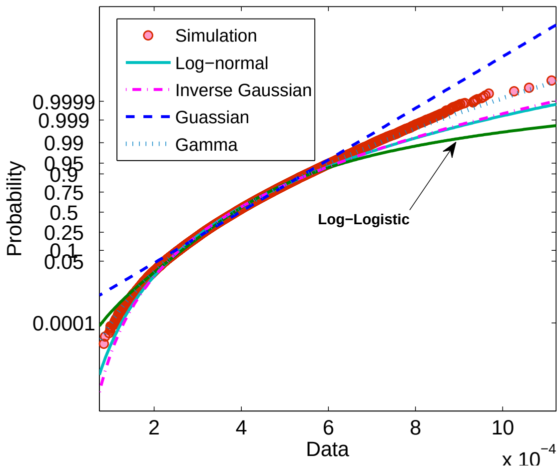

(b) Probability plots for different distribution vs. simulation results

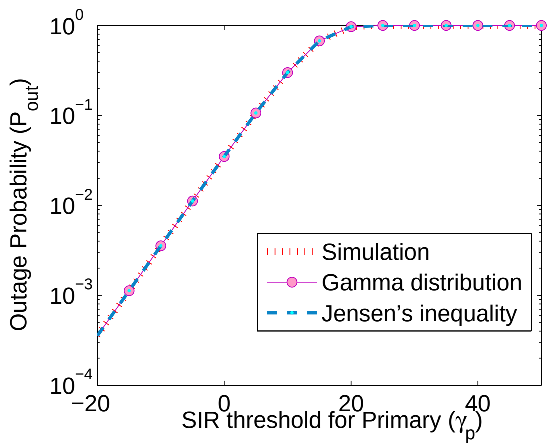

(c) CGF based method vs. moment matching method for varying SIR threshold ($\lambda_s^{TX} = 0.01, \alpha = 4, \eta = 1, r_e = 5, r_p = 2, \gamma_b = 10$ dB).

Figure 5.3: Moment matching for the interference PDF and comparison of different approaches for computing the OP.

Another important observation which follows from Fig. 5.4a is regarding the dependence of the OP on the type of detector employed at the secondary transmitters. As illustrated, the OP of the primary when the MF is employed at the CR transmitters is significantly less than the OP when ED is employed by CRs for a fixed γ_p and equal probability of false alarm. As discussed previously (Section 5.3), this superior performance of the MF is governed by the fact that the MF assumes that complete knowledge of the primary's beacon is available at the CR transmitter. Another interesting observation from Fig. 5.4a is the difference in the sensitivity of MF and ED to the change in the P_{FA}. Although for both MF and ED OP increases with a decrease in the probability of false alarm (since a decrease in P_{FA} is achieved at the cost of an increase in P_{MD} (probability of mis-detection)) when all other parameters are constant, however, the amount by which it is increased in the case of MF is not the same as in the case of ED for an equal decrease in P_{FA}. This essentially follows from the Eq.(5.4) and (5.5), which shows that the required SNR threshold for beacon detection is more suseptible to the changes in P_{FA} for MF as compared to ED.

b) Impact of distance between P_{RX} and P_{TX}: Fig. 5.4b highlights how changes in the distance between primary transmitter and primary receiver affect the OP of the primary link while operating in the presence of a spectrum sensing Poisson field of CRs. The results presented in Fig. 5.4b are quite intuitive. The OP of the primary link increases with increase in the link distance.

c) Impact of secondary user density: Following the legacy of Gupta and Kumar [93] type scaling laws, it can be observed from Fig. 5.3c that the OP of the primary's link increases with an increase in the density of secondary transmitters. Moreover from (5.31) and (5.13), it can be easily shown that the OP of the primary's link scales as $O\left(\sqrt{\lambda_s^{TX}}\right)$. Since outage capacity (OC) can be easily obtained from OP, it can also be shown that OC scales in a similar manner. Ideally, in the presence of an exclusion region and spectrum sensing, it is expected that secondary transmitters will not cause similar deterioration as may be caused by other primary transmitters which do not perform any spectrum sensing. However, this proposition is not true and CR transmitters can cause similar deterioration. The main reason behind this stems from many sources; the prime factors involved are uncertainty in the primary's channel, uncertainty in the medium access and uncertainty in the network geometry. Besides these uncertainites of traditional networks, additional uncertainty of the interference channel and spectrum sensing process also impact CRNs. Since an increase in the secondary transmitter density for constant P_{FA} corresponds to an increase in the amount of potential interferers or more specifically, an increase in the amount of interference, the OP increases with an increase in the secondary transmitters as shown in Fig. 5.3c. The difference in the sensitivity to P_{FA} is also reflected in the OP.

Scaling of OP with the secondary user density.

d) Impact of secondary medium access: The MAP introduced in Section 5.2, models the self-coexistence constraint on secondary network. We will discuss the importance of considering self-coexistence in our later discussion. However, as depicted in Fig. 5.3d, the OP decreases with a decrease in the MAP. A decrease in MAP effectively corresponds to a decrease in the number of interferers and so in the interference. Consequently, the OP decreases with a decrease in a MAP.
e) Impact of power ratio (η): Another important design parameter is the power ratio η (primary transmission power to secondary transmission power). The importance of this parameter was shown in [113, 114] where the TC of CRN is studied. Although in this chapter we have restricted ourselves to the constant transmit power case (i.e., considering η as constant), however, when either primary or secondary employ power adaptation, η is also a random parameter. As highlighted in Fig. 5.5e the OP decreases with the increase in η. Since increase in η corresponds to the increase in the primary's transmit power relative to the secondary's transmission power, with increasing η the SIR of the primary link improves and hence the OP for a fixed SIR threshold γ_p decreases.
f) Impact of primary exclusion region and beacon channel SNR: Before highlighting the impact of variations in the beacon channel SNR on the OP of the primary as shown in Fig. 5.5f, we will discuss the impact of a variation in the exclusion region of the secondary. Fig. 5.5 illustrates how the OP of the primary is affected by changes in the radius of the exclusion region. Furthermore, these results are presented for different values of path loss exponent (corresponding to different propagation environments). The numeric values of path-loss exponent are selected from the 802.22 standard. Fig. 5.5 presents some interesting results which cannot be deduced intuitively.

It is shown that before a particular threshold value of $\tilde{r_e}$, the OP of the primary does not decrease with increase in the exclusion radius r_e. This threshold value $\tilde{r_e}$ depends on the path-loss exponent, i.e., the smaller the path-loss exponent the higher is the threshold. Moreover, after a certain increase in the exclusion radius the OP does not depend upon the choice of detector employed at the secondary transmitter. In other words, CRs employing either ED or MF cause the same OP at the primary for equal probability of false alarm.

A closer inspection of (5.13) in the Rayleigh fading scenario reveals that as r_e increases, the first term (containing difference of Gamma and upper Gamma) and the second term (containing upper Gamma) increases with increase in r_e^{α}. However, the the term $r_e^{d-\alpha n}$ decreases with increase in the exclusion region r_e. This increase obviously depends on the α path-loss exponent. Hence this increase and decrease balance each other up to a particular threshold beyond which the decreasing term is dominant and hence the cumulants for the interference tend to zero (i.e., the OP decreases). This peculiar behavior stems from the fact that for a constant transmit power depending on the path-loss exponent, most of the nearby CR transmitters will not cause significant interference because these transmitters are able to sense the primary's presence with high probability. So increasing the exclusion region does not readily translate into a proportional decrease in the number of interferers. However, after a certain threshold value $\tilde{r}_e$, which depends on the path-loss exponent, increase in the exclusion region ultimately results in a reduction in the number of interferers.

The interesting observation here is that there exists an optimal radius of exclusion region corresponding to the desired OP and this radius depends on the environment in which the network is operational. As a result, the exclusion region should be selected according to the operational environment and the OP constraint. Moreover as the radius of the exclusion region is increased, the nearest interferers, which may also be dominant interferers for the primary receiver, are silenced. The secondary interferer (operating very far away) does not cause a significant amount of interference. Furthermore the detection performance of the CR transmitters is so poor that it does not matter which type of detector is employed at the CR. However, it is also important to note that the critical value of r_e also depends on the power ratio η.

Critical value of beacon channel SNR.

Lastly, as depicted in Fig.5.5f there also exists a critical value of SNR γ_b for the beacon channel beyond which the OP decreases with increase in γ_b. The reasoning follows similar to the reasoning employed for the exclusion region since the second term of the cumulant (5.13) shows similar behavior with γ_b. Also note that the ED may perform superior to the MF when both operate in different environments (different path-loss exponent). This is obvious from the intersection of the OP curves in Fig. 5.5f.

5.4.5.2 *Impact of parametric variations on the OP for RX based spectrum sensing*

As discussed earlier, a receiver based spectrum sensing strategy may provide performance gain in terms of decrease in the OP or it may further deteriorate the performance, depending upon the spatial configuration of receiver. Since we consider two extreme cases, i.e. the worst and the best case spatial configuration of the CR receiver, it is natural to study performance loss and gain in terms of OP for these two configurations respectively. Hence we define two new metrics,

$$G_{RX} = \frac{P_{out}^{TX} - P_{out}^{RX}}{P_{out}^{TX}} \times 100\%, \tag{5.32}$$

$$L_{RX} = \frac{P_{out}^{RX} - P_{out}^{TX}}{P_{out}^{TX}} \times 100\%, \tag{5.33}$$

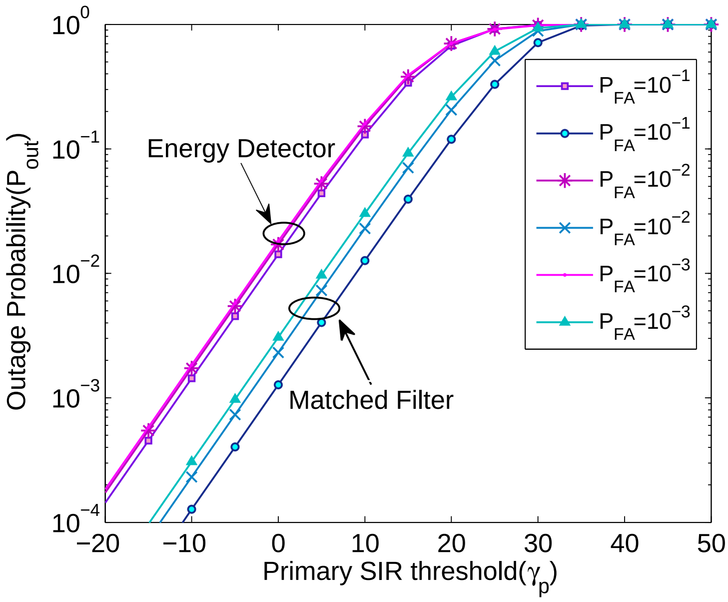

(a) OP of primary with varying SIR threshold for TX based sensing for $\lambda_s^{TX} = 10^{-2}, p = 1, \alpha = 4, r_e = 5, r_p = 2, \eta = 1$and $\gamma_b = 10$ dB (see Eqs. (5.13) and (5.31)).

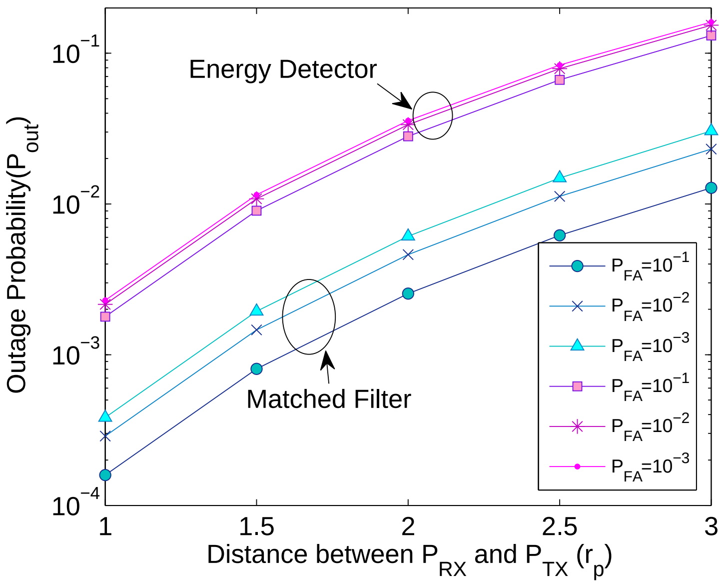

(b) OP of primary with varying link distance for TX based sensing for $\lambda_s^{TX} = 10^{-2}, p = 1, \alpha = 4, r_e = 5, \gamma_p = 3$ dB$, \eta = 1$ and $\gamma_b = 10$ dB (see Eqs. (5.13) and (5.31)).

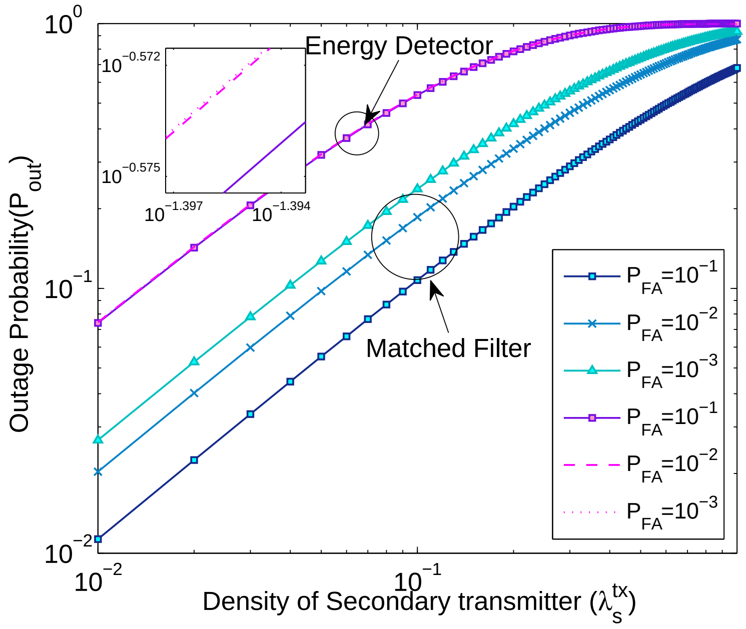

(c) OP of primary with varying density of secondary TX for TX based sensing for $p = 1, \alpha = 4, r_e = 5, \gamma_p = 6$ dB, $\eta = 1$ and $\gamma_b = 3$ dB (see Eqs. (5.13) and (5.31)).

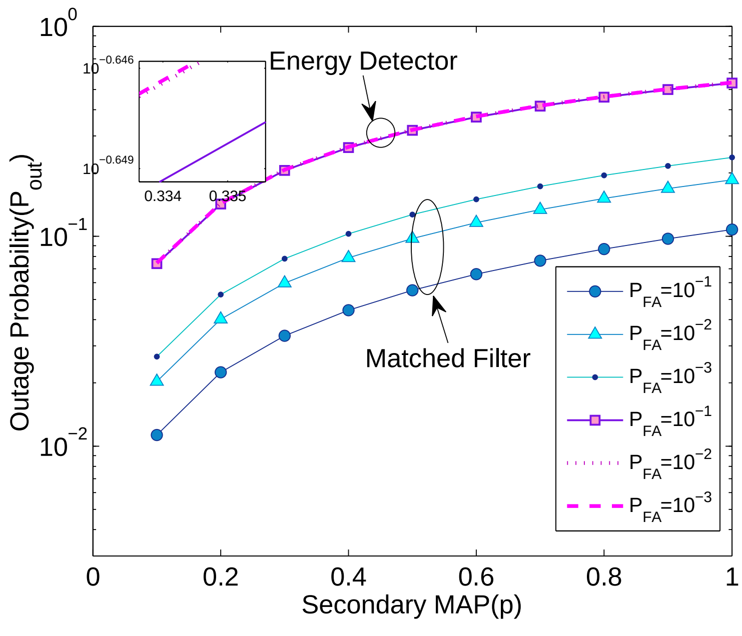

(d) OP of primary with varying MAP of secondary TX's for TX based sensing for $\lambda_s^{TX} = 10^{-1}$,$\alpha = 4$,$r_e = 5$,$\gamma_p = 6$dB,$\eta = 1$and $\gamma_b = 3$dB (see Eqs. (5.13) and (5.31)).

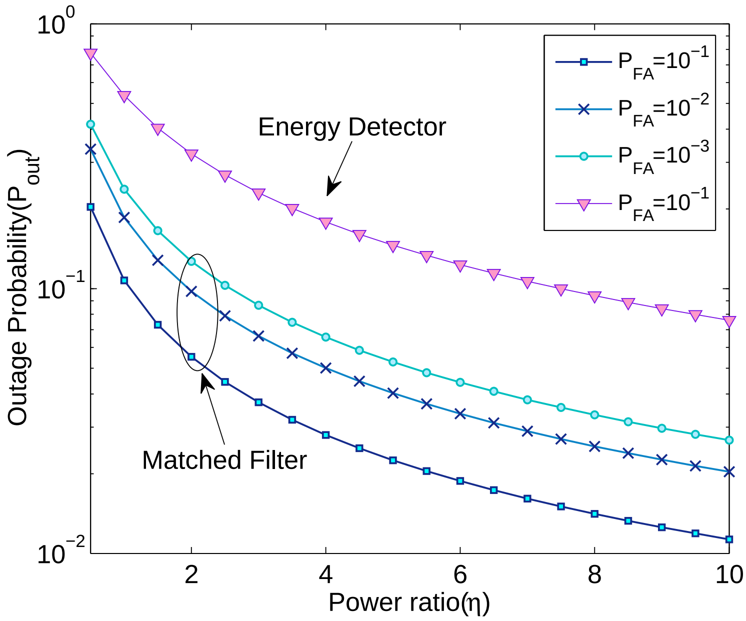

(e) OP of primary with varying power ratio for TX based sensing for $\lambda_s^{TX} = 10^{-1}, p = 1, \alpha = 4, r_e = 5, \gamma_p = 6$ dB, and $\gamma_b = 3$ dB (see Eqs. (5.13) and (5.31)).

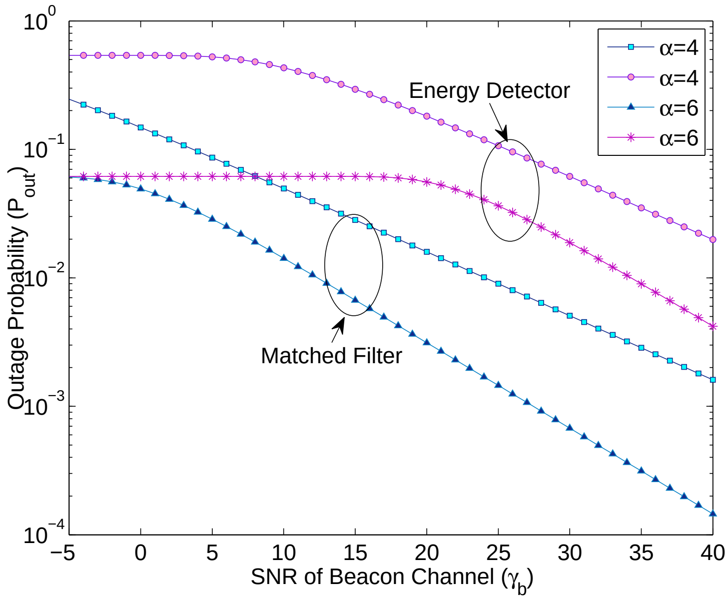

(f) OP of primary with varying SNR of beacon channel for TX based sensing for $\lambda_s^{TX} = 10^{-1}, p = 1, r_p = 2, r_e = 5, P_{FA} = 0.1, \gamma_p = 6$ dB and $\eta = 1$(see Eqs. (5.13) and (5.31)).

Figure 5.4: Impact of parametric variations on the OP of the primary link.

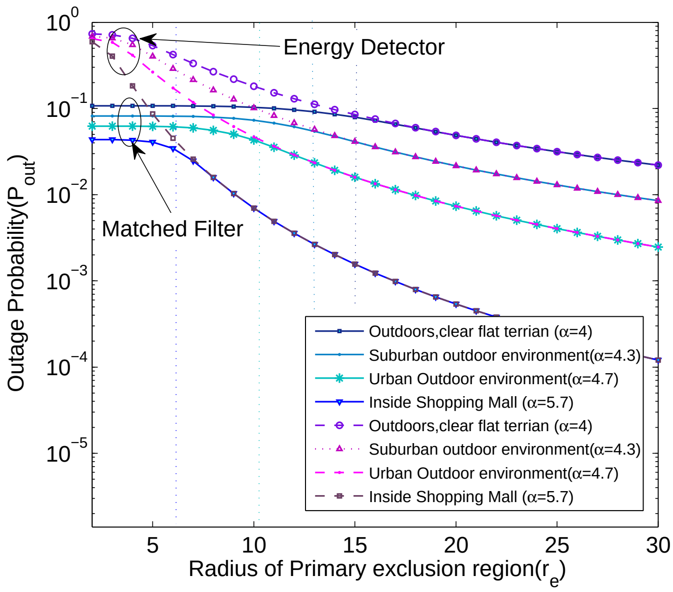

Figure 5.5: The OP of the primary versus the radius of the primary's exclusive region for TX based sensing for $\lambda_s^{TX} = 10^{-1}, p = 1,\ r_p = 2, P_{FA} = 10^{-1}, \gamma_p = 6\,\text{dB}$ and $\eta = 1$ (see Eqs. (5.13) and (5.31)).

where G_{RX} (gain) and is L_{RX} (loss) are percentage differences in the OP between the two schemes. Fig. 5.6a shows that the gains in the best case configuration are huge in the low SIR regime. In other words, when the primary link has less stringent QoS requirements and the spatial configuration of the receiver is the best, it is optimal to employ the receiver based spectrum sensing. Another important observation from Fig. 5.6a is that both the MF and the ED exercise the same order of increase in the gain for an equal decrease in the coefficient of distance variation for the best case configuration (c_B). A closer look at points A,B and C reveals that the choice of optimal detector depends on γ_p, as the MF with relatively less better configuration of CR receiver compared to the ED will still provide better performance in terms of gain. As shown by the dotted red line in Fig. 5.6a, the ED can attain gains similar to those of the MF by sensing for longer duration (i.e., by increasing time bandwidth product). As discussed before, not all CR receivers in a CRN will be in the best spatial configuration. Hence, only a fraction of CR receivers can be delegated the task of spectrum sensing. Consequently, the resulting gain is upper-bounded by G_{RX}.

The lower values of desired SIR threshold is of particular interest because primary user's are more sensitive to the secondary interference in this regime.

Fig. 5.6b depicts the losses encountered when the spatial configuration of the CR receiver is worse relative to the CR transmitter. Again the losses in terms of OP performance are huge for lower values of γ_p. However, the magnitude of decrease in loss is not same for a MF and an ED when subjected to a proportional reduction in the coefficient of distance variation (c_W). It is obvious that an ED is not very sensitive to variations in c_B. This is due to the fact that an ED by default results in a higher OP of the primary as compared to the MF. Moreover, the detection performance of the MF is more sensitive to the variation in SNR as compared to the ED. Hence there exists a trade off between the insensitivity to the spatial configuration, the complexity of implementation and the OP of the primary. The ED is less complex to implement, less sensitive to variation in P_{FA} and the location of receiver but provides poor OP in comparison with the MF which is more complex to implement, requires complete knowledge of the primary's beacon and is more sensitive to the receiver configuration when implemented in receiver based sensing mode. Notice, that these losses characterize the penalty incurred by a CRN, when CR TXs wrongly delegate the task of spectrum sensing to CR RXs. This penalty can be easily translated in terms of reduction in the CR's MAP (Section 5.7).

Complexity of Implementation vs. Sensitivity trade-off.

Finally in Fig. 5.7c we study how the OP of the primary link changes with variation in coefficient of distance variation c for fixed γ_p. Note that $c < 1$ corresponds to best case spatial configuration of a CR receiver, while $c = 1$ implies that the CR receiver has a configuration as good as that of the CR transmitter and $c > 1$ refers to a worse case configuration of a CR receiver. Since the CR transmitter based scheme is independent of c it provides a constant OP with respect to c when all other parameters are fixed. Fig. 5.7c provides some interesting insights. The OP for a receiver based scheme is less than the OP when a transmitter based scheme is adopted for $c < 1$, and greater for $c > 1$ for both an ED and a MF. However, it is obvious that the difference in terms of OP for a TX based scheme and RX based scheme when a MF is employed is significantly greater than the difference when an ED is employed. This consolidates our previous argument that an ED is less sensitive to the worst spatial configuration and can provide constant OP beyond a certain threshold value of c. Fig. 5.7c is divided into four regions. In Region I, RX based detection employing an ED is optimal; in region II, RX based detection employing MF is optimal; in region III and IV, TX based detection employing a MF is optimal. However, a more interesting observation in region IV is that RX based detection employing MF performs worse than TX based detection employing ED. This reveals how the geometry of a CR receiver can also affect the choice of optimal detector.

5.4.5.3 *Impact of parametric variations on the OP for Greedy transmitter strategy*

Figs. 5.7a and 5.7b compare the greedy strategy with the TX and RX based spectrum sensing strategy for worst and best spatial configurations of the CR receiver. Since both TX and RX jointly sense the spectrum the overall P_{FA} and P_{MD} is greater than that of the individual ones. Hence, the greedy strategy results in a higher OP than achieved by employing either RX or

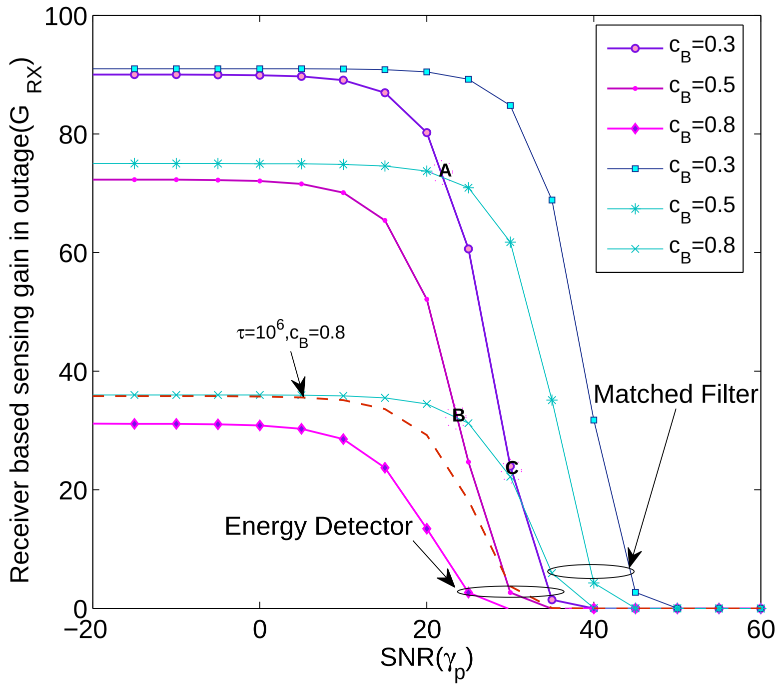

(a) Receiver based sensing gain varying SIR threshold for RX based sensing for $\lambda_s^{TX} = 10^{-2}, p = 1, \alpha = 4, r_e = 5, r_p = 2, \eta = 1, P_{FA} = 10^{-1}$and $\gamma_b = 10$ dB (see Eqs. (5.18) and (5.31)).

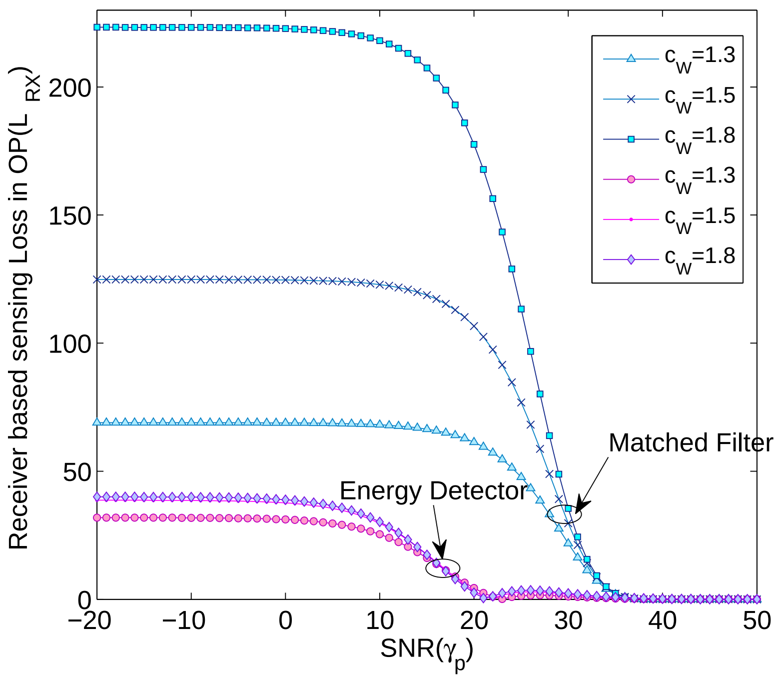

(b) Receiver based sensing loss varying SIR threshold for RX based sensing for $\lambda_s^{TX} = 10^{-2}, p = 1, \alpha = 4, r_e = 5, r_p = 2, \eta = 1, P_{FA} = 10^{-1}$and $\gamma_b = 10$ dB (see Eqs. (5.19) and (5.31)).

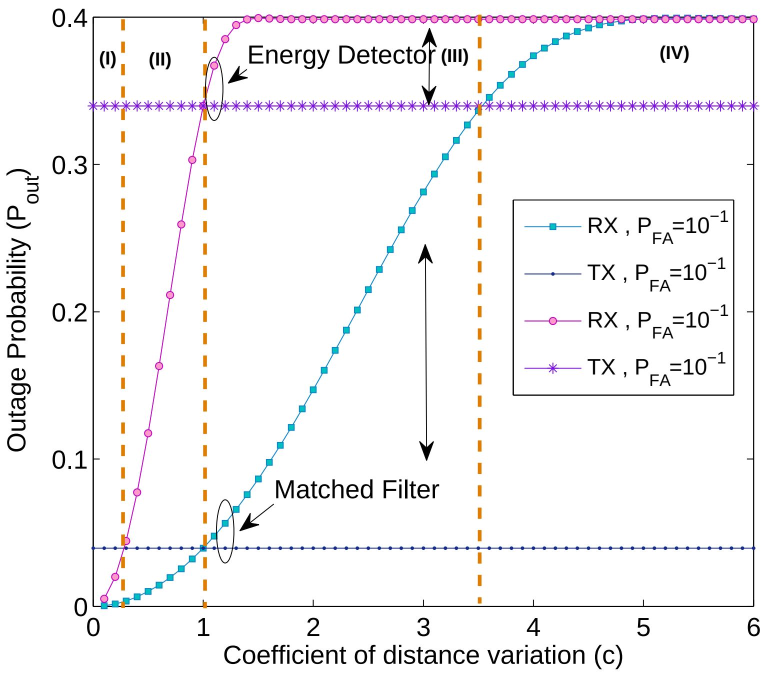

(c) OP of primary with varying coefficient of distance variation for RX based sensing for $\lambda_s^{TX} = 10^{-2}$, $p = 1, \alpha = 4, r_e = 5, \gamma_p = 15\,\mathrm{dB}, \eta = 1$ and $\gamma_b = 10\,\mathrm{dB}$ (see Eqs. (5.17) and (5.31)).

Figure 5.6: Impact of parametric variations on OP of the primary link when CRN performs RX based Sensing

TX based strategy. The OP in the case of heterogeneous detection presents some interesting results. In the case when a MF is employed at TX and an ED is employed at RX the OP of the greedy strategy is about the order of OP when ED is employed at RX only. This is intuitive since greedy behavior is dominated by the worst detector from RX and TX. Similarly in the case of ED-MF, the OP of the primary is about the same as when ED is employed at TX only.

Lastly, Fig. 5.8c presents the variation in the OP when the coefficient of distance variation c is subjected to changes. Different regions indicate different 'crossings' and optimal detector for the region. Results consolidate the previous arguments. We will skip the detailed discussion since intuitive reasoning can be provided as in the previous cases.

5.4.5.4 *Impact of parametric variations on the OP for Content transmitter strategy*

To conclude this section, we will discuss the impact of variation in c on the OP of the primary link when the CRN adopts content transmitter based spectrum sensing strategy. Results similar to those discussed previously are skipped due to space limitations.

Fig. 5.8 presents some interesting insights specially for the case of heterogeneous detectors. When content transmitter strategy is adapted with an ED at TX and a MF at RX irrespective of spatial configuration of the CR receiver, the detection performance is dominated by the MF. Since the MF has a better detection performance than the ED and if it fails to detect a beacon from primary, then the probability that the ED at TX will detect the beacon depends on the value of coefficient of distance variation c as indicated in Tables 5.1 and 5.2. Note that simulation results show that the MF at the receiver is selected by the system since it is better than an ED at TX for varying c, hence selecting the optimal detector. When a MF is employed at TX and an ED at RX, ED is selected up to a certain value of c (see Tables 5.1 and 5.2) after which a MF at TX becomes optimal in terms of minimizing the OP. When both TX and RX employ a MF, RX based sensing is used for the best spatial configuration of receiver and TX based sensing dominates for worst configuration hence content transmitter strategy provides minimum OP for all values of c. Similarly when an ED is employed at both TX and RX, an ED at RX dominates for choice of the best spatial configuration of the CR receiver while TX dominates in the worst spatial condition. Thus a content transmitter strategy provides better performance then employing an ED alone at either TX or RX but worse performance then employing a MF at both TX and RX. These insights reveal how the CRN designer can employ an optimal spectrum sensing strategy to minimize the OP of the primary given different desirable characteristics of the network and information about its operational environment.

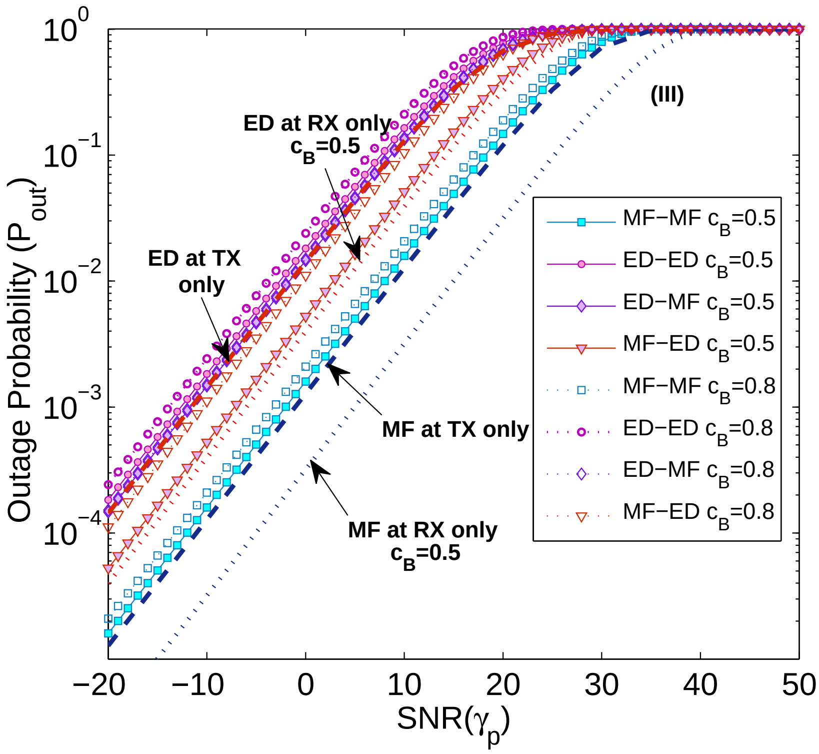

(a) OP of the primary link with varying SIR threshold for Greedy transmitter sensing strategy (Best RX configuration), $\lambda_s^{TX} = 10^{-2}, p = 1, \alpha = 4, r_e = 5, r_p = 2, \eta = 1, P_{FA} = 10^{-1}$ and $\gamma_b = 10$dB (see Eqs. (5.22) and (5.31)).

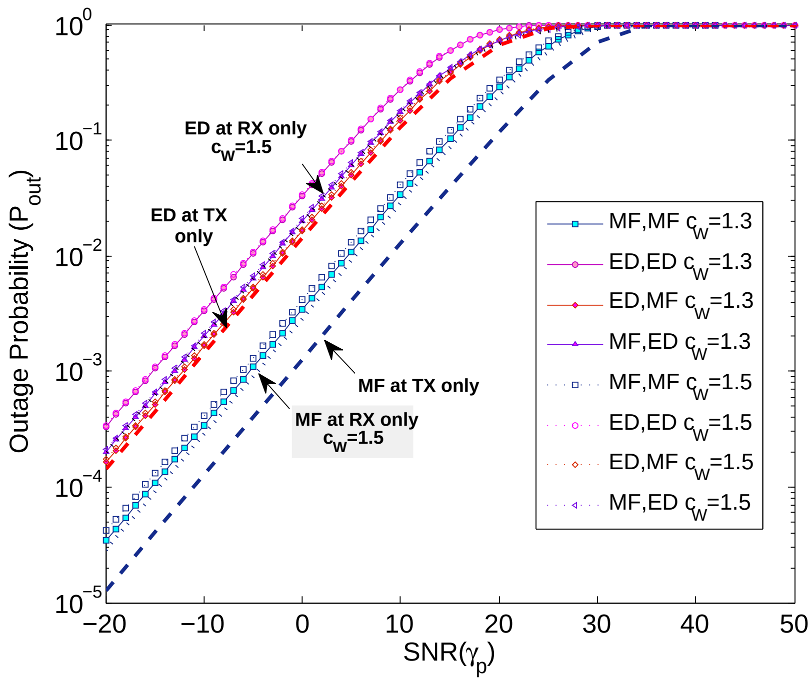

(b) OP of the primary link with varying SIR threshold for Greedy transmitter sensing strategy (worst RX configuration), $\lambda_s^{TX} = 10^{-2}, p = 1, \alpha = 4, r_e = 5, r_p = 2, \eta = 1, P_{FA} = 10^{-1}$ and $\gamma_b = 10$ dB (see Eqs.(5.23) and (5.31)).

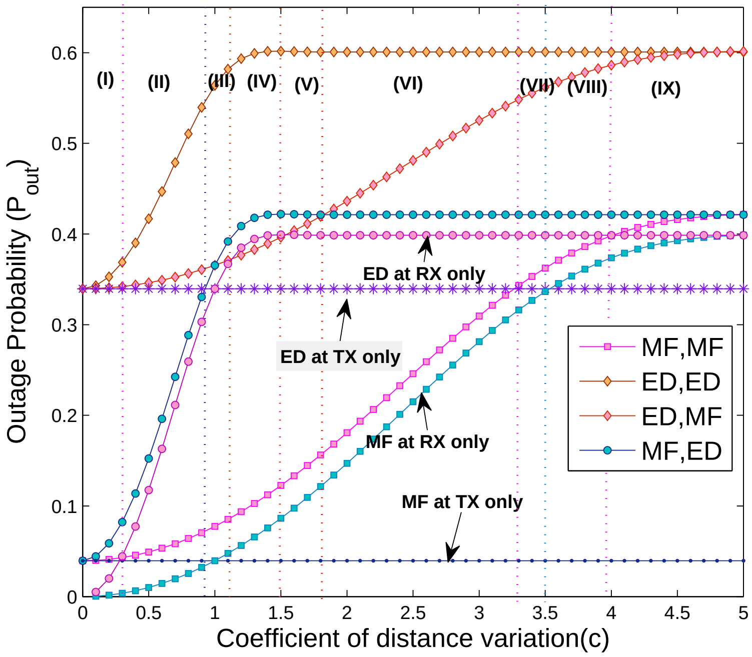

(c) OP of primary with varying coefficient of distance variation for Greedy transmitter based sensing strategy for $\lambda_s^{TX} = 10^{-2}$, $p = 1, \alpha = 4, r_e = 5, \gamma_p = 15$ dB, $\eta = 1$ and 10 dB (see Eq.(5.31)).

Figure 5.7: Impact of parametric variations on the OP of the primary link when the CRN performs greedy transmitter based sensing.

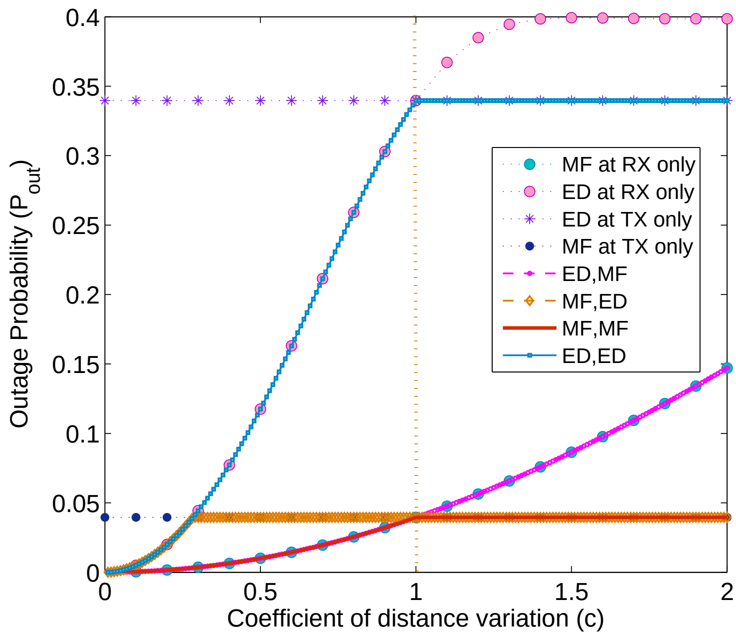

Figure 5.8: OP of primary with varying coefficient of distance variation for Content transmitter based sensing strategy for $\lambda_s^{TX} = 10^{-2}$, $p = 1, \alpha = 4, r_e = 5, \gamma_p = 15$ dB, $\eta = 1$ and $\gamma_b = 10$ dB (see Eq. (5.31) and Table. (5.3)).

5.5 THROUGHPUT OF THE PRIMARY LINK

In the previous section, we established a comprehensive analytical framework for studying the OP of the primary link in the presence of a Poisson field of secondary interferers employing different spectrum sensing strategies. Besides OP another important metric for the primary is the throughput of primary. The throughput of primary is defined as,

$$T_p = P_{suc}(\gamma_p) \log_2(1 + \gamma_p) \quad \text{(bits/sec/Hz)}. \tag{5.34}$$

This definition assumes that Shannon's formula for channel capacity holds. However, in the presence of non-Gaussian interference the above formula serves as a lower bound on actual throughput. Fig. 5.9 shows the variation in throughput with varying QoS requirements of the primary. As the SIR threshold increases (stringent QoS requirements) the throughput of the primary decreases (P_{suc} also decreases). Moreover, the throughput of the primary increases with the decrease in the density of secondary transmitters or decrease in MAP. Intuitively, decreasing either of these two corresponds to a decrease in the interference or in other terms increases the probability of success, hence increase in the throughput. Note that the throughput of the primary link is also coupled with the type of detector employed by the

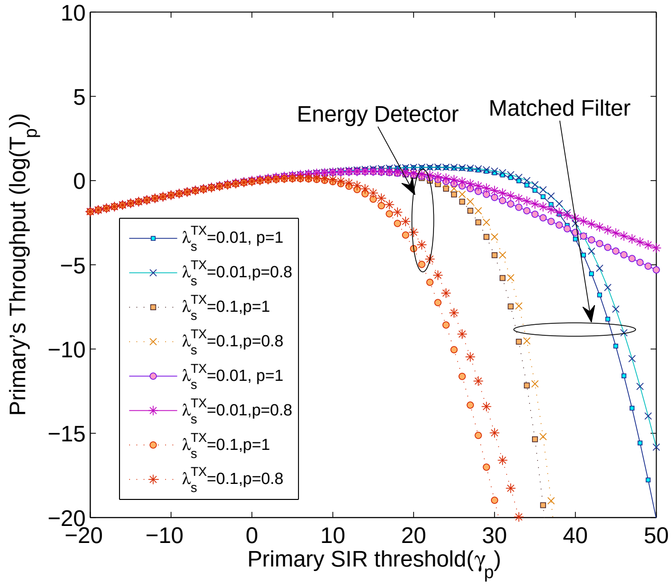

Figure 5.9: Throughput of the primary with varying SIR threshold γ_p for ED and MF with $\alpha = 4, \eta = 1, r_p = 2, r_e = 5, P_{FA} = 10^{-1}$and $\gamma_b = 10$ dB (see Eq. (5.34)).

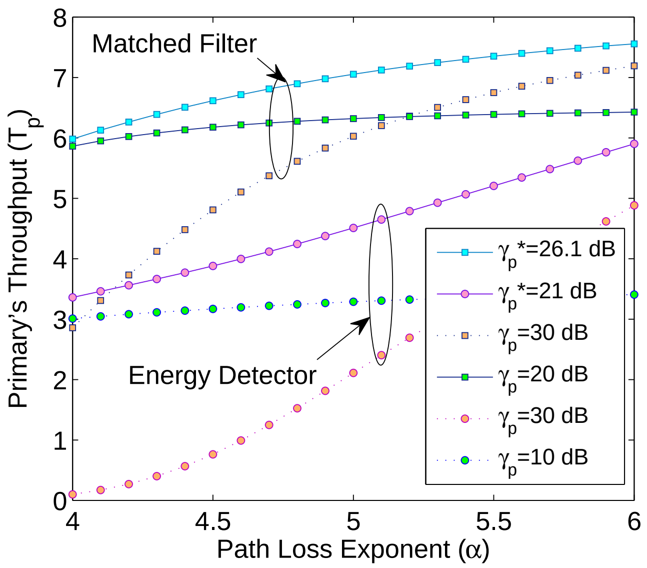

Figure 5.10: Throughput of the Primary with varying path-loss exponent for optimum SIR threshold with $\eta = 1, r_p = 2, r_e = 5, P_{FA} = 10^{-1}$ and $\gamma_b = 10$ dB (see Eq.(5.34)).

CRN. The MF results in superior throughput since it reduces interference by superior detection performance as compared to ED. Another interesting observation here is that there exists an optimal SIR threshold γ_p^* for which throughput is maximized.

Optimum SIR threshold for the Throughput of Primary

Proposition 5.3 *Considering all other parameters fixed, the throughput of the primary T_p is maximized for*

$$\gamma_p^* = \exp\left(\mathcal{W}\left(\frac{\eta}{r_p^\alpha \kappa_1}\right)\right) - 1, \tag{5.35}$$

where $\mathcal{W}(.)$ is the Lambert W function or product log function.

PROOF: Consider the probability of success (5.29) then

$$T_p = \exp\left(-\frac{\kappa_1 r_p^\alpha \gamma_p}{\eta}\right) \log_2(1+\gamma_p), \tag{5.36}$$

Solving by using first derivative and the definition of Lambert W function [122],

$$\gamma_p^* = \exp\left(\mathcal{W}\left(\frac{\eta}{r_p^\alpha \kappa_1}\right)\right) - 1. \tag{5.37}$$

□

Fig. 5.10 shows throughput of the primary versus path loss exponent. Note that the throughput is maximum for an optimum SIR threshold γ_p^*. Although increasing γ_p from γ_p^* should decrease the throughput since the QoS constraint becomes more stringent, this is not true for a decrease in γ_p. As shown in Fig. 5.10, decreasing γ_p from γ_p^* also decreases the throughput which consolidates the argument that γ_p^* is the optimal SIR threshold. Since the throughput of the primary is a function of $P_{suc} = 1 - P_{out}$, all other factors which impact the OP have a complementary affect on throughput. For instance, an increase in secondary user density will decrease the throughput as shown in Fig. 5.9 because it increases the OP. Hence, an optimal choice of the detector when the primary's throughput is of interest can be found as discussed previously.

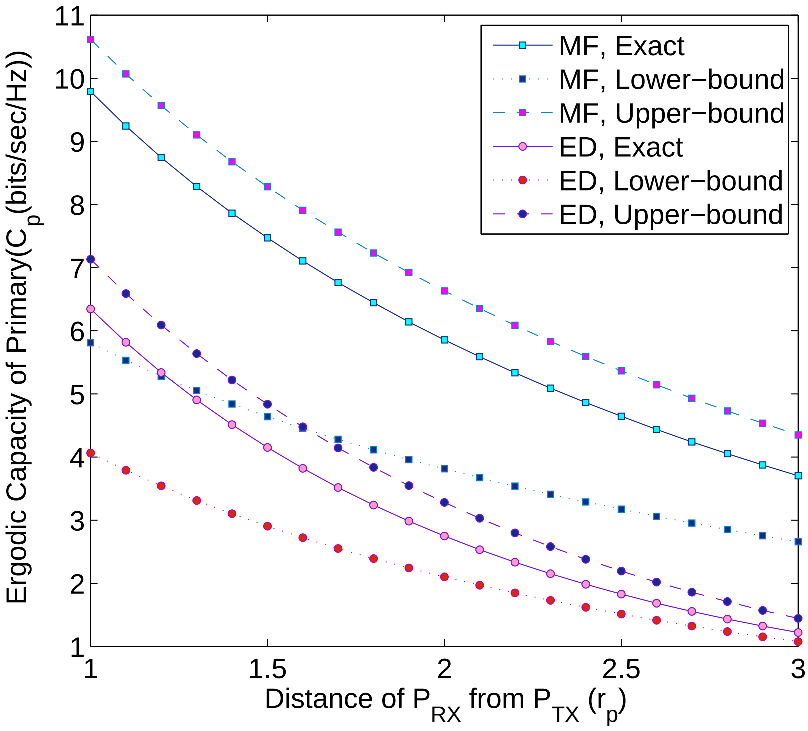

Figure 5.11: Ergodic capacity of the primary with varying link distance with $\eta = 1, r_p = 2, r_e = 5, P_{FA} = 10^{-1}$ and $\gamma_b = 10$ dB (see Eq. (5.40)).

5.6 ERGODIC CAPACITY OF THE PRIMARY

The ergodic capacity of the primary is another important metric. Ergodic capacity can be defined in terms of the OP P_{out} as,

$$\begin{aligned} C_p &= \mathbb{E}\left(\log_2\left(1+\mathrm{SIR}\right)\right) \quad \text{(bits/sec/Hz)}, && (5.38)\\ &= \int \log_2\left(1+\gamma_p\right) dP_{out}(\gamma_p). && (5.39) \end{aligned}$$

Ergodic capacity of the primary

Proposition 5.4 *Considering all other parameters fixed, the ergodic capacity of the primary in the presence of Poisson field of secondary interferers is given by,*

$$C_p = \frac{\exp\left(-\frac{\kappa_1 r_p^{\alpha}}{\eta}\right)}{\ln(2)} E_1\left(\frac{\kappa_1 r_p^{\alpha}}{\eta}\right). \tag{5.40}$$

PROOF: Considering (5.38) and (5.29)[5],

$$C_p = c_1 \int_0^{\infty} \log_2(1+\gamma_p) \exp(-\gamma_p c_1) d\gamma_p,$$

where $c_1 = \frac{\kappa_1 r_p^{\alpha}}{\eta}$. Substituting $\gamma = 1+\gamma_p$,

$$C_p = \frac{c_1 \exp\left(c_1\right)}{\ln(2)} \underbrace{\int_1^{\infty} \ln(\gamma) \exp(-\gamma c_1) d\gamma}_{A}.$$

Now,

$$A = \int_1^{\infty} \ln(\gamma) \exp(-\gamma c_1) d\gamma,$$

can be solved through using integration by parts and the exponential integral $E_1(x) = \int_1^{\infty} x^{-1} \exp(-x) dx$ to give

$$C_p = \frac{\exp\left(\frac{\kappa_1 r_p^{\alpha}}{\eta}\right)}{\ln(2)} \mathrm{E}_1\left(\frac{\kappa_1 r_p^{\alpha}}{\eta}\right). \tag{5.41}$$

5 The main reason behind utilizing a CGF based approximation is its exponential form which yields analytical, tractable solutions.

□

Upper (C_p^{up}) and lower (C_p^{lower}) bounds on the ergodic capacity of the primary can be established from the fact that,

$$\frac{1}{2}\exp(-x)\ln\left(1+\frac{2}{x}\right) < \mathrm{E}_1(x) < \exp(-x)\ln\left(1+\frac{1}{x}\right). \quad (5.42)$$

So,

$$C_p^{lower} = \frac{1}{2}\ln\left(1+\frac{2\eta}{\kappa_1 r_p^\alpha}\right) \text{ and } C_p^{up} = \ln\left(1+\frac{\eta}{\kappa_1 r_p^\alpha}\right). \quad (5.43)$$

As shown in Fig. 5.11 the ergodic capacity when secondary radios employ MF's is greater than the ergodic capacity when an ED is employed while considering TX based spectrum sensing. Moreover the ergodic capacity decreases with an increase in the link distance.

5.7 SELF-COEXISTENCE AND OPTIMAL MAP FOR SECONDARY

The most important aspect concerning the design of the MAC for a CRN is guaranteeing an uninterrupted/smooth operation of the primary link. The primary on the other hand wants to achieve a desired QoS. This QoS constraint dictates the primary's SIR requirements and success probability. Mathematically, the QoS translates into

$$P_{suc} = \Pr\{\mathrm{SIR} > \gamma_p\} \leq \rho. \quad (5.44)$$

If the secondary network is aware of such a QoS constraint, it can modify its MAP such that it guarantees desired QoS for the primary. This MAP not only depends upon the primary's QoS parameters (γ_p, ρ) but also on the *type and architecture* for the detection employed at the secondary.

Optimal MAP.

Proposition 5.5 *There exists an optimum MAP p_{opt} for the secondary network such that it guarantees the desired QoS parameters (γ_p, ρ) of the primary. In other words secondary transmitters maintain an interference level below a tolerable interference threshold. Such an optimum MAP p_{opt} can be calculated as,*

$$p_{opt} = \min\left(1, \frac{-\ln(\rho)}{\tilde{k}\ln\left(1+\frac{\gamma_p r_p^\alpha}{\eta}\tilde{\theta}\right)}\right), \quad (5.45)$$

where $\tilde{k} = k|_{p=1}$ and $\tilde{\theta} = \theta|_{p=1}$.

PROOF: From (5.44) and (5.31),

$$P_{suc} = \frac{1}{\left(1 + \frac{\tilde{\theta} r_p^{\alpha} \gamma_p}{\eta}\right)^{p\tilde{k}}} \leq \rho, \tag{5.46}$$

where $\tilde{k}$ and $\tilde{\theta}$ are independent of p or in other words evaluated considering $p = 1$. Taking the natural logarithm at both sides and solving for p gives,

$$p_{opt} = \min\left(1, \frac{-\ln(\rho)}{\tilde{k} \ln\left(1 + \frac{\gamma_p r_p^{\alpha}}{\eta}\tilde{\theta}\right)}\right).$$

□

5.7.1 *Discussion*

5.7.1.1 *Optimal MAP (p_{opt})*

The optimal MAP (p_{opt}) decreases as the primary's desired SIR threshold (γ_p) increases for a fixed success rate ρ as illustrated in Fig. 5.12a. Fig. 5.12a also illustrates that p_{opt} always guarantees the QoS constraint for the primary. Hence the primary's performance is only limited by the randomness in its own communication channel and its transmit power and not by the interference generated from the secondary transmitters. Note that as illustrated in Fig. 5.12a, p_{opt} also depends upon the type of detector employed by the secondary transmitter and the spectrum sensing architecture. Notice that the secondary transmitters employing ED have to adopt a lower MAP than those employing MF to compensate for the inferior detection performance. Moreover, up to a certain threshold value of γ_p, secondary transmitters have a positive non-zero MAP which may in turn reflect the usefulness of the secondary network.

5.7.1.2 *Self-coexistence constraint*

The self-coexistence constraint plays a central role in characterizing the interference experienced by the primary receiver from cognitive users. However as discussed earlier, studies in the past have overlooked the fact that the CRs also need to coexist among themselves. In other words, all of them cannot transmit simultaneously even if all of them want to communicate with their intended receivers. The MAC employed at the CRs is solely responsible for ensuring such a peaceful coexistence. Studies in the past do not cater for the MAC in the secondary network. Consequently, these studies [20, 51, 112, 124] have overestimated the interference encountered by a

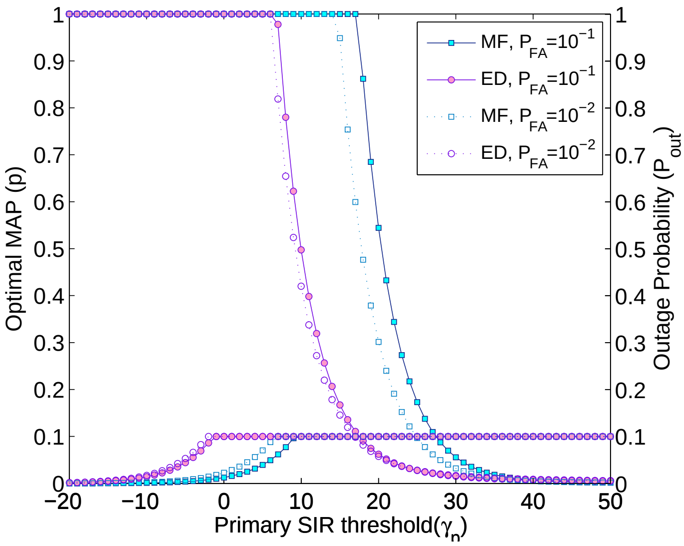

(a) Optimal MAP p for secondary network employing TX-based detection for varying QoS requirement of primary for $\lambda_s^{TX} = 10^{-1}, \eta = 1, r_p = 2, r_e = 5, P_{FA} = 10^{-1}, \rho = 0.9$ and $\gamma_b = 10$ dB (see Eq. (5.45)).

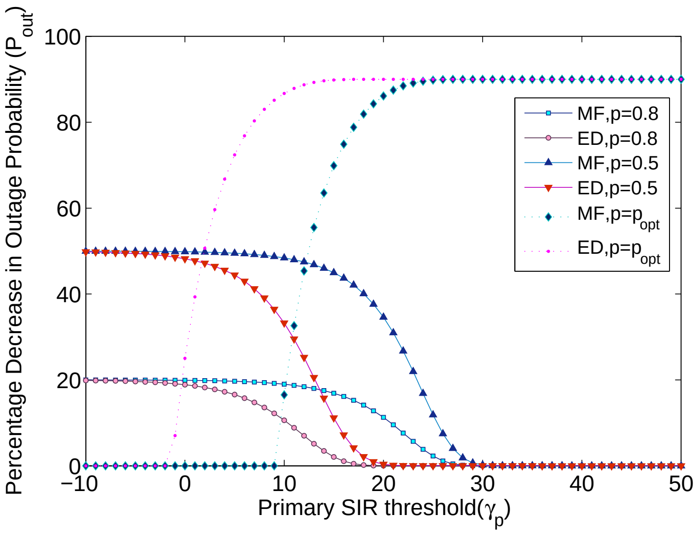

(b) Percentage decrease in OP under self-coexistence constraint,$\lambda_s^{TX} = 10^{-1}, \eta = 1, r_p = 2, r_e = 5, P_{FA} = 10^{-1}$ and $\gamma_b = 10$ dB .

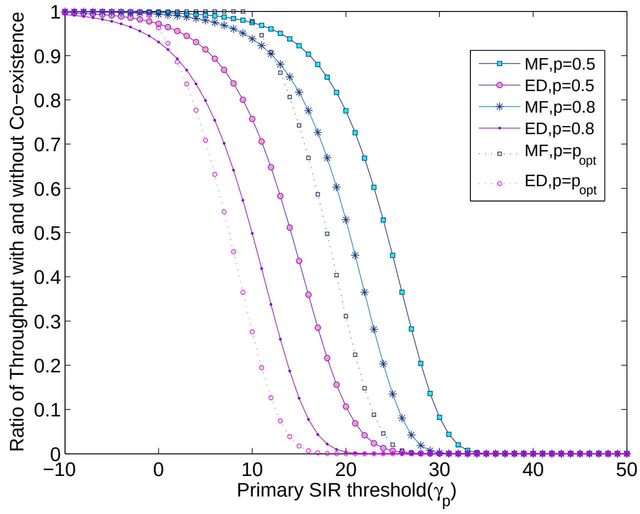

(a) Ratio of throughput with and without coexistence constraint $\lambda_s^{TX} = 10^{-1}, \eta = 1, r_p = 2, r_e = 5, P_{FA} = 10^{-1}$ and $\gamma_b = 10\,\text{dB}$.

Figure 5.12: Optimal MAP p for desired primary QoS and impact of the self-coexistence on outage and throughput

typical primary receiver in the presence of a collocated CRN. This overestimation may motivate a CRN designer to design overprotective protocols with a higher interference margin for the CRN, which will in turn decrease the spectral efficiency and hence the usefulness of CRNs.

In this work, we cater for the self-coexistence constraint in the form of Slotted ALOHA MAC. Our motivation (like other studies [44, 111]) for restricting the discussion to the Slotted ALOHA is mainly due to its simple model which provides some fundamental insights. More complicated MACs, such as CSMA/CA[6] possess additional dependence between spectrum sensing and the carrier sensing processes. Consequently, analysis of such a MAC scheme may obscure fundamental insights which can be obtained by studying simple MAC protocols such as ALOHA.

Fig. 5.12b shows the percentage decrease $\left(\frac{P_{out}|_{p=1} - P_{out}|_{p<1}}{P_{out}|_{p=1}} \times 100\%\right)$ in the OP of the primary link when CRs operate under the self-coexistence constraint. As indicated in Fig.5.12b even for the high values of MAP ($p = 0.8$),

6 To the best of our knowledge even for wireless ad hoc networks, no closed form expressions are known for the Laplace transform of interference under CSMA/CA MAC. In [62] the authors demonstrated that such an ad hoc network forms Matern hardcore process of type II. In order to simplify analysis, most of the studies approximate dependent thinning of Matern's hardcore process by independent thining with retention probability $p = \frac{1-\exp(-\lambda b_d r^d)}{\lambda b_d r^d}$ [61], where r is the inhibition radius between the points retained after thinning a stationary marked PPP. This implies that a rough estimate of performance for CSMA/CA can be obtained by simply adjusting the MAP to $p = \frac{1-\exp(-\lambda \pi r_c^2)}{\lambda \pi r_c^2}$. In this case, r_c is the carrier sensing range of the CSMA/CA protocol.

the percentage decrease is significant. Moreover, it is also obvious that the percentage decrease in OP is proportional to $1 - p$ (i.e. the probability by which any CR defers its transmission). In case of more complex protocols like CSMA, the probability of deferring the transmission is different for different CRs. This is due to the fact that the spatial configuration of neighbors determines the MAP of a particular secondary receiver. Fig. 5.12b also shows that the percentage difference in OP can be as high as ρ when an optimum MAP is employed by the secondary transmitters. Fig. 5.12a shows the ratio of throughput with and without coexistence. The decreasing ratio shows that a significant throughput gain can be exercised when the primary SIR threshold γ_p is high and the CRN operates under the self-coexistence constraint.

5.8 CONCLUDING REMARKS

In this chapter, we have developed a comprehensive statistical model of the interference encountered by a typical primary receiver due to the secondary transmitters in a collocated CRN. We considered that spectrum sharing between the primary user and secondary transmitters is achieved by using explicit beaconing and interweave spectrum access method. Secondary users utilize a matched filter or an energy detector to detect the primary's beacon based on the degree of their knowledge about the beacon signal. We explored the OP of the primary receiver when the CRN can employ three different spectrum sensing architectures, namely, TX-based spectrum sensing, RX-based spectrum sensing and TX-RX joint spectrum sensing. Several parametric variations and their impact on the OP of the primary for all the stated sensing architectures is investigated in a comprehensive manner.

6

TRANSMISSION CAPACITY ANALYSIS OF COGNITIVE RADIO NETWORKS

CRNs are envisioned to eradicate the artificial scarcity caused by today's stringent spectrum allocation policy. In this chapter, we develop a comprehensive statistical framework to study the transmission capacity (TC) of the primary network in the presence of collocated CRN operating under self-coexistence constraint. Considering a system model based on stochastic geometry and the primary beacon enabled interweave spectrum sharing model, OP of a typical primary receiver is studied. Scaling laws for the OP of a typical primary receiver are established. With the help of simulations it is shown that TC of the primary network decreases with increasing number of secondary users and degree of the self-coexistence.

Primary objective:
- *To characterize the transmission capacity of a large scale primary network.*
- *To study the impact of the secondary network's density on the transmission capacity of the primary network.*

6.1 INTRODUCTION

In the previous chapter, we developed a statistical framework to characterize the performance of a single primary link operating in the presence of collocated CRN. The focus of this chapter is to extend the analysis for a large scale primary network.

As mentioned earlier the past studies [20, 51, 125] have devoted significant attention towards modeling the interference at a primary receiver surrounded by a Poisson field of secondary users. However, these studies ignore some of the fundamental operational and design constraints on the CRs. Firstly, these studies consider a single primary and multiple secondary user ad hoc network model, where all secondary users transmit and hence potentially cause the outage at the primary receiver [20]. Nevertheless, in practice not only multiplicity of both primary and secondary users is exercised, but *'self-coexistence'* constraint on secondary users is also enforced. Under such a self-coexistence constraint only a fraction of secondary transmitters are allowed to transmit at a particular time instant according to some medium access control (MAC) scheme. Moreover, even with sophisticated MAC schemes, the self-interference/inter-network interference is unavoidable. In other words, a typical primary receiver not only suffers from interference from the secondary users which fail to detect the primary but also from the other primary transmitters utilizing the same frequency band for concurrent transmissions. Hence the outage incurred at a typical primary receiver is characterized by both the primary and secondary users under co-existence constraints. A complex but interesting question for a CRN designer is how outage of the primary network is coupled with the amount of multiplicity (density) of users in both the primary and secondary networks? This indeed warrants the study of the scaling properties of the OP, which are addressed in this chapter. Another important question is how the effective capacity of the ad hoc primary network is affected by the density of users? Since even after significant efforts, the capacity region of the ad hoc network still remains an unsolved puzzle, it might be impossible to obtain such a region considering both the primary and secondary ad hoc networks. However, as adopted by the ad hoc networking community, an alternate metric of *transmission capacity* (TC) can be employed for the study of CRNs. The TC of the ad hoc network represents the number of successful transmissions per unit area subject to a certain outage constraint (see Section 6.4for the formal definition and details). To the best of our knowledge, TC of the primary network in the presence of CRN has not been studied before. Hence in this chapter, we take the first step in this direction and establish the TC of the primary network in presence of a CRN.

6.2 RELATED WORK AND OUR CONTRIBUTION

To the best of our knowledge, none of the studies in the past have explored the TC in the context of CRNs. The only work which closely relates to this chapter is [72]. In [72], authors have studied the capacity trade-off for co-existing ad hoc and cellular networks sharing the spectrum using *spectrum underlay* or *spectrum overlay* mechanisms. However, the study considers traditional ad hoc networks where transmission decisions are not based upon the inference drawn from the spectrum sensing process. The TC for ad hoc networks was primarily introduced by Weber et. al. in [46]. Numerous studies in the past have employed TC to study different design and performance mechanisms for ad hoc wireless networks. Interested readers are refered to [126] and the references therein. Another closely related area is the study of outage and interference (with and without self-coexistence constraints) in the context of both traditional ad hoc networks and cognitive ad hoc networks. Interested readers are directed to [63, 125] for details.

Contributions and Organization

As previously discussed, this chapter is the first step in the direction of exploring TC of a primary ad hoc network in presence of a collocated CRN. So in this chapter:

☐ We consider a network model (Section 6.3) where the spatial distribution of the primary and secondary nodes is characterized by the Poisson point process. We formalize the stochastic geometry based network model and the underlying intuition. We then discuss the classification of the nodes based on their role at an arbitrary time instant. We formalize the notion of self-coexistence and highlight its importance.

☐ Based on the network and spectrum sharing model introduced in Section 6.3, in Section 6.4:

i) We develop a statistical framework for quantifying OP of a typical primary receiver in the presence of multiple primary and secondary interferers, considering the *self-coexistence* constraint;

ii) Scaling Laws for the OP of a typical primary receiver are established;

iii) Statistical framework for evaluating the TC of the primary network is derived from the OP analysis.

☐ Lastly, with the help of simulations (in Section 6.5) we study how the TC of the primary network is affected by the parametric variations such as the multiplicity or density of users, MAP and the signal to interference ratio (SIR) threshold.

6.3 STOCHASTIC GEOMETRY BASED NETWORK MODEL

6.3.1 *Geometry of the Primary and Secondary Network*

6.3.1.1 *Node Distribution*

In this chapter, we consider that the spatial distribution of primary and secondary users can be accurately characterized by a homogeneous Poisson point process (HPPP). More specifically, the location of the nodes of the primary network at any arbitrary time instant[1] constitutes a HPPP $\Phi_p(\lambda_p)$ with intensity λ_p. The intensity/density λ_p quantifies the number of primary users per unit area. Similarly, the location of the nodes of the secondary network form a HPPP $\Phi_s(\lambda_s)$ with intensity λ_s. Note that both $\Phi_p(\lambda_p)$ and $\Phi_s(\lambda_s)$ are collocated over an infinite Euclidean plane and by the Superposition theorem [60], the overall network formed by both the primary and secondary users follows a HPPP $\Phi(\lambda) = \Phi_p(\lambda_p) \cup \Phi_s(\lambda_s)$ with intensity $\lambda = \lambda_p + \lambda_s$. It is worth mentioning that the HPPP is a very well established statistical model for the spatial distribution of the nodes in ad hoc wireless networks [63]. There is a wealth of literature utilizing the HPPP for modeling the spatial distribution of nodes and many studies in the past [20, 51] have utilized the HPPP for modeling the spatial distribution of the secondary network. At this juncture, it is worth mentioning that the HPPP assumption comes with two fundamental constraints on the spatial distribution of the nodes:

1 In other words, we consider an arbitrary snapshot of the network.

1. *Poisson distribution of nodes:* Considering $\Phi_i(B)$ $(i \epsilon \{s, p\})^2$ as a counting process defined over a bounded Borel set B, the number of nodes (i.e., points of Φ_i in B) have a Poisson distribution with a finite mean $\lambda_i v_d(B)$ for some constant λ_i. $v_d(B)$ is the Lebesgue measure defined on the measurable space $[\mathbb{R}^d, B^d]$. In other words, $v_d(B)$ is the volume of a $d-$dimensional bounded Borel set B . If B is a $d-$dimensional sphere $v_d(B) = b_d r^d$, where r is the radius of the sphere and b_d is the volume of the unit sphere in $\mathbb{R}^d$, then $b_d = \sqrt{\pi^d}/\Gamma(1+d/2)$with $\Gamma(a) = \int_0^\infty x^{a-1} \exp(-x) dx$.

2. *Independence:* The number of primary/secondary nodes in m disjoint bounded subsets B of $\mathbb{R}^d$ form m independent random variables, for an arbitrary m. It is natural to assume such a constraint because in real life, the node movements in ad hoc networks are independent of each other. Hence, considering a typical snapshot of such a network, the number of nodes in disjoint areas is independent and identically distributed (i.i.d.).

Note that, by construction both the primary and secondary networks satisfy the above-mentioned properties.

6.3.1.2 *Classification of Nodes*

At a given instant, any arbitrary primary/secondary node can act either as a transmitter or a receiver. We formulate this classification of nodes by employing the Superposition theorem. The HPPP $\Phi_i(\lambda_i)$ can be constructed by the superposition of two independent HPPPs $\Phi_i^{tx}(\lambda_i^{tx})$ and $\Phi_i^{rx}(\lambda_i^{rx})$ with intensity λ_i^{tx} and λ_i^{rx} respectively, such that $\lambda_i = \lambda_i^{tx} + \lambda_i^{rx}$, with:

$$\lambda_i^{tx} = \lambda_i \rho_i \text{ and } \lambda_i^{rx} = (1 - \rho_i)\lambda_i. \tag{6.1}$$

where $0 \leq \rho_i \leq 1$. ρ_i can be interpreted as the medium access probability (MAP) for Slotted ALOHA type MAC. MAP is one of the important parameters and of significant importance while modeling the interference in CRN. Indeed, MAP is used to model the self-coexistence constraint in CRN. In particular, even if every secondary transmitter always has data to transmit to some secondary receiver, not all of them can transmit at the same time. This constraint stems from the fact that, if all the secondary transmitters transmit data all the time none of them will be successful in their transmission. Such a self-coexistence constraint is ignored by the past studies [20, 51]. Consequently, these studies over-estimate the interference encountered by a typical primary receiver. Since the interference analysis is fundamentally

2 We utilize the notation of i instead of s or p to avoid repetition, when both primary and secondary networks can be treated under the same framework.

concerned with the distribution of the transmitters, we can invoke the above-mentioned property to model the spatial distribution of the transmitters in the primary/secondary network. An alternative but equivalent model can be constructed using the theory of Marked point processes [60]. However, for the sake of clarity and simplicity, we adhere to the model introduced.

6.3.1.3 *Reference Primary Node*

We introduce a reference/probe node in the point process formed by the locations of the primary nodes, it does not effect the overall distribution of the nodes. In order to keep the mathematical analysis simple (like most of the studies [72, 126]), we introduce a reference node at the origin. However, note that the analysis is valid for any *typical point* of the point process. Putting it in a more concrete way, complementary cumulative density function (CCDF) of the interference at a typical primary receiver located at the origin and measure of quality of service (QoS) (will be discussed later) are sufficient to characterize the transmission capacity and other performance measures. Like the past studies [72, 126], we assume that the reference primary transmitter is located at a distance r_o from the reference primary receiver.

6.3.1.4 *Primary Exclusion Region*

In the case of ad hoc networks, the primary's exclusion region is defined by a disk of radius r_e, centered at the primary receiver. Hence, the exclusion disk defines the interference region in which any concurrent transmission on the same frequency band will cause significant interference at primary receiver. Alternatively, it is also possible to center the exclusion disk on the primary transmitter rather than the primary receiver [93]. The detailed discussion on the primary's exclusion region (also refered to as the primary guard zone) can be found in [64]. It is worth highlighting that the primary's exclusion region is an important design parameter which is indeed dictated by the maximum tolerable interference threshold, secondary node density, fading, environment dependent path-loss and the MAC mechanism. Perhaps, it should be highlighted that incorporating for the exclusion region of primary receiver might increase the complexity of analysis. However, an advantage of such a regulatory constraint is that it inherently avoids the singularity [127] for power-law type path-loss model. Interested readers are refered to [125] for details.

6.3.2 *Channel Model*

The large scale path-loss between any arbitrary transmitter $y_t \epsilon \Phi_i^{tx}(\lambda_i^{tx})$ and the reference receiver is given by $l(\|y_t - 0\|)$, where, $l(.)$ is a distance dependent path-loss function and $\|.\|$ corresponds to the Euclidean distance. Generally, the large scale path-loss is modeled by considering the power law function, i.e., $l(R) = CR^{-\alpha} R \geq 1$, where C is the frequency dependent constant, R is the distance between the transmitter and the receiver and $\alpha > 2$ is the terrain or environment dependent path-loss exponent. In the specific case where $y_t \epsilon \Phi_s^{tx}(\lambda_s^{tx})$, the constraint on path-loss function becomes $R \geq r_e \geq 1$. This is required to cater for the primary's exclusion region, as described previously.

The channel effects due to multipath impairment process between any arbitrary transmitter $y_t \epsilon \Phi_i^{tx}(\lambda_i^{tx})$ and the reference receiver can be modeled using a random variable H with the probability distribution function (PDF) $f_H(.)$, cumulative distribution function (CDF) $F_H(.)$ and mean μ. We also consider that H is independent and identically distributed (i.i.d.) both in the spatial and temporal domain. The overall impact of the communication channel is modeled using a random variable $G = Hl(r)$.

6.3.3 *Spectrum Sensing Model*

Secondary transmitters must follow several prescribed spectrum etiquettes to ensure peaceful coexistence with the primary network. As proposed by the FCC, it is obligatory for the secondary transmitters to detect the presence of the primary user, before initiating their own communication session. Many studies have investigated several potential algorithms to detect the presence of the primary. It is beyond the scope of this chapter to elaborate the discussion on this topic. Interested readers may refer to [8] for an overview of the primary detection algorithms and spectrum sharing models [3].

We consider a beacon/control channel based spectrum sensing model. The primary transmitter explicitly sends a control signal such as '*grant*' and '*inhibit*' when it leaves or enters the transmission mode. Such a scheme is also known as *out of band* sensing [20]. Numerous studies on the interference modeling [20, 51] have utilized this model. In this chapter, we assume that beacon channel is interference free. In practice this is assured by the control packets such as CTS/RTS of the primary network . In such a network all primary users which receive CTS from a primary in their contention domain, refrain to send their own beacon. Hence before initiating its communication a primary receiver can send inhibit beacon without suffering significant interference. This assumption may seem trivial however note that it is rather critical to keep analysis tractable.

6.4 TRANSMISSION CAPACITY ANALYSIS OF PRIMARY NETWORK

In this section, we develop a comprehensive framework for evaluating the TC of the primary network in the presence of a collocated CRN. The TC of an ad hoc primary network is characterized by the OP of a typical primary receiver; which is in turn governed by the accumulative interference from both the collocated[3] primary and secondary users. Since this chapter (to the best of our knowledge) is the first work on the TC based analysis of CRN, it is worth providing a formal definition of TC in terms of the underlying factors which characterize it.

Transmission capacity of the primary network.

Definition 6.1 *The number of concurrent successful transmissions occurring per unit area in the primary network, subject to some OP constraint in the presence of collocated secondary network, is defined as the transmission capacity (TC) of the primary network. Mathematically,*

$$C(q) = p_{out}^{-1}(q)(1-q) \quad q \,\epsilon\, (0,1), \tag{6.2}$$

where $p_{out}(\lambda)$ is the OP of a typical primary receiver subject to the constraint β (will be defined shortly) on accumulative interference caused by the Poisson field of interferers with intensity λ and q is the network-wide QoS measure.

In stochastic geometric sense, $p_{out}^{-1}(q)$ corresponds to the spatial intensity of the transmissions associated with the OP q, thinned by the probability of success $(1-q)$. Note that our definition of TC is mainly motivated by the definition of Weber et al. in [126] in the context of ad hoc networks.

6.4.1 *Outage Probability*

By virtue of Definition 1, the TC of the primary network is characterized by the OP p_{out} of a typical primary receiver. Hence, in this subsection we establish an analytical framework for the OP by considering the reference primary receiver located at the origin (Section 3.1.3).

The OP of a reference primary receiver $x_o \,\epsilon\, \Phi_p \cup \{0\}$ located at the origin is defined as the probability that SIR[4] at the receiver is below a specified threshold β,

$$\begin{aligned} p_{out}(\Lambda) &= \Pr\left\{\mathrm{SIR} < \beta\right\}, \\ &= \Pr\left\{\frac{P_p H_o l(r_o)}{\sum_{i \epsilon \Phi_{int}(\Lambda)} P_i H_i l(R_i)} < \beta\right\}. \end{aligned} \tag{6.3}$$

where, P_p is the transmit power of the primary transmitter , H_o is the channel gain between the reference primary transmitter and receiver separated by a distance r_o, $l(.)$ is path-loss function, H_i is the channel gain of the interferer i ,P_i is the transmit power of the interferer i , R_i is the distance between

3 Here the term 'collocated' is not confined to the spatial collocation, rather it also implies that interfering nodes transmit in same frequency band as that of the reference pair.

4 Throughout the analysis we consider that the network is interference limited. However thermal noise can also be accommodated in the same framework.

the interferer i and the reference primary receiver and β is the threshold SIR which depends on the desired bit error rate (BER) and data transmission rate. Both H_o and H_i are drawn from the distribution $F_H(.)$ and are i.i.d.

The point process of the interferer $\Phi_{int}(\Lambda)$ in the case of CRN plays a central role while evaluating the OP of a typical primary receiver. Primary transmitters, which operate in the same frequency band as that of the reference pair, and the secondary users which fail to detect the beacon from the primary, both contribute towards the accumulative interference. Past studies on the interference modeling [20, 51], consider only a single primary transmitter and receiver pair in the presence of Poisson distributed secondary users. In these studies, only the secondary users which fail to detect the primary's beacon are considered as the source of interference. However, in practice, primary ad hoc network also suffers from the interference from the other primary users when employing MAC schemes such as Slotted ALOHA or even CSMA/CA. Hence, in this chapter we consider both primary and secondary transmitters as the potential interferers.

$$\begin{aligned} \Phi_{int}(\Lambda) &= \Phi_s^{md,tx}(\lambda_s^{md,tx}) \cup \Phi_p^{tx}(\lambda_p^{tx}), \\ \Lambda &= \lambda_s^{md,tx} + \rho_p \lambda_p. \end{aligned} \tag{6.4}$$

where, $\Phi_s^{md,tx}(\lambda_s^{md,tx})$ is the point process formed by the secondary transmitters which lie outside the primary's exclusion region and fail to detect the *inhibit* beacon from the primary. Such a point process is constructed using *dependent thinning* [60] of the HPPP of the secondary transmitters $\Phi_s^{tx}(\lambda_s^{tx})$.

A secondary transmitter located at a distance r from the primary receiver is able to detect the beacon if the SNR of the beacon channel is above some fixed threshold γ_{th}. Mathematically,

$$\mathbb{1}_{md}(\gamma(r)) = \begin{cases} 1 & \gamma(r) < \gamma_{th} \\ 0 & \gamma(r) \geq \gamma_{th} \end{cases}, \tag{6.5}$$

where $\mathbb{1}_{md}(\gamma(r))$ is the indicator random variable, i.e., the detection process can be expressed as a Bernoulli trial with the probability of misdetection $\Pr\{\gamma(r) < \gamma_{th}\}$ and probability of detection $1 - \Pr\{\gamma(r) < \gamma_{th}\}$. The SNR $\gamma(r) = \frac{P_b l(r) H}{N_o}$, where P_b is the beacon transmission power, H is the channel gain between the primary receiver and the secondary transmitter and N_o is the noise power at secondary transmitter. Note that the point process formed by such dependent thinning is non-homogeneous. The intensity of $\Phi_s^{md,tx}(\lambda_s^{md,tx})$ in polar coordinates is given as,

$$\lambda_s^{md,tx}(r) = d b_d \rho_s \lambda_s r^{d-1} \mathbb{1}_{md}(\gamma(r)). \tag{6.6}$$

With the complete characterization of interferers at our disposal, we now revert back to the original problem of evaluating OP for the reference primary receiver.

OP and MGF of the Interference.

Lemma 6.1 *Considering H_o to be exponentially distributed with mean $\mu = 1$, the OP of a typical primary receiver is completely characterized by the product of the moment generating functions (MGF) of the shot noise random field of the primary interferers (primary transmitters transmitting concurrently) and secondary interferers (secondary transmitters failing to detect the primary, hence continuing their transmission).*

PROOF: From (6.3),

$$\begin{aligned} p_{out}(\Lambda) &= \Pr\left\{H_o < \frac{\beta \sum_{i\epsilon\Phi_{int}(\Lambda)} P_i H_i l(r_i)}{P_p l(r_o)}\right\}, \\ &= 1 - \mathbb{E}\left(\exp\left(-sI_{sec}\right)\right)\Big|_{s=\frac{\beta\eta}{l(r_o)}} \mathbb{E}\left(\exp\left(-sI_{pri}\right)\right)\Big|_{s=\frac{\beta}{l(r_o)}} \\ &= 1 - M_{I_{sec}}\left(\frac{\beta\eta}{l(r_o)}\right) M_{I_{pri}}\left(\frac{\beta}{l(r_o)}\right). \end{aligned} \tag{6.7}$$

where, $I_{sec} = \sum_{i\epsilon\Phi_s^{md,tx}(\lambda_s^{md,tx})} H_i l(r_i)$, $I_{pri} = \sum_{i\epsilon\Phi_p^{tx}(\lambda_p^{tx})} H_i l(r_i)$, $\eta = \frac{P_s}{P_p}$ is the ratio of secondary transmit power P_s to the primary transmit power P_p, $M_{I_{sec}}$ and $M_{I_{pri}}$ are the MGFs of the shot noise random field of the secondary and primary interferers respectively.

□

MGF of the aggregate interference inflicted by the secondary users.

Theorem 6.1 *The MGF of the accumulative interference due to the secondary transmitters which fail to detect an inhibit beacon from a reference primary node over a Rayleigh faded channel (i.e., exponential channel gain H_i with $\mu = 1$) can be closely approximated as*

$$M_{I_{sec}}(s) = \frac{1}{(1+\theta s)^k}. \tag{6.8}$$

where, $k = \frac{\kappa_1^2}{\kappa_2}$ and $\theta = \frac{\kappa_2}{\kappa_1}$ with κ_n being the n^{th} cumulant of the interference.

$$\kappa_n = \frac{d\rho_s\lambda_s b_d}{\alpha n - d}\left[\gamma_{low}\left(n, \bar{\gamma}_{th}\right) r_e^{d-\alpha n} + \left(\frac{\bar{\gamma}_{th}}{r_e^{\alpha}}\right)^{\frac{d}{\alpha}-n} \gamma_{up}\left(\frac{d}{\alpha}, \bar{\gamma}_{th}\right)\right]. \tag{6.9}$$

with $\gamma_{low}(a,b) = \int_0^b x^a \exp(-x)dx$, $\gamma_{up}(a,b) = \int_b^\infty x^a \exp(-x)dx$ *and* $\bar{\gamma}_{th} = \gamma_{th} N_o r_e^\alpha$.

PROOF: see Appendix F. □

MGF of the accumulative primary interference.

Theorem 6.2 *The MGF of the accumulative interference due to the primary transmitters concurrently transmitting with the reference primary node over a Rayleigh faded channel (i.e., exponential channel gain H_i with $\mu = 1$) is given as*

$$M_{I_{pri}}(s) = \exp\left(-\rho_p \lambda_p b_d s^{\frac{d}{\alpha}} \mathbb{E}_H\left(H^{\frac{d}{\alpha}} \gamma_{low}(1-\frac{d}{\alpha}, sH)\right)\right). \quad (6.10)$$

for $\frac{d}{\alpha} = \frac{1}{2}$ *this reduces to*

$$M_{I_{pri}}(s) = \exp\left(-\frac{\rho_p \lambda_p b_d \sqrt{s}}{2}\left(\pi - \arctan\left(\frac{1}{\sqrt{s}}\right) + \frac{\sqrt{s}}{(s+1)}\right)\right). \quad (6.11)$$

PROOF: see Appendix F. □

Utilizing Lemma 1, Theorem 1 and Theorem 2, $p_{out}(\Lambda)$ can be easily deduced.

6.4.2 *Scaling Laws for the Outage Probability*

Gupta and Kumar in their seminal paper [93] introduced scaling laws to delineate the capacity of an ad-hoc network with increasing number of nodes. Such an analysis has provoked a race amongst the wireless networking researchers towards better theoretical underpinning of ad hoc paradigm. To the best of our knowledge, the scaling laws for the OP of CRN (in stochastic geometric sense) are never studied before. Since the TC of the primary network depends on the OP of a typical primary receiver, understanding the scaling laws for the OP provides a significant insight on how the TC scales with increasing number of primary and secondary users.

Scaling of OP with primary transmitters.

Theorem 6.3 *The OP of a typical primary receiver exponentially increases with the increase in the number of concurrent primary transmitters. Equivalently, the probability of successful (SP) transmission decreases exponentially with increasing λ_p.*

PROOF: Given $\lambda_s^{md,tx} = 0$

$$\lim_{\lambda_p \to \infty} p_{out}(\lambda_p) = \lim_{\lambda_p \to \infty} \left(1 - c_1 \exp(-\rho_p \lambda_p)\right) = 1. \quad (6.12)$$

□

Scaling of OP with secondary transmitters.

Theorem 6.4 *The OP of a typical primary receiver increases in a power law manner with increase in the number of secondary transmitters miss-detecting the beacon.*

PROOF: Given $\lambda_p = 0$

$$\lim_{\lambda_s^{md,tx} \to \infty} p_{out}(\lambda_s^{md,tx}) = \lim_{\lambda_s^{md,tx} \to \infty} \left(1 - \frac{1}{c_2^{\lambda_s^{md,tx}}}\right) = 1. \quad (6.13)$$

□

Having comprehensive framework for modeling OP of CRN, we conclude by establishing our original objective, i.e., the quantification the TC of the primary network.

TC of the primary network.

Theorem 6.5 *The TC of the primary network, i.e., the number of concurrent successful transmissions occurring per unit area in the primary network, subject to some OP constraint p is*

$$C(q) = \frac{(1-q)\ln\left[(1-q)(1+\beta\eta r_o^\alpha \theta)^k\right]^{-1}}{\rho_p b_d \sqrt{\beta r_o^\alpha}\left(\frac{\pi}{2} - 0.5\arctan\left(\frac{1}{\sqrt{\beta r_o^\alpha}}\right) + \frac{0.5\sqrt{r_o^\alpha \beta}}{(r_o^\alpha \beta + 1)}\right)}. \quad (6.14)$$

PROOF: This can be obtained using Lemma 8.1, Theorem 8.1 and Theorem 8.2. □

6.5 RESULTS AND DISCUSSION

In this section, we discuss some key results obtained from the analytical framework of the TC developed in this chapter. There are many parameters which affect the TC of the primary system. It is natural to ask questions such as how does the path-loss exponent impact the TC of the primary network? or does detection sensitivity of the secondary users (dictated by the SIR threshold γ_{th}) significantly affects the TC of primary network? How-

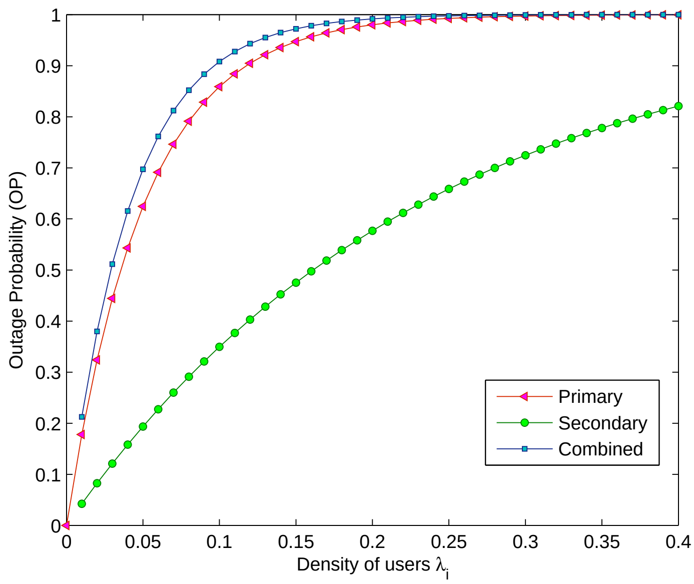

Figure 6.1: OP with varying density of primary and secondary users $\beta = 12$ dB, $\alpha = 4$,$\gamma_{th} = -20$ dB $r_o = \rho_p = \rho_s = 1$ and $\eta = 1$ (see(6.14))

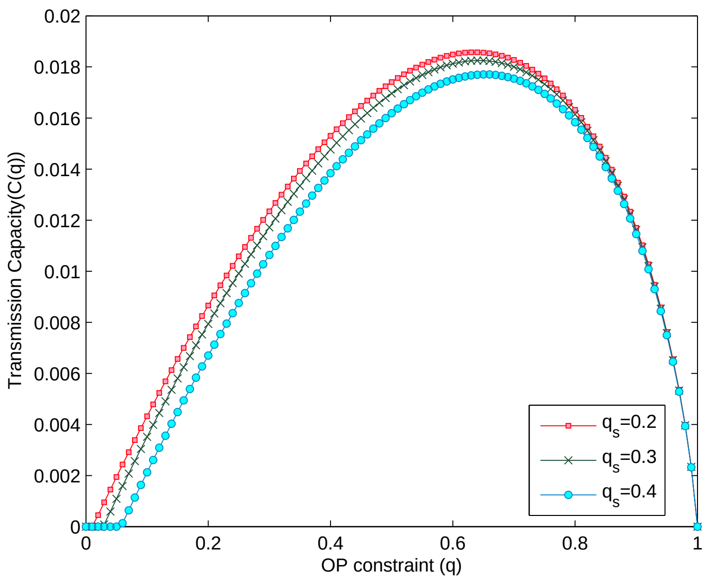

Figure 6.2: Transmission Capacity with varying q_s, $\beta = 12$ dB,$\alpha = 4$,$\gamma_{th} = -20$ dB,$\eta = 1$ and $r_o = 1$(see(6.14)).

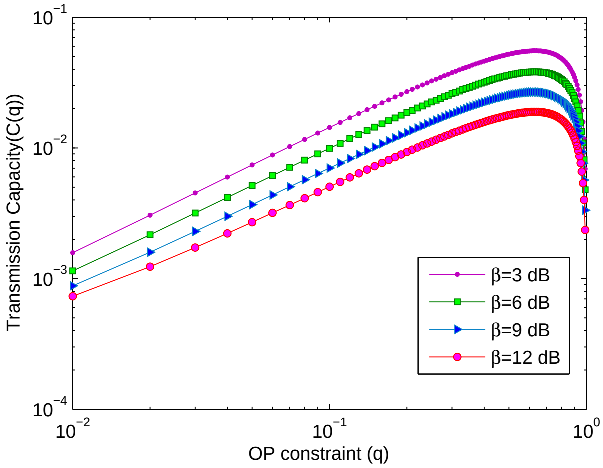

Figure 6.3: Transmission Capacity with varying SIR threshold $\lambda_s^{tx} = \lambda_p^{tx} = 0.01$, $\rho_p = \rho_s = 1$,$\alpha = 4$,$\gamma_{th} = -20\,\text{dB}$,$\eta = 0.1$ and $r_o = 1$(see(6.14)).

ever, we restrict our discussion to key parametric variations which provide significant insight.

Fig. 1 illustrates that the OP of the primary network increases with the increasing density of secondary or primary users. This verifies our claim in Theorem 3 and 4. Fig. 1 illustrates scaling behavior of the OP for three distinct cases, i.e., (i) when there are no secondary transmissions or equivalently all secondaries detect the presence of primary with probability 1; (ii) when there is no self-interference in the primary network and the misdetecting secondaries are the only source of interference; (iii) when both sources of interference, i.e., primary and secondary are operational. As depicted in Fig. 1 an increase in the primary or secondary user density for case (i) and (ii) clearly shows a distinct behavior since depending on the selection of parameters one can dominate the other and hence drive the primary user towards outage. In other words, the selection of operational parameters determine whether self-interference or interference from the secondary will dominantly contribute towards outage.

Consider $\bar{\lambda}_s$ such that $p_{out}(\Lambda) = p_{out}(\bar{\lambda}_s)\big|_{\lambda_p=0} \leq q_s$, i.e., the density of the secondary transmitters such that secondary network satisfies the QoS constraint q_s, then for such $\bar{\lambda}_s$ the TC of the primary network is shown in Fig. 2. It is obvious that there is a one to one correspondence between q_s and the density of secondary network $\bar{\lambda}_s$. As the QoS constraint is relaxed, the number of transmissions satisfying the constraint also increase, hence, primary network suffers from more interference. This increasing interference essentially deteriorates the primary's performance and consequently decreases the primary's TC. It can also be shown that decreasing MAP for the case of slotted ALOHA corresponds to a proportional reduction in secondary interferers, thereby, increasing the primary's TC. Note that in Fig. 2, for $q_s = 0.4$, TC is zero up to a certain value of q. This behavior stems from the fact that below this threshold value of q it is not possible to satisfy primary's outage constraint since the QoS/outage constraint on the secondary network is non-zero and hence it is not possible to ensure interference free communication under such a constraint.

Lastly, as depicted in Fig. 3, the TC decreases with the increasing SIR thresholdβ for fixed λ_s^{tx} and λ_p^{tx}. This is intuitive since as the required SIR for achieving better performance at the primary increases, outages become un-avoidable. In 802.11 legacy networks, rate and code adaptation schemes are utilized, which trade the effective communication rate for the reliability of the transmission.

6.6 CONCLUSION

In this chapter, we have developed a stochastic geometry based statistical model to characterize the TC of the primary network in the presence of a collocated CRN. A practical scenario is considered where the performance of the primary network is governed by both inter-network and intra-network interference. We also consider a realistic network where Slotted ALOHA type MAC is employed to assure self-coexistence. The TC of the primary network is studied under both geometric uncertainties in transmission/reception/sensing distances and channel uncertainties due to multipath impairment process encountered by both the primary and secondary networks. Scaling laws for the outage probability were established. Lastly, the impact of the primary and secondary user density, QoS constraint on the secondary network and the SIR threshold on TC was studied with the help of simulations.

7

REVISITING THE OUTAGE AND THROUGHPUT IN SPECTRUM SENSING CRNS

In this chapter, we present a novel closed-form expression for an upper bound on the OP of a primary receiver operating in the presence of a Poisson field of spectrum sensing CRs. We consider that the CRs employ either a matched filter (MF) or an energy detector (ED) to detect the presence of the primary user. Slotted ALOHA MAC is also enforced on the mis-detecting CRs. In order to demonstrate the tightness of the proposed bound, we corroborate our analytical results with a Monte Carlo simulations. The upper bound on the OP is employed to characterize the spatial/transport throughput of the primary link (bit m/s/Hz). It is shown that the transport throughput decreases with an increase in either the primary's QoS requirement or the secondary's medium access probability/transmitter density. Our results indicate that there exists an optimal SIR threshold and link distance for which the primary's throughput is maximized.

Primary objective:
■ *To obtain an upperbound on the Laplace transform of the aggregate interference.*
■ *To quantify the performance of the primary user in presence of the secondary network.*

7.1 INTRODUCTION

In this chapter, we revisit the analysis of primary user's outage probability (presented in chapter 5) with the focus on deriving near exact closed form upper-bound. We further explore the spatial throughput of the primary network in the presence of spectrum sensing CRN.

7.1.1 *Motivation*

The authors in [20, 53, 123] have investigated the probability distribution function (PDF) of the aggregate interference in the presence of a *spectrum sensing* CRN. However, all of these approaches rely on the moment matching approach. Consequently, different authors have proposed *different distributions* for approximating the true distribution of the aggregate interference. Essentially, all of these studies have either of the following limitations:

- They characterize the aggregate *interference distribution* and not the *distribution of the signal to interference ratio* (SIR). For a CRN designer, the outage probability (OP) of the primary $(\Pr\{\text{SIR} < \gamma_{th}\})$ is a more meaningful performance metric than the probability that the aggregate interference exceeds a certain threshold $(\Pr\{I > I_{th}\})$. Further analysis based on the approximate distributions in the literature is intricate if not impossible. The widely utilized distributions such as the *shifted-Lognormal* or *Lognormal* distribution do not possess a closed-form expression for their Laplace transforms. Hence, the characterization of the OP is difficult even when the primary communication channel suffers from *Rayleigh fading* .

- Since all of these approaches rely on *approximations* and not *bounds*, the analysis based on these distributions *cannot provide* any performance *guarantees*. Most of these approximations are only valid for a limited choice of parameters. Notice that in [123] *Gamma* distribution, while in [53] *truncated* $\alpha-$*stable* distribution was proposed to model the aggregate interference. Both distributions possesses a closed-form expression for the corresponding Laplace transform. However, both [123] and [53] provide approximations for the OP and not the bounds.
- The spectrum sensing mechanism is *either not generic* [20, 53, 123] (see Section 7.2) or *completely ignored* [51, 112]. Furthermore, the *medium access control* (MAC) which also enforces the *self-coexistence constraint* in a CRN, is only studied in [123].

7.1.2 *Contribution & Organization*

In this chapter, we derive a novel closed-form tight upper bound on the OP (Section 7.3) of the primary receiver in the presence of a Poisson field of CR interferers (Section 7.2). This bound is obtained by computing a tight lower bound on the Laplace transform of the aggregate interference. In order to demonstrate the generality of our proposed bound, we consider Nakagami$-m$ fading for both the primary communication and the secondary interference links (Section 7.2). CRs are assumed to either employ a matched filter (MF) or an energy detector (ED) for detecting the primary user. A slotted ALOHA based MAC is employed by the CRs to schedule their transmissions. The upper bound on the OP is employed to quantify the spatial/transport throughput (i.e., bit meter/s/Hz) performance of the primary link. The impact of the primary user's QoS requirements and the secondary user's medium-spectrum access on the throughput is also studied. To the best of our knowledge, neither closed-form bounds for the OP of the primary exist in the literature nor any study in the past has considered Nakagami$-m$ fading with the possibility of using either a MF or an ED with Slotted ALOHA. The spatial throughput of the primary user in spectrum sensing CRN is also not quantified in the existing studies.

7.2 SYSTEM MODEL

7.2.1 *Network Geometry*

We consider a single primary link operating in the presence of a collocated spectrum-sensing CRN. The primary communication link ($P_{RX} \rightarrow P_{TX}$) is comprised of a primary receiver (P_{RX}) located at the origin and a primary transmitter (P_{TX}) located at a distance r_p from P_{RX}. The *spatial no-talk zone* (also known as the *primary's exclusive region* [64]) is modeled by a disk of radius r_e centered at P_{RX}. Secondary transmitters located inside this region are obliged to maintain silence. The radius of the exclusive region (r_e) is defined in terms of the primary's link distance as, $r_e = r_p + \Delta$, where Δ is the width of an additional spatial guard-zone.

The spatial distribution of the secondary transmitters at any arbitrary time instant is captured by a *homogeneous Poisson point process* (HPPP) [60] Φ_s^{TX} on $\mathbb{R}^d \backslash b(o, r_e)$ with intensity λ_s^{TX}. Here $b(o, r_e)$ represents a $d-$dimensional ball of radius r_e centered at the origin and λ_s^{TX} quantifies the number of secondary transmitters per unit area/volume. More specifically, the probability of finding $n \in \mathbb{N}$ secondary transmitters inside a region $\mathcal{A} \subset \mathbb{R}^d$ is given by

$$\mathbb{P}(\Phi_s^{TX}(\mathcal{A}) = n) = \frac{\left(\lambda_s^{TX} v_d(\mathcal{A})\right)^n}{n!} \exp\left(-\lambda_s^{TX} v_d(\mathcal{A})\right), \qquad (7.1)$$

where, $v_d(\mathcal{A}) = \int_{\mathcal{A}} dx$ is the Lebesgue measure [60]. If $\mathcal{A}$ is a $d-$dimensional sphere then $v_d(\mathcal{A}) = b_d r^d$, where r is the radius of the sphere and b_d is the volume of the unit sphere in $\mathbb{R}^d$, with $b_d = \sqrt{\pi^d}/\Gamma(1+d/2)$ and $\Gamma(a) = \int_0^\infty x^{a-1} \exp(-x) dx$.

7.2.2 *Channel Model*

We use $\mathcal{G}(k, \theta)$ to represent a Gamma distribution with shape parameter k and scale parameter θ.

A narrowband Nakagami-m block-fading channel is assumed for both the primary communication link ($P_{TX} \rightarrow P_{RX}$) and the secondary interference link ($x \in \Phi_s^{TX} \rightarrow P_{RX}$). The overall channel gain between P_{TX} and P_{RX} is given by $H_{pp} l(r_p)$, where $H_{pp} \sim \mathcal{G}\left(m_p, 1/m_p\right)$ and $l(r_p) = C r_p^{-\alpha}$ is a distance dependent power-law path-loss function. Here, C is the frequency dependent constant and $\alpha > 2$ is the terrain or environment dependent path-loss exponent. Similarly, the channel gain between an arbitrary secondary transmitter $x \in \Phi_s^{TX}$ and P_{RX} is modeled as $H_x l(R_x)$, where $H_x \sim \mathcal{G}\left(m_s, 1/m_s\right)$, $l(R_x) = C R_x^{-\alpha}$ and $R_x = \|P_{RX} - x\|$. The fading channel gains are mutually independent and identically distributed (i.i.d.) across secondary interference links. Without loss of generality, we will assume $C = 1$ for the rest of the discussion. Our main motivation is to characterize the OP of the primary link in a Rayleigh fading environment, while also demonstrating the generality of the analysis.

We use $\|a - b\|$ to denote distance between points a and b.

7.2.3 *Spectrum Sensing and Medium Access Control*

Secondary user's spectrum sensing and medium access mechanism play a vital role in characterizing the primary's OP. In this chapter, we consider the *out-of-band* beacon enabled *interweave* spectrum access [3] approach. Although the out-of-band beaconing requires a dedicated control channel, it does not enforce a stringent detection constraint as in the case of *in-band* sensing. For the sake of completeness, we summarize the spectrum and medium access mechanism for secondary users as follows:

7.2.3.1 *Primary's out-of-band beaconing*

Before initiating their communication session, both the P_{TX} and the P_{RX} employ some sort of handshaking protocol (e.g. RTS-CTS). The P_{RX} then transmits a beacon over a dedicated control channel. Secondary users listen on the beacon channel for the primary's signal.

7.2.3.2 *Beacon detection*

CRs employ a detection mechanism to detect the presence of the primary's beacon. In this paper, we consider two well known detection algorithms, i.e., the MF or the ED. Notice that these two architectures correspond to the *degree of knowledge* possessed by the CRs about the primary's beacon. The detection performance of these two detectors is summarized in Propositions 1 and 2.

Detection performance of the MF.

Lemma 7.1 *(See [120]) The probability of successfully detecting the primary beacon (when it is present) by employing the matched filter at a CR $x \in \Phi_s^{TX}$ is,*

$$P_D = Q\left(Q^{-1}\left(P_{FA}\right) - \sqrt{2\gamma(H_x, R_x)\tau}\right), \tag{7.2}$$

where $Q(z) = \frac{1}{\sqrt{2\pi}}\int_z^\infty \exp(-\frac{y^2}{2})dy$, P_{FA} is the probability of false alarm, τ is the time-bandwidth product for the beacon signal and $\gamma(H_x, R_x) = \frac{P_b H_x l(R_x)}{\sigma^2} = \gamma_b H_x l(R_x)$ is the beacon channel SNR (where the beacon transmit power is P_b, σ^2 is the noise power and $\gamma_b = {}^{P_b}/_{\sigma^2}$ is the beacon channel SNR in the absence of fading and path-loss).

Notice that τ is the product of the detectors observation time interval and the channel bandwidth. Moreover, the time-bandwidth product τ approximately reperesents the number of samples employed to establish the presence of the primary user's beacon.

Detection Performance of the ED.

Lemma 7.2 *(See [128]) The probability of successful beacon detection when an energy detector is employed at a CR is*

$$P_D = Q\left(\frac{Q^{-1}(P_{FA}) - \sqrt{\tau}\gamma(H_x, R_x)}{1+\gamma(H_x, R_x)}\right), \tag{7.3}$$

where, $Q(.)$ τ,P_{FA} and $\gamma(H_x, R_x)$ are as previously defined.

Interested readers should refer to [20] and references therein, for the detailed discussion. Also notice that, the coherence bandwidth for the CR operating in TV bands may significantly exceed from the separation between the adjacent channels.

Note that (7.3) is based on the Guassian approximation of the test statistic distribution, which is accurate for moderate to large τ. Like previous studies ([20, 51]), we consider that the out-of-band beacon channel and the secondary data channel experience the same propagation conditions. This is reasonable assumption when both channels lie in a proximity and the coherence bandwidth is sufficiently large .

In [128] authors employed the un-normalized received energy as the test statistic, i.e., $T_{ED} = \sum_{i=1}^{\tau} |r_i^2|$, where r_i is the i^{th} sample of the received beacon signal at the CR transmitters. Similar to [128], we utilize T_{ED} for its analytical simplicity (in contrast to its normalized counterpart, i.e., $\bar{T}_{ED} = \frac{1}{\tau}\sum_{i=1}^{\tau} |r_i^2|$)[1].

The analytical forms of (7.2) and (7.3) do not allow further analysis. However, for a fixed and a high detection threshold $\bar{P}_D$ (i.e., $\bar{P}_D \geq 0.5$) and a constant probability of false alarm $\bar{P}_{FA}$, mis-detection of the beacon at an arbitrary CR transmitter can be modeled as an indicator or Bernoulli random variable $\mathbb{1}_{\gamma_{th,t}}^{MD}(\gamma(H_x, R_x))$. The indicator random variable is defined as:

We use t to denote the type of the detector i.e., an ED or a MF for those parameters which depend on the detection mechanism. For instance, in the case of an ED, $\gamma_{th,t}$ corresponds to $\gamma_{th,ED}$ and for a MF it corresponds to $\gamma_{th,MF}$.

$$\mathbb{1}_a(b) = \begin{cases} 1 & b \leq a \\ 0 & b > a \end{cases}, \tag{7.4}$$

Fig. 7.1 sketches the detection performance of the ED and the MF against the varying beacon channel SNR. Notice that for a fixed small value of P_{FA} the detector's performance curve has a steep transition. This serve as a main motivation behind the approximation of P_D by an indicator random variable (as proposed in [121]). Employing the indicator random variable approximation an arbitrary CR transmitter detects with probability 1 (see Fig. 7.1) if

1 The probability of successful beacon detection when $\bar{T}_{ED}$ is used as the test statistic is given by

$$P_D = Q\left(\frac{Q^{-1}(P_{FA}) - \sqrt{\tau}\gamma(H_x, R_x)}{\sqrt{1+2\gamma(H_x, R_x)}}\right).$$

Further analysis requires solving this expression for the required SNR (γ) when a fixed detection threshold $\bar{P}_D$ is required. Notice that this is much easier considering (7.3) and hence motivates our choice of T_{ED} as test statistic.

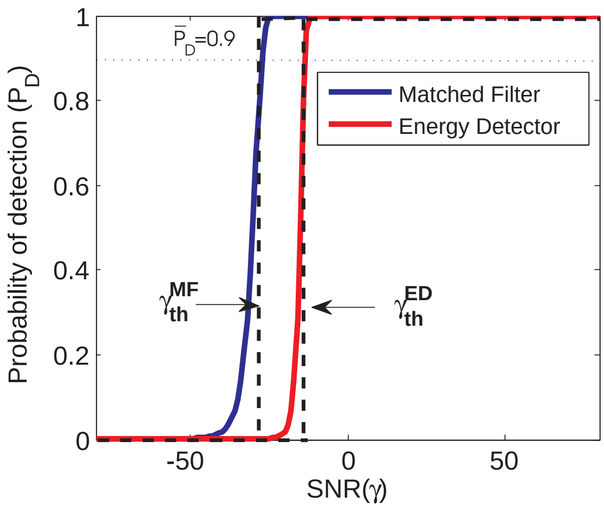

Figure 7.1: Detection performance of MF vs. ED. Solid line represents P_D as a function of γ for constant $P_{FA} = 10^{-3}$ and $\tau = 10^4$. The dotted line step function represents a simplified analytical model for P_D as a function of γ (see (7.2) and (7.3)).

the SNR of the received beacon signal exceeds a certain threshold $\gamma_{th,t}$. The threshold values can be computed from (7.2) and (7.3) by setting the probability of detection to a fixed high detection threshold $\bar{P}_D$.

$$\begin{aligned} \gamma_{th,MF} &= \frac{\left[Q^{-1}\left(\bar{P}_{FA}\right) - Q^{-1}\left(\bar{P}_D\right)\right]^2}{2\tau}, \\ \gamma_{th,ED} &= \frac{Q^{-1}\left(\bar{P}_{FA}\right) - Q^{-1}\left(\bar{P}_D\right)}{\sqrt{\tau} + Q^{-1}\left(\bar{P}_D\right)}. \end{aligned} \tag{7.5}$$

Considering the recommendations of the IEEE 802.22 work-group, we have typical values of $\bar{P}_D \geq 0.9$ and $\bar{P}_{FA} \leq 0.1$. Notice that the detection architecture used in this chapter is generic and hence neither we fix $\bar{P}_D = 0.5$ as in the previous work [20] nor do we restrict our discussion to the ED sensing method.

7.2.3.3 *Medium Access*

CR transmitters which fail to detect the primary's presence, falsely presume a transmission opportunity. We assume that these CR transmitters employ a Slotted ALOHA MAC protocol to schedule their transmissions. In brief, each CR transmitter which mis-detects the beacon transmits with a probability p in the current time slot or defers its transmission with probability $1 - p$.

7.3 OUTAGE AND TRANSPORT THROUGHPUT OF THE PRIMARY USER

In this section, we derive a novel closed-form upper bound on the OP of the primary user considering a collocated spectrum sensing CRN. We then utilize this bound to quantify the transport throughput of the primary user.

OP of the Primary under Nakagami-m fading.

Theorem 7.1 *Consider that the interfering CR transmitters form an inhomogenous Poisson point process $\Phi_I \subseteq \Phi_s^{TX}$, then the OP of the primary link when the communication channel between P_{RX} and P_{TX} suffers from Nakagami$-m_p$ fading is given by*

$$P_{out}^{\{p\}}(\gamma_p, r_p) = \begin{cases} 1 - \sum_{i=0}^{m_p-1} \frac{(-s)^i}{i!} \frac{d^i \mathcal{L}_I(s)}{ds^i}\Big|_{s=\frac{m_p \gamma_p r_p^\alpha}{\eta}} & m_p \in \mathbb{Z}^+ \\ \sum_{i=0}^{\infty} \frac{(-s)^{m_p+i}}{(m_p+i)!} \frac{d^{m_p+i} \mathcal{L}_I(s)}{ds^{m_p+i}}\Big|_{s=\frac{m_p \gamma_p r_p^\alpha}{\eta}} & m_p \geq 1/2 \end{cases}, \quad (7.6)$$

where, $I = \sum_{x \in \Phi_I} H_x l(R_x)$ is the aggregate interference, $\mathcal{L}_I(s)$ is the Laplace transform of the interference and $\eta = P_p/P_s$ is the ratio of the primary and secondary user transmit powers. Also, Φ_I depends on the spectrum sensing and the medium access mechanisms and will be characterized later.

PROOF: The OP ($P_{out}^{\{p\}}$) of the interference-limited primary link is given by,

$$\begin{aligned} P_{out}^{\{p\}}(\gamma_p, r_p) &= 1 - \Pr\{\text{SIR} > \gamma_p\}, \quad (7.7) \\ &= 1 - \mathbb{E}_I\left[\Pr\left\{H_{pp} > \frac{\gamma_p r_p^\alpha}{\eta} I \,\Big|\, I\right\}\right], \end{aligned}$$

Employing the cumulative distribution function (CDF) of H_{pp} we have

$$P_{out}^{\{p\}}(\gamma_p, r_p) = 1 - \mathbb{E}_I\left[\frac{\Gamma\left(m_p, \frac{m_p \gamma_p r_p^\alpha}{\eta} I\right)}{\Gamma(m_p)}\right], \quad (7.8)$$

where $\Gamma(a, b) = \int_b^\infty x^{a-1} \exp(-x) dx$ is the upper-incomplete Gamma function. For an integer m_p, after some mathematical manipulations (similar to [63]), we obtain

$$P_{out}^{\{p\}}(\gamma_p, r_p) = 1 - \sum_{i=0}^{m_p-1} \frac{(-s)^i}{i!} \frac{d^i \mathcal{L}_I(s)}{ds^i}\Big|_{s=\frac{m_p \gamma_p r_p^\alpha}{\eta}},$$

For non-integer m_p, we employ series expansion of the incomplete Gamma function from [?]

$$\Gamma\left(a,z\right)=\Gamma(a)\left[1-\sum_{i=0}^{\infty}\frac{z^{i+a}\exp\left(-z\right)}{\Gamma(i+a+1)}\right], \tag{7.9}$$

Expanding (7.8) by employing (7.9), we obtain the expression for the OP (non-integer $m_p \geq 1/2$) as

$$P_{out}^{\{p\}}(\gamma_p,r_p)=\sum_{i=0}^{\infty}\frac{(-s)^{m_p+i}}{(m_p+i)!}\frac{d^{m_p+i}\mathcal{L}_I(s)}{ds^{m_p+i}}\bigg|_{s=\frac{m_p\gamma_p r_p^{\alpha}}{\eta}}.$$

□

From (7.6), it is obvious that for non-integer values of m_p, computation of the OP for the primary link requires computing an infinite summation. Although it is possible to obtain a good approximation by truncating the infinite series in (7.6) at a few terms, we develop an alternative upper bound in the following corollary for non-integer m_p.

Bounds on the OP for non-integer m

.

Corollary 7.1 *The OP of the primary communication link ($P_{RX} \to P_{TX}$) when primary user's channel experiences Nakagami-m_p fading and co-channel interference from collocated cognitive transmitter is upper-bounded by*

$$P_{out}^{\{p\}}(\gamma_p,r_p)\leq\left[1-\exp\left(\frac{c_1 m_p\gamma_p r_p^{\alpha}}{\eta}\frac{\partial}{\partial s}\mathcal{L}_I(s)\bigg|_{s=0}\right)\right]^{m_p}, \tag{7.10}$$

where

$$c_1=\begin{cases}\left[\Gamma(1+m_p)\right]^{1/m_p} & if\, 0<m_p<1\\ 1 & if\, m_p>1\end{cases}. \tag{7.11}$$

PROOF: From ([129]), we have that

$$1-\frac{\Gamma(m_p,x)}{\Gamma(m_p)}\leq\left(1-\exp\left(-c_1x\right)\right)^{m_p}, \tag{7.12}$$

where c_1 is defined in (7.11). Employing (7.12) and (7.8), we obtain

$$P_{out}^{\{p\}}(\gamma_p,r_p)\leq\mathbb{E}_I\left[\underbrace{\left(1-\exp\left(-\frac{c_1 m_p\gamma_p r_p^{\alpha}}{\eta}I\right)\right)^{m_p}}_{g(I)}\right]. \tag{7.13}$$

Noticing that the function $g(I)$ is concave with respect to I, we employ the Jensen's inequality (i.e., $\mathbb{E}(g(X)) \leq g(\mathbb{E}(X))$ for a concave $g(X)$) to arrive at (7.10). □

OP under Rayleigh fading.

Corollary 7.2 *The OP of the primary link suffering from Rayleigh fading and interference from mis-detecting active CR transmitters (Φ_I) can be characterized as*

$$P_{out}^{\{p\}}(\gamma_p, r_p) = 1 - \mathcal{L}_I(s)\Big|_{s=\frac{\gamma_p r_p^\alpha}{\eta}}. \tag{7.14}$$

PROOF: (7.14) is the special case of (7.6) with $m_p = 1$. This is consistent with the previous studies [44] and [126]. □

An interesting observation which follows from (7.14), is that the upper bound presented in (7.10) reduces to equality for the Rayleigh fading environment ($m_p = 1$). This indicates that the bounds derived in (7.10) are sufficiently tight.

Both (7.6) and (7.14) indicate that the Laplace transform of the aggregate interference generated by the CRN plays a central role in quantifying the primary's outage probability. To the best of our knowledge, closed-form expressions or bounds for $\mathcal{L}_I(s)$ do not exist in the current literature.

In order to derive the closed-form bounds for $\mathcal{L}_I(s)$, we will first characterize the in-homogenous Poisson point process (IHPPP) of the secondary interferers Φ_I constructed as follows:

1) Let $\Phi^{MD} \subseteq \bar{\Phi}_s^{TX}$ denote the set of CR transmitters which mis-detect the primary's beacon. In terms of stochastic geometry formalism, $\bar{\Phi}_s^{TX} \subseteq \Phi_s^{TX}$ is a Marked Poisson point process (MPPP) [60] on $\mathbb{R}^d \backslash b(o, r_e) \times \mathbb{R}^+$, such that each point in x is paired with an i.i.d. mark $H_x \sim \mathcal{G}(m_s, 1/m_s)$. Then Φ^{MD} is constructed by a location dependent thinning of the HPPP Φ_s^{TX} as

$$\Phi^{MD} \quad = \quad \{[x\,;\,H_x] \in \bar{\Phi}_s^{TX} : \mathbb{1}_{\gamma_{th,t}}^{MD}(\gamma(H_x, R_x)) = 1\}, \tag{7.15}$$

$$\lambda^{MD}(h, r) = \lambda_s^{TX} f_H(h) d b_d r^{d-1} \mathbb{1}_{\gamma_{th,t}}^{MD}(\gamma(h, r)). \tag{7.16}$$

Eq. (7.16) is obtained by transforming Φ_s^{TX} to polar coordinates using the Mapping theorem and then applying the theory of MPPP [60].

2) According to the Slotted-ALOHA MAC, each CR transmitter in Φ^{MD} transmits with probability p. Consequently, $\Phi_I \subseteq \Phi^{MD}$is constructed by an independent $p-$thinning of the MPPP Φ^{MD}. The intensity function of Φ_I is given by

$$\lambda_I(h, r) = \lambda_s^{TX} p f_H(h) d b_d r^{d-1} \mathbb{1}_{\gamma_{th,t}}^{MD}(\gamma(h, r)). \tag{7.17}$$

Laplace transform of the aggregate interference.

Notice that the number of CR interferers is proportional to the medium access probability (MAP), p.

Theorem 7.2 *The Laplace transform $\mathcal{L}_I(s)$ of the aggregate interference (I) generated by a spectrum-sensing CRN operating under the Slotted ALOHA MAC and Nakagami$-m_s$ fading channel is lower-bounded by*

$$\mathcal{L}_I(s) \geq \exp\left(-\lambda_s^{TX} p b_d \left[f_1(s) + f_2(s)\right]\right), \tag{7.18}$$

where $f_1(s)$ and $f_2(s)$ are given by (7.19) and (7.20) respectively. The normalized threshold detection SNR ($\bar{\gamma}_{th,t}$) in (7.19) and (7.20) is defined as $\bar{\gamma}_{th,t} = {}^{\gamma_{th}}/{}_{\gamma_b}$ and $\gamma_l(x,y) = \int_0^y t^{x-1}\exp(-t)dt$ is the lower incomplete Gamma function.

$$\begin{aligned} f_1(s) = {} & \left(\frac{s}{m_s}\right)^{d/\alpha} \frac{\gamma_l\left(1 - d/\alpha, s\bar{\gamma}_{th,t}\right)\gamma_l\left(m_s + d/\alpha, m_s\bar{\gamma}_{th,t} r_e^\alpha\right)}{\Gamma(m_s)} \\ & + \frac{r_e^d m_s^{m_s}}{\Gamma(m_s)} \frac{\gamma_l\left(m_s, \left(m_s r_e^\alpha + s\right)\bar{\gamma}_{th,t}\right)}{\left(s r_e^{-\alpha} + m_s\right)^{m_s}} - \frac{r_e^d \gamma_l\left(m_s, m_s\bar{\gamma}_{th,t} r_e^\alpha\right)}{\Gamma(m_s)}. \end{aligned} \tag{7.19}$$

$$\begin{aligned} f_2(s) = {} & \left(\frac{s}{m_s}\right)^{d/\alpha} \frac{\gamma_l\left(1 - d/\alpha, s\bar{\gamma}_{th,t}\right)\Gamma\left(m_s + d/\alpha, m_s\bar{\gamma}_{th,t} r_e^\alpha\right)}{\Gamma(m_s)} \\ & - \left(\frac{\bar{\gamma}_{th,t}^{-1}}{m_s}\right)^{d/\alpha} \frac{\Gamma\left(m_s + d/\alpha, m_s\bar{\gamma}_{th,t} r_e^\alpha\right)}{\Gamma(m_s)} \left(1 - \exp\left(-s\bar{\gamma}_{th,t}\right)\right). \end{aligned} \tag{7.20}$$

PROOF: The Laplace transform of the aggregate interference generated by the CR transmitters is given by

$$\begin{aligned} \mathcal{L}_I(s) &= \mathbb{E}_I(\exp(-sI)) = \mathbb{E}_{\Phi_I}\left(\exp\left(-s\textstyle\sum_{x\in\Phi_I} H_x l(R_x)\right)\right), \\ &= \mathbb{E}_{\Phi_I}\left(\prod_{[x;H_x]\in\Phi_I} \exp\left(-sH_x l(R_x)\right)\right). \end{aligned} \tag{7.21}$$

Using the definition of the Generating functional for the Poisson point process

$$\mathcal{G}(f(x)) = \mathbb{E}\left(\prod_{x\in\Phi} f(x)\right) = \exp\left(-\int_{\mathbb{R}^d}(1 - f(x))\lambda(dx)\right), \tag{7.22}$$

then (7.21) can be written as,

$$\mathcal{L}_I(s) = \exp\left(-\underbrace{\int_0^\infty \int_{r_e}^\infty \left(1 - \exp\left(-shr^{-\alpha}\right)\right) \lambda_I(h,r) drdh}_{A}\right). \quad (7.23)$$

The detailed derivation of an upper bound on A can be found in the Appendix F. Notice that $\mathcal{L}_I(s)$ is exponentially decreasing with increasing A. Hence, an upper bound on A results in a lower bound on $\mathcal{L}_I(s)$ (which is also the success probability ($P_{suc}^{\{p\}} = 1 - P_{out}^{\{p\}}$) in the case of a Rayleigh fading channel (see Corollary 1)). □

An upper bound on $P_{out}^{\{p\}}$ can be easily obtained using Theorems 1 and 2. The upper bound on $P_{out}^{\{p\}}$ is much simplified when both the primary communication link and the secondary interference links suffer from Rayleigh fading (i.e., $m_p = m_s = 1$).

Transport/Spatial throughput.

Corollary 7.3 *The transport throughput of the primary user operating in the presence of a collocated interfering spectrum-sensing CRN can be quantified as*

$$\mathcal{T}_p = r_p P_{suc}^{\{p\}}\left(\gamma_p, r_p\right) \log_2\left(1+\gamma_p\right) \ \ (\textit{bit m/s/Hz}), \quad (7.24)$$

where r_p is the distance of the primary's communication link, γ_p is primary's desired SIR and $P_{suc}^{\{p\}}\left(\gamma_p, r_p\right)$ is the probability of successfully establishing the link for given $\left(\gamma_p, r_p\right)$.

A lower bound on the transport throughput of the primary user can be computed using (7.18), (7.6) and (7.14). Such a lower bound characterizes the worst case achievable bit meter per second per Hertz performance for the primary user. For the Rayleigh faded primary channel,

$$\begin{aligned} \mathcal{T}_p \ &\leq \ r_p \exp\left(-\lambda_s^{TX} p b_d \left[f_1\left(\frac{\gamma_p r_p^\alpha}{\eta}\right) + f_2\left(\frac{\gamma_p r_p^\alpha}{\eta}\right)\right]\right) \quad (7.25) \\ &\times \ \log_2\left(1+\gamma_p\right) \ \ (\text{bit m/s/Hz}). \end{aligned}$$

As indicated by (7.25), the transport throughput of the primary user is not only coupled with the primary's QoS requirements $\left(\gamma_p, r_p\right)$ but also depends upon the secondary's medium and spectrum access mechanism through $P_{suc}^{\{p\}}$.

7.4 RESULTS & DISCUSSION

In this section, we corroborate our previously derived analytical results through Monte Carlo simulations, and also study the impact of several parametric variations on the primary's transport throughput.

7.4.1 *Outage Probability*

Fig. 7.2 depicts the OP of the primary link as a function of the primary's desired SIR threshold. Solid and dashed lines represent the analytical upper bound on the OP of the primary link obtained from (7.14) and (7.18) for the secondary MAP values of $p = 1$ and $p = 0.7$ respectively. Monte Carlo simulation results are indicated by '□' markers and were performed by generating 10^5 realizations for both Φ_s^{TX} (with intensity $\lambda_s^{TX} = 10^{-3}$) and the fading-channel gains for each SIR threshold (γ_p). As indicated by Fig. 7.2, the upper bound obtained using (7.18) is a tight upper bound. We also investigated the tightness of the upper bound considering several parametric variations.

Fig. 7.2 shows that the OP of the primary link increases with an increase in the desired γ_p. Considering all other parameters to be fixed, an increase in γ_p corresponds to an increase in the primary user's desired QoS. Intuitively, such an increase corresponds to a decreasing tolerance for the secondary interference. With a non-zero aggregate secondary interference, if the primary's desired QoS constraint is raised to the point where it cannot be fulfilled, then $P_{out}^{\{p\}}$ converges to unity. Also notice (see Fig. 7.2) that the OP of the primary link decreases with the decreasing MAP and the superior spectrum sensing mechanism. This is because both the superior performance of the MF (obtained at the cost of complete knowledge of the beacon) and decrease in the MAP reduce the aggregate interference generated by the CRN.

7.4.2 *Transport Throughput*

Fig. 7.3 shows how the $\mathcal{T}_p$ of the primary link is coupled with the primary's own desired QoS. An important observation which follows from Fig. 7.3 is that there exists an optimal value for the QoS constraint (γ_p, r_p), say (γ_p^*, r_p^*), for which $\mathcal{T}_p$ is maximized. Such an optimal operating point for the primary exists because $r_p \log_2(1 + \gamma_p)$ is increasing in terms of r_p or γ_p, while $P_{suc}^{\{p\}}(\gamma_p, r_p)$ decreases with an increase in γ_p or r_p. Moreover, as indicated by Figs. 7.3a and 7.3b the choice of detector employed by the CR plays a vital role in characterizing the primary's $\mathcal{T}_p$. It should be noticed that for a fixed (γ_p, r_p), the primary user can attain a higher $\mathcal{T}_p$ when a MF is employed at the CRs as compared to the use of an ED. Hence the primary

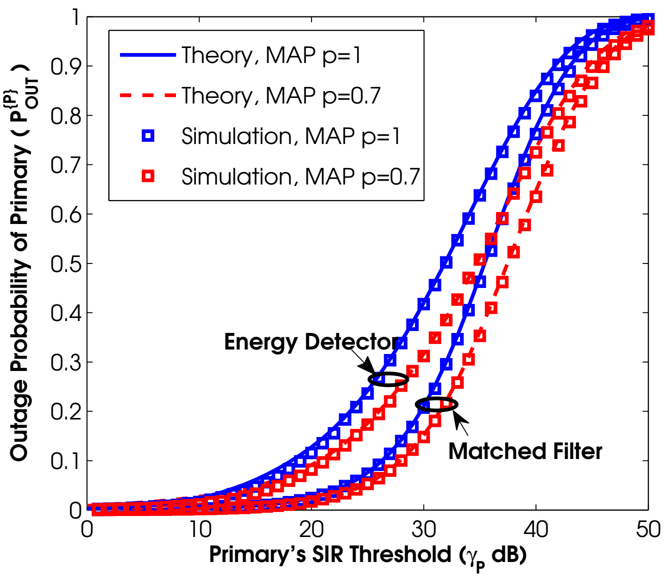

(a) Analytical and simulated outage probability ($P_{out}^{\{p\}}$) of the primary user in the presence of a CRN with $d = 2$, $\alpha = 4$, $\lambda_S^{TX} = 10^{-3}$, $\bar{P}_{FA} = 10^{-1}$, $\bar{P}_{DET} = 0.9$, $\eta = 1$, $r_e = 5$, $r_p = 2$, $\tau = 10^4$,$\gamma_B = 10$ dB, $m_p = m_s = 1$ and $p = \{0.7, 1\}$. (see eqs.(7.14)& (7.18))

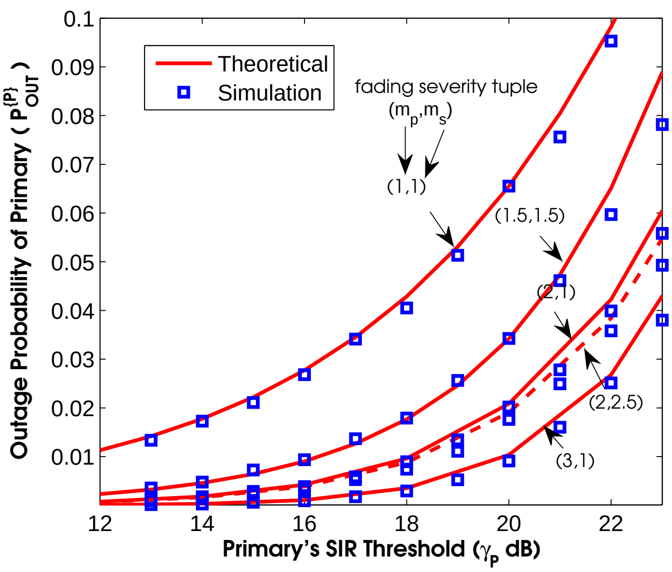

(b) Analytical and simulated outage probability ($P_{out}^{\{p\}}$) of the primary user in the presence of a CRN with $d = 2$, $\alpha = 4$, $\lambda_S^{TX} = 10^{-3}$, $\bar{P}_{FA} = 10^{-1}$, $\bar{P}_{DET} = 0.9$, $\eta = 1$, $r_e = 5$, $r_p = 2$, $\tau = 10^4$ and $\gamma_B = 20$ dB,. (see eqs .(7.6),(7.10)& (7.18))

Figure 7.2: Outage Probability of the Primary User.

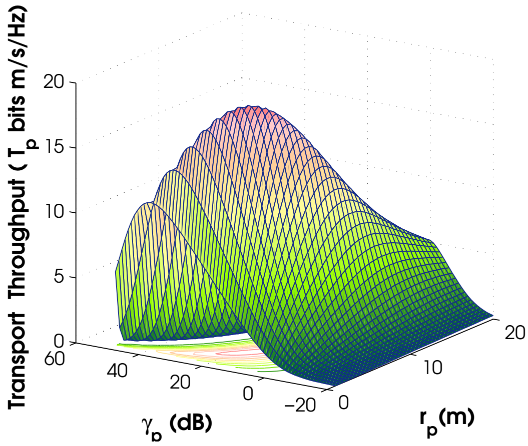

(a) Transport throughput ($\mathcal{T}_p$) of the primary user in the presence of a CRN employing MF.

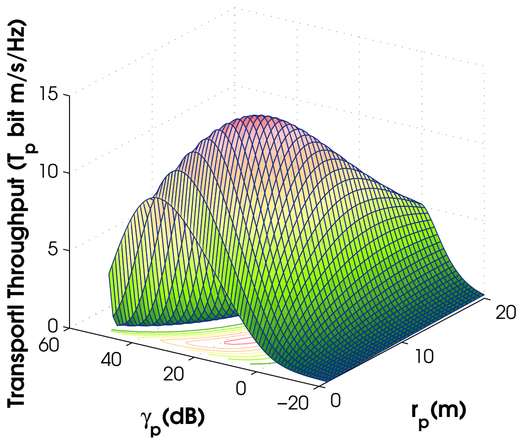

(b) Transport throughput ($\mathcal{T}_p$) of the primary user in the presence of a CRN employing ED.

Figure 7.3: Primary user's Transport throughput ($\mathcal{T}_p$) for $d = 2$, $\alpha = 4$, $\lambda_S^{TX} = 10^{-3}$, $\bar{P}_{FA} = 10^{-1}$, $\bar{P}_{DET} = 0.9$, $\eta = 1$, $\Delta = 2$, $\tau = 10^4$,$\gamma_B = 10$ dB, $m_p = m_s = 1$ and $p = 1$. (see eq.(7.25)

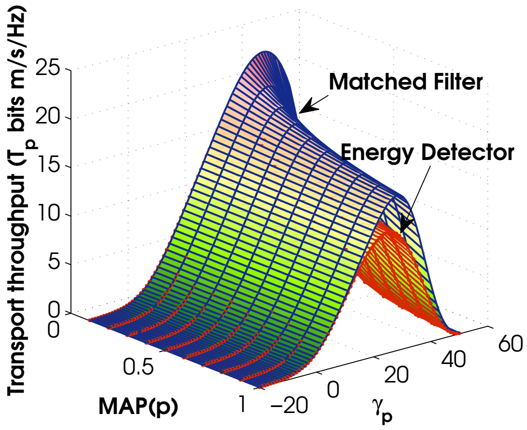

(a) Impact of the secondary's MAP(p) on the transport throughput ($\mathcal{T}_p$) of the primary user.

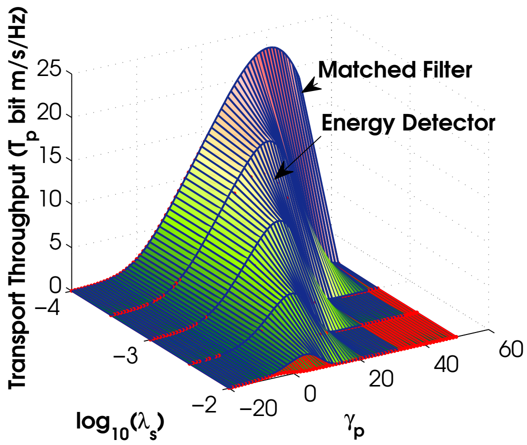

(b) Impact of the secondary user density (λ_s^{TX}) on the primary user's transport throughput ($\mathcal{T}_p$).

Figure 7.4: Primary user's Transport throughput ($\mathcal{T}_p$) versus Secondary's MAP (p) and transmitter density (λ_s^{TX}) for $d = 2$,$\alpha = 4$, $\bar{P}_{FA} = 10^{-1}$, $\bar{P}_{DET} = 0.9$, $\eta = 1$, $\Delta = 2$, $r_p = 2$, $\tau = 10^4$,$\gamma_B = 10$ dB, $m_p = m_s = 1$, $\lambda_S^{TX} = 10^{-3}$(in (a)) and $p = 1$(in (b)). (see eq.(7.25)

user can potentially improve its throughput by sharing the exact signaling information with the CRs.

Fig. 7.4a shows the impact on $\mathcal{T}_p$ of increasing the MAP (p). As expected, $\mathcal{T}_p$ decreases with increasing p due to the increase in the aggregate secondary interference. However, notice that for fixed γ_p, the decrease in $\mathcal{T}_p$ with increasing p for the ED, is much higher than that of the MF. In Fig. 7.4b we study $\mathcal{T}_p$ as a function of the secondary transmitter density (λ_s^{TX}). Increasing λ_s^{TX} (for fixed p) decreases $\mathcal{T}_p$ to zero irrespective of the the detection mechanism, due to the increasing aggregate interference.

7.5 CONCLUSION

In this chapter, we revisited the modeling of the aggregate interference in spectrum sensing cognitive radio networks. Departing from the traditional cumulant based approximation approach, we derived a novel upper-bound on the outage probability of the primary user in the presence of mis-detecting cognitive radios. Corresponding to the dergee of knowledge about the primary user, two different detectors, i.e., matched-filter and energy-detector were considered for establishing the presence of the active primary link. The upper-bound on the outage probability is employed to quantify the minimum transport throughput of the primary link. It is shown that their exists an optimal SIR threshold and a link distance which maximize the transport throughput of the primary.

Part III

ENERGY EFFICIENCY OF AD-HOC WIRELESS NETWORKS

8

ON THE ENERGY EFFICIENCY OF LARGE SCALE INTERFERENCE LIMITED WIRELESS AD HOC NETWORKS

The key objective of this chapter is to explore how aggregate interference impacts the energy efficiency in large scale ad hoc networks.

ABSTRACT

Efficient utilization of power resources, frequently termed *energy efficiency* (EE) of a large scale network, quantifies the number of bits that can be successfully transferred between an arbitrary pair of nodes at the cost of one Joule of energy. Quantitative characterization of EE is vital to explore the design space for low-power wireless networks. With this in mind, in this chapter, we present an *analytical approach* to quantify the EE of a large scale *interference limited* wireless ad hoc network. Our quantitative investigation addresses energy consumption at the *physical*, *medium access control* (MAC) and *routing* layers. Specifically, we analytically characterize the energy consumption of a large scale wireless ad hoc network, where users wish to communicate with their intended destinations under a certain *quality of service* (QoS) constraint. The *Slotted ALOHA* (S-ALOHA) MAC protocol is employed by users to share a common wireless medium. At an arbitrary S-ALOHA time slot, the spatial configuration of the users/nodes is modeled by a *stationary Poisson point process*. User/node level energy expenses are quantified by analyzing the power consumption of *communication hardware*. Inspired by current trends in radio transceiver design, our analysis considers three popular transceiver architectures. It is assumed that nodes which defer their own transmission (under S-ALOHA protocol), assist other nodes by acting as relays. In essense, an arbitrary source communicates with its destination via *multihop* transmission. Although, we do not consider a particular *routing* scheme, the forwarding strategy is similar to *long-hop/greedy routing* (GR).While quantifying the overall EE of the network, the *geometry of the forwarding* areas resulting from different GR type relaying stratgies is also explicitly addressed. Unlike prior studies, the link model is formulated by considering: (i) the large-scale path-loss and the small-scale Rayleigh fading; (ii) the co-channel network interference; and (iii) the user's desired QoS requirements. Recognizing that the EE of a large scale ad hoc network is strongly coupled with connectivity attributes, the link and routing models are employed to establish two critical quantities, i.e., the *single hop maximum forward progress* and the *node isolation probability*. The *number of hops* required by an arbitrary source to connect with its destination is quantified from single hop maximum forward progress. Finally, the user level hardware power consumption model, the MAC protocol, the desired QoS constraint, the single hop forward progress, the node isolation probability and hop count statistics are all combined to establish an analytical expression for EE of large scale ad hoc network. Both analytical and Monte-Carlo simulations are employed to investigate the impact of several parametric variations on the connectivity attributes and the EE. Our results indicate, that several hypotheses established in existing literature which *ignore* the network interference and the fading break down for a large scale interference limited network. We also demonstrate that medium access probability (MAP) is a cross-layer parameter and there exists an optimum MAP which maximizes the EE.

8.1 MOTIVATION

In recent years, the world has witnessed an enormous proliferation of wireless communication devices in day-to-day activities. Such a ubiquitous computing paradigm has triggered a sky-rocketing demand for the deployment of large scale wireless ad hoc networks. Bestowed with intrinsic self-configuration capabilities, large scale ad hoc networks can be dynamically formed without any pre-established infrastructure. This indeed facilitates rapid deployment and on-the-fly reconfiguration for a wide variety of applications. But it comes at the cost of several formidable design challenges.

Ensuring an energy efficient communication in large scale wireless ad hoc networks is one of the key challenges that network designers face today. Due to the absence of a dedicated infrastructure, the ad hoc networks are intrinsically energy limited. A significant amount of energy is wasted in combating various uncertainties that are inherent to the wireless channel. More specifically, communication on a wireless channel is constrained by various *propagation conditions*, additive *thermal noise* and *network interference* at a receiver front-end. In order to design energy efficient communication protocols, accurate quantification of energy consumption considering these uncertainties is unavoidable. To this end, in this chapter we develop a comprehensive statistical framework to quantify the energy efficiency (EE) of a large scale wireless ad hoc networks. In accordance with the existing literature [130, 131], *the EE of large scale ad hoc network is defined as the number of bits which can be successfully transferred from an arbitrary source to its destination (separated by a fixed distance* r_{SD}*) at the cost of one joule of energy.*

8.2 CONTRIBUTIONS

Characterization of the EE of a large scale ad hoc wireless network is a cross-layer issue [59, 132]. In the past, numerous studies [70, 130, 131, 133–145] have dedicated their efforts to quantify the EE of an ad hoc wireless network. However, most of these studies:

1. Restrict their investigation to a particular layer in the OSI protocol stack [130, 131, 133, 137, 138, 140–142, 146, 147]. In other words, these studies focus on quantifying the EE of a wireless network by considering the energy expenditure at a particular layer. Although this approach *simplifies* the analysis, it also obfuscates the useful insights. For example, restricting the analysis to the physical layer, it may be concluded that there exists an optimum value of M for an $M-$ary modulation scheme that will *maximize* the EE of the network [130, 131]. However, this is only true for an ideal MAC which guarantees 100% interference free operation (Section 8.6). Considering the *cross-layer nature* of the problem, in this chapter, we consider all *three bottom layers* of OSI model, i.e., physical, MAC and routing layer. Motivated by current trends in wireless local area network (WLAN) radios, we consider a few popular transceiver architectures (Section 8.5). For these architectures, we quantify the EE under Slotted-ALOHA (S-ALOHA) MAC and generic routing strategies (Section 8.4).

2. Adopt a simplified link formation model. More specifically, most of the studies [70, 71, 131, 143, 148–150] employ a deterministic 'disk model', where transmission is always successful within some fixed deterministic radius. In other words, channel impairments such as multipath propagation are completely overlooked. Ignoring the inherent uncertainty in the wireless channel results in an *over-optimistic* characterization of the EE [59, 132, 151]. In practice, small-scale multipath fading *increases* the link *outage probability* and hence a significant amount of energy is wasted due to transmission failures. In this chapter, we quantify the EE of an ad hoc wireless network where links suffer from both *large-scale path-loss* and *small-scale Rayleigh fading* (Section 8.4).

3. Completely ignore the co-channel network interference [70, 71, 130, 131, 133, 134, 143–145, 148, 150, 152, 153]. Communication in wireless ad hoc networks is primarily limited by the network interference [154]. Hence, the amount of energy consumed in combating the interference is non-negligible. Ignoring the network interference while quantifying the EE of a wireless ad hoc network results in an over-estimation of network performance. Interference not only *decreases* the probability of successful packet reception but it also *decreases* the spatial progress of the packet towards its destination (Section 8.6). Consequently, it

is important to consider co-channel interference in the EE analysis. In this study, we *explicitly* consider co-channel *interference* resulting from simultaneous transmissions under *S-ALOHA MAC* protocol. To the best of our knowledge, none of the studies in past have analytically characterized the EE of interference limited large scale ad hoc wireless network. Our results suggest that :

a) the performance of a large scale ad hoc network is *limited by interference* more than by any other factor.

b) in an interference limited network, the probability that an arbitrary transmitter cannot connect to any receiver for a fixed QoS requirement is *independent of the user density* (see Section IV-Claim 1). This is contrary to the previous results which ignore network interference [70, 71, 142, 150].

c) in an interference limited network, the average *number of hops* required to connect an arbitrary transmitter with its receiver *increases with an increase in the user density*. Increase in the user density corresponds to an increase in the number of relays under S-ALOHA protocol. This conclusion is also contrary to the past studies which predict that with a growing number of relays the average number of required hops decreases [70, 142, 149, 150] (see Section 8.6- Claim 2).

d) in an interference limited network, there exists an optimal medium access probability (MAP) which maximizes the EE (see Section 8.6-Theorem 1). We also demonstrate that the optimal MAP is a cross-layer parameter which depends on the routing strategy and modulation scheme. Moreover, the MAP which *maximizes* the EE also *minimizes* the node isolation probability and *maximizes* the average forward progress. Several other important results characterizing the impact of the modulation scheme, hardware platform, sleep scheduling, routing strategy and user density control are detailed in Section 8.6.

4. Do not explicitly address the spatial distribution of transmitters/receivers in the network. According to [59], wireless networks cannot be studied by considering a static network graph. Ignoring the underlying spatial distribution of the transmitters results in the widely accepted belief that interference can be modeled by a Gaussian random process [135, 136]. However, in reality, despite the large number of transmitters, the central limit theorem (CLT) may not hold due to the power-law decay of a signal [63]. To this end, in this chapter, we explicitly address the spatial distribution of nodes by employing techniques from *stochastic geometry*.

5. Do not explicitly consider users desired quality of service (QoS) requirement. The notion of link in ad hoc wireless networks does not have an absolute meaning [59]. In other words, existence of link depends on the channel conditions, modulation scheme, signal processing techniques and also on the user's desired QoS. Links which exist at a particular QoS requirement may not exist at a higher QoS requirement. Hence, the EE of the overall network cannot be characterized in isolation with the QoS requirements of the constituent nodes. Consequently, in this chapter we consider link formation *under certain desired QoS* requirements (Section 8.6-B).

6. Do not consider multihop communication. Most of the studies [131, 133, 140], restrict their attention to a point-to-point communication scenario. In this chapter, we consider a possibility of *multihop communication* between transmitter and its destination. To the best of our knowledge, none of the studies in the past have characterized the EE of a large scale interference limited network considering multihop communication.

8.2.1 *Organization*

Section 8.3 provides a detailed survey of related work. The network, channel, MAC and routing models are specified in Section 8.4. The energy consumption model for the transceiver platforms is detailed in Section 8.5. Section 8.6-A establishes a macroscopic view of the network. In Section 8.6-B, we study routing strategies while accommodating the user's QoS demand. The geometry of the relaying areas resulting from various long hop routing protocols is considered in Section 8.6-C. The analytical framework for quantifying the EE of interference limited wireless ad hoc network is developed in Section 8.6-D. Several insights into the EE and the connectivity attributes supported by analysis and Monte Carlo simulations are also detailed in Section 8.6-D. Lastly, in Section 8.7, we give conclusions.

8.3 RELATED WORK

In their seminal articles, both Goldsmith et al.[132] and Ephremides [59] demonstrated that the investigation of energy consumption in wireless ad hoc networks is a cross-layer issue. In [132] authors presented a brief overview of ad hoc wireless networks with their military and commercial applications. They also investigated several link and network level design issues. Ephremides in [59] examined the notion of wireless link in details. Like [132], he also explored several viable options which can be adapted to realize an energy efficient wireless ad hoc network. He also highlighted that it is important to distinguish between energy constrained and energy efficient operations. In this chapter, we are primarily interested in quantifying the EE of large scale wireless ad hoc networks. However, our results are generic and can be extended in a straightforward manner to quantify network life time and connectivity attributes of energy constrained networks[1].

EE is a cross layer metric.

Inspired by the proposals of [132], the authors in [135] studied the cross-layer design for maximizing the life time of interference limited wireless sensor networks. Authors in [135] formulated the problem of information flow, link schedule and power control as a non-linear optimization problem. They demonstrated that such a non-linear optimization problem can be solved by employing various standard techniques for certain link schedules. In [136] authors extended their previous work [135] by considering a more realistic model of a radio transceiver. Notice that both [135] and [136] address energy constrained network where topology of the network is fixed. It is assumed that a link between transmitter and receiver can be established, if the received power at receiver exceeds a certain threshold value. As argued in [59] the notion of link between a transmitter and receiver in an ad hoc network is completely relative. Consequently, in the light of [59], assuming a fixed network topology and the notion of links without considering the QoS may result in under-estimation of energy consumption.

EE models should cater for the spatial dynamics and QoS dependence in the notion of link between two nodes.

Though analytical results on the energy consumption in large scale ad hoc networks are rare, there exists a plenty of literature on energy efficient design of wireless sensor networks. As discussed earlier, quantifying the energy consumption of a large scale wireless ad hoc networks is a cross-layer issue. However, most of the existing studies either study energy constrained networks or focus their attention on optimization of a particular layer. In the following discussion, we will briefly survey the relevant literature on energy consumption at each layer. Interested readers may refer to references cited in the surveyed literature to obtain a more detailed discussion:

1) Energy consumption at Physical Layer: Feeney et al. in [133] empirically investigated the energy consumption of a wireless network interface in ad hoc network. Shih et al. in [140] proposed physical layer driven design of protocols and algorithms for energy efficient wireless sensor networks. They introduced a realistic hardware model for quantifying the energy consumption of wireless sensor node. Based on the introduced hardware model, they studied the design of physical layer protocols and algorithms that will maximize the network life time. They also highlighted that due to non-zero transient times, switching the idle nodes to *sleep mode* may further increase the energy consumption of a network. Motivated by [140], in [131] Cui et al. stud-

1 The term 'energy constrained network' refers to a network such as a battery operated wireless sensor network or a satellite network. In such a network energy sources can not be replenished easily. On contrary, the term 'energy efficient network' refers to a network where energy sources can be replenished easily. However, longevity of batteries or other energy sources is a prime concern.

ied optimization of a modulation scheme for an energy-constrained hardware platform. Authors in [131] considered a realistic direct conversion radio transceiver and showed that up to 80% energy saving is possible by optimizing the transmission time and modulation scheme. Extending [131], Holland et al. in [130] also considered optimization of physical layer parameters for wireless networks. Both [131] and [140] quantified energy consumption at physical layer considering a point-to-point communication link. However, in this chapter, our primary focus is to characterize the energy consumption of a large scale wireless ad hoc networks by considering realistic wireless transceivers. Notice that this problem inherently involves addressing intricate dynamics at node, link and network level. Although, in [130] authors consider the impact of hop distance on energy efficiency, however, they do not explicitly treat hop counts and they do not address the co-channel interference.

2) Energy consumption at MAC Layer: In [155], authors presented a detailed comparison of various MAC protocols for wireless local networks based on the metric of battery power consumption. Unlike our study, they considered a wireless network with a fixed infrastructure. In [141], Zhao et al. proposed an energy efficient architecture for sensor networks with mobile agents. Authors employed opportunistic ALOHA based MAC protocol. Different from our study, authors in [141] only consider a single hop transmission between sensors and mobile agents. A detailed survey on MAC for wireless sensor networks is provided in [156] and [157]. Notice, that unlike energy-constrained wireless sensor networks, large scale ad hoc wireless networks do not have a single destination (sink). As indicated in [44, 154], S-ALOHA or CSMA/CA type protocol is more suited for large scale wireless ad hoc networks. The seminal paper of Baccelli et al. [44] has sparked significant interest in the research community to employ stochastic geometry and S-ALOHA protocol for performance analysis of large scale networks. Interested readers are directed to a recent tutorial by Win et al. [63] for a detailed discussion. Motivated by [44, 154], in this chapter we consider S-ALOHA based MAC for large scale wireless networks.

3) Energy consumption at Routing Layer: In [143] Zhao et al. established scaling laws for the EE in a large scale wireless networks. Authors in [143] considered proactive and reactive routing approaches. They explicitly addressed the impact of wake up schemes, message duty cycles, fading rates and node mobility on the EE of a large scale wireless networks. Unlike our study, the authors in [143] do not consider the presence of multiple sources in the network. In other words, [143] does not cater for interference. Moreover, [143] abstracts topological variations due to fading. Like other studies, authors consider a deterministic circular 'disk based' communication model, which has several short comings as indicated in [151]. Haenggi in [151] addressed the routing problem in large scale ad hoc networks with Rayleigh fading channels. He also explicitly addressed the random spatial distribution of nodes using stochastic geometry. Although [151] addresses multihop communication, it does not consider interference. Under noise limited conditions, [151] showed that it is beneficial to route over a small amount of long hops as compared to large number of short hops. Haenggi et al. in [158] further consolidated his argument of routing over long hops [151] by providing 18 reasons why short hop routing is not beneficial. Motivated by the arguments in [158], in this chapter we consider long hop routing to quantify the EE of a wireless ad hoc network. In [147] Weber et al. introduced longest edge and random edge routing. Authors focus on exploiting buffer diversity and assume that every node in a network has a packet for any node it can connect with. They study the spatial density of progress under these considerations. Since in practice, it is not possible to ensure that every node has a packet for every other node, we do not make such an assumption. While authors in [147] have considered single hop transmissions, our focus is on multihop communication. In a separate line of work, geographic random forwarding protocol (GeRaF) was proposed by Zorzi and Rao in [70] and [144]. Then [70] was extended to accommodate fading in [145]. GeRaF belongs to a broad class of geographical information forwarding (GIF) protocols. GIF protocols such as GeRaF, GAF, LEACH, DREAM, STEM, SPAN and GEAR [70] focus on long hop routing. The main focus of GIF is to minimize the delay and the energy consumption. Unfortunately all of these protocols are designed without considering the co-channel interference and channel dynamics. Most of the literature focuses on single source and destination networks. However, in reality large scale ad hoc networks are formed by multiple sources which are scheduled under certain MAC schemes. Some of the recent literature has focused on channel awareness [142] and its impact on such GIF strategies. However, to the best of our knowledge none of the studies in past has addressed the energy efficiency of these protocols in the presence of interference. A detailed survey of energy efficient routing is presented in [146].

In [148, 149, 152, 159–161] the authors have characterized the hop counts and connectivity attributes of a random network. All these studies, consider the deterministic 'disk based' model which breaks down under fading environment. In [137] and [138] fading is explicitly addressed. Nevertheless, the authors obtain a recursive probability density function (PDF) and cumulative density function (CDF) for hop counts. Such recursive PDF's are not only intricate to deal with but also void useful insights. In [162] Hekmat et al. has empirically studied the degree distribution and hop count in wireless ad hoc networks. He also pointed some links between random geometric graphs and SNR graphs of the large scale ad hoc networks. All of the studies mentioned before consider single source and destination networks. Consequently, they do not address interference. In [134] and [139] Gurosy et al.

quantified the EE, considering the QoS constraints. Authors address only noise limited case, i.e., interference is not addressed. Unlike this chapter, the spatial distribution for nodes is not addressed.

8.4 NETWORK & SYSTEM MODEL

The EE of a wireless ad hoc network *cannot* be quantified without thorough understanding of *system* and *network level* dynamics. Interaction amongst several layers across the communication protocol stack including the actual *hardware platform* host manifests the system/node level dynamics. Network level dynamics are stimulated by *active network topology*, *information flow/routing* and *MAC* mechanisms. The overall network behavior is partially shaped by the system level activity of various users and partially by the inherent dynamics of the wireless channel, i.e., *fading*, *additive noise*, *path-loss*, *shadowing* and *interference*. In a nutshell, both *system* and *network* level dynamics shape the *connectivity* and *coverage* attributes of a typical user and in turn quantify the EE of network.

In this section, we detail the system and network model considering the above-mentioned dynamics. In subsequent sections, we will build our discussion around the models presented in this section.

8.4.1 *Network Model*

Large scale ad hoc network with nodes forming Poisson point process.

In this chapter, we consider an infinitely *extended* large ad hoc wireless network. The spatial distribution of nodes/users is captured by a *homogeneous Poisson point process* (HPPP) Φ with intensity λ. In other words, the *number of users* in any bounded region are *Poisson distributed* with mean $\lambda \times$ [area of the region], while their locations are *uniformly distributed.* More formally, considering $\Phi(B)$ as a counting process defined over a bounded Borel set B, the number of nodes (i.e., points of Φ in B) has a Poisson distribution with finite mean $\lambda v_d(B)$ for some constant λ. Mathematically,

$$\mathrm{P}(\Phi(B) = k) = \frac{(\lambda v_d(B))^k}{k!} \exp\left(-\lambda v_d(B)\right). \tag{8.1}$$

where $v_d(B)$ is the Lebesgue measure defined on the measurable space $[\mathbb{R}^d, B^d]$. Alternatively, $v_d(B)$ can be regarded as the volume of a $d-$dimensional bounded Borel set B. If B is a $d-$dimensional sphere $v_d(B) = b_d r^d$, where r is the radius of the sphere and b_d is the volume of the unit sphere in $\mathbb{R}^d$, i.e., $b_d = \sqrt{\pi^d}/\Gamma(1+d/2)$ with $\Gamma(a) = \int_0^\infty x^{a-1}\exp(-x)dx$ [163].

8.4.2 *Medium Access Control (MAC)*

Considering the distributed nature of ad hoc wireless networks, ALOHA, CSMA/CA and their derivative protocols are an appealing choice for multiple access communication. Baccelli et al. in [44] demonstrated that the performance of properly tuned S-ALOHA protocol is *comparable* to that of CSMA/CA. S-ALOHA also has low implementation complexity due to its simple nature. Hence, we will consider the S-ALOHA MAC protocol for the wireless ad hoc network.

In S-ALOHA, time is discretized into slots of length T_{slot}. At the start of a slot, a user can independently decide either to transmit with a probability p or defer its transmission with a probability $1 - p$. We assume that all users always have one or more packets to transmit. This assumption is widely prevalent in the literature, mainly because it simplifies the analysis by abstracting queuing details. We also consider that all nodes are half-duplex and may serve as relays if they defer their own transmission. Each S-ALOHA time slot can accommodate a single packet with n_D data bits and n_H header bits.

Header bits contribute to energy overhead.

8.4.3 *Physical Layer Model*

We assume that all transmitters in the network transmit with a constant power P which is upper bounded by some regulatory peak power constraint $P \leq P_{max}$. All receivers suffer from additive white Gaussian noise and co-channel interference from simultaneous transmissions by other nodes. We assume that communication is interference limited, i.e., the noise power is significantly lower than the aggregate interference power and hence can be ignored. Such a scenario practically corresponds to a network operating under saturated traffic conditions. Since outages due to noise and interference can be treated separately [151], the generality of analysis is preserved even if the noise power is comparable to the interference power.

Rayleigh fading and power-law attenuation path-loss model.

The channel gain between an arbitrary transmitter Y[2] and a receiver X is modeled by $H_{XY} l(\|Y - X\|)$, where, $l(.)$ is a distance dependent path-loss function and H_{XY} is a unit mean *exponentially* distributed random variable. H_{XY} accounts for the small scale Rayleigh fading channel. Generally, the large scale path-loss is modeled by considering the *power law function*, i.e., $l(R) = CR^{-\alpha}$, where C is a frequency dependent constant, R is the distance between the transmitter and the receiver and $\alpha \geq 2$ is the terrain or environment dependent path-loss exponent. Although this type of path-loss model suffers from a singularity near zero, it is quite accurate in the far-field region.

2 Note that Y and X corresponds to the location of the transmitter and receiver respectively. In context of this chapter, both $Y = (Y_1, Y_2, .., Y_d)$ and $X = (X_1, X_2, ..., X_d)$ are random vectors with X_i or Y_i being uniformly distributed random variables ($\forall i = 1, ..., d$).

The channel gains are assumed to be independent and identically distributed (i.i.d.) both in the spatial and temporal domains (i.e., across different links in space and different slots on the same link).

8.4.4 *Routing*

We consider a routing strategy based on *geographical information forwarding* (GIF). Geographical information forwarding or greedy routing (GR) is a contention based state-free routing scheme. We assume that nodes are aware of their own position and possess some knowledge about the destination. The latter can be obtained from the broadcasted data itself. In order to maintain generality, we do not assume any specific greedy routing protocol. We rather focus on the best case routes which can be established between an arbitrary source and destination.

Poisition based geographical information forwarding.

Geographical routing has been investigated extensively in the literature. Nevertheless, most of the studies restrict their analysis to simplistic network models. To the best of our knowledge, most of the existing literature [70, 130, 138, 142–145, 148, 150, 155, 161] investigates a single source-destination pair with multiple relaying terminals at their disposal. In reality not only multiple users will seek to transmit at the same time but the availability of relaying terminals is also subject to the MAC. The *spatial reuse* of the spectral resources *cannot* be ignored. It is this spatial reuse which results in inter-network interference. Consequently, a receiver/relay can only decode the packets if its SIR is above a certain capture threshold. Ignoring interference in the analysis entirely changes the state of affairs. Users in a large scale ad hoc network have desired QoS requirements. As per our earlier discussion the notion of a link is tightly coupled with these QoS requirements. Hence the *physical (or topological) connectivity* of nodes (considering received power $P \geq P_{min}$) does not reflect *actual connectivity* (SIR $\geq \beta$). In brief, simplistic models with one source and a destination may lead to unrealistic conclusions and insights. In this chapter, we modify the existing GR protocol to explicitly address the QoS constraints. We will defer the detailed discussion to Section IV.

8.4.5 *Notation and Symbols*

Table 1 summarizes frequently used geometric symbols. Throughout the chapter, we use $\mathbb{E}(.)$ to denote expectation, $f_X(.)$ to denote probability density function (PDF) and $\mathcal{F}_X(.)$ to denote the cumulative distribution function (CDF) of random variable X. Random variables are represented by uppercase symbols and boldface italic symbols are used to denote random sets.

Symbol	Description
$b(x,r)$	Ball of radius r centered at point x.
$b^c(x,r)$	Complementary region of $b(x,r)$, i.e., $\mathbb{R}^2 - b(x,r)$.
$lens(x_1,r_1,r_2)$	Area of intersection between two balls, i.e., $b(x_1,r_1) \cap b(x_2,r_2)$ with $x_1 = (a,b)$ and $x_2 = (a+r_2,b)$ with $a,b \in \mathbb{R}$.
$lune(x_1,r_1,r_2)$	Area of upper lune formed by intersection of two balls, i.e., $b(x_2,r_2) - lens(x_1,r_1,r_2)$ with $x_1 = (a,b)$ and $x_2 = (a+r_2,b)$ with $a,b \in \mathbb{R}$.
$Sec(x,\phi,r)$	Sector with radius r and central angle ϕ centered at point x.
$Sec^c(x,\phi,r)$	Complementary region of $Sec(x,\phi,r)$, i.e., $\mathbb{R}^2 - Sec(x,\phi,r)$.

Table 8.1: Geometric symbols and their description.

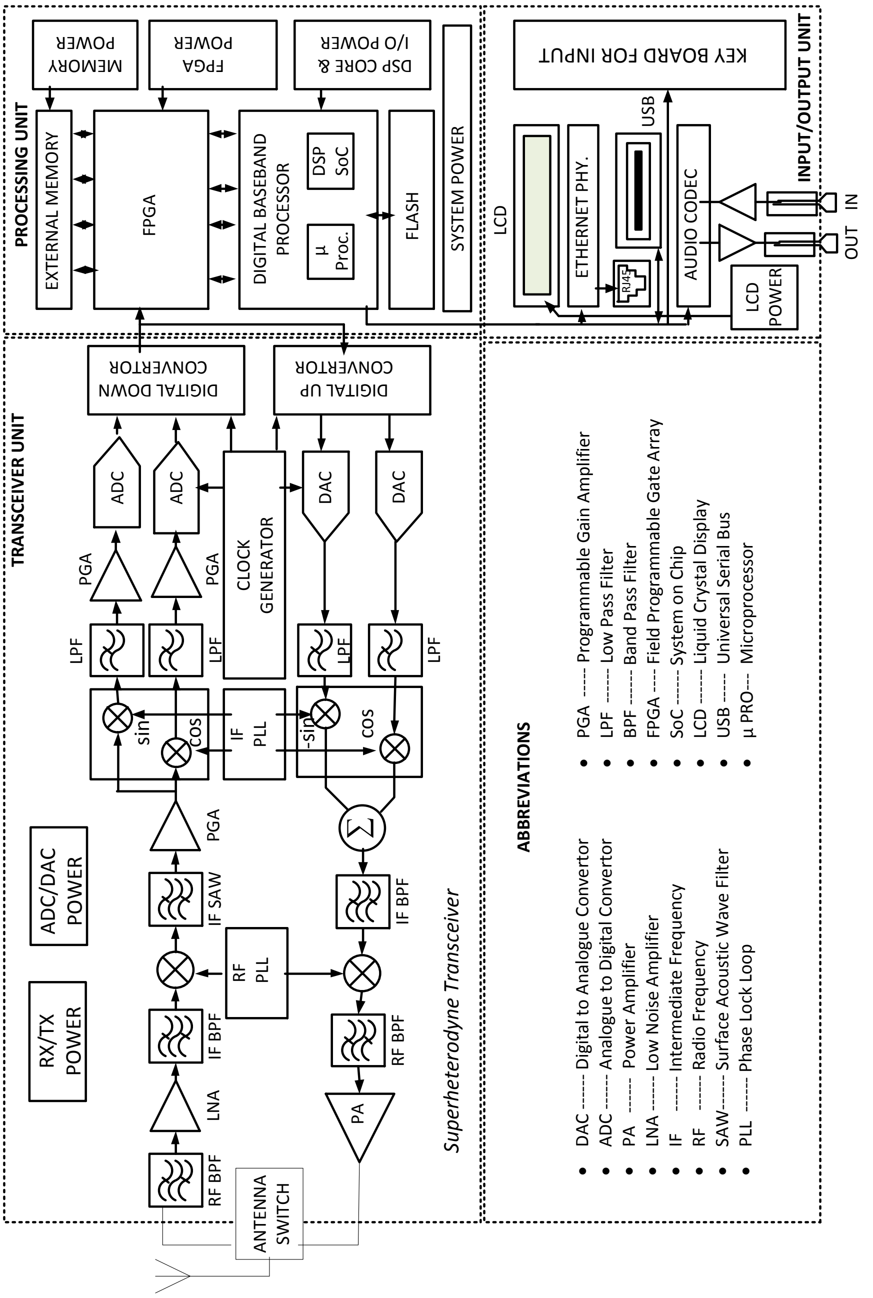

Figure 8.1: Block Diagram of a Communication Hardware Platform with Superheterodyne Transceiver.

8.5 ENERGY CONSUMPTION MODEL FOR TRANSCEIVER

The *hardware architecture* of the communication transceiver employed by an individual user *cannot* be neglected while characterizing the EE. In reality, the communication hardware may vary from one user to another. It is difficult, if not impossible, to characterize the EE of a large scale ad hoc network formed by heterogeneous hardware platforms. To this end, in this study we assume homogeneity between users in terms of device capabilities and architecture. Without loss of analytical generality, we consider a generic software defined radio (SDR) type hardware architecture as depicted in fig. 8.1. Our choice of architecture is mainly motivated by the Texas Instrument (TI) recommendation [164] and current trends in 802.11 WLAN radios [165].

Energy consumption model cannot ignore the underlying hardware model.

In order to quantify the overall power consumption of the radio platform, we employ component by component power consumption analysis as in [130] and [131]. On a broader scale radio hardware may not be manufactured using discrete components. Currently, two different industrial trends are being witnessed: (i) radio transceiver, PHY, MAC all fabricated in a single CMOS chip, while an external SiGe or GaAs power amplifier chip is employed. (ii) single chip CMOS PHY+MAC and a separate SiGe BiCMOS power amplifier and radio is employed. The single chip fabrication may reduce the energy expenditure of a radio platform. However, such reduction can be addressed by appropriate scaling of power consumption parameters in a straightforward manner.

The choice of process technology, i.e., CMOS or SiGe BiCMOS is not an arbitrary decision. Indeed, process choices are subject to several technical and non-technical considerations, for e.g. flicker noise, transconductance, DC coupling, availability of modeling tools, accuracy in modeling, production and marketing times etc. Selection of a particular process technology also plays a vital role in crafting the overall *energy consumption* of the *radio frequency integrated circuit* (RFIC) [165]. In this chapter, we do not confine our analysis to a particular technology. Our generic component by component parametrization facilitates analysis for different process technologies. However, for the purpose of simulations, we will consider the power consumption parameters for SiGe BiCMOS RFIC.

The radio platform depicted in fig. 8.1 can be partitioned into three distinct units according to their functionalites, i.e., the transceiver unit, the processing unit and the input/output (IO) unit. There are three alternative choices for transceiver architecture:

1. Superheterodyne (SH) transceiver (fig. 8.1 transceiver unit);
2. Low intermediate frequency (LIF) transceiver (fig. 8.2);
3. Zero intermediate frequency (ZIF)/Direct Conversion (DC) transceiver (fig. 8.2).

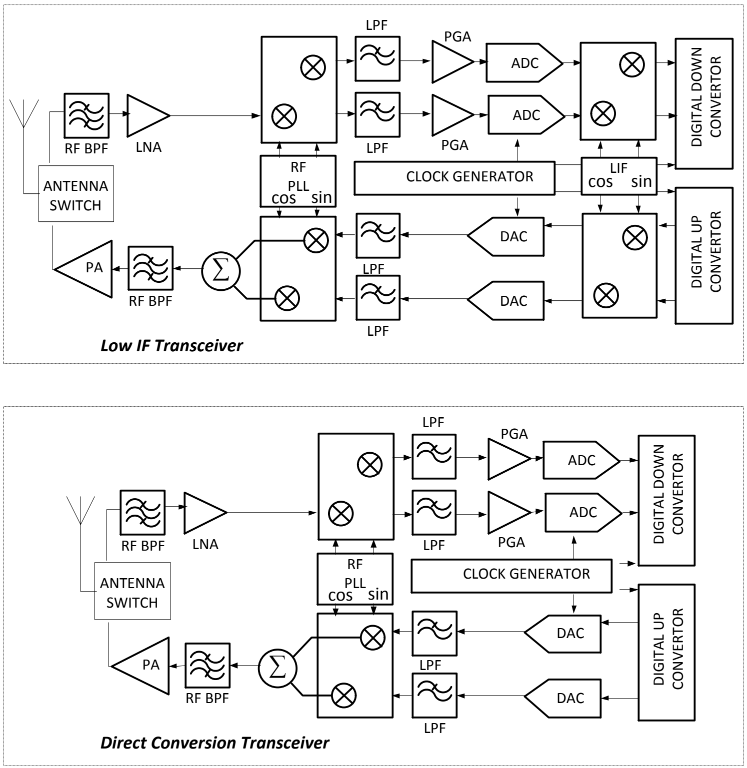

Figure 8.2: Alternate Architectural Options for the Transceiver Block.

Each of the transceiver architectures has its own merits and demerits. The choice of a particular architecture depends on the intended application. Detailed discussion on the selection of a particular architecture is out of the scope of this study. Interested readers are directed to [165] and [166] for insightful discussions. Due to the architectural differences between these transceivers, their power consumption is also different. Table 8.2 enumerates typical values for the power consumption of different components involved in the transmit and receive chain. The power consumption of the DSP varies depending on the usage patterns of different on-chip resources. We assume that a typical device has 60% processing load. This choice of load is arbitrary and purely based on the availability of the numerical value for power consumption from the datasheet [167]. Power consumption values in Table 8.2 are obtained from several research papers describing the state of the art research in RF IC design. The effective power consumption of a typical node in transmit mode is given by

$$P_{TX} = P_{TX}^{EF} + (1 + \alpha_{amp})P, \quad (8.2)$$

$$P_{TX}^{EF} = P_{PU} + P_{TU} + P_{IOU}, \quad (8.3)$$

where P is the transmit power of the node, P_{PU} is the power consumption of processing unit, P_{TU} is the power consumption of the transmission circuitry, P_{IOU} is the power consumption of the IO unit, $\alpha_{amp} = \frac{\xi}{\eta} - 1$ is the amplifier efficiency of class A amplifier [131]. Note that amplifier efficiency is coupled with the drain efficiency η and the Peak to Average Ratio (PAR) ξ. The PAR for an amplifier depends on the modulation scheme and its constellation size[3]. Similarly the power consumption of the receiver is

$$P_{RX} = P_{PU} + P_{RU} + P_{IOU}, \tag{8.4}$$

where P_{RU} is the energy consumption of the receiver circuitry. The numerical values for P_{PU}, P_{RU}, P_{IOU} and P_{TU} can be calculated using the block diagrams 8.1, 8.2 and Table 8.2.

8.6 ENERGY EFFICIENCY OF INTERFERENCE LIMITED AD HOC NETWORK

Section II and III, presented a detailed sketch of network and user level parameters which are critical for characterizing the EE. Based on our prior discussion, our focus in this section is to develop a generic statistical framework for quantifying the EE.

8.6.1 *Macroscopic Picture of the Network*

Half-duplex nodes with those defering transmission serving as relays.

Consider a snapshot of the network at the beginning of an arbitrary S-ALOHA time slot. This snapshot consists of two distinct type of nodes, i.e., transmitters and receivers. Since users are distributed according to the HPPP Φ (Section III), S-ALOHA MAC can be incorporated by the construction of a Marked Poisson point process (MPPP) [163] as

$$\bar{\Phi} = \{[x_i, \mathbb{1}(x_i)] \; : \; x_i \in \Phi\}, \tag{8.5}$$

where,

$$\mathbb{1}(x_i) = \begin{cases} 1 & \text{with probability} \quad p \\ 0 & \text{with probability} \quad 1-p \end{cases},$$

is the medium access indicator and p is the MAP. Alternatively, $\bar{\Phi}$ can be represented as a pair of independent HPPPs, i.e.,

$$\begin{aligned} \Phi_{TX} &= \{x_i : \mathbb{1}(x_i) = 1\} \text{ with intensity } \lambda p, \text{ and} \\ \Phi_{RX} &= \{x_i : \mathbb{1}(x_i) = 0\} \text{ with intensity } \lambda(1-p). \end{aligned} \tag{8.6}$$

3 For uncoded M-QAM, the amplifier efficiency is given by $\alpha_{amp} = 3\frac{\sqrt{M}-1}{\sqrt{M}+1}$ [130, 131].

Component	Power Consumption(mW)	Description
P_{LPF}	30	2^{nd} order Low pass filter [168]
P_{BPF}	48.6	4^{th} order Band pass filter [169, 170]
P_{LNA}	14.4	Low Noise Amplifier [171]
$P_{Q,MIX}$	66.6	Quadrature Modulator [172]
P_{MIX}	85.5	Mixer with Buffer [173]
P_{PGA}	36	Programmable Gain Amplifier [174]
P_{RFPLL}/P_{IFPLL}	50	RF and IF Phase Lock Loop [131]
P_{DUC}/P_{DDC}	250	Digital Up/Down Converter [175]
P_{CLOCK}	650	Clock generator (CDC E949) [176]
$P_{\mu PRO}$	0.44	MSP430F1232 Microprocessor [177]
P_{FPGA}	800	65nm FPGA [178]
P_{DSP}	$0.93 \times 10^{-6}B$	TMS 320 DSP @600 MHz [167]
P_{DAC}	$15.4 + 1.8 \times 10^{-7}B$	Digital to Analog convert or [131]
P_{ADC}	$6.6 + 1.313 \times 10^{-5}B$	Analog to Digital converter [131]

Table 8.2: Power consumption of various components in a DC radio platform. (The power consumption of DAC, ADC and DSP depends on the signal bandwidth B taken in hertz).

We envision a scenario, where each transmitter $x_j \in \Phi_{TX}$ wants to communicate with its desired destination x_{des}^j (located at a distance r_{SD}) in a multihop manner. Receivers from Φ_{RX} serve as intermediate relays between transmitters and their destinations. Destinations are not assumed to be a part of the point process Φ. Notice that for a certain class of routing protocols the distance r_{SD} may change from one time slot to another depending on the net progress of the packet. Each transmitted packet is routed by a QoS aware greedy routing (Section IV-B) strategy towards its intended destination via multihop relaying. It is assumed that each node has a large buffer to store packets and then forward them on the basis of best-effort service.[4]

8.6.2 *QoS Aware Greedy Forwarding*

Recall, that the notion of link is coupled with the desired QoS.

Given a realization of a HPPP of transmitters Φ_{TX}, receivers Φ_{RX} and destinations associated with each transmitter, the QoS aware greedy forwarding operates as follows:

Condition 1: *Any receiver $x \epsilon \Phi_{RX}$ is considered as a potential relay for a transmitter $y \in \Phi_{TX}$ in a particular S-ALOHA time slot, iff the SIR of the packet received from y at x is above certain threshold β.*

The threshold β reflects the users' desired QoS requirements. Additionally, it also dictates the number of transmitters associated with each relay. For $\beta \geq 1$, at maximum there is *one and only one unique* transmitter associated with each receiver. This is intuitive, since for $\beta \geq 1$, the SIR constraint is only satisfied if the signal power from a certain transmitter individually exceeds the aggregate power contributed by all other transmitters. Later in our discussion, it will become clear that β is always greater than 1 for an uncoded modulation scheme and narrow band transmissions.

Condition 2: *A receiver $x \in \Phi_{RX}$ which fulfills the SIR requirements (Condition 1) can serve as a relay for a transmitter $y \in \Phi_{TX}$, iff it provides maximum progress of the packet towards its desired destination. In other words, if $\boldsymbol{R_y} \subseteq \Phi_{RX}$ is the (random) set of relays that satisfy SIR requirement for a particular transmitter y at a particular time slot, then node x is selected as a relay iff*

$$x = \arg\min_{x \in \boldsymbol{R_y}} \left(r_{SD} - \|y - x\| \right). \tag{8.7}$$

At this juncture, it is important to highlight that the above formulation addresses both interference and QoS requirements by employing SIR based connectivity and the relaying model. These two aspects have been completely ignored in most of the relevant literature.

4 We do not quantify the end-to-end delay incurred by each packet. Detailed analysis of end-to-end delay is beyond the scope of this chapter. Interested readers may refer to [179] for a comprehensive discussion of end-to-end delay with different problem setups.

8.6.3 *Selection of Forwarding Areas*

A closer look at condition 2 reveals that even if there exists one or more relays satisfying the QoS constraint, they may not be useful unless they lie in a certain *specific region*. More specifically, only those relays which can guarantee a *positive forward progress* without sacrificing the *desired link quality* are critical in quantifying the EE. In the classical setup[5], the specific region in which existence of a relay guarantees a positive progress towards the destination is often referred to as the *forwarding area* for GR. Different GR protocols result in a different geometry for the forwarding areas [150]. In essence, protocol designers can leverage the geometry of the forwarding area to control the *overall directionality* of a routing protocol. In turn, directionality of the routing protocol characterizes the average number of hops traveled by each packet before reaching its desired destination and hence shapes the overall EE of a network. In this study, we consider three different shapes for the forwarding area resulting from three different forwarding strategies:

1. *Generalized Lower Bound (GLB):* Confining relays to a certain geographical area often results in an intractable analysis. The main reason behind this is the intricate geometry of the forwarding area. Specially, for networks which are represented as a higher dimensional HPPP ($d > 3$) it is extremely difficult to obtain closed-form expressions for average number of hops under the GR protocol[6]. However, for generic d-dimensional networks, a lower bound on the hop count can be established by ignoring the forward progress constraint. In other words, the minimum number of hops required for communication between an arbitrary source and its intended destination is obtained by assuming that *any progress made in a network is exactly in the intended direction.* Such a lower bound is similar in spirit to Shannon's approach for capacity. It equips network designers with a clear idea about the best case achievability. In this chapter, we name such a lower bound the

5 Note that in classical setup [70, 142, 143, 145, 150] existence of relay with a positive forward progress means physical existence of relay within a certain area $\mathcal{A}$. $\mathcal{A}$ is the common area between some hypothetical shape centered at the destination and a ball of radius r centered at the source. The radius of the circle (r) quantifies the node's audibility/transmission radius. However, in this study we argue that the physical existence of the relay does not guarantee a positive forward progress unlessthe relay also satisfies Condition 1 (Section V-B). Moreover, due to the presence of fading terrain and interference, the audibility region of a source cannot be represented by a perfect circle of radius r.

6 It might be argued that real world networks do not exist in higher dimensional spaces $\mathbb{R}^d$ ($d > 3$). As a matter of fact, physically network nodes do not form a HPPP in a higher dimensional space. Nevertheless, the different *dynamics* of the network, nodes often finish up in forming a higher dimensional point process. For instance, consider a case where network nodes form a HPPP in $\mathbb{R}^3$. Each node is activated whenever it has a packet to transmit. Assuming that inter-arrival time of packets follow an exponential distribution and packet arrivals form a HPPP in $\mathbb{R}$. Then the overall network forms a Poisson point process in a product space $\mathbb{R}^3 \times \mathbb{R}$ or simply a HPPP in $\mathbb{R}^4$.

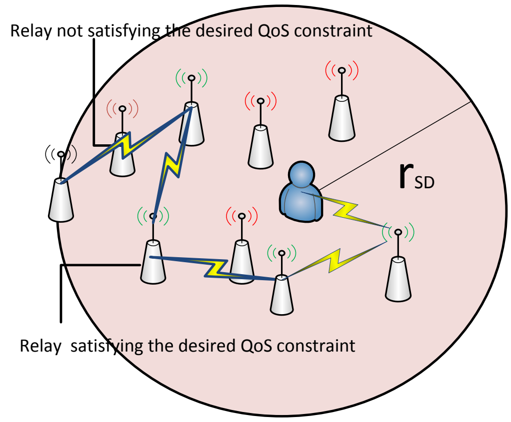

(a) Geometry of the forwarding area which results in GLB for QoS aware GR.

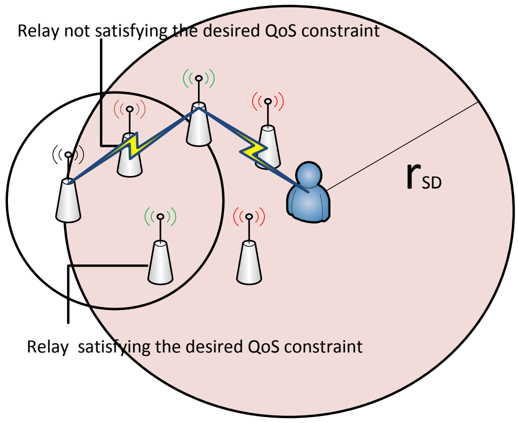

(b) Geometry of the forwarding area under MFA based QoS aware GR.

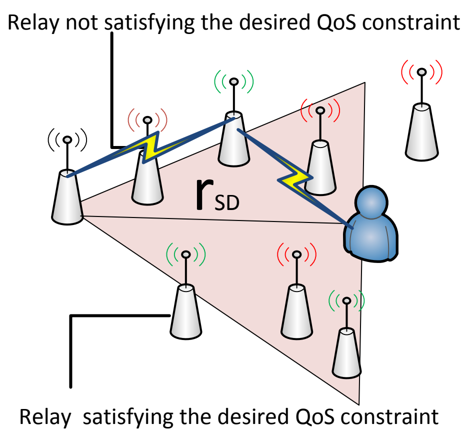

(c) Geometry of the forwarding area under RSA based QoS aware GR.

Figure 8.3: Selection of the forwarding Area.

Generalized Lower Bound (GLB). Note that the GLB does not propose any specific forwarding scheme. However, while quantifying the EE of an ad hoc network under different forwarding schemes we treat the GLB in a similar context. Fig. 8.3a provides a graphical illustration for the GLB.

2. *Maximum Forward Area (MFA)*: Maximum forward area based GR for 2-D networks is very well established in the literature [70, 71, 143, 145, 149, 150, 160]. In this study, we consider a modified version of MFA for QoS aware GR. Consider that the network nodes form a HPPP Φ in $d = 2$. Moreover, consider a typical transmitter y located at origin o with its intended destination x_{des} located at $(r_{SD}, 0)$. Let $\boldsymbol{R}_y$ be the set of relays at which y's QoS constraint is satisfied. Then the receiver $x_i \in \boldsymbol{R}_y$ located at distance r from the origin, provides maximum forward progress towards the destination *iff there does not exist any other receiver* $x_j \in \boldsymbol{R}_y$ *in a* $lune\left(o, r, \frac{r_{SD}}{2}\right)$ (See tab. 8.1). Fig. 8.3b provides a graphical illustration of the MFA based GR strategy. Note that all relays lying on the periphery of $b(o, r)$ (lower bounding the lune) provide *equal forward progress* towards the destination. In short, MFA based QoS aware greedy routing selects a relay in $lens\left(o, r, \frac{r_{SD}}{2}\right)$ which provides maximum forward progress and satisfies the SIR criterion.

3. *Radian Sector Forwarding (RSF)*: In RSF based forwarding, the next hop relay is selected in a radial sector with central angle ϕ around the line connecting the transmitter and its intended destination. Considering the QoS aware GR, a typical transmitter y gets maximum forward progress of $r\cos(\theta)$ *iff there exists a relay in circular sector* $Sec(o, \phi, r)$ *satisfying the desired SIR constraint and* $Sec^c(o, \phi, r)$ *does not contain any such relay*. Considering the best case scenario, $\cos(\theta) \approx 1$ and hence maximum forward progress is given by the random variable r. Fig. 8.3c depicts RSF based forwarding strategy.

Routing across the QoS voids.

At this juncture, it is important to highlight that in the context of this study routing voids or dead ends are not only manifested by physical absence of relays but they also result from the user's QoS requirement. Voids which exist at a particular QoS requirement may not necessarily exist for a different QoS requirement. When voids exist in MFA or RSF based strategies, GLB can be employed to investigate the feasibility of routing around the voids.

8.6.4 *Energy Efficiency*

Maximum forward progress under GLB

Lemma 8.1 *Given a realization of the HPPP of transmitters Φ_{TX}, their associated destinations and the HPPP of receivers/relays Φ_{RX}, the probability that the single hop maximum forward progress ζ from a typical transmitter $y \in \Phi_{TX}$ towards its intended destination x^{y}_{des} does not exceed r is given by*

$$\begin{aligned} \mathcal{F}^{GLB}_{\zeta}(r) &= \Pr\{\zeta \leq r\}, \\ &= \exp\left(-\frac{(1-p)}{p}\frac{\sin(\delta)}{\delta\beta^{\frac{\delta}{\pi}}}\exp\left(-\frac{\lambda p b_d \beta^{\frac{\delta}{\pi}}\delta}{\sin(\delta)}r^d\right)\right) \end{aligned} \tag{8.8}$$

where, $\delta = \frac{d\pi}{\alpha}$ is constant for given path loss exponent α, network dimension d and β is the previously defined SIR threshold.

PROOF: Consider a snapshot of the network at an arbitrary S-ALOHA time slot. From (8.6), it is known that the location of transmitters and receivers can be represented by HPPPs Φ_{TX} and Φ_{RX} respectively. Since the HPPP Φ_{TX} is stationary, by Slivnyak's theorem [163] adding a single point at an arbitrary location does not change the distribution of the point process. For analytical convenience, we add a probe transmitter at the origin $\Phi_{TX} \cup \{o\}$. Also, the stationarity of Φ_{TX} implies that the distribution of the maximum forward progress ζ is not affected by the choice of any particular transmitter. Hence, without any loss of generality, we focus on the progress made by the packet transmitted from the probe transmitter. The SIR with respect to the probe transmitter, measured at an arbitrary receiver/relay located at distance r from the origin is given by

$$\begin{aligned} \gamma(r, H_{xo}, I) &= \frac{H_{xo}P_s l(r)}{\sum_{j\in\Phi_{tx}\setminus\{o\}} H_{jo}P_s l(R_j)}, \\ &= \frac{H_{xo} l(r)}{I} \end{aligned} \tag{8.9}$$

where, $I = \sum_{j\in\Phi_{tx}\setminus\{o\}} H_{jo} l(R_j)$ is the accumulated interference experienced at an arbitrary relay. Notice that $\gamma(r, H_{xo}, I)$ does not depend on the transmit power. Define a MPPP Φ_{REL}, constructed by assigning position dependent QoS marks, i.i.d. fading and interference marks to each point in Φ_{RX}. QoS marks ensure that only receivers which satisfy Condition 1 will contend for relaying the packet.

$$\mathbb{1}_{QoS}(\gamma(r, H_{xo}, I)) = \begin{cases} 1 & \gamma(r, H_{xo}, I) \geq \beta \\ 0 & \gamma(r, H_{xo}, I) < \beta \end{cases}, \tag{8.10}$$

$$\Phi_{REL} = \{[x, \mathbb{1}_{QoS}(\gamma(\|x-o\|, H_{xo}, I)), H_{xo}, I] : x \in \Phi_{RX}\}. \tag{8.11}$$

By construction, Φ_{REL} is an inhomogeneous Poisson point process (IHPPP). Since, H_{xo}'s are i.i.d. random variables, we will drop the subscript for ease of presentation. The intensity function of Φ_{REL} can be obtained by employing the Marking theorem [163],

$$\lambda_{REL}(r, h, i) = \lambda(1-p)db_d r^{d-1} f_H(h) f_I(i) \mathbb{1}_{QoS}(\gamma(r, h, i)). \tag{8.12}$$

The mean measure for Φ_{REL} is given by,

$$\begin{aligned}
\Lambda(B) &= \int_0^\infty \int_0^\infty \int_B \lambda_{REL}(r) dr dh di, \qquad (8.13)\\
&= \int_0^\infty \int_0^\infty \int_B \lambda(1-p)db_d r^{d-1} \mathbb{1}_{QoS}(\gamma(r,h,i)) f_H(h) f_I(i) dr dh di,\\
&= \int_0^\infty \int_0^\infty \int_B \lambda(1-p)db_d r^{d-1} \mathbb{1}_{QoS}\left(h \geq i\beta r^\alpha\right) f_H(h) f_I(i) dr dh di,\\
&= \int_0^\infty \int_B \lambda(1-p)db_d r^{d-1} \left[\int_0^\infty \mathbb{1}_{QoS}\left(h \geq i\beta r^\alpha\right) f_H(h)\right] dh f_I(i) dr di,\\
&= \int_0^\infty \int_B \lambda(1-p)db_d r^{d-1} \left(1 - \mathcal{F}_H(i\beta r^\alpha)\right) f_I(i) dr di,\\
&= \int_B \lambda(1-p)db_d r^{d-1} \left[\int_0^\infty \exp\left(-i\beta r^\alpha\right) f_I(i) di\right] dr,\\
&= \int_B \lambda(1-p)db_d r^{d-1} \underbrace{\mathbb{E}_I\left(\exp\left(-i\beta r^\alpha\right)\right)}_{A} dr.
\end{aligned}$$

By definition of the Laplace transform,

$$\mathcal{L}_I(s) = \mathbb{E}_I\left(\exp\left(-si\right)\right). \tag{8.14}$$

Hence, $A = \mathcal{L}_I(s) \mid_{s=\beta r^\alpha}$ can be solved as,

$$\begin{aligned}
\mathcal{L}_I(s) &= \mathbb{E}_{\Phi,H}\left(\exp\left(-s \sum_{i \epsilon \phi_{tx} \setminus \{o\}} H_{io} l(R_i)\right)\right), \qquad (8.15)\\
&\stackrel{B}{=} \mathbb{E}_\Phi\left(\prod_{i \in \phi_{tx} \setminus \{o\}} \mathbb{E}_H\left(\exp(-sHl(R_i))\right)\right)
\end{aligned}$$

where, B follows from the i.i.d assumption. Using the definition of the Generating functional for the Poisson point process [163],

$$\begin{aligned} \mathcal{G}(f(x)) &= \mathbb{E}_\Phi\left(\prod_{x\in\phi} f(x)\right), \\ &= \exp\left(-\int_{\mathbb{R}^d}(1-f(x))\lambda(dx)\right). \end{aligned} \tag{8.16}$$

The Laplace transform of the interference can be written as,

$$\mathcal{L}_I(s) = \exp\left(\int_0^\infty (1-\mathbb{E}_H(\exp(-sHr^{-\alpha})))\lambda(dr)\right). \tag{8.17}$$

Eq. (8.17) can be solved as in [154] and [44],

$$\mathcal{L}_I(s) = \exp\left(-\lambda p b_d s^{\frac{d}{\alpha}} \frac{\pi\frac{d}{\alpha}}{\sin(\pi\frac{d}{\alpha})}\right). \tag{8.18}$$

Consequently,

$$A = \exp\left(-\frac{\lambda p b_d \beta^{\frac{\delta}{\pi}}\delta}{\sin(\delta)} r^d\right) \tag{8.19}$$

where, $\delta = \frac{d\pi}{\alpha}$ is constant for fixed d and α .Using eq. (8.15), (8.13) can be simplified,

$$\Lambda(B) = \int_B \lambda(1-p) d b_d r^{d-1} \exp\left(-\frac{\lambda p b_d \beta^{\frac{\delta}{\pi}}\delta}{\sin(\delta)} r^d\right) dr. \tag{8.20}$$

The single hop maximum forward progress ζ is at most r provided there does not exist any potential relay in the region $b^c(0,r)$, i.e.,

$$\begin{aligned} \mathcal{F}_\zeta^{GLB}(r) &= \Pr\{\Phi_{REL}(\Lambda(b^c(0,r))) = 0\}, \\ &= \exp\left(-\int_r^\infty \lambda(1-p) d b_d r^{d-1} \exp\left(-\frac{\lambda p b_d \beta^{\frac{\delta}{\pi}}\delta}{\sin(\delta)} r^d\right) dr\right), \\ &= \exp\left(-\frac{(1-p)}{p}\frac{\sin(\delta)}{\delta\beta^{\frac{\delta}{\pi}}} \exp\left(-\frac{\lambda p b_d \beta^{\frac{\delta}{\pi}}\delta}{\sin(\delta)} r^d\right)\right). \end{aligned} \tag{8.21}$$

□

Maximum Forward Progress under MFA & RSF)

Lemma 8.2 *Considering MFA/RSF based GR, the probability that the single hop maximum forward progress ζ from a typical transmitter $y \in \Phi_{TX}$ towards its destination is at most r can be quantified as*

$$\mathcal{F}^{j}_{\zeta}(r) = \exp\left(-\kappa^{j}\frac{(1-p)}{p}\frac{\sin(\delta)}{\delta\beta^{\frac{\delta}{\pi}}}\exp\left(-\frac{\lambda p\pi\beta^{\frac{\delta}{\pi}}\delta}{\sin(\delta)}r^2\right)\right) \quad (8.22)$$

where $j \in \{MFA, RSF\}$, $\kappa^{MFA} = \frac{\cos^{-1}(\frac{r}{r_{sd}})}{\pi}$ *and* $\kappa^{RSF} = \frac{\phi}{2\pi}$.

PROOF: Both MFA and RSF restrict the selection of potential relays to a certain area (Section V-B). Consequently, (8.13) needs to accommodate this geometric constraint. For $d = 2$, the mean measure of the IHPPP Φ_{REL} formed by the relays under RSF is given by,

$$\begin{aligned}\Lambda(Sec^{c}(o,\phi,r)) &= \int_{\theta_1}^{\theta_2} 2\pi\int_0^{\infty}\int_0^{\infty}\int_r^{\infty}\lambda(1-p)r \\ &\times \mathbb{1}_{QoS}(\gamma(r,h,i))f_H(h)f_I(i)f_{\Theta}(\theta)drdhdid\theta,\end{aligned} \quad (8.23)$$

where, θ is angle of a typical relay from the line connecting the transmitter $y \in \Phi_{TX}$ and its intended destination x^{y}_{des}. Since, relays are originally distributed according to a HPPP Φ_{RX}, θ is uniformly distributed between $[0, 2\pi]$. RSF restricts relay selection in a sector with a central angle ϕ,

$$\begin{aligned}\Lambda^{RSF}(Sec^{c}(o,\phi,r)) &= \int_{-\frac{\phi}{2}}^{\frac{\phi}{2}}\int_0^{\infty}\int_0^{\infty}\int_r^{\infty}\lambda(1-p)r \\ &\times \mathbb{1}_{QoS}(\gamma(r,h,i))f_H(h)f_I(i)drdhdid\theta, \quad (8.24) \\ &= \lambda\phi(1-p)\int_r^{\infty} r\exp\left(-\frac{\lambda p\pi\beta^{\frac{\delta}{\pi}}\delta}{\sin(\delta)}r^2\right)dr.\end{aligned}$$

Hence,

$$\mathcal{F}^{RSF}_{\zeta}(r) = \exp\left(-\frac{\phi}{2\pi}\frac{(1-p)}{p}\frac{\sin(\delta)}{\delta\beta^{\frac{\delta}{\pi}}}\exp\left(-\frac{\lambda p\pi\beta^{\frac{\delta}{\pi}}\delta}{\sin(\delta)}r^2\right)\right).$$

Similarly in the case of MFA, θ_1 and θ_2 are the angles at which $b(o,r)$ and $b\left(\left(\frac{r_{SD}}{2},0\right),\frac{r_{SD}}{2}\right)$ intersect.

$$\begin{aligned}\Lambda^{MFA}\left(lune\left(o,r,\frac{r_{SD}}{2}\right)\right) &= \int_{-\cos^{-1}\left(\frac{r}{r_{SD}}\right)}^{\cos^{-1}\left(\frac{r}{r_{SD}}\right)}\int_0^{\infty}\int_0^{\infty}\int_r^{r_{SD}\cos(\theta)}\lambda(1-p)r \\ &\times \mathbb{1}_{QoS}(\gamma(r,h,i))f_H(h)f_I(i)drdhdid\theta.\end{aligned}$$

Consequently,

$$\mathcal{F}_{\zeta}^{MFA}(r) = \exp\left(-\frac{\cos^{-1}(\frac{r}{r_{sd}})}{\pi}\frac{(1-p)}{p}\frac{\sin(\delta)}{\delta\beta^{\frac{\delta}{\pi}}}\exp\left(-\frac{\lambda p\pi\beta^{\frac{\delta}{\pi}}\delta}{\sin(\delta)}r^2\right)\right), \quad 0 \leq r \leq r_{SD}.$$

□

Remarks on Lemma 1 & 2:

1. Lemma 1, quantifies the best case single hop spatial progress (ζ) that can be attained by an arbitrary packet under a particular QoS constraint. Employing Riemann–Stieltjes integral representation and integration by parts, average progress (ζ_{GLB}) made by an arbitrary transmission towards its intended destination can be expressed as

$$\begin{aligned}\zeta_{GLB} &= \mathbb{E}(\zeta) = \int_0^{\infty}\left(1-\mathcal{F}_{\zeta}^{GLB}(r)\right)dr, \qquad (8.25)\\ &= \int_0^{\infty}\left(1-\exp\left(-\frac{(1-p)}{p}\frac{\sin(\delta)}{\delta\beta^{\frac{\delta}{\pi}}}\exp\left(-\frac{\lambda p b_d\beta^{\frac{\delta}{\pi}}\delta}{\sin(\delta)}r^d\right)\right)\right)dr.\end{aligned}$$

   Notice that ζ_{GLB} does not depend on the distance between the transmitter and its intended destination (r_{SD}). This indicates that an optimal QoS aware routing scheme should be designed in such a manner that it always ensures constant single hop progress, irrespective of the transmitter-destination separation r_{SD}. From a practical perspective, it is difficult to design a routing protocol which is independent of r_{SD} and also ensures desired routing directionality (defined in Section V-B).

2. Similar to Lemma 1, Lemma 2 can be employed to quantify the average single hop progress (ζ_{MFA}/ζ_{RSF}) made by an arbitrary transmission under MFA/RSF based GR. The average single hop progress ζ_{MFA} strictly depends on the distance between transmitter and its destination r_{SD}. This is not true for RSF, at least while considering the best case scenario[7]. This dependence implies that progress in slot i depends on the progress of the packet in slot $i-1$. This is because distance between transmitter and destination r_{SD} changes from one slot to another. Hence considering the progress in say m slots, then $\zeta_1, \zeta_2, \ldots, \zeta_m$ are dependent random variables.

This observation will be very useful in our later discussion.

3. Both Lemma 1 and Lemma 2, suggest that single hop maximum forward progress (ζ) depends on: (i) *Average forwarding node degree* (Number of receivers/relays per transmitter, i.e., $\frac{1-p}{p}$); (ii) *Path loss expo-*

7 In this chapter, we only focus on best case forwarding under RSA. In other words, we assume $\cos(\theta) \approx 1$ for the sake of analytical tractability.

Modulation	SIR threshold β
BPSK/QPSK	$0.5\left(Q^{-1}\left(P_b^{th}\right)\right)^2$
M-PSK	$\frac{0.5}{\log_2(M)}\left(\frac{Q^{-1}\left(\frac{P_b^{th}\log_2(M)}{2}\right)}{\sin\left(\frac{\pi}{M}\right)}\right)^2$
M-QAM	$\frac{M-1}{3\log_2(M)}\left(Q^{-1}\left(\frac{\log_2(M)P_b^{th}}{4(1-1/\sqrt{M})}\right)\right)^2$

Table 8.3: Selection of SIR threshold β for fixed BEP threshold P_b^{th} .

nent α (through δ); (iii) *QoS Constraint* (through SIR threshold β); (iv) *Density of transmitters* (λ) and (v) *Directionality of routing protocol* (through κ). Except for the path loss exponent (α), all other parameters represent the degrees of freedom (DoF) available to a network designer. An optimal network design will leverage these DoF to maximize the forward progress.

4. The maximum single hop forward progress (ζ) depends on the desired QoS constraint through the SIR threshold β. Hence, the choice of a particular value for β is not arbitrary. The SIR threshold β depends on the modulation and coding scheme employed by the transmitter. Considering a fixed threshold for the bit error probability (BEP) P_b^{th}, β for $M-$PSK and $M-$QAM can be obtained from Table 8.3. Fixing P_b^{th} to 10^{-3} results in $\beta \approx 6$ dB for BPSK modulation. This implies that for uncoded $M-$PSK or $M-$QAM, the typical value of β always exceeds unity when P_b^{th} is fixed to a realistic threshold. Hence in accordance with our previous discussion, there is *one and only one unique* transmitter associated with each receiver.

Fig. 8.4a and 8.4b display network snapshots which corroborate our statements. Notice that increasing the MAP decreases both the number of potential relays for a typical transmitter and the forward progress obtained while selecting a relay. A closer look at eq. 8.25 reveals this two fold impact of increasing p,

$$\zeta_{GLB}=\int_0^\infty \left(1-\exp\left(-\underbrace{\frac{(1-p)}{p}}_{\text{Avg. out degree}\downarrow\text{with}\uparrow p}\frac{\sin(\delta)}{\delta\beta^{\frac{\delta}{\pi}}}\underbrace{\exp\left(-\frac{\lambda p b_d \beta^{\frac{\delta}{\pi}}\delta}{\sin(\delta)}r^d\right)}_{\text{Probability of successful connection}\downarrow\text{ with }\uparrow p}\right)\right)dr.$$

Fig. 8.5 depicts the CDF (8.8,8.22) for forward progress (ζ) under BPSK/QPSK and 16−QAM considering all three forwarding strategies. The dashed lines in Fig. 8.5 correspond to Monte Carlo simulations. Monte Carlo simulations were performed by averaging the single hop progress over 10^5 realizations

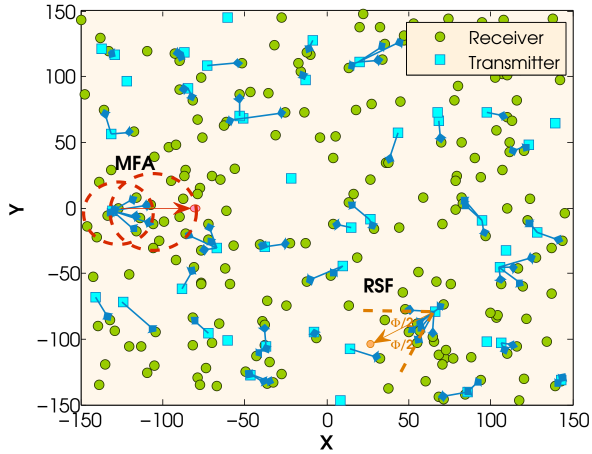

(a) Network Snapshot considering BPSK Modulation Scheme with $P_b^{th} = 10^{-3}$and MAP $p = 0.025$.

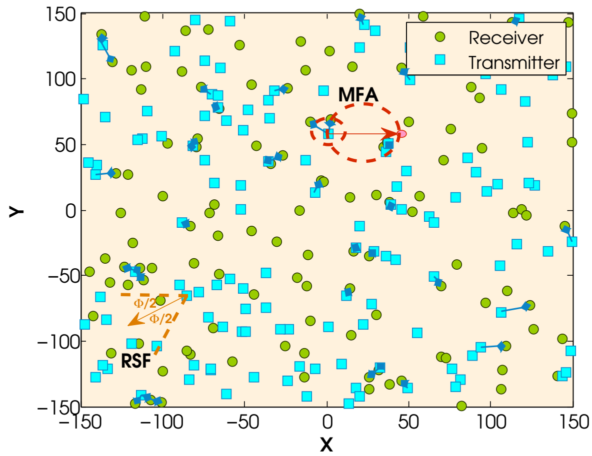

(b) Network Snapshot considering BPSK Modulation Scheme with $P_b^{th} = 10^{-3}$and MAP $p = 0.5$.

Figure 8.4: Snapshots of Network

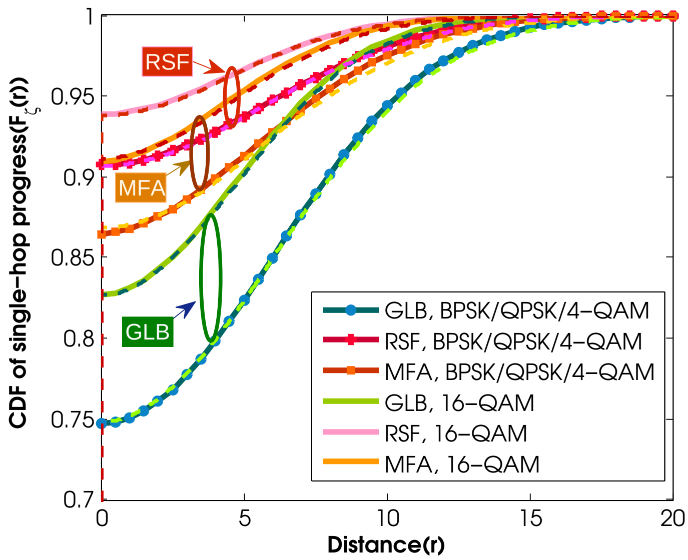

Figure 8.5: CDF (see Eq. (8.8)) of the single-hop progress ζ, with $\lambda = 3 \times 10^{-3}$,$\alpha = 4$,$d = 2$,$r_{SD} = 50$,$\phi = \frac{2\pi}{3}$ and $p = 0.5$. Monte Carlo Simulation results are sketched with dashed line.

of a HPPP Φ with intensity $\lambda = 3 \times 10^{-3} \left(\frac{30 \text{ users}}{100 \times 100 \text{ sq. meter}} \right)$, $p = 0.5$, $r_{SD} = 50$ meter and $\phi = \frac{2\pi}{3}$ for each value of β. Notice that the theoretical and simulation results presented in Fig. 8.5 closely agree with each other.

The CDF of ζ belongs to the family of extreme value distributions [180] and is closely related to the Generalized Gumbel distribution. Like the Gumbel distribution, the CDF possesses a discontinuity at zero [181, 182]. This discontinuity accounts for the fact that there is a positive probability that no progress can be made by a transmission. In other words, there exists a non-zero probability p_{ISO} with which a typical node is isolated in the network. We should reiterate that isolation does not necessarily imply that node cannot communicate with any other node in the network. Rather isolation has a broader meaning in the context of this chapter, i.e., nodes which cannot communicate with another node while fulfilling their desired QoS requirement are considered as isolated. Hence nodes which are isolated for a certain QoS requirement, may not be isolated at lower QoS requirements. Note that the single hop progress ζ is a mixed-type random variable, where $\zeta = 0$ occurs with probability p_{ISO}. From Fig. 8.5, it is obvious that p_{ISO} is *considerably high* for an SIR limited ad hoc network. Moreover, p_{ISO} *increases* with an increase in the desired QoS requirements[8]. Switching from BPSK

8 Increase in a desired QoS requirement corresponds to an increase in the desired transmission rate, i.e., increased bits per symbol ($b = \log_2(M)$) for a fixed bandwidth B and a fixed BER threshold P_b^{th}.

Energy consumption in the network is function of the connectivity in the network.

to 16−QAM results in an increase of void probabilities by 8.4%, 4.2% and 3% for GLB, RSF and MFA respectively (see 8.5). The isolation probability p_{ISO} is an important parameter from the EE perspective. Nodes which are isolated under a certain desired QoS constraint, may spend *infinite energy* without attaining *any forward progress*.

Claim 1: *In an interference limited ad hoc wireless network, the isolation probability (p_{ISO}) of a typical transmitter does not depend on the density of the users.*

PROOF: The isolation probability p_{ISO} can be determined as,

$$\begin{aligned} p^j_{ISO} &= \Pr\{\Phi_{REL}(\Lambda^j(b(0,\infty))) = 0\}, \\ &= \exp\left(-\kappa^j_1 \frac{(1-p)}{p} \frac{\sin(\delta)}{\delta\beta^{\frac{\delta}{\pi}}}\right), \end{aligned} \tag{8.26}$$

where $j \in \{GLB, MFA, RSF\}$, $\kappa^{GLB}_1 = 1$, $\kappa^{MFA}_1 = 0.5$ and $\kappa^{RSF}_1 = \frac{\phi}{2\pi}$. From (8.26), it is obvious that p_{ISO} is independent of λ (density of users) and only depends on *MAP* p, *path-loss exponent* α, *modulation scheme* (through SIR threshold β) and *geometry of the forwarding area* (through κ_1). □

Remarks on Claim 1:

There exists plenty of literature which suggests that p_{ISO} can be potentially *reduced to zero* by *increasing the number of relays* in the network [70, 71, 142, 150, 153]. Apparently, Claim 1 implies a *contrary conclusion* to all these studies. Perhaps, it should be emphasized that extreme care is required while interpreting the connectivity results prevalent in the literature. The major difference between the conclusions of Claim 1 and the existing literature stems from the choice of the network model. Many of the existing studies [70, 71, 142, 150, 153] focus on a scenario, where a single source-destination pair wants to communicate. This communication is facilitated by multihop relaying. Relays are assumed to follow a HPPP, say Φ_R, with intensity λ. Results obtained under such a setup cannot be extended to the case of multiple source-destination pairs. Moreover, it is extremely difficult (both in terms of network design and cost) to deploy a very large population of dedicated relaying terminals. In fact, a more practical approach would be the deployment of dedicated base stations. In real life ad hoc networks, nodes may opt to cooperate with each other subject to their own priority. In other words, nodes which are denied access to the shared wireless medium for a particular time slot may serve as relays. Indeed, Claim 1 quantifies the isolation probability p_{ISO} for a typical transmitter under this scenario. In this case, the number of relays can be increased by one of the following two mechanisms:

1. *By increasing the density of users* λ: Increasing the density of users for a fixed non-zero MAP p will definitely increase the number of relays. However, it also increases the number of transmitters. Hence, the aver-

age number of relays per transmitter remains *unchanged* and the average forward progress will *decrease* due to the *increased interference.* In short, as per Claim 1, node isolation probability p_{ISO} is independent of the user density and cannot be decreased by increasing λ, while such an increase in λ will worsen the EE of the network.

2. *By decreasing the MAP p:* For fixed λ, decreasing the MAP p will reduce the isolation probability p_{ISO}. Nevertheless, the maximum possible reduction of p to zero will imply that no one in the network transmits. Of course, if there is no transmission, energy consumption is zero and the network is trivially energy efficient. Thus, it will violate the purpose of the existence of the network. This means that there exists a *trade off* between *spatial reuse of spectrum*, *connectivity* and the *EE* of the ad hoc network.

In real life the world is cruel and he users are selfish so everybody wants to talk and only a few want to listen, i.e., the number of relays will typically be small as compared to transmitters. In short, it is the *average number of receivers per transmitter* $\left(\frac{1-p}{p}\right)$ under certain MAC which define the isolation and not the *absolute* number of transmitters and receivers.

The complementary isolation probability is indeed the probability of connectivity.

Fig. 8.6 depicts *complementary isolation probability* ($\bar{p}_{ISO} = 1 - p_{ISO}$) of all three forwarding schemes under different parametric variations. The complementary isolation probability $\bar{p}_{ISO}$ plays an important role in quantifying the bits/Joule performance of the ad hoc network. Consequently, the impact of different parameters on $\bar{p}_{ISO}$ should be addressed in detail. To this end, we summarize key observations from fig. 8.6:

- The complementary isolation probability of RSF $\bar{p}_{ISO}^{RSF}$ and MFA $\bar{p}_{ISO}^{MFA}$ are always less than the complementary isolation probability under GLB $\bar{p}_{ISO}^{GLB}$. This holds independent of other parameters (see 8.6). A more general observation is,

$$\bar{p}_{ISO}^{RSF} \leq \bar{p}_{ISO}^{MFA} \leq \bar{p}_{ISO}^{GLB}.$$

  Since GLB represent the best case scenario, it is intuitive to expect a higher connectivity than MFA or RSF under desired QoS requirements. As discussed earlier both MFA and RSF ensure proper directionality for communication. This of course, comes at the cost of increased $\bar{p}_{ISO}$. Both geographical and QoS voids equally contribute towards the $\bar{p}_{ISO}^{MFA}$ and $\bar{p}_{ISO}^{RSF}$, while only QoS voids dominantly contribute towards $\bar{p}_{ISO}^{GLB}$.

- The complementary isolation probability $\bar{p}_{ISO}$ for all three forwarding strategies, decreases with an increase in the desired QoS requirement. Figs. 8.6a, 8.6b and 8.6c clearly depict this decreasing trend. This further consolidates our argument, that a void at a particular QoS requirement may not exist at a lower QoS requirement. Notice that the rate at

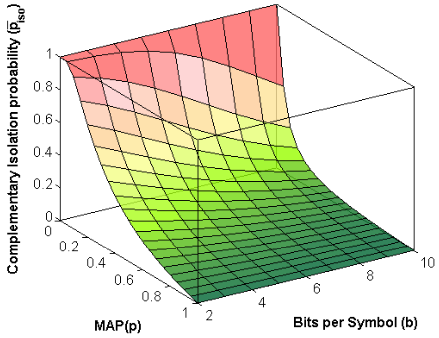

(a) Complementary isolation probability $\bar{p}_{ISO}$ under GLB with $\alpha = 4$, varying MAP p and modulation order M.

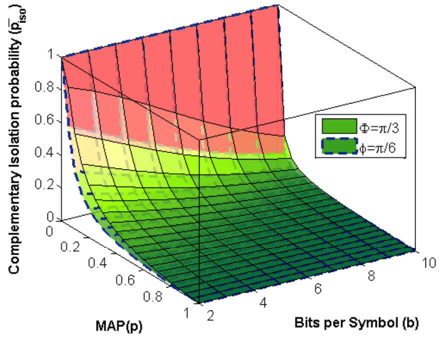

(b) Complementary isolation probability $\bar{p}_{ISO}$ under RSF with $\alpha = 4$, varying MAP p, modulation order M and sector angle ϕ.

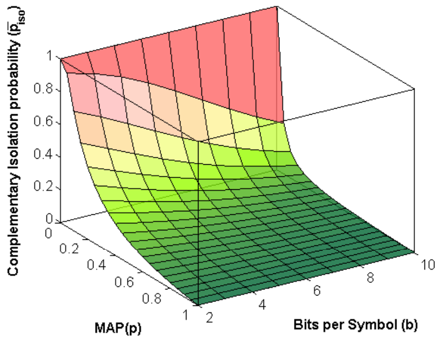

(c) Complementary isolation probability $\bar{p}_{ISO}$ under MFA with $\alpha = 4$, varying MAP p and modulation order M.

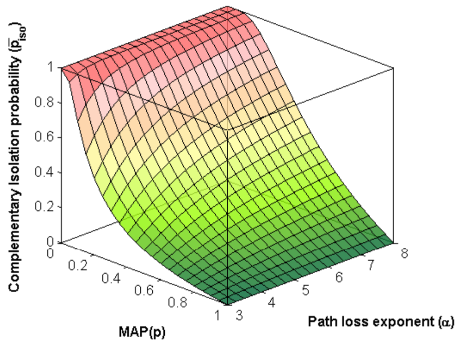

(d) Complementary isolation probability $\bar{p}_{ISO}$ under GLB employing BPSK with varying MAP p and path-loss exponent α.

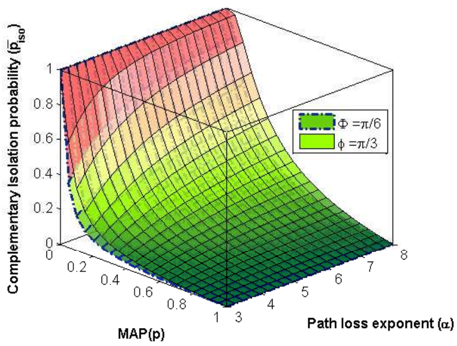

(e) Complementary isolation probability $\bar{p}_{ISO}$ under RSF employing BPSK with varying MAP p, path-loss exponent α and sector angle ϕ.

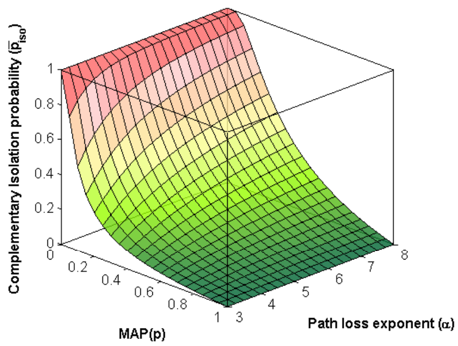

(f) Complementary isolation probability $\bar{p}_{ISO}$ under MFA employing BPSK with varying MAP p and path-loss exponent α.

Figure 8.6: Complementary isolation probability $\bar{p}_{ISO}$ with desired threshold BER $P_b^{th} = 10^{-3}$ (see eq. (8.26)).

which $\bar{p}_{ISO}$ decreases is higher in case of RSF and MFA as compared to GLB.

- The complementary isolation probability $\bar{p}_{ISO}$ increases with an increase in the path loss exponent. This trend is evident from figs. 8.6d, 8.6e and 8.6f. At the first appearance, this may seem counter intuitive. However, the higher the value of path-loss exponent, the faster is the signal decay. This indeed implies that under a high path-loss exponent, interference encountered at typical receiver decreases. Consequently, $\bar{p}_{ISO}$ increases with an increase in the path loss exponent for a fixed modulation scheme and MAP.
- Lastly, in the case of RSF, the complementary isolation probability $\bar{p}^{RSF}_{ISO}$ decreases with a decrease in the central angle of the forwarding area ϕ (see figs. 8.6b and 8.6e). Intuitively, a decrease in ϕ corresponds to an increase in the directionality of communication. In other words, it is very difficult for a transmitter to find a relay which can decode its transmission in a very small region. Hence, the geometry of forwarding region is also critical in shaping the connectivity and EE of an ad hoc network.

Average number of hops.

Lemma 8.3 *In an interference limited large scale ad hoc network , the average number of hops h^j required by a typical transmitter $y \in \Phi_{TX}$ to communicate with its intended destination x^y_{des} located at a distance r_{SD} can be quantified as,*

$$\begin{aligned} h^j &= \mathbb{E}(\#\ of\ hops) \approx \frac{r_{SD}}{\mathbb{E}(\zeta)}, \\ &= \frac{r_{SD}}{\int_{\mathbb{R}^+}(1-\mathcal{F}^j_\zeta(r))dr}, \end{aligned} \tag{8.27}$$

where $j \in \{GLB, MFA, RSF\}$.

PROOF: Assume that a destination located at a distance r_{SD} from the probe transmitter can be reached in $\bar{h}$ hops, then

$$\sum_{i=1}^{\bar{h}} \zeta_i \geq r_{SD}. \tag{8.28}$$

For GLB and RSF $\zeta_1, \zeta_2, \zeta_3, ..., \zeta_{\bar{h}}$ are i.i.d random variables with mean $\mathbb{E}(\zeta)$. Let us define another stochastic process Ξ such that,

$$\Xi_i = \sum_{t=1}^{i} \zeta_t - i\mathbb{E}(\zeta), \tag{8.29}$$

The stochastic process $\Xi_1, \Xi_2, \Xi_3, ..., \Xi_{\bar{h}}$ actually represents stopped random walk with $\mathbb{E}(\Xi) = 0$ [183]. Using eq. (8.29),

$$\Xi_{\bar{h}} = \sum_{t=1}^{\bar{h}} \zeta_t - \bar{h}\mathbb{E}(\zeta),$$

Taking expectation on both sides,

$$\mathbb{E}(\Xi_{\bar{h}}) = \mathbb{E}\left(\sum_{t=1}^{\bar{h}} \zeta_t\right) - \mathbb{E}\left(\bar{h}\right)\mathbb{E}(\zeta),$$

$$\mathbb{E}(\bar{h}) = \frac{\mathbb{E}\left(\sum_{t=1}^{\bar{h}} \zeta_t\right)}{\mathbb{E}(\zeta)}. \tag{8.30}$$

Using the lower bound on $\mathbb{E}\left(\sum_{t=1}^{\bar{h}} \zeta_t\right)$ from eq. (8.28) ,

$$h = \mathbb{E}(\bar{h}) \approx \frac{r_{SD}}{\mathbb{E}(\zeta)}. \tag{8.31}$$

The expectation $\mathbb{E}(\zeta)$ for GLB and RSF can be quantified as discussed in eq. (8.25). In the case of MFA, as discussed earlier, progress in each hop depends on the prior progress. In [184], the authors introduced the notion of negative quadrant dependence (NQD) of random variables. More specifically, two random variables ζ_i and ζ_j are considered NQD iff,

$$\Pr\left\{\zeta_i \geq r_1, \zeta_j \geq r_2\right\} = \Pr\left\{\zeta_i \geq r_1\right\}\Pr\left\{\zeta_j \geq r_2\right\}. \tag{8.32}$$

It can be easily shown that under MFA ζ_i and ζ_j satisfy this definition and hence are NQD random variables. Applying the strong law of large numbers (SLLN) for NQD random variables [184],

$$h \approx \frac{r_{SD}}{\mathbb{E}(\zeta)}. \tag{8.33}$$

□

Claim 2: *Assuming all other parameters are fixed, the average number of hops required by an arbitrary transmitter $y \in \Phi_{TX}$ to communicate with its destination located at a distance r_{SD} increases with an increase in the number of users (λ) in an ad hoc network.*

PROOF: For instance, consider the average number of hops required by the probe transmitter to reach its destination under GLB;

$$h = \frac{r_{SD}}{\underbrace{\int_0^\infty \left(1 - \exp\left(-\frac{(1-p)}{p}\frac{\sin(\delta)}{\delta\beta^{\frac{\delta}{\pi}}}\exp\left(-\frac{\lambda p b_d \beta^{\frac{\delta}{\pi}}\delta}{\sin(\delta)}r^d\right)\right)\right)dr}_{A_1}}. \tag{8.34}$$

The integral in denominator A_1 represents the expected forward progr-ess; it decreases with an increasing λ. Consequently, the average number of hops required to communicate with destination increases with increase in λ. □

Remarks on Claim 2:

Again, the conclusion of Claim 2 is *contrary to what has been reported in past studies* [70, 71, 142, 145, 150]. As discussed earlier, in an interference limited ad hoc network, an increase in the number of users λ will result in a corresponding increase in the interference. Due to this *increased interference, progress can only be made in large number of short hops.* Notice that the number of relays per transmitter can not increase unbounded, while keeping the number of transmitters fixed. Hence, the claim that increasing number of relays will decrease the number of hops is not valid for any positive fixed MAP p. Increasing number of relays per transmitter by decreasing the MAP comes at the cost of an increased energy consumption and decreased spatial reuse of the spectrum. Care must be exercised while making any design conclusion for the large scale wireless ad hoc networks; a simple idealistic model may lead to wrong design conclusions. Fig. 8.7b vouches the Claim 2, considering variations in user density (λ) and transmitter-destination separations (r_{SD}). For a very dense network the average hop count is of the order of hundreds (fig. 8.7b), mainly due to the high amount of interference experienced at relays. *Interference forms an ultimate bottleneck* on the performance of dense multihop networks, as increased number of hops correspond to increased latency, decreased probability of successful packet delivery, lower throughput, unreliable connections and increased energy consumption.

Fig. 8.7a depicts the impact of the modulation scheme and forwarding strategy on the average number of hops (h) required to connect an arbitrary transmitter with its intended destination. Notice that both analytical and simulation results closely match each other. In the best case scenario (GLB), the numeric value of the average number of hops required to connect a transmitter-destination pair is typically less than their separation distance under BPSK and 16−QAM modulation. This clearly reflects that the *number of hops* required to connect a *transmitter and its destination* depends on *the desired QoS.* As in our previous discussion, the average forward progress under MFA and RSF based GR is lesser than GLB. Hence, h^{RSF} and h^{MFA} typically assume

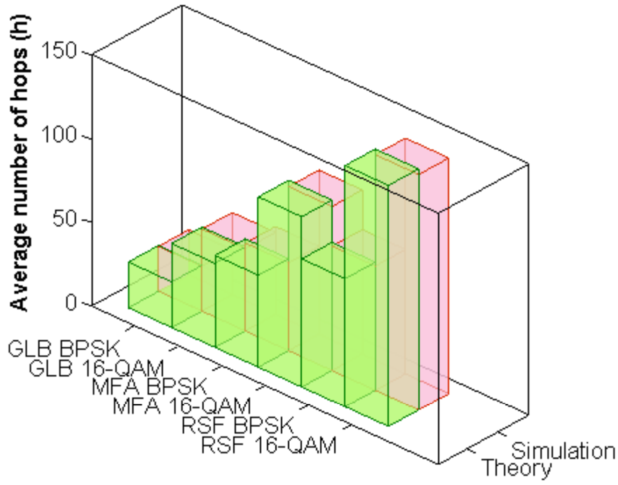

(a) Impact of varying β on average number of hops h required for a typical transmitter to reach its destination at distance $r_{SD} = 50$ with $p = 0.5$, $\alpha = 4$, $\phi = \frac{2\pi}{3}$ and $\lambda = 3 \times 10^{-3}$.

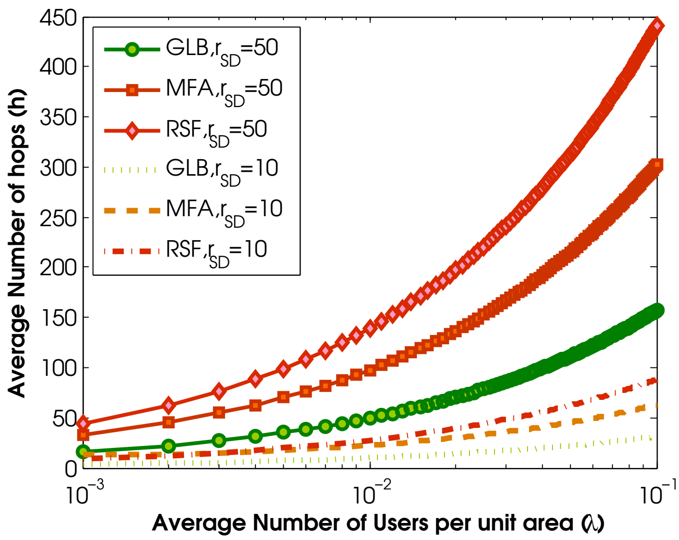

(b) Impact of varying λ on average number of hops h required for a typical transmitter to reach its destination at distance $r_{SD} = 10, 50$ with $\alpha = 4$,$\phi = \frac{2\pi}{3}$ and $p = 0.5$ for BPSK/QPSK/4-QAM.

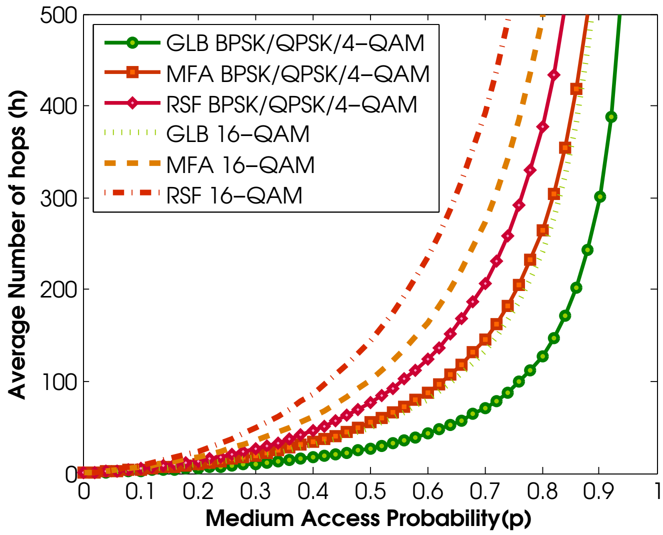

(c) Impact of varying p on average number of hops h required for a typical transmitter to reach its destination at distance $r_{SD} = 50$ with $\alpha = 4$, $\phi = \frac{2\pi}{3}$ and $\lambda = 3 \times 10^{-3}$.

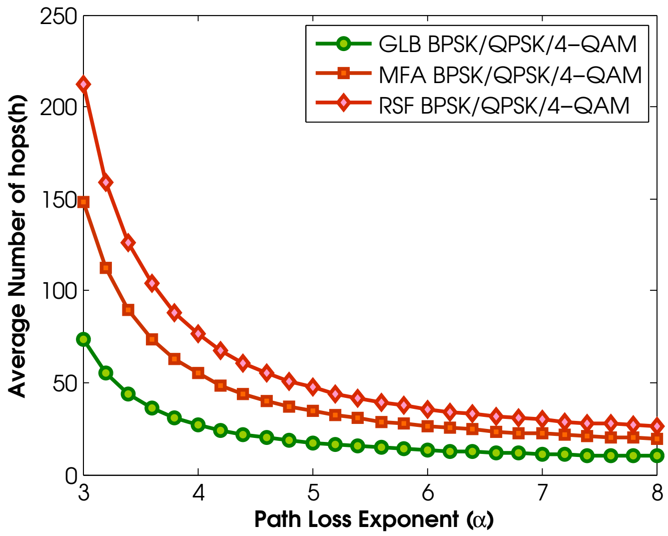

(d) Impact of varying α on average number of hops h required for a typical transmitter to reach its destination at distance $r_{SD} = 50$ with $p = 0.5$, $\phi = \frac{2\pi}{3}$ and $\lambda = 3 \times 10^{-3}$.

Figure 8.7: Impact of parametric variations on hop count in large scale interference limited ad hoc network (See eq. (8.27)).

high values as compared to h^{GLB} for same separation distance. The average number of hops required to connect an arbitrary transmitter with its destination may become *infinite* for a very high QoS requirement. This indeed reflects that at such QoS requirements, *it is impossible to find a connecting path* between the source and destination, mainly due to non-zero interference and channel impairment process.

Fig. 8.8c depicts that h *increases with increasing* MAP p. This is intuitive as increasing p corresponds to *increase in average number of transmitters per unit area and a decrease in the average number of receivers* per unit area. In other words, an increase in p corresponds to a decrease in the average forwarding node degree. Simultaneously, an increase in p results in the *reduction of the typical hop length due to the increased interference.* Note that for $p = 1$, the number of hops required to communicate with the destination become unbounded due to the interference. Fig. 8.8d depicts that h *decreases with increase in the path-loss exponent* α. As discussed earlier, an increase in α might reduces the link distance, but it reduces the interference as well. Hence, the increase in α can be helpful in terms of the number of hops required for communication. Unfortunately, α is not in the system designers control and depends on the environment in which the network is deployed.

EE for a large scale ad-hoc network

Theorem 8.1 *Consider an ad hoc wireless network, where the medium is shared by transmitters forming a HPPP* Φ_{TX}. *In such an ad hoc network,* λp *transmission sessions originate in a given S-ALOHA time slot. Each session requires* h^j *hops before it terminates at a destination located at a distance* r_{SD} *from a typical transmitter. Each packet is relayed by an arbitrary receiver in* Φ_{RX} *iff they satisfy certain QoS and routing constraints (Section V-B). Then the EE (bits/Joule) of such a large scale interference limited ad hoc network is given by,*

$$\eta_{EE}^j = \frac{B \log_2 M \bar{p}_{ISO}^{h^j}}{\left[\left\{P_{TX} + \left(\frac{1-p}{p}\right) P_{RX}\right\}\left(1 + \frac{n_H}{n_D}\right) + \rho\right] h^j} \frac{bits}{J} \tag{8.35}$$

where, $j \in \{GLB, MFA, RSF\}$ *and* ρ *accounts for the energy consumption due to switching from transmit to receive mode. It can be quantified as,*

$$\rho = \frac{4(1-p) B \log_2 M P_{RFPLL} T_{tr}}{n_D}.$$

PROOF: The average transmit energy consumption (E_{TX}) per unit area in a typical S-ALOHA time slot can be computed using eq. (8.3) as,

$$E_{TX} = \lambda p P_{TX} T_{slot}, \tag{8.36}$$

Similarly, the average receive energy consumed per unit area can be evaluated with the help of eq. (8.4),

$$E_{RX} = \lambda(1-p)P_{RX}T_{slot}, \tag{8.37}$$

An additional energy cost is incurred due to switching from the transmit to receive mode and vice versa,

$$E_{SW} = 4\lambda p(1-p)P_{RFPLL}T_{tr} \tag{8.38}$$

where T_{tr} is the transient time for phased lock loop (PLL). Notice that we have approximated the switching energy by only considering the dominant energy consumer involved in the process [131]. In practice, shifting from one mode to another might incur additional costs due to switching of other components besides the RF PLL. The average energy consumption per unit area of the network in a h^j hop transmission session is given by,

$$E_{TOTAL} = h^j(E_{RX} + E_{TX} + E_{SW})\ \frac{J}{m^2}. \tag{8.39}$$

Considering that $M-$ary modulation is employed by each transmitter, then

$$T_{slot} = \frac{(n_D + n_H)T_{sym}}{\log_2 M} = \frac{n_D + n_H}{B\log_2(M)}, \tag{8.40}$$

$$\begin{aligned} E_{TOTAL} &= \left[\lambda p \left\{P_{TX} + \left(\frac{1-p}{p}\right) P_{RX}\right\} \frac{(n_D + n_H)}{B\log_2 M}\right. \\ &+ \left. 4\,(1-p)\,P_{RFPLL}T_{tr}\right] h^j\ \frac{J}{m^2}. \end{aligned} \tag{8.41}$$

The total number of traffic sessions originating at a given snapshot of network is λp. The probability that each session can successfully terminate at a desired destination r_{SD} away in h^j hops is $\bar{p}^{h^j}_{ISO}$. Since each traffic session contributes n_D bits of useful information the total successful throughput of the network in h^j hops is given by

$$C_{TOTAL} = \lambda p \bar{p}^{h^j}_{ISO} n_D\ \frac{J}{m^2}. \tag{8.42}$$

Consequently, the EE in successful bits per joule of large scale interference limited ad hoc network can be quantified from eq. (8.42) and (8.41)

$$\begin{aligned} \eta^j_{EE} &= \frac{E_{TOTAL}}{C_{TOTAL}}\ \frac{bits}{J}, \\ &= \frac{B\log_2 M \bar{p}^{h^j}_{ISO}}{\left[\left\{P_{TX} + \left(\frac{1-p}{p}\right) P_{RX}\right\}\left(1 + \frac{n_H}{n_D}\right) + \rho\right] h^j}\ \frac{bits}{J}. \end{aligned} \tag{8.43}$$

□

Discussion on Theorem 1:
The definition of EE formulated in Theorem 1 captures several key aspects of a large scale ad hoc wireless network. For instance, the ratio of the number of header bits n_H to the number of data bits n_D in a packet quantifies the overhead incurred per packet. This additional overhead will increase the energy consumption at both transmitter and its associated receiver. The factor $\left(1 + \frac{n_H}{n_D}\right)$ in the denominator of eq. (8.35) captures this energy consumption due to overhead. Another interesting observation from eq. (8.35) follows by noticing the factor $\left(\frac{1-p}{p}\right) P_{RX}$. This term reflects that for each transmission the power consumption contributed by the receivers is proportional to the average forwarding node degree. Hence the formulation of the EE in eq. (8.35) inherently addresses several performance determinants.

From eq. (8.35) it is obvious that the EE of the network *decreases* with an *increase* in the average number of hops h^j. As discussed earlier, the average number of hops h^j is in turn coupled with the *transmitter-destination separation* r_{SD}, *MAP* p, *forwarding area for relay selection* (through κ), *number of users* λ, *modulation order* M (through β) and *path-loss exponent* α. The EE also *decreases* with a *decrease* in the complementary isolation probability $\bar{p}_{ISO}$. As per our previous discussion, the complementary isolation probability $\bar{p}_{ISO}$ of a node can be completely characterized by the same parameters which influence h^j, except for the user density λ (see Claim 1). Unfortunately, none of these parameters are in the system designer's control with an exception of λ, p ,ϕ and M.

a) Impact of ϕ on the EE of an Interference Limited Network: Increasing ϕ will *increase* the complementary isolation probability $\bar{p}_{ISO}$ of a typical node when RSF based GR is employed. In effect, it may potentially *increase* the EE of the network. However, care must be taken before drawing any final conclusion. Notice that we consider the best case scenario for RSF, i.e., the maximum forward progress $r\cos(\theta)$ can be approximated with r. This assumption implies that $\cos(\theta) \approx 1$. This holds when ϕ is small. In short, by *increasing* ϕ, the *directionality of the transmission* is lost and the transmission is forced to go through a longer routes (the average number of hops (h) increases). The additional cost of transmission/reception due to a longer route may *offset the energy gain obtained by increasing* ϕ. Moreover, in practice it might deteriorate the performance of network. The longer the packet is routed in the network, the greater is the chance that it will hit a void and hence all energy spent in the transmission is wasted.

b) Impact of the User density λ on EE : *Decreasing* the user density λ will *reduce* the interference in the network. As discussed before, it will *increase* the average forward progress and hence *decrease* the h. However, it does not affect the complementary isolation probability $\bar{p}_{ISO}$. Thus admission control or any other method of reducing the number of users (λ) can be useful. In-

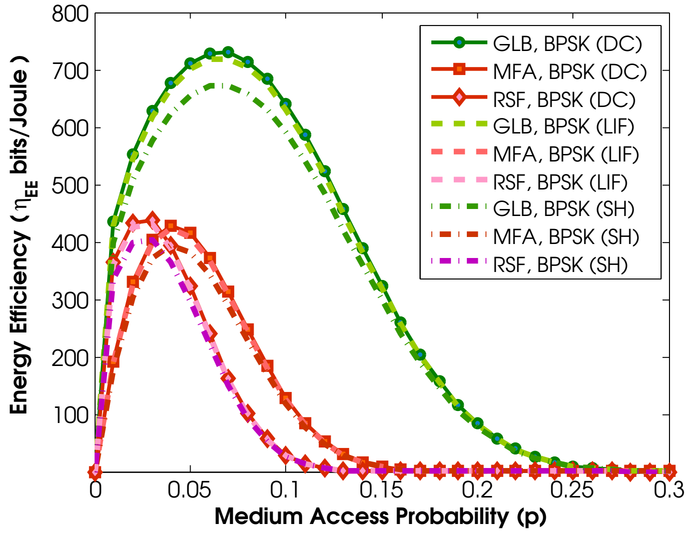

(a) Energy Efficiency of an ad hoc network with varying p, where $r_{SD} = 50$, $\phi = \frac{2\pi}{3}$, $\lambda = 3 \times 10^{-3}$, $P_b^{th} = 10^{-3}$and $\alpha = 4$ (see eq.(8.35)).

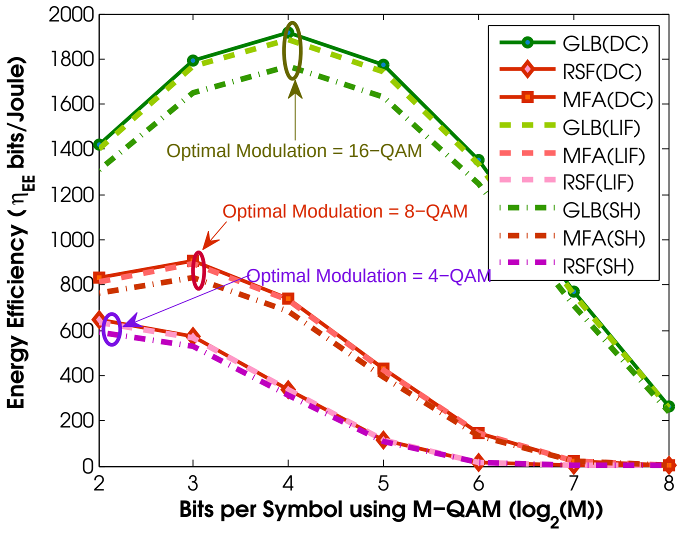

(b) Energy Efficiency of an ad hoc network with varying M, where $r_{SD} = 50$, $\phi = \frac{2\pi}{3}$, $\lambda = 3 \times 10^{-3}$,$p = 5 \times 10^{-1}$and $\alpha = 4$ (see eq.(8.35)).

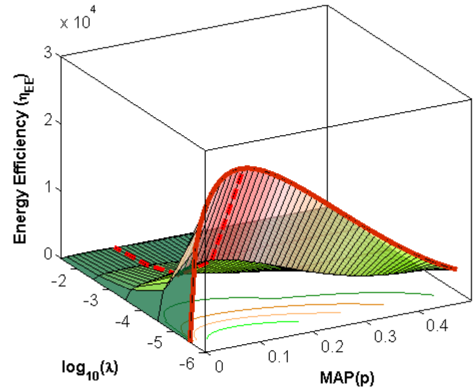

(c) Impact of varying p and λ on the best case (GLB) EE of an ad hoc network with DC/ZIF transceivers, $r_{SD} = 50$, $P_b^{th} = 10^{-3}$and $\alpha = 4$ (see eq.(8.35)).

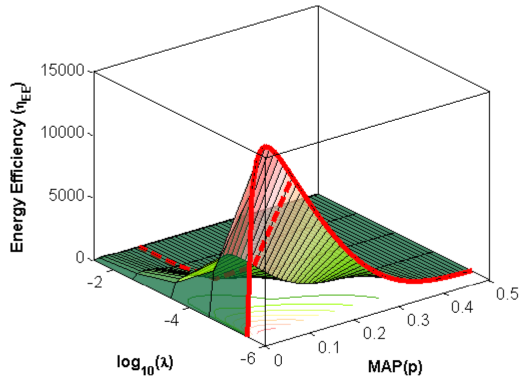

(d) EE considering ad hoc network employing DC/ZIF transceivers and RSF based GR with varying p and λ, $r_{SD} = 50$, $P_b^{th} = 10^{-3}$and $\alpha = 4$ (see eq.(8.35)).

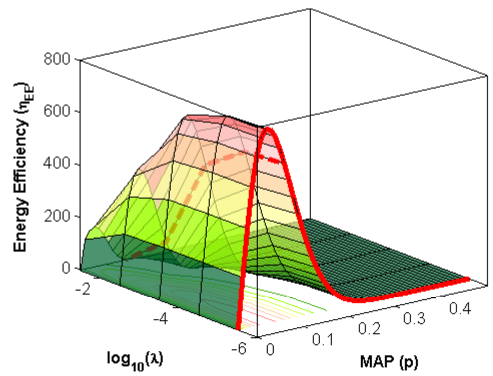

(e) EE considering ad hoc network with DC/ZIF transceivers and MFA based GR with varying p and λ, $r_{SD} = 50$, $P_b^{th} = 10^{-3}$and $\alpha = 4$ (see eq.(8.35)).

Figure 8.8: Energy Efficiency of a large scale interference limited ad hoc wireless network.

terference reduction is a compelling alternative to user density control. This requires the application of intelligent signal processing and networking algorithms. We will briefly discuss a few potential approaches to accomplish interference mitigation in Section VI.

Figs. 8.9c,8.9d and 8.9e depict the impact of decreasing λ on the EE of a large scale ad hoc network. Notice that the number of successful bits transmitted per joule increases with a decrease in λ. However, the rate at which the EE increases depends on a particular forwarding scheme. In particular, the scaling behavior of the EE for RSF and MFA is slightly different when subjected to a similar decrease in the user density λ. For dense wireless (high λ) ad hoc networks, MFA performs better than RSF in terms of EE. Nevertheless, for sparse networks RSF is significantly better than MFA.

c) Impact of Modulation order M ***on EE :*** *Decreasing* the modulation order M will *decrease* the number of hops h required for communication with destination. However, it also *reduces* the EE by decreasing the $\log_2 M$ factor in (8.35). The average number of hops h, the complementary isolation probability $\bar{p}_{ISO}$ and amplifier efficiency α_{amp} (Section IV) are all functions of M. For M-QAM, amplifier efficiency ($\alpha_{amp} = 3\frac{\sqrt{M}-1}{\sqrt{M}+1}$ [130, 131]) decreases with an increase in M . In other words, transmit energy consumption *increases* with *increase* in M. Hence, the relationship of M with EE is not straightforward. It can be shown that there exists an optimal M which will maximize the EE of an interference limited network. Nevertheless, this optimal value of M only exists for a very small MAP p. This optimal value of M is different for different forwarding strategies and is independent of the transceiver architecture. Fig. 8.8b corroborates these arguments by simulating (8.35). Note that the MAP p in fig. 8.8b is quite small. It can be easily shown that even for $p = 0.1$, there does not exist any optimal $M > 2$. Indeed, BPSK becomes an optimal choice for any MAP $p \geq 0.1$. In summary, the *widely prevalent hypothesis* [130, 131] that *there exists an optimal* M which maximizes the EE is *only valid for interference free* networks (i.e., very small MAP p) and breaks down as soon as interference is considered. Perhaps it should also be highlighted that for fixed P_b^{th}, an increase in M reflects increasing QoS requirement. As discussed before, it may not be possible to meet the high QoS in the presence of non-zero interference. Consequently, for high QoS requirement, QoS voids are very frequent which result in zero forward progress with infinite energy expense (EE is zero, see fig 8.8b).

d) Impact of MAP p ***on EE :*** *Decreasing* MAP p *increases* EE by *decreasing* h and *increasing* $\bar{p}_{ISO}$. However, reduction in p *increases* the average forwarding node degree $\frac{1-p}{p}$. Such an increase in the average forwarding node degree implies that most of the nodes will deplete their energy in the *listening* mode. Consequently, there exists an optimal value of p for which the EE of the network is maximized. Fig. 8.8a shows the EE of network with GLB, MFA and RSF against varying p. An optimal value of p depends on the forwarding strategy and is independent of the transceiver architecture. This implies that the MAP p is a cross layer parameter and in order to maximize the overall EE of the network, MAP p should be selected in conjunction with the routing strategy.

The optimal value of p lies near 0.1 or even below for a fixed user density $\lambda = 3 \times 10^{-3}$. Notice that the optimal MAP (say p^*_{op}) depends on the user density λ. Higher values of p^*_{op} can be obtained by *decreasing* λ or equivalently by *mitigating the co-channel interference.* Figs. 8.9c ,8.9d and 8.9e depict the optimal value of p for varying user density λ.

At this juncture, we should highlight that the selection of an optimal MAP p^*_{op} may only be optimal considering the EE of interference limited network. Other important parameters which can not be neglected while optimizing p are the network connectivity and average forward progress. We are interested in the question that whether a particular choice of p is optimal in terms of all parameters, i.e., it maximizes the average progress ζ, minimizes the complementary isolation probability $\bar{p}_{ISO}$ and also maximizes the EE of the network. The optimum MAP p^*_ϵ is the MAP which ensures that the probability of isolation p_{ISO} for a typical transmitter is less than ϵ. From 8.26,

$$p^*_\epsilon = \frac{\sin(\delta)\kappa_1^j}{\kappa_1^j \sin(\delta) - \delta\beta^{\frac{\delta}{\pi}} \ln(\epsilon)}. \tag{8.44}$$

Fig. 8.9a depicts the $\epsilon-$optimal MAP with varying modulation order M. This further consolidates our argument, i.e., optimal MAP is a cross layer parameter which depends on both physical layer parameters such as modulation order M and routing mechanism (see 8.9a). Also note that the value of $\epsilon-$optimal MAP p^*_ϵ in fig. 8.9a is of the same order as of the MAP which optimizes the EE p^*_{op}. Fig. 8.9b depicts average forward progress with varying MAP p. It is clear from 8.9b that the MAP which maximizes the average forward progress is also of the same order as p^*_ϵ and p^*_{op}. In summary, optimizing the MAP p to attain ϵ-isolation probability or to maximize forward progress will also result in a network with good EE performance.

d) Impact of Transceiver Architecture & Sleep Scheduling on EE: Fig. 8.8a shows the overall EE of the network where users employ one of the three different transceiver architectures introduced in Section III. Due to the low power consumption, the DC/ZIF architecture is more energy efficient than LIF and the traditional SH transceiver. Consequently, the DC transceiver can support a successful transmission of approximately 100 additional bits per joule as compared to the SH transceiver at p^*_{op}. The LIF transceiver consumes more power than a DC transceiver. However, its power consumption is lesser than that of a SH transceiver. Resultantly, the LIF transceiver provides a comparable performance to the DC transceiver. From fig. 8.8a, it is obvious that the power consumption of the underlying transceiver architecture plays an important role in shaping the overall EE of the network.

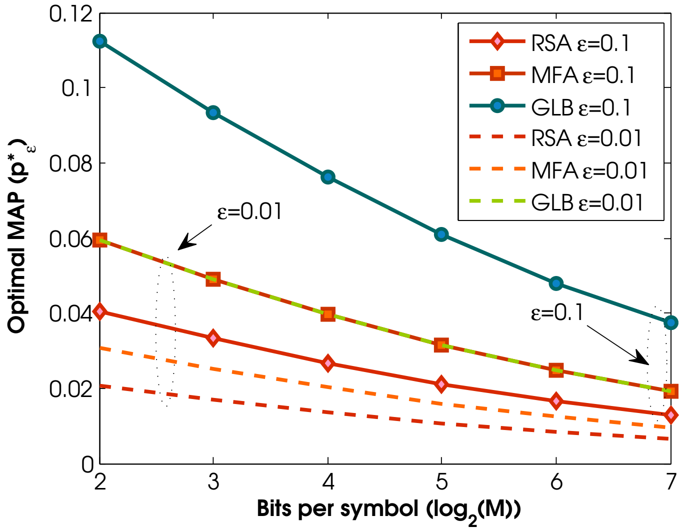

(a) ϵ-optimal MAP p^*_{op} with varying M-QAM modulation and ϵ with $\alpha = 4$(See eq.(8.44)).

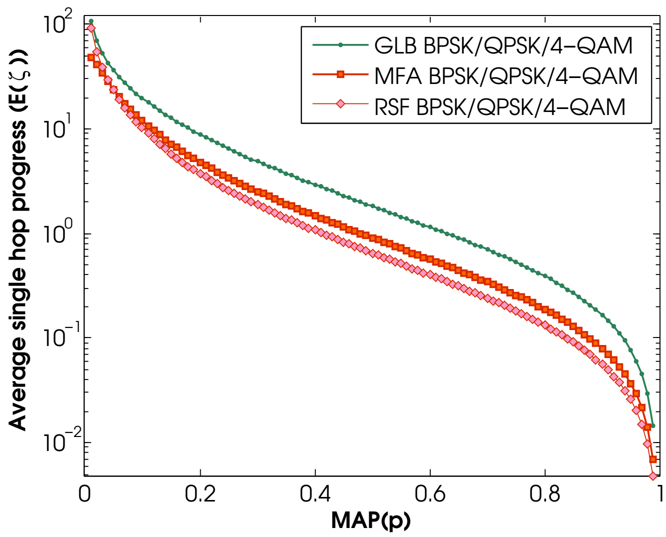

(b) Average single hop forward progress with varying MAP p, with $r_{SD} = 50$,$\alpha = 4$, $\phi = \frac{2\pi}{3}$,$P_b^{th} = 10^{-3}$ and $\lambda = 3 \times 10^{-3}$(See eq.(8.25)).

Figure 8.9: Optimal MAP p considering network connectivity and average progress.

Hence, optimization of hardware to ensure low power operation can bring significant gains in terms of network EE.

Sleep scheduling, is often employed to reduce energy consumption in wireless networks. The key idea behind sleep scheduling is to reduce energy consumption by idle listening [140]. However, in large scale interference limited wireless networks, sleep scheduling will reduce the density of relays. Consequently, it may further deteriorate the EE of the network. From a practical perspective, it is difficult to implement sleep scheduling for S-ALOHA or CSMA/CA type protocols.

8.7 CONCLUSIONS

In this chapter, we quantified the EE of a large scale interference limited ad hoc wireless network by considering three bottom layers of the OSI protocol stack. Utilizing the techniques from stochastic geometry, we modified traditional GR to accommodate the user's QoS constraints. We quantified the average single hop forward progress, node isolation probability and the average number of hops required to connect an arbitrary transmitter to its destination. We employed these statistics to quantify the overall EE of the large scale ad hoc network. Our quantification explicitly addresses the geometry of forwarding areas, co-channel interference, spatial configuration of nodes and the channel impairment process. Moreover, we also considered the power consumption of the user's communication hardware by considering three different transceiver architectures.

Part IV

CONCLUSION AND FUTURE WORK

9

CONCLUSION & FUTURE WORK

9.1 SUMMARY

In this thesis, we developed a stochastic geometric models for characterizing the aggregate interference in the large scale cognitive radio network (CRN). We demonstrated that the operational environment for both the primary and the secondary user's is determined by the co-channel interference. In turn, co-channel interference is function of several link and node level dynamics. The aggregate interference is performance bottleneck from both spectral and energy efficiency perspective. Consequently, the network and protocol operations should be engineered to shape the interference environment such that deployment can attain maximum spectral efficiency at the cost of minimum energy expense. Thus in the light of current thesis, we argue that cognition has a broader meaning than usual interpretation. Effectively, cognition is a way forward to enable intelligent co-existence for efficient utilization of infinitely renewable spectrum.

In their basic form dynamic spectrum access (DSA) algorithms provisioned by employing cognitive radios (CRs) are essentially co-existence mecahnisms. The secondary or CR users must implement co-existence mechanism in terms of interference control, avoidance and/or coordination with the legacy users.

In chapter 2, we investigated the DSA paradigm where spectrum sharing is provisioned by introducing a spatial no-talk zone for controlling the aggregate interference. We computed the minimum radius of the guard-zone which is required to ensure that the primary user's link success probability (SP) remains above its desired threshold. It was shown that the radius of the no-talk region: (i) reduces with the a reduction in the isolation probability threshold mainly due to a reduction in the medium access probability (MAP); (ii) decreases with an increase in the directionality of the forwarding protocol; (iii) increases with an increase in secondary user density. Since multihop transmission in large scale CRNs are highly directional towards the intended destination, the required radius of guard-zone at primary receiver may be very small. This indeed implies that increasing the directionality of transmission in the employed packet forwarding mechanism and a small MAP provides CRs with huge spatial foot-print which can be treated as a white-space. However, the spatial white-space comes at the cost of low duty cycle, which is due to employing a lower value of MAP. Hence temporal white-space is traded for spatial white-space. A key design insight from such temporal vs. spatial tradeoff is that the aggregate interference can be managed using multiple dimensions. As a matter of the fact more effective scheme should distribute the aggregate interference across these dimensions in an optimal manner. The definition of 'optimal' in current context is optimal in the sense of spectral efficiency.

While implementing, the guard-zone based interference protection is straightforward for a large scale CRN co-existing with a single PU link, this is not the case in the presence of multiple active PU links. With multiplicity in PU links, CRs are effectively required to track whether they are inside or outside such no-talk zones. This translates the interfernece control problem into the interference avoidance issue. In such a case, it is natural to explore other dimensions (besides spatial dimension) which can be exploited to provision the interference control. As noted in the previous discussion, one such dimension is MAP. In chapter 3, we studied the spatial throughput of the multi-antenna multi-hop CRN under MAP adaptation. A QoS aware routing was proposed for relaying the data from the CR source to its intended destination. MIMO MRC and MRT were employed on hop-by-hop basis. It was shown that there exists an optimal MAP which maximizes the spatial throughput of the secondary network. However, this MAP may lie beyond the permissible operational regime enforced by the primary network. The optimal MAP is strongly coupled with the number of antennas employed by the secondary user. It was also shown that multiple antennas result in a win-win situation for both the primary and the secondary users.

The existence of the optimal MAP motivated us to inspect the design space of the cognitive underlay networks in more comprehensive manner. It was shown that there exists another degree of freedom, i.e., the transmit power which can be employed to extend the operational regime. The so called adapt-and-optimize strategy was proven to be optimal for all the considered networking paradigms. Several interesting properties of the optimal operating points were studied (see chapter 4).

Departing from the interference control, the second part of this thesis focused on interference avoidance strategies for co-existence between the primary and the secondary users.In chapter D, we investigated analyzed the performance of the primary link in the presence of the co-channel interference from the mis-detecting CRN. The key results can be summarized as follows:

- In TX based sensing, CR transmitters perform spectrum sensing using a MF or an ED. Based on the inference drawn from the spectrum sensing process, the CR TXs transmit with a probability p or defer their transmission with a probability $(1 - p)$. In such a scenario,
  - An increase in the secondary user density (λ_s^{TX}) or equivalently an increase in the MAP (p) increases the OP of the primary link or equivalently decreases the primary's throughput and ergodic capacity.

  - An increase in the required SIR threshold (γ_p) of the primary which partially reflects the stringent QoS constraint or an increase in the link distance of primary (r_p) results in a higher OP of the primary user.
  - The OP of the primary user decreases with an increase in the beacon channel SNR (γ_b) or with an increase in the ratio of primary's transmit power to the secondary's transmit power (η).
  - The OP of the primary also depends upon its own exclusion region. Interestingly the OP of the primary does not readily decrease with an increase in the radius of the exclusion region until a certain value of r_e. This threshold value of r_e depends upon the path loss exponent α. Beyond the threshold value of r_e the OP of the primary decreases with increase in r_e or equivalently the throughput and ergodic capacity increases.
  - The OP of primary user scales as $O\left(\sqrt{\lambda_s^{TX}}\right)$. In the case of traditional ad hoc networks similar scaling is observed with respect to primary users. This indicates that although spectrum sensing and MAC are employed by the secondary transmitters, they are still capable of causing comparable performance deterioration as caused by interfering primary users which do not employ spectrum sensing.

- In RX based spectrum sensing, CR receivers perform spectrum sensing using a MF or an ED. Since the distance between the primary receiver and the CR TX and the link distance between the CR RX and the primary receiver is not the same, the CR RX can provide superior or inferior detection performance depending on the coefficient of distance variation (c). Hence the CR TX can minimize the outage incurred at the primary receiver by delegating sensing responsibility to the CR RX when spatial configuration of the CR RX is better than the CR TX relative to P_{RX}. We have studied two extreme spatial configurations for the CR RX, i.e., worst and best case configuration. Moreover,
  - The ED is less sensitive to the spatial configuration of the receiver than is the MF in the worst case scenario. This reveals that there exists a trade off between OP performance, complexity of implementation and insensitivity to the spatial configuration of receiver.
  - The MF, which is more sensitive to the spatial configuration, can at worse perform as bad as the ED for certain values of c.

- In TX-RX based spectrum sensing, both the CR TX and RX perform the spectrum sensing. The inferences drawn from the spectrum sensing process are combined using either greedy or content strategy. Furthermore, CR TX and RX may each employ different type of detectors. This results in four possible combination of detectors (MF,MF), (ED,ED), (ED,MF) and (MF, ED).

- In Greedy strategy, if either the CR TX or RX fail to detect the primary's beacon, the CR TX assumes the channel to be free. The greedy strategy is dominated by the worst detector from the CR TX and RX.
- In Content strategy, if both the CR TX and RX fail to detect the beacon, the CR TX assumes the channel to be free. The content strategy is dominated by best detector from the CR TX and RX.

- The throughput of the primary user depends on the OP in a complementary manner. Hence network parameters which may cause an increase in the OP equivalently cause a decrease in throughput. Also there exists a distinct SIR threshold γ_p^* of the primary for which throughput is maximized.
- The ergodic capacity of the primary can be calculated by using the OP function of the primary as distribution of SIR. The ergodic capacity of the primary user decreases with increase in the OP.
- The self-coexistence constraint plays a vital role in characterizing the OP of the primary receiver. Ignoring self-coexistence results in an over-estimation of the outage incurred by the primary user.
- We have shown that there exists an optimal MAP (p_{opt}) for which the primary's desired QoS parameters are always satisfied.

The developed moment matching approach for modeling the distribution of aggregate interference is employed in chapter 6 to study the transmission capacity(TC) of the primary network. It is shown that the TC scales exponentially with the density of the primary network, while the scaling with respect to the secondary network density follows a power-law behavior.

In chapter 7, we revisit the problem of interference modeling for quantifiying the OP of the primary user. A novel upper-bound for near exact characterization of the Laplace transform of the aggregate interference is presented. It is shown that there exists an optimal value of desired SIR threshold and link distance which will maximize the primary user's performance. While we attempted to explore the design space of cognitive interweave networks at its fullest there are still huge technical challenges which can be stated as open issues. We will defer the discussion of these issues untill the next section.

Since the aggregate interference not only characterizes the spectral performance but it also shapes the energy consumption in large scale network, we dedicated third part to explore the relevant issues.In chapter , we developed stochastic geometric model to characterize the energy efficiency of the interference limited ad hoc network. Our results demonstrated that:

- Network interference is the ultimate bottleneck on the energy efficiency performance of a dense wireless ad hoc network.
- An optimal routing protocol should be designed to provide a constant forward progress irrespective of the source-destination separation.
- The user density, routing strategy, modulation scheme and average forwarding node degree are the only degree of freedom which network designer can exploit to maximize (average) single-hop progress.
- The node isolation probability can not be decreased to zero by increasing the number of relays, either by increasing the user density or by decreasing the MAP. As a matter of fact, the node isolation probability is independent of the user density.
- The number of hops required by an arbitrary source to reach its destination increases with an increase in the user density. In other words, in an interference limited network progress can only be made by a large number of small hops.
- Both node isolation and hop count are relative to the desired QoS.
- The EE of the network can be increased by mitigating interference or by implementing user density control.
- There exists an optimal MAP which maximizes the energy efficiency of the large scale ad hoc network. This MAP is cross-layer parameter and depends on both the routing and the modulation schemes.
- The MAP which maximizes the energy efficiency, also minimizes the node isolation probability and maximizes the average forward progress.
- There may not exist any $M > 2$ (for an $M-$ary modulation scheme) which will maximize the energy efficiency of the network. In such a case BPSK is always optimal.
- The communication hardware platform of user's can be optimized to realize large gains in terms of energy efficiency.

The key take-away from this thesis is that in order to optimize either the energy or the spectral efficiency, interference environment should be shaped using the avialable degree of freedoms in an optimal manner.

9.2 FUTURE WORK

Lastly, we would like to summarize some of the promising research directions which have been identified as the result of this study.

9.2.1 *Guard-zone Empowered Interference Control*

In light of the aforementioned conclusions, it is obvious that secondary users should employ a very low MAP which inturn will result in small guard-zone for the primary and more spatial white-space for the secondary users. If the secondary network is deployed in a finite area, reduction in the radius of the guard-zone implies that more secondary users can be accomodated. However, notice that the reduction in radius is obtained at the cost of lower MAP, i.e. reduction in the density of the active users. Furthermore, the density of the active transmitters dictates the network wide area spectral efficiency. Hence, there exists an optimal MAP which will maximize the area spectral efficiency. This optimal MAP will correspond to the point where gain obtained by recovering more network area will offset the reduction expereinced due to decrease in density. Quantification of this optimal point still remains an open issue.

Another interesting observation from chapter 2 is that the increase in directionality of the forwarding protocol reduces the radius of the guard-zone. We notice that directional antennas can also improve the directionality of the transmission. Hence, we believe that geometric configurations of antenna arrays such as uniform linear array (ULA) or uniform circular array (UCA) can be employed to reduce the radius of the guard-zone. More interestingly, the OP of the primary can be employed as a constraint to design the geometry of the array such that co-existence is guaranteed. While the geometry of the transmit array is constrained, the geometry of the receive array may be exploited to increase the throughput of the secondary network.

Guard-zone empowered interference control is of prime importance in context of emerging small-cell paradigm. The small-cellular networks are envisioned to maximize the spectral performance by aggresive reuse of the Hertzian medium. Such aggresive re-use may require small cells to share the same spectrum as with existing macro base stations. Due to the high transmit power of the macro (specially in the cell center), small cells can only utilize the same spectrum towards the cell edges. This naturally induces a guard-zone on the primary, i.e., macro base station. In this context, the geometry and tilts of antenna array provide a degree of freedom which can be exploited to harness more spatial transmission opportunites. Notice that there is no multi-hop transmission in this context hence directionality can not be tuned by employing routing protocol with highly directional geometry.

9.2.2 *Underlay Networks with MAP and Transmit Power Adaptation*

The future research directions are envisoned to address the following design issues:

1. MIMO MRC and MRT based forwarding requires the potential relays to provide principle eigen-vector as a feedback to the transmitter. In characterizing the performance of the MIMO multihop CRN, we assumed that feedback channel is error free. However, in more practical setup the feedback channel will have propagation errors, delays, quantization noise etc. Hence the framework needs to be extended to quantify the losses due to imperfect channel state information.

2. We also notice that the performance of the MIMO MRC networks can be improved by exploiting multiple antennas at receiver to cancel some of the interference (see [84]). While cancelling interference from primary network may be difficult, CRs can still partially cancel the inter-network interference.

3. Antenna selection can be employed by at CRs as an alternative to the MIMO MRC scheme. The key advantage is that the amount of feedback required will be significantly reduced.

4. As indicated by the chapter 4, performance of the MIMO multi-hop networks can be further improved by adapting the transmission power. Optimal transmission power is expected to be the function of the number of antennas and adopted modulation scheme. Characterization of the optimal power remains an open issue.

Again in the context of the emerging small cellular paradigm, Slotted-ALOHA can be implemented in the frequency domain. Then the problem studied in chapter 3 and 4 can be restated with some modifications into more interesting problem of spectrum sharing between femto and macro cells. Notice that multiple antennas provide an additional degree of freedom which can be exploited for the interference management in such small cellular 5G networks.

9.2.3 *Interference Modeling in Interweave Networks*

9.2.3.1 *Performance Evaluation of the Secondary User*

Taking a step further, we would like to highlight some of the open issues in the domain of statistical characterization of the interference in spectrum sensing CRN. Besides interference, outage, throughput and ergodic capacity of the primary, a CRN designer is also interested in similar metrics for the secondary network. All these metrics require statistical characterization of interference encountered by a secondary receiver. Note that the amount of interference encountered by a CR receiver depends upon its location and hence varies from CR to CR. This is due to the fact that the primary user also causes interference for CRs which mis-detect the presence of the primary. Consequently, the interference experienced at any CR receiver is caused by other CRs transmitting concurrently and also by the primary transmitter. Treatment of both these interferences which are indeed coupled by the spectrum sensing process poses a great challenge and still remains a open issue. We would also like to point out that, some approximations for such a scenario can be made by using the theory of second order intensity re-weighted [60] point processes. The issue of interference characterization becomes further intricate when multiple primary users are also present. So complete characterization of all four interferences, i.e., primary to primary, secondary to secondary, secondary to primary and primary to secondary remains an open issue when both primary and secondary networks exercise multiplicity.

9.2.3.2 *Impact of Threshold Model*

In quantifying the performance of the primary network, the detectors performance curve is often approximated by an indicator function. This because the exact expression for the probability of detection cannot be employed for further analysis. Under such an approximation the aggregate interference is under-estimated as the CRs satisfying the threshold criteria also interfere with a non-zero probability. Hence an alternative route needs to be devised for exact analysis.

9.2.4 *Energy Efficiency in Large Scale Networks*

In the chapter 8, we demonstrated that the EE of a large scale ad hoc network is predominantly limited by interference. The optimal MAP which guarantees maximum EE of the network is quite small. Consequently, the spatial reuse of the spectrum is quite low. A MAP with larger p can be provisioned by *decreasing the user density* or by *mitigating the interference*. There are several intelligent signal processing algorithms which can be employed to attain these objectives. Our work can be extended to study the following viable options:

- Power control: Although power control will reduce the amount of interference, it is difficult to devise a power control algorithm for long hop routing. While it might be feasible to obtain channel state information (CSI) from the nearest neighbor, it is extremely difficult to do the same for the farthest.
- Interference Cancellation: Interference cancellation (IC) can potentially improve the EE of wireless networks. However, the overhead associ-

ated in performing IC may offset the energy gains. It is far from obvious, whether there exists such an operational regime in which IC maximizes the network energy efficiency.

- Interference Alignment: Interference alignment (IA) can also provide large gains in terms of EE. However, the feasibility of IA in random networks with various dynamics is still an open question.
- MIMO communication: MIMO communication such as transmit and receive beamforming will reduce the amount of interference. Consequently, it will improve the EE of the large scale network. However, the number of transceiver radio chains also increases with the number of antennas. In other words, MIMO radio platforms consume more energy than SISO platforms. Whether there exists an optimum number of antennas that maximizes the EE of wireless network is also an open issue.
- CR enabled spectrum sharing: Both the problem of EE and spectrum scarcity originate from the same source, i.e., increase in high bit rate applications. Hence it is intuitive to ask whether CRs can address both aspects. There has been alot of buzz that CRs are key enablers for the green communication. However, we firmly believe that this is an over-statement. CRs require more awarness to manage the aggregate interference. Consequently, a CR platform may spend more energy than traditional radio transceiver. We believe that the only possibility of implementing the EE communication using CRs is by exploiting the inherent geometric randomness. More specifically, CRs can trade their cooperation as a price for inflicting interference. Mutual cooperation across the networks can be studied under game-theoretic framework. We firmly believe that such trading will be the key enablers for CRs to improve the network-wide EE.

Part V

APPENDIX

A

STATISTICAL PRELIMINARIES

A.1 MEASURES

σ- additivity:

Definition A.1 *The property of σ-additivity implies that the volume of the set function on a set that can be divided into countable union of subsets should be equal to the sum of the values of the set function on the subsets.*

σ-algebra:

Definition A.2 *If a system of subsets $\mathcal{X}$ of a ground set X satisfies the following conditions;*

$X \in \mathcal{X}$,

If $A \in \mathcal{X}$ *then* $A^c \in \mathcal{X}$,

If $A_1, A_2, \cdots \in \mathcal{X}$ *then* $\bigcup_{k=1}^{\infty} A_k \in \mathcal{X}$.

Then $\mathcal{X}$ is the σ-algebra of X.

The following properties correspondingly become evident from the above;

$\emptyset \in \mathcal{X}$,

If $A_1, \cdots A_n \in \mathcal{X}$ *then* $A_1 \bigcap \cdots A_n \in \mathcal{X}$, $A_1 \bigcup \cdots \bigcup A_k \in \mathcal{X}$,

If $A, B \in \mathcal{X}$ then $A \backslash B \in \mathcal{X}$.

Astraight forward example of σ-algebra is the power set of X.

Borel Set $\mathcal{B}^d$:

Definition A.3 *The smallest σ-algebra on $\mathbb{R}^d$ that contains all open subsets of $\mathbb{R}^d$ is called the borel set.*

Measurable Space:

Definition A.4 *The set X and its σ-algebra $\mathcal{X}$, together form a measurable space $[X, \mathcal{X}]$.*

A function $f : X \to \mathbb{R}$ is said to be $\mathcal{X}$- measurable if for all Borel sets $B \in \mathcal{B}^1$ the inverse image $f^{-1}(B) = \{x \in X : f(x) \in B\}$ *belongs to the σ-algebra $\mathcal{X}$ associated with X.*

Ball

The d-dim. ball $(d \in \mathbb{N})$ with radius $r \in \mathbb{R}_+$ is:

$$b_d(c, r) \equiv \{x \in \mathbb{R}_d : |x - c \leq r|\},$$

where c is the center of the ball such that $c \in \mathbb{R}_d$.

Lebesgue Measure:

Definition A.5 *It is a way to standardize the length, area and volume of the subsets in Euclidean space. For a family of Borel sets defined in Euclidean space, it is defined over the measure space $[\mathbb{R}^d, \mathcal{B}^d]$ as;*

$v_d(Q) = (v_1 - u_1) \cdots (v_d - u_d)$

where, $Q = [u_1, v_1] \times \ldots \times [u_d, v_d]$.

Lebesgue measure for $d = 1$ corresponds to length, $d = 2$ to area and $d = 3$ to the volume measure.

The d- dimensional ball has the Lebesgue measure

$$b_d(c, r) = c_d r^d$$

where

$$c_d \equiv \begin{cases} \frac{\pi^{d/2}}{(d/2)!} & \text{even } d \\ \frac{1}{d!}\pi^{d-1/2}2^d\left(\frac{d-1}{2}\right)! & \text{odd } d \end{cases}$$

A.2 POISSON POINT PROCESS

General Poisson point process [60]:

Definition A.6 A general Poisson point process Π with intensity measure Λ(diffuse Radon measure) on $\mathbb{R}^2$ is a point process with the following two properties:

1) Poisson distribution of point-counts: the number of points in a bounded region $\mathcal{A} \subseteq \mathbb{R}^2$ follows the Poisson law with mean $\Lambda(\mathcal{A})$. If the Radon measure [60] Λ has density with respect to the Lebesgue measure then it is given by

$$\Lambda(\mathcal{A}) = \int_{\mathcal{A}} \lambda(\boldsymbol{x}) \boldsymbol{dx}. \tag{A.1}$$

where, $\lambda(x)$ is called the intensity function of the general Poisson point process. The General Poisson point process with intensity measure of the form (A.1) is also known as Non-homogeneous Poisson point process (NHPPP). The definition of HPPP (discussed earlier) follows from (A.1) with $\Lambda(\mathcal{A}) = \lambda \int_{\mathcal{A}} \boldsymbol{dx}$.

2) Independent Scattering: the number of points in k disjoint compact subsets of $\mathbb{R}^2$ form k independent random variables.

Void Probability:

Definition A.7 *For a Poisson point process Π containing points $\{x_i\}$,the probability that there are no points in a ball $b_d(o,r)$ given as*

$$\mathbb{P}\left(\Pi(b_d(o,r)) = 0\right) = e^{-\lambda c_d r^d}$$

is called the void probability. Here, c_d is as defined earlier.

Mapping Theorem:

Definition A.8 *Let Φ be an in- homogeneous PPP on $\mathbb{R}_d$ with intensity function Λ, and let $f : \mathbb{R}_d \to \mathbb{R}_s$ be measurable and $\Lambda\left(f^{-1}\{y\}\right) = 0$ for all $y \in \mathbb{R}_s$. Assume further that $\mu(B) = \Lambda(f^{-1}(B))$ satisfies $\mu(B) < \infty$ for all bounded B. Then $f(\Phi)$ is a non-homogeneous PPP on $\mathbb{R}_s$ with intensity measure μ.*

Definition A.9 *Let* Π_1 $=\{x_i\}$ *, be a PPP in* $\mathbb{R}^d$ *of intensity* λ*, and* Π_2 $\{t_i\}$ *, a PPP in* $\mathbb{R}$ *of intensity* 1*. Then:*

Distance Mapping :

$$\lambda c^d \left|x_i\right|^d = 2\left|t_i\right|, \quad i \in \mathbb{N}$$

A.3 THINNED POINT PROCESS

The thinning operation over a HPPP Π uses a definite set of rules to delete certain points of Π. The resulting process $(\Pi_t \subseteq \Pi)$ is known as thinned point process.

p-thinning :

Definition A.10 *A p-thinned Poisson point process $\Pi_t \subseteq \Pi$ on $\mathbb{R}^2$ is constructed by retaining each point of a HPPP (Π) with probability p and deleting it with probability $1 - p$. The retaining operation of a point is independent of the other points and the location of the point.*

It can be easily shown that the p-thinning of a HPPP with intensity λ results in another HPPP with intensity λp.

Position dependent thinning :

Definition A.11 Consider a measurable function $f : \mathbb{R}^2 \rightarrow \mathbb{R}$ and an indicator random variable

$$\mathbb{1}(f(\boldsymbol{x})) = \begin{cases} 1 & f(\boldsymbol{x}) \geq c \\ 0 & f(\boldsymbol{x}) < c \end{cases}, \tag{A.2}$$

where c is an arbitrary constant. Then a position dependent thinning of a HPPP Π is defined as

$$\Pi_t = \{\boldsymbol{x} \in \Pi : \mathbb{1}(f(\boldsymbol{x})) = 1\}. \tag{A.3}$$

The density of a point process resulting from the position dependent thinning of a HPPP is given by $\Lambda(\mathcal{A}) = \lambda \int_{\mathcal{A}} \mathbb{1}(f(\boldsymbol{x}))\boldsymbol{dx}$. The position dependent thinning can also be treated as a Marked Poisson point process (MPPP) (see [60] for details).

Generating functional of HPPP [60] :

Definition A.12 Let $f : \mathbb{R}^2 \to [0, \infty)$ be a measurable function on a HPPP Π, then the probability generating functional (PGFL) of Π is given by

$$\begin{aligned} \mathcal{G}(f) &= \mathbb{E}\left(\prod_{x\in\Pi} f(\boldsymbol{x})\right), \\ &= \exp\left(-\int (1 - f(\boldsymbol{x}))\, \Lambda(\boldsymbol{dx})\right), \end{aligned} \tag{A.4}$$

where, $\mathbb{E}(.)$ represents statistical expectation.

Silvnyak & Mecke Theorem [60] :

Definition A.13 For a HPPP the reduced Palm distribution equals the distribution of HPPP (i.e., $\mathbb{P}^{!o} \equiv \mathbb{P}$). Consequently, if an additional point is introduced at some location x in a HPPP it does not change the distribution of the point process.

Shot Noise process :

Definition A.14 A (sum) SN process is a real-valued random process $\Sigma(x)$, indexed by the continuous parameter $x \in \mathbb{R}_d$, that is a functional of an underlying (stationary) point process = Π_1 =$\{x_i\} \subset \mathbb{R}_d$, where

$$\Sigma^l_\Pi(x) \equiv \Sigma_{i\in\Pi} h_i \left(l\, |x_i - x|\right) \quad x \in \mathbb{R}^d$$

Here $l : \mathbb{R}_+ \to \mathbb{R}_+$ is a linear time-invariant impulse response function and $\{h_i\}$ is a collection of i.i.d. nonnegative RVs.

Stable RV and distribution. :

Definition A.15 *Let $x \sim F$ and$(x_1, ..., x_n)$ be iid from F. Say x is a stable RV (F is a stable distribution) if for each $n \in N$, there exists numbers(a_n, b_n) such that*

$$a_n x + b_n = x_1 + ... + x_n.$$

B

APPENDIX TO CHAPTER 3

CDF OF MAXIMUM EIGENVALUE OF $H^\dagger H$

From (3.9) , the $(i,j)^{th}$ entry of the $\Psi_c(z)$ can be written as

$$\{\Psi_c(z)\}_{i,j} \;=\; (i+j-2)!\left(1-\textstyle\sum_{k=0}^{i+j-2}\frac{\exp(-z)z^k}{k!}\right). \tag{B.1}$$

Taking the derivative of (3.6) and evaluating the determinant, the PDF of the maximum eigenvalue can be written as

$$\begin{aligned} f_{\Lambda_{max}}(x) &= \frac{1}{\left[\prod_{k=1}^{N_p}(N_p-k)!\right]^2}\frac{d}{dx}\det(\Psi_c(x)), \\ &= \frac{\sum_{i=1}^{N_p}\exp(-ix)\sum_{m=0}^{2N_pi-2i^2}a_{i,m}x^m}{\left[\prod_{k=1}^{N_p}(N_p-k)!\right]^2}, \end{aligned} \tag{B.2}$$

where $a_{i,m}$ is the constant coefficient which depends on m and i. Integrating (B.2), we obtain the CDF as

$$\begin{aligned} \mathcal{F}_{\Lambda_{max}}(z) &= \frac{\sum_{i=1}^{N_p}\sum_{m=0}^{2N_pi-2i^2}a_{i,m}\gamma(m+1,iz)}{i^{m+1}\left[\prod_{k=1}^{N_p}(N_p-k)!\right]^2}, \\ &\underset{(a)}{=} \sum_{i=1}^{N_p}\sum_{m=0}^{2N_pi-2i^2}d_{i,m}\left(1-\exp(-iz)\sum_{k=0}^{m}\frac{(iz)^k}{k!}\right) \end{aligned} \tag{B.3}$$

where (a) follows from (3.9) and $d_{i,m}$is given by

$$d_{i,m} = \frac{m!a_{i,m}}{i^{m+1}\left[\prod_{k=1}^{N_p}(N_p-k)!\right]^2}. \tag{B.4}$$

Noticing that the CDF is in the form of weighted sum of elementary Gamma CDFs

$$\sum_{i=1}^{N_p}\sum_{m=0}^{2N_pi-2i^2}d_{i,m} = 1. \tag{B.5}$$

Finally, (3.8) is obtained by substituting (B.5) into (B.3).

C

APPENDIX TO CHAPTER ??

DERIVATION OF THE LAPLACE TRANSFORM OF THE AGGREGATE INTERFERENCE

Using the definition of the Generating functional for the Marked Poisson point process [60], we can write (7.21) as

$$\mathcal{L}_I(s) = \exp\left(-\underbrace{\int_0^\infty\int_0^\infty \left(1-\exp\left(-shr^{-\alpha}\right)\right)\lambda_I(h,r)drdh}_{A}\right)$$

Now A can be computed as

$$\begin{aligned}
A &= \mathbb{E}_H\left(\int_0^\infty \left(1-\exp\left(-shr^{-\alpha}\right)\right)\lambda_s^{TX}db_d r^{d-1}\mathbb{1}_{I_{th}}\left(r,h\right)dr\right),\\
&= \mathbb{E}_H\left(\int_0^\infty \left(1-\exp\left(-shr^{-\alpha}\right)\right)\lambda_s^{TX}db_d r^{d-1}\mathbb{1}_{I_{th}}\left(P_s hr^{-\alpha}\leq I_{th}\right)dr\right),\\
&= \mathbb{E}_H\left(\int_0^\infty \left(1-\exp\left(-shr^{-\alpha}\right)\right)\lambda_s^{TX}db_d r^{d-1}\mathbb{1}_{I_{th}}\left(r\geq \left(h/\bar{I}_{th}\right)^{1/\alpha}\right)dr\right),\\
&= \mathbb{E}_H\left(\underbrace{\int_{\left(h/\bar{I}_{th}\right)^{1/\alpha}}^\infty \left(1-\exp\left(-shr^{-\alpha}\right)\right)\lambda_s^{TX}db_d r^{d-1}}_{B}\right)dr,
\end{aligned}$$

Let $z = \left(h/\bar{I}_{th}\right)^{1/\alpha}$ and $\delta = \frac{d}{\alpha}$, then B can be evaluated by using integration by parts as

$$\begin{aligned}
B &= \lambda_s^{TX}b_d\left[\left(1-\exp\left(-shr^{-\alpha}\right)\right)r^d\Big|_z^\infty + \alpha\int_z^\infty shr^{d-\alpha-1}\exp(-shr^{-\alpha})dr\right],\\
&= \lambda_s^{TX}b_d h^\delta\left[s^\delta\gamma_l\left(1-\delta,s\bar{I}_{th}\right)-\left(1-\exp\left(-s\bar{I}_{th}\right)\right)\bar{I}_{th}^{-\delta}\right].
\end{aligned}$$

Finally, using B then

$$\begin{aligned}
A &= \lambda_s^{TX}b_d\mathbb{E}_H\left(h^\delta\right)\left\{s^\delta\gamma_l\left(1-\delta,s\bar{I}_{th}\right)-\left(1-\exp\left(-s\bar{I}_{th}\right)\right)\bar{I}_{th}^{-\delta}\right\}, \qquad \text{(C.1)}\\
&= \lambda_s^{TX}b_d\mathbb{E}_{\bar{G}_1,G_2}\left(\left(\bar{G}_1G_2\right)^\delta\right)\left\{s^\delta\gamma_l\left(1-\delta,s\bar{I}_{th}\right)-\left(1-\exp\left(-s\bar{I}_{th}\right)\right)\bar{I}_{th}^{-\delta}\right\},\\
&= \lambda_s^{TX}b_d\exp\left(\frac{\mu^2}{2}\right)\frac{\Gamma\left(m_{sp}+\delta\right)}{\Gamma(m_{sp})}\left\{s^\delta\gamma_l\left(1-\delta,s\bar{I}_{th}\right)-\left(1-\exp\left(-s\bar{I}_{th}\right)\right)\bar{I}_{th}^{-\delta}\right\}.
\end{aligned}$$

where $\mu = \left(\frac{d\left(\sigma_{pp}+\sigma_{ps}\right)\zeta}{\alpha}\right)$.

D

APPENDIX TO CHAPTER 5

D.1 CUMULANTS FOR THE AGGREGATE INTERFERENCE (κ_n) UNDER TX BASED DETECTION

In this section, we derive a closed form expression for the aggregate interference experienced at the primary receiver when CRs employ either MF or ED at transmitters to sense the presence of the primary.

$$
\begin{aligned}
\kappa_n &= \int_0^\infty \int_{\mathbb{R}^d \setminus b(0,r_e)} (h\tilde{l}(r))^n \lambda_{INT}(h,r) dr f_H(h) dh, \\
&= p\lambda_s^{TX} d b_d \mathbb{E}_H \left[\int_{r_e}^\infty h^n r^{d-\alpha n-1} \mathbb{1}_{MD}^t(\gamma(h,r)) dr \right], \qquad \text{(D.1)} \\
&= p\lambda_s^{TX} d b_d \mathbb{E}_H \left[\int_{r_e}^\infty h^n r^{d-\alpha n-1} \mathbb{1}_{MD}^t \left(\frac{P_b h}{\sigma_b^2 r^\alpha} < \gamma_{th}^t \right) dr \right], \\
&= p\lambda_s^{TX} d b_d \mathbb{E}_H \left[\int_{r_e}^\infty h^n r^{d-\alpha n-1} \mathbb{1}_{MD}^t \left(r > \left(\frac{P_b h}{\sigma_b^2 \gamma_{th}^t} \right)^{\frac{1}{\alpha}} \right) dr \right], \\
&= p\lambda_s^{TX} d b_d \int_0^\infty \int_{\max\left(r_e, \left(\frac{\gamma_b h}{\gamma_{th}^t}\right)^{\frac{1}{\alpha}}\right)}^\infty h^n r^{d-\alpha n-1} dr f_H(h) dh, \\
&= p\lambda_s^{TX} d b_d \left[\int_0^{\frac{\gamma_{th}^t r_e^\alpha}{\gamma_b}} \int_{r_e}^\infty h^n r^{d-\alpha n-1} dr f_H(h) dh \right. \\
&+ \left. \int_{\frac{\gamma_{th}^t r_e^\alpha}{\gamma_b}}^\infty \int_{\left(\frac{\gamma_b h}{\gamma_{th}^t}\right)^{\frac{1}{\alpha}}}^\infty h^n r^{d-\alpha n-1} dr f_H(h) dh \right], \\
&= \frac{p\lambda_s^{TX} d b_d}{\alpha n - d} \left[\left\{ \Gamma(n+1) - \Gamma\left(n+1, \frac{\gamma_{th}^t r_e^\alpha}{\gamma_b}\right) \right\} r_e^{d-\alpha n} \right. \\
&+ \left. \Gamma\left(\frac{d}{\alpha}+1, \frac{\gamma_{th}^t r_e^\alpha}{\gamma_b}\right) \left(\frac{\gamma_{th}^t}{\gamma_b}\right)^{n-\frac{d}{\alpha}} \right].
\end{aligned}
$$

Employing the fact that $\gamma_l(a,b) = \Gamma(a) - \Gamma(a,b)$ with $\mu_1 = n+1$ and $\mu_2 = \frac{d}{\alpha}+1$, we obtain t

$$\begin{aligned}\kappa_n &= \frac{p\lambda_s^{TX} d b_d}{\alpha n - d}\left[\gamma_l\left(\mu_1, \frac{\gamma_{th}^t r_e^\alpha}{\gamma_b}\right) r_e^{d-\alpha n}\right. \\ &+ \left.\Gamma\left(\mu_2, \frac{\gamma_{th}^t r_e^\alpha}{\gamma_b}\right)\left(\frac{\gamma_{th}^t}{\gamma_b}\right)^{n-\frac{d}{\alpha}}\right].\end{aligned} \tag{D.2}$$

D.2 COMPUTATION OF THE CUMULANTS UNDER CONTENT TRANSMITTER STRATEGY

In this section, we evaluate the cumulants of the aggregate interference inflicted by CRN under content transmitter strategy.

$$\begin{aligned}\kappa_{n,(t_1,t_2)}^{content} &= p\lambda_s^{TX} d b_d \int_0^\infty \int_{r_e}^\infty h^n r^{d-\alpha n-1} \mathbb{1}_{MD}^{t_1}(\gamma(h,r)) \\ &\times \mathbb{1}_{MD}^{t_2}(\gamma(h,\tilde{r})) dr f_H(h) dh, \\ &= p\lambda_s^{TX} d b_d \int_0^\infty \int_{r_e}^\infty h^n r^{d-\alpha n-1} \mathbb{1}_{MD}^{t}\left(\frac{\gamma_b h}{r^\alpha} < \gamma_{th}^{t_1}\right) \\ &\times \mathbb{1}_{MD}^{t}\left(\frac{\gamma_b h}{c^\alpha r^\alpha} < \gamma_{th}^{t_2}\right) dr f_H(h) dh, \\ &= p\lambda_s^{TX} d b_d \int_0^\infty \int_{\max\left(r_e, \left(\frac{\gamma_b h}{\gamma_{th}^{t_1}}\right)^{\frac{1}{\alpha}}, \left(\frac{\gamma_b h}{c^\alpha \gamma_{th}^{t_2}}\right)^{\frac{1}{\alpha}}\right)}^\infty h^n \\ &\times r^{d-\alpha n-1} dr f_H(h) dh, \\ &= p\lambda_s^{TX} d b_d \int_0^\infty \int_{\max\left(r_e, \eta_1 h^{\frac{1}{\alpha}}, \eta_2 h^{\frac{1}{\alpha}}\right)}^\infty h^n \\ &\times r^{d-\alpha n-1} dr f_H(h) dh, \\ &= p\lambda_s^{TX} d b_d \int_0^\infty \int_{\max\left(r_e, \max(\eta_1,\eta_2) h^{\frac{1}{\alpha}}\right)}^\infty h^n \\ &\times r^{d-\alpha n-1} dr f_H(h) dh,\end{aligned} \tag{D.3}$$

where, $\eta_1 = \left(\frac{\gamma_b}{\gamma_{th}^{t_1}}\right)^{\frac{1}{\alpha}}$ and $\eta_2 = \left(\frac{\gamma_b}{c^\alpha \gamma_{th}^{t_2}}\right)^{\frac{1}{\alpha}}$.

E APPENDIX TO 6

E.1 DERIVATION FOR THE MGF OF THE AGGREGATE INTERFERENCE GENERATED BY THE PRIMARY USER

As discussed earlier, the accumulative interference from the secondary transmitters employing ALOHA type MAC is

$$I_{sec} = \sum_{i \epsilon \Phi_s^{md,tx}(\lambda_s^{md,tx})} H_i l(r_i) \tag{E.1}$$

the MGF of I_{sec} is given by

$$\begin{aligned} M_{I_{sec}} &= \mathbb{E}\left(\exp\left(-sI_{sec}\right)\right) \\ &= \mathbb{E}\left(\exp\left(-s \sum_{i \epsilon \Phi_s^{md,tx}(\lambda_s^{md,tx})} H_i l(r_i)\right)\right) \\ &= \mathbb{E}\left(\prod_{i \epsilon \Phi_s^{md,tx}(\lambda_s^{md,tx})} \mathbb{E}_H\left(\exp\left(-sH_i l(r_i)\right)\right)\right) \end{aligned} \tag{E.2}$$

Using the PGFL of Poisson point process MGF can be written as

$$M_{I_{sec}}(s) = \exp\left(-\int_o^\infty \int_{r_e}^\infty \left(1 - \exp\left(-shl(r)\right)\right) \lambda_s^{md,tx}(r) f_H(h) dr dh\right) \tag{E.3}$$

This MGF cannot be expressed in closed form. Hence, using the cumulant generating function (CGF)

$$\begin{aligned} K_{I_{sec}}(s) &= \ln(M_{I_{sec}}(s)) \\ &= -\int_o^\infty \int_{r_e}^\infty \left(1 - \exp\left(-shl(r)\right)\right) \lambda_s^{md,tx}(r) f_H(h) dr dh \end{aligned} \tag{E.4}$$

Then n^{th} cumulant can be expressed as

$$\begin{aligned}
\kappa_n &= \frac{d^n K_{I_{sec}}(s)}{ds^n} \qquad\qquad \text{(E.5)}\\
&= \int_0^\infty \int_{r_e}^\infty h^n l(r)^n \lambda_s^{md,tx}(r) f_H(h) dr dh \\
&= \int_0^\infty \int_{r_e}^\infty h^n r^{-\alpha n} f_H(h) d b_d \rho_s \lambda_s r^{d-1} \mathbb{1}_{md}(\gamma(r)) dr dh \\
&= d b_d \lambda_s \rho_s \int_0^\infty h^n f_H(h) \int_{\max\left(r_e, \left(\frac{h}{\gamma_{th}}\right)^{\frac{1}{\alpha}}\right)}^\infty r^{d-\alpha n-1} dr dh \\
&= \frac{d\rho_s \lambda_s b_d}{\alpha n - d} \left[\gamma_{low}\left(n, \bar{\gamma}_{th}\right) r_e^{d-\alpha n} + \left(\frac{\bar{\gamma}_{th}}{r_e^\alpha}\right)^{\frac{d}{\alpha}-n} \gamma_{up}\left(\frac{d}{\alpha}, \bar{\gamma}_{th}\right)\right]
\end{aligned}$$

The PDF of the aggregate interference can be obtained from the cumulants using the Method of Moments [20]. Authors in [20] have employed a similar approach in the absence of self-coexistence to model the interference by the log-normal or shifted log-normal distribution. Note that it is well established in the literature that the Gaussian approximation is not valid for interference due to its skewed and fat-tailed behavior [20]. The main problem with these distributions is that although they closely fit in the body, they do not fit accurately in the tail for all parameters. Moreover, the expressions for matching such moments (see [20]) are quite complex. An alternative choice can be the log-logisitic distribution. However, it does not result in a good fit both in body and tail. It is possible to accurately fit the distribution using simulation and maximum likelihood estimate or L-moments type statistics. After conducting several experiments and goodness of fit testing, we found that the Gamma distribution is the best fit for the interference distribution. An added advantage with the Gamma distribution is that moment matching expressions lend themselves into a very simple form. Hence interference $I \sim \mathcal{G}amma(k, \theta)$ with k being the shape parameter and θ is the scale parameter with

$$k = \frac{\kappa_1^2}{\kappa_2} \text{ and } \theta = \frac{\kappa_2}{\kappa_1}. \qquad \text{(E.6)}$$

The accuracy of Gamma distribution is verified using simulations and goodness of fit testing. Hence MGF of Gamma distribution can be used to approximate the MGF of interference contributed by the secondary transmitters.

$$M_{I_{sec}}(s) = \frac{1}{(1+\theta s)^k}. \qquad \text{(E.7)}$$

E.2 DERIVATION FOR THE MGF OF THE AGGREGATE INTERFERENCE GENERATED BY PRIMAY USERS

The aggregate interference power from other primary users utilizing slotted ALOHA type transmission scheme is

$$I_{pri} = \sum_{i \epsilon \Phi_p^{tx}(\lambda_p^{tx})} H_i l(r_i) \tag{E.8}$$

the MGF of I_{pri} is given by

$$\begin{aligned} M_{I_{pri}} &= \mathbb{E}\left(\exp\left(-sI_{pri}\right)\right) \\ &= \mathbb{E}\left(\exp\left(-s \sum_{i\epsilon\Phi_p^{tx}(\lambda_p^{tx})} H_i l(r_i)\right)\right) \\ &= \mathbb{E}\left(\prod_{i\epsilon\Phi_p^{tx}(\lambda_p^{tx})} \mathbb{E}_H\left(\exp\left(-sH_i l(r_i)\right)\right)\right) \end{aligned} \tag{E.9}$$

Using the definition of PGFL

$$M_{I_{pri}} = \exp\left(\underbrace{-\int_o^\infty \int_1^\infty \left(1-\exp\left(-shl(r)\right)\right)\lambda_p^{tx}(r) f_H(h) drdh}_{A}\right) \tag{E.10}$$

$$A = -\int_o^\infty \int_1^\infty \left(1-\exp\left(-shl(r)\right)\right)\lambda_p^{tx}(r) f_H(h) drdh$$

Using the change of variables

$$A = \lambda_p \rho_p b_d \int_0^\infty f_H(h) \underbrace{\int_1^\infty \left(1-\exp\left(-s\frac{h}{z}\right)\right) z^{\frac{d}{\alpha}-1} dz}_{B}\, dh$$

Note that B is

$$B = \mathbb{E}\left(\left(\frac{sH}{Z}\right)^{-\frac{d}{\alpha}}\right)$$

where Z is exponential random variable with unit mean, Hence

$$A = \lambda_p \rho_p b_d s^{\frac{d}{\alpha}} \int_0^\infty h^{\frac{d}{\alpha}} \gamma_{low}\left(1-\frac{d}{\alpha}, hs\right) f_H(h) dh$$

Subsituting A in MGF expression

$$M_{I_{pri}}(s) = \exp\left(-\rho_p \lambda_p b_d s^{\frac{d}{\alpha}} \mathbb{E}_H\left(H^{\frac{d}{\alpha}} \gamma_{low}(1-\frac{d}{\alpha}, sH)\right)\right).$$

For $\frac{d}{\alpha} = \frac{1}{2}$,

$$M_{I_{pri}}(s) = \exp\left(-\rho_p \lambda_p b_d \sqrt{s} \mathbb{E}_H \left(\sqrt{H} \gamma_{low}(\frac{1}{2}, sH)\right)\right)$$

Using the fact that H is exponential

$$M_{I_{pri}}(s) = \exp\left(-\rho_p \lambda_p b_d \underbrace{\int_0^\infty \sqrt{sh} \gamma_{low}(\frac{1}{2}, sh) \exp(-\frac{sh}{s}) dh}_{C}\right)$$

$$C = \int_0^\infty \sqrt{sh} \gamma_{low}(\frac{1}{2}, sh) \exp(-\frac{sh}{s}) dh$$

Using change of variable $x = sh$ and $w = \frac{1}{s}$,

$$C = w \int_0^\infty \sqrt{x} \gamma_{low}(\frac{1}{2}, x) \exp(-wx) dx$$

Using the fact that $\gamma_{low}(\frac{1}{2}, x) = \sqrt{\pi} \text{erf}\left(-\sqrt{x}\right)$

$$\begin{aligned}
C &= w\sqrt{\pi} \int_0^\infty \text{erf}\left(-\sqrt{x}\right) \sqrt{x} \exp(-wx) dx \\
&= w\sqrt{\pi} \int_0^\infty \left(\text{1-erfc}\left(-\sqrt{x}\right)\right) \sqrt{x} \exp(-wx) dx \\
&= \underbrace{w\sqrt{\pi} \int_0^\infty \sqrt{x} \exp(-wx) dx}_{D} + \underbrace{w\sqrt{\pi} \int_0^\infty \text{erfc}\left(-\sqrt{x}\right) \sqrt{x} \exp(-wx) dx}_{E}
\end{aligned}$$

D can be solved using $\Gamma(.)$, Gamma function defined previously and E can be solved using [185]. Hence after mathematical simplification and manipulation,

$$M_{I_{pri}}(s) = \exp\left(-\rho_p \lambda_p b_d \sqrt{s} \left(\frac{\pi}{2} - 0.5 \arctan\left(1/\sqrt{s}\right) + \frac{\sqrt{s}}{2(s+1)}\right)\right).$$

F

APPENDIX TO 7

F.1 DERIVATION FOR THE UPPERBOUND

In this appendix we derive an upper-bound on A in (7.23). So from (7.17) and (7.23) we have

$$A = \lambda_s^{TX} p b_d \int_0^\infty \int_{r_e}^\infty \left(1 - \exp\left(-shr^{-\alpha}\right)\right) dr^{d-1} \mathbb{1}_{\gamma_{th,t}}^{MD}(\gamma(h,r)) dr f_H(h) dh.$$

Then after some algebraic manipulations

$$A = \lambda p b_d \left[\underbrace{\int_0^{\bar{\gamma}_{th,t} r_e^\alpha} \Xi(r_e) f_H(h) dh}_{\bar{f}_1(s)} + \underbrace{\int_{\bar{\gamma}_{th,t} r_e^\alpha}^\infty \Xi\left(\left(\frac{h}{\bar{\gamma}_{th,t}}\right)^{\frac{1}{\alpha}}\right) f_H(h) dh}_{f_2(s)} \right] \quad \text{(F.1)}$$

where,

$$\Xi(x) = \int_x^\infty \left(1 - \exp(-shr^{-\alpha})\right) dr^{d-1} dr. \quad \text{(F.2)}$$

Performing the integration by parts and then some mathematical manipulations

$$\Xi(x) = (sh)^{d/\alpha} \gamma_l \left(1 - d/\alpha, shx^{-\alpha}\right) - \left[1 - \exp\left(-shx^{-\alpha}\right)\right] x^d. \quad \text{(F.3)}$$

Substituting (F.3) into (F.1) we have

$$\begin{aligned} \bar{f}_1(s) &= \underbrace{\int_0^{\bar{\gamma}_{th,t} r_e^\alpha} (sh)^{d/\alpha} \gamma_l \left(1 - d/\alpha, shr_e^{-\alpha}\right) f_H(h) dh}_{B_1} \quad \text{(F.4)} \\ &- \underbrace{\int_0^{\bar{\gamma}_{th,t} r_e^\alpha} \left[1 - \exp\left(-shr_e^{-\alpha}\right)\right] r_e^d f_H(h) dh.}_{B_2} \end{aligned}$$

Now B_2 can be evaluated exactly as

$$B_2 = \frac{r_e^d m_s^{m_s}}{\Gamma(m_s)} \frac{\gamma_l\left(m_s, \left(m_s r_e^\alpha + s\right) \bar{\gamma}_{th,t}\right)}{\left(s r_e^{-\alpha} + m_s\right)^{m_s}} - \frac{r_e^d \gamma_l\left(m_s, m_s \bar{\gamma}_{th,t} r_e^\alpha\right)}{\Gamma(m_s)}. \quad \text{(F.5)}$$

For B_1 a tight upper bound can be computed as follows. First we can write

$$B_1 = \frac{s^{d/\alpha} m_s^{m_s}}{\Gamma(m_s)} \int_0^{\bar{\gamma}_{th,t} r_e^\alpha} h^{d/\alpha + m_s - 1} \gamma_l\left(1 - d/\alpha, shr_e^{-\alpha}\right) \exp(-m_s h) dh. \quad \text{(F.6)}$$

Applying integration by parts with $u = \gamma_l\left(1 - {}^{d}/_{\alpha}, shr_e^{-\alpha}\right)$ and $dv = h^{d/\alpha + m_s - 1}$ $\exp(-m_s h)dh$ and after some mathematical manipulations, we obtain

$$B_1 = \left(\frac{s}{m_s}\right)^{d/\alpha} \frac{\gamma_l\left(1 - {}^{d}/_{\alpha}, s\bar{\gamma}_{th,t}\right)\gamma_l\left(m_s + {}^{d}/_{\alpha}, m_s\bar{\gamma}_{th,t}r_e^{\alpha}\right)}{\Gamma(m_s)} - I_1, \tag{F.7}$$

where,

$$I_1 = \frac{sr_e^{d-\alpha}}{m_s^{d/\alpha}\Gamma(m_s)} \int_0^{\bar{\gamma}_{th,t}r_e^{\alpha}} h^{-d/\alpha} \exp(-shr_e^{-\alpha})\gamma_l\left(m_s + {}^{d}/_{\alpha}, m_s h\right) dh \tag{F.8}$$

can be ignored to obtain a tight upper bound on B_1. Thus $\bar{f}_1(s) \leq f_1(s)$ (see (7.19) and (F.1)).

The second term in (F.1), i.e. $f_2(s)$, can be exactly computed as

$$f_2(s) = \int_{\bar{\gamma}_{th,t}r_e^{\alpha}}^{\infty} h^{d/\alpha} f_H(h)dh \left[s^{d/\alpha}\gamma_l\left(1 - {}^{d}/_{\alpha}, s\bar{\gamma}_{th,t}\right) - \frac{\{1 - \exp(-s\bar{\gamma}_{th,t})\}}{\bar{\gamma}_{th,t}^{d/\alpha}}\right],$$

which results in (7.20).

BIBLIOGRAPHY

[1] A. Ericsson, "Traffic and market data report–on the pulse of the networked society," 2011. [Online]. Available: http://hugin.info/1061/R/1561267/483187.pdf (Cited on page 1.)

[2] E. Hossain, D. Niyato, and Z. Han, *Dynamic spectrum access and management in cognitive radio networks*. Cambridge University Press New York, NY, USA, 2009. (Cited on page 1.)

[3] A. Goldsmith, S. Jafar, I. Maric, and S. Srinivasa, "Breaking spectrum gridlock with cognitive radios: An information theoretic perspective," *Proceedings of the IEEE*, vol. 97, no. 5, pp. 894–914, 2009. (Cited on pages 2, 3, 4, 8, 26, 40, 109, 116, 164, and 176.)

[4] M. McHenry, P. Tenhula, D. McCloskey, D. Roberson, and C. Hood, "Chicago spectrum occupancy measurements & analysis and a long-term studies proposal," in *Proceedings of the First International Workshop on Technology and Policy for Accessing Spectrum*. ACM, 2006. (Cited on page 2.)

[5] M. McHenry, "NSF spectrum occupancy measurements project summary," *Shared Spectrum Company*, 2005. (Cited on page 2.)

[6] E. FCC, "Docket No 02-135," *Spectrum Policy Task Force*, 2002. (Cited on page 2.)

[7] M. Buddhikot, "Understanding dynamic spectrum access: Models taxonomy and challenges," in *2nd IEEE International Symposium on New Frontiers in Dynamic Spectrum Access Networks*, 2007, pp. 649–663. (Cited on page 2.)

[8] Q. Zhao and B. Sadler, "A survey of dynamic spectrum access," *IEEE Signal Processing Magazine*, vol. 24, no. 3, pp. 79–89, 2007. (Cited on pages 2, 8, and 164.)

[9] R. Tandra, S. Mishra, and A. Sahai, "What is a spectrum hole and what does it take to recognize one?" *Proceedings of the IEEE*, vol. 97, no. 5, pp. 824–848, 2009. (Cited on pages 3 and 110.)

[10] S. Haykin, "Cognitive radio: brain-empowered wireless communications," *IEEE Journal on Selected Areas in Communications*, vol. 23, no. 2, pp. 201–220, 2005. (Cited on pages 3 and 4.)

[11] R. Zhang, X. Kang, and Y.-C. Liang, "Protecting primary users in cognitive radio networks: Peak or average interference power constraint?" in *IEEE International Conference on Communications*, 2009, pp. 1–5. (Cited on page 4.)

[12] X. Kang, R. Zhang, Y.-C. Liang, and H. K. Garg, "On outage capacity of secondary users in fading cognitive radio networks with primary user's outage constraint," in *IEEE Global Telecommunications Conference*, 2009, pp. 1–5. (Cited on page 4.)

[13] A. Conti, M. Win, M. Chiani, and J. Winters, "Bit error outage for diversity reception in shadowing environment," *IEEE Communications Letters*, vol. 7, no. 1, pp. 15–17, 2003. (Cited on page 4.)

[14] C. E. Shannon and W. Weaver, "A mathematical theory of communication," 1948. (Cited on page 4.)

[15] T. Clancy, "Achievable capacity under the interference temperature model," in *26th IEEE International Conference on Computer Communications*, 2007, pp. 794–802. (Cited on page 4.)

[16] ——, "Achievable capacity under the interference temperature model," in *26th IEEE International Conference on Computer Communications*. IEEE, 2007, pp. 794–802. (Cited on page 4.)

[17] E. FCC, "Docket no 03-237 notice of inquiry and notice of proposed rulemaking," *ET Docket*, no. 03-237, 2003. (Cited on page 4.)

[18] J. Mitola, "Cognitive radio: An integrated agent architecture for software defined radio," *Doctor of Technology, Royal Inst. Technol.(KTH), Stockholm, Sweden*, pp. 271–350, 2000. (Cited on page 5.)

[19] H. Kim and K. Shin, "In-band spectrum sensing in ieee 802.22 wrans for incumbent protection," *IEEE Transactions on Mobile Computing*, vol. 9, no. 12, pp. 1766–1779, 2010. (Cited on page 6.)

[20] A. Ghasemi and E. Sousa, "Interference aggregation in spectrum-sensing cognitive wireless networks," *IEEE Journal of Selected Topics in Signal Processing*, vol. 2, no. 1, pp. 41–56, 2008. (Cited on pages 6, 7, 11, 113, 118, 132, 133, 154, 159, 161, 162, 164, 166, 173, 174, 177, 178, and 264.)

[21] W. Ren, Q. Zhao, and A. Swami, "Power control in cognitive radio networks: how to cross a multi-lane highway," *IEEE Journal on Selected Areas in Communication*, vol. 27, no. 7, p. 1283, 2009. (Cited on pages 6 and 116.)

[22] M. Cardenas-Juarez and M. Ghogho, "Spectrum sensing and throughput trade-off in cognitive radio under outage constraints over nakagami fading," *IEEE Communications Letters*, vol. 15, no. 10, pp. 1110–1113, 2011. (Cited on page 7.)

[23] Y.-C. Liang, Y. Zeng, E. Peh, and A. T. Hoang, "Sensing-throughput tradeoff for cognitive radio networks," *IEEE Transactions on Wireless Communications*, vol. 7, no. 4, pp. 1326–1337, 2008.

[24] Y. F. Sharkasi, S. Zaidi, and M. Ghogho, "Revisiting spectrum sensing-throughput trade-off in cognitive radio networks under fading channels and detection uncertainty," *submitted to IEEE Transactions on Vehicular Technology*, 2013. (Cited on page 7.)

[25] S. Mangold, A. Jarosch, C. Monney, and S. Innovations, "Operator assisted cognitive radio and dynamic spectrum assignment with dual beacons-detailed evaluation," in *First International Conference on Communication System Software and Middleware*, 2006, pp. 1–6. (Cited on page 7.)

[26] S. Sengupta, M. Chatterjee, and R. Chandramouli, "A coordinated distributed scheme for cognitive radio based IEEE 802.22 wireless mesh networks," in *IEEE International Conference on Communications Workshops*, 2008, pp. 461–465.

[27] A. Tajer and X. Wang, "Beacon-assisted spectrum access with cooperative cognitive transmitter and receiver," *| IEEE Transactions on Mobile Computing*, pp. 112–126, 2009. (Cited on page 7.)

[28] F. No, "03-322," *Notice of Proposed Rule Making and Order*, 2003. (Cited on pages 7 and 116.)

[29] R. Menon, R. M. Buehrer, and J. H. Reed, "Outage probability based comparison of underlay and overlay spectrum sharing techniques," in *First IEEE International Symposium on New Frontiers in Dynamic Spectrum Access Networks*. IEEE, 2005, pp. 101–109. (Cited on pages 8 and 11.)

[30] M. Maso, M. Debbah, and L. Vangelista, "A distributed approach to interference alignment in ofdm-based two-tiered networks," *IEEE Transactions on Vehicular Technology*, vol. PP, no. 99, pp. 1–1, 2013. (Cited on page 8.)

[31] M. Uppal, G. Yue, Y. Xin, X. Wang, and Z. Xiong, "A dirty-paper coding scheme for the cognitive radio channel," in *IEEE International Conference on Communications (ICC)*, 2010, pp. 1–5. (Cited on page 8.)

[32] J. G. Andrews, R. K. Ganti, M. Haenggi, N. Jindal, and S. Weber, "A primer on spatial modeling and analysis in wireless networks," *IEEE Communications Magazine*, vol. 48, no. 11, pp. 156–163, 2010. (Cited on pages 9 and 69.)

[33] M. Haenggi, J. Andrews, F. Baccelli, O. Dousse, and M. Franceschetti, "Stochastic geometry and random graphs for the analysis and design of wireless networks," *IEEE Journal on Selected Areas in Communications*, vol. 27, no. 7, pp. 1029–1046, 2009. (Cited on pages 9 and 11.)

[34] E. Sousa and J. Silvester, "Optimum transmission ranges in a direct-sequence spread-spectrum multihop packet radio network," *IEEE Journal on Selected Areas in Communications*, vol. 8, no. 5, pp. 762–771, 1990. (Cited on pages 9 and 133.)

[35] A. Mawira, "Estimate of mean C/I and capacity of interference limited mobile ad-hoc networks," in *International Zurich Seminar on Broadband Communications, Access, Transmission, Networking.*, 2002, pp. 51–1.

[36] J. Ilow and D. Hatzinakos, "Analytic alpha-stable noise modeling in a Poisson field of interferers or scatterers," *IEEE Transactions on Signal Processing*, vol. 46, no. 6, pp. 1601–1611, 1998. (Cited on page 133.)

[37] V. Mordachev and S. Loyka, "On node density-outage probability tradeoff in wireless networks," in *IEEE International Symposium on Information Theory*, 2008, pp. 191–195.

[38] R. Hekmat and P. Van Mieghem, "Interference in wireless multi-hop ad-hoc networks and its effect on network capacity," *Wireless Networks*, vol. 10, no. 4, pp. 389–399, 2004.

[39] O. Dousse, F. Baccelli, and P. Thiran, "Impact of interferences on connectivity in ad hoc networks," *IEEE/ACM Transactions on Networking*, vol. 13, no. 2, pp. 425–436, 2005.

[40] H. Nguyen, F. Baccelli, and D. Kofman, "A stochastic geometry analysis of dense ieee 802.11 networks," in *26th IEEE International Conference on Computer Communications.* IEEE, 2007, pp. 1199–1207.

[41] P. Pinto and M. Win, "Communication in a Poisson field of interferers-Part I: Interference distribution and error probability," *IEEE Transaction on Wireless Communication*, 2009.

[42] ——, "Communication in a Poisson field of interferers-Part II: Channel capacity and interference spectrum," *IEEE Transaction on Wireless Communication*, 2009.

[43] F. Baccelli and B. Blaszczyszyn, *Stochastic geometry and wireless networks.* Now Publishers Inc, 2009, vol. 1. (Cited on pages 68 and 72.)

[44] F. Baccelli, B. Blaszczyszyn, and P. Muhlethaler, "An Aloha protocol for multihop mobile wireless networks," *IEEE Transactions on Information Theory*, vol. 52, no. 2, pp. 421–436, 2006. (Cited on pages 27, 38, 39, 45, 115, 156, 181, 197, 200, and 214.)

[45] A. Hunter, J. Andrews, and S. Weber, "Transmission capacity of ad hoc networks with spatial diversity," *IEEE Transactions on Wireless Communications*, vol. 7, no. 12, pp. 5058–5071, 2008.

[46] S. P. Weber, X. Yang, J. G. Andrews, and G. De Veciana, "Transmission capacity of wireless ad hoc networks with outage constraints," *IEEE Transactions on Information Theory*, vol. 51, no. 12, pp. 4091–4102, 2005. (Cited on pages 77 and 160.)

[47] K. Gulati, B. Evans, J. Andrews, and K. Tinsley, "Statistics of Co-Channel Interference in a Field of Poisson and Poisson-Poisson Clustered Interferers," *IEEE Transaction on Signal Processing, Submitted.*

[48] Y. Shobowale and K. Hamdi, "A unified model for interference analysis in unlicensed frequency bands," *IEEE Transactions on Wireless Communications*, vol. 8, no. 8, pp. 4004–4013, 2009.

[49] E. Salbaroli and A. Zanella, "Interference analysis in a Poisson field of nodes of finite area," *IEEE Transactions on Vehicular Technology*, vol. 58, no. 4, pp. 1776–1783, 2009.

[50] H. S. Dhillon, R. K. Ganti, F. Baccelli, and J. G. Andrews, "Modeling and analysis of k-tier downlink heterogeneous cellular networks," *IEEE Journal on Selected Areas in Communications*, vol. 30, no. 3, pp. 550–560, 2012. (Cited on page 9.)

[51] M. Vu, S. Ghassemzadeh, and V. Tarokh, "Interference in a cognitive network with beacon," in *IEEE Wireless Communications and Networking Conference*, 2008, pp. 876–881. (Cited on pages 11, 113, 116, 154, 159, 161, 162, 164, 166, 174, and 177.)

[52] J. Lee, J. Andrews, and D. Hong, "Spectrum-sharing transmission capacity," *IEEE Transactions on Wireless Communications*, no. 99, pp. 1–11, 2011. (Cited on page 37.)

[53] A. Rabbachin, T. Quek, H. Shin, and M. Win, "Cognitive network interference," *IEEE Journal on Selected Areas in Communication*, vol. 29, no. 2, 2011. (Cited on pages 113, 173, and 174.)

[54] P. Mitran, "Interference scaling laws in cognitive networks," in *24th Biennial Symposium on Communications*, 2008, pp. 282–285.

[55] C. Yin, L. Gao, T. Liu, and S. Cui, "Transmission capacities for overlaid wireless ad hoc networks with outage constraints," in *IEEE International Conference on Communications*. IEEE, 2009, pp. 1–5. (Cited on pages 37, 51, and 113.)

[56] N. Shankar and C. Cordeiro, "Analysis of aggregated interference at DTV receivers in tv bands," in *Cognitive Radio Oriented Wireless Networks and Communications, 3rd International Conference on*, 2008, pp. 1–6.

[57] M. Hanif and P. Smith, "On mimo cognitive radios with antenna selection," in *IEEE Wireless Communications and Networking Conference*. IEEE, 2010, pp. 1–6. (Cited on pages 34, 36, and 37.)

[58] S. A. R. Zaidi, D. McLernon, and M. Ghogho, "On outage and interference in 802.22 cognitive radio networks under deterministic network geometry," in *ACM Mobicom*, 2009. (Cited on page 11.)

[59] A. Ephremides, "Energy concerns in wireless networks," *IEEE Wireless Communications*, vol. 9, no. 4, pp. 48–59, 2002. (Cited on pages 11, 37, 193, 194, 195, and 196.)

[60] D. Stoyan, W. Kendall, J. Mecke, and D. Kendall, *Stochastic geometry and its applications*. Wiley New York, 1995. (Cited on pages 11, 22, 23, 26, 29, 34, 39, 41, 43, 55, 115, 123, 124, 161, 163, 166, 175, 181, 246, 253, 254, 255, and 259.)

[61] M. Haenggi, "Interference in large wireless networks," *Foundations and Trends in Networking*, vol. 3, no. 2, pp. 127–248, 2009. (Cited on pages 11, 40, and 156.)

[62] F. Baccelli and B. Błaszczyszyn, "Stochastic geometry and wireless networks," *NOW: Foundations and Trends in Networking*. (Cited on pages 11, 39, and 156.)

[63] M. Win, P. Pinto, and L. Shepp, "A mathematical theory of network interference and its applications," *Proceedings of the IEEE*, vol. 97, no. 2, pp. 205–230, 2009. (Cited on pages 11, 38, 113, 160, 161, 179, 194, and 197.)

[64] M. Vu, N. Devroye, and V. Tarokh, "On the primary exclusive region of cognitive networks," *IEEE Transactions on Wireless Communications*, vol. 8, no. 7, pp. 3380–3385, 2009. (Cited on pages 21, 22, 115, 163, and 175.)

[65] S. Anand and R. Chandramouli, "On the secrecy capacity of fading cognitive wireless networks," in *Proc. IEEE CROWNCOM*, 2008, pp. 1–5. (Cited on page 21.)

[66] A. Bagayoko, P. Tortelier, and I. Fijalkow, "Impact of shadowing on the primary exclusive region in cognitive networks," in *Proc. IEEE EW*, pp. 105–110. (Cited on page 21.)

[67] J.-M. Dricot, G. Ferrari, F. Horlin, and P. De Doncker, in *Proc. IEEE ICC*, May 2010, pp. 1 –5. (Cited on page 21.)

[68] I. Akyildiz, W. Lee, and K. Chowdhury, "Crahns: Cognitive radio ad hoc networks," *Ad Hoc Networks*, vol. 7, no. 5, pp. 810–836, 2009. (Cited on page 21.)

[69] T. Lin and J. Hou, "Interplay of spatial reuse and sinr-determined data rates in csma/ca-based, multi-hop, multi-rate wireless networks," in *Proc. IEEE INFOCOM*, 2007, pp. 803–811. (Cited on pages 24 and 29.)

[70] M. Zorzi and R. Rao, "Geographic random forwarding (GeRaF) for ad hoc and sensor networks: multihop performance," *IEEE Transactions on Mobile Computing*, vol. 2, no. 4, pp. 337–348, 2004. (Cited on pages 24, 193, 194, 198, 201, 209, 211, 220, and 225.)

[71] D. Chen, J. Deng, and P. Varshney, "Selection of a forwarding area for contention-based geographic forwarding in wireless multi-hop networks," *IEEE Transactions on Vehicular Technology*, vol. 56, no. 5, pp. 3111–3122, 2007. (Cited on pages 24, 35, 53, 193, 194, 211, 220, and 225.)

[72] K. Huang, V. Lau, and Y. Chen, "Spectrum sharing between cellular and mobile ad hoc networks: transmission-capacity trade-off," *IEEE Journal on Selected Areas in Communications*, vol. 27, no. 7, pp. 1256–1267, 2009. (Cited on pages 33, 37, 51, 160, and 163.)

[73] S. Zaidi, D. McLernon, and M. Ghogho, "Quantifying the primary's guard zone under cognitive user's routing and medium access," *IEEE Communications Letters*, vol. PP, no. 99, pp. 1 –4, 2012. (Cited on page 33.)

[74] Q. Li, G. Li, W. Lee, M. il Lee, D. Mazzarese, B. Clerckx, and Z. Li, "Mimo techniques in wimax and lte: a feature overview," *IEEE Communications Magazine*, vol. 48, no. 5, pp. 86 –92, may 2010. (Cited on page 34.)

[75] S. Alamouti, "A simple transmit diversity technique for wireless communications," *IEEE Journal on Selected Areas in Communications*, vol. 16, no. 8, pp. 1451–1458, 1998. (Cited on page 34.)

[76] V. Tarokh, N. Seshadri, and A. Calderbank, "Space-time codes for high data rate wireless communication: Performance criterion and code construction," *IEEE Transactions on Information Theory*, vol. 44, no. 2, pp. 744–765, 1998. (Cited on page 34.)

[77] E. Telatar, "Capacity of multi-antenna gaussian channels," *European Transactions on Telecommunications*, vol. 10, no. 6, pp. 585–595, 1999. (Cited on page 34.)

[78] V. Cadambe and S. Jafar, "Interference alignment and degrees of freedom of the k-user interference channel," *IEEE Transactions on Information Theory*, vol. 54, no. 8, pp. 3425 –3441, aug. 2008. (Cited on page 34.)

[79] G. Scutari, D. Palomar, and S. Barbarossa, "Cognitive mimo radio," *IEEE Signal Processing Magazine*, vol. 25, no. 6, pp. 46–59, 2008. (Cited on pages 34 and 36.)

[80] C. Gao, Y. Shi, Y. Hou, and S. Kompella, "On the throughput of mimo-empowered multi-hop cognitive radio networks," *IEEE Transactions on Mobile Computing*, 2011. (Cited on page 37.)

[81] R. Vaze, "Transmission capacity of spectrum sharing ad hoc networks with multiple antennas," *IEEE Transactions on Wireless Communications*, no. 99, pp. 1–7, 2010. (Cited on pages 37 and 51.)

[82] R. Zhang and Y. Liang, "Exploiting multi-antennas for opportunistic spectrum sharing in cognitive radio networks," *IEEE Journal of Selected Topics in Signal Processing*, vol. 2, no. 1, pp. 88–102, 2008. (Cited on pages 34, 36, and 37.)

[83] M. Kang and M. Alouini, "Largest eigenvalue of complex wishart matrices and performance analysis of mimo mrc systems," *IEEE Journal on Selected Areas in Communications*, vol. 21, no. 3, pp. 418–426, 2003. (Cited on pages 35, 38, 43, and 44.)

[84] J. Pena-Martin, J. Romero-Jerez, G. Aguilera, and A. Goldsmith, "Performance comparison of mrc and ic under transmit diversity," *IEEE Transactions on Wireless Communications*, vol. 8, no. 5, pp. 2484–2493, 2009. (Cited on pages 35, 38, 44, and 245.)

[85] L. Zhang and Y. Zhang, "Energy-efficient cross-layer protocol of channel-aware geographic-informed forwarding in wireless sensor networks," *IEEE Transactions on Vehicular Technology*, vol. 58, no. 6, pp. 3041–3052, 2009. (Cited on page 35.)

[86] B. Karp and H. Kung, "Gpsr: greedy perimeter stateless routing for wireless networks," in *Proceedings of the 6th Annual International conference on Mobile Computing and Networking*. ACM, 2000, pp. 243–254. (Cited on page 35.)

[87] C. Li and H. Dai, "On the throughput scaling of cognitive radio ad hoc networks," in *Proceedings of IEEE INFOCOM*, april 2011, pp. 241 –245. (Cited on pages 37 and 51.)

[88] A. Maaref and S. Aissa, "Closed-form expressions for the outage and ergodic shannon capacity of mimo mrc systems," *IEEE Transactions on Communications*, vol. 53, no. 7, pp. 1092–1095, 2005. (Cited on pages 38 and 44.)

[89] C. Khatri, "Distribution of the largest or the smallest characteristic root under null hypothesis concerning complex multivariate normal populations," *The Annals of Mathematical Statistics*, vol. 35, no. 4, pp. 1807–1810, 1964. (Cited on pages 43 and 44.)

[90] P. Dighe, R. Mallik, and S. Jamuar, "Analysis of transmit-receive diversity in rayleigh fading," *IEEE Transactions on Communications*, vol. 51, no. 4, pp. 694–703, 2003. (Cited on pages 43 and 44.)

[91] K. Ahn, "Performance analysis of mimo-mrc system in the presence of multiple interferers and noise over rayleigh fading channels," *IEEE Transactions on Wireless Communications*, vol. 8, no. 7, pp. 3727–3735, 2009. (Cited on page 38.)

[92] R. Louie, M. McKay, and I. Collings, "Open-loop spatial multiplexing and diversity communications in ad hoc networks," *IEEE Transactions on Information Theory*, vol. 57, no. 1, pp. 317–344, 2011. (Cited on page 38.)

[93] P. Gupta and P. Kumar, "The capacity of wireless networks," *IEEE Transactions on Information Theory*, vol. 46, no. 2, pp. 388–404, 2000. (Cited on pages 38, 135, 163, and 168.)

[94] M. Souryal, B. Vojcic, and R. Pickholtz, "Information efficiency of multihop packet radio networks with channel-adaptive routing," *IEEE Journal on Selected Areas in Communications*, vol. 23, no. 1, pp. 40–50, 2005. (Cited on page 38.)

[95] W. Johnson, "The curious history of faà di bruno's formula," *The American mathematical monthly*, vol. 109, no. 3, pp. 217–234, 2002. (Cited on pages 46 and 77.)

[96] J. Proakis, *Digital communications*. McGraw-hill, 1987, vol. 1221. (Cited on pages 49 and 52.)

[97] L. Tong, Q. Zhao, and S. Adireddy, "Sensor networks with mobile agents," in *IEEE Military Communications Conference*, vol. 1. IEEE, 2003, pp. 688–693. (Cited on page 59.)

[98] Y. Sun, R. Jover, and X. Wang, "Uplink interference mitigation for ofdma femtocell networks," *IEEE Transactions on Wireless Communications*, vol. 11, no. 2, pp. 614–625, 2012. (Cited on page 67.)

[99] Y. Zhang, R. Yu, M. Nekovee, Y. Liu, S. Xie, and S. Gjessing, "Cognitive machine-to-machine communications: visions and potentials for the smart grid," *IEEE Network*, vol. 26, no. 3, pp. 6–13, 2012. (Cited on page 68.)

[100] P. Jänis, C. Yu, K. Doppler, C. Ribeiro, C. Wijting, K. Hugl, O. Tirkkonen, and V. Koivunen, "Device-to-device communication underlaying cellular communications systems," *International Journal of Communications, Network and System Sciences*, vol. 2, no. 3, pp. 169–178, 2009. (Cited on page 68.)

[101] K. Doppler, M. Rinne, C. Wijting, C. Ribeiro, and K. Hugl, "Device-to-device communication as an underlay to lte-advanced networks," *IEEE Communications Magazine*, vol. 47, no. 12, pp. 42–49, 2009. (Cited on page 68.)

[102] P. Chen, S. Cheng, W. Ao, and K. Chen, "Multi-path routing with end-to-end statistical qos provisioning in underlay cognitive radio networks," in *2011 IEEE Conference Computer Communications Workshops (INFOCOM WKSHPS) on*. IEEE, 2011, pp. 7–12. (Cited on page 71.)

[103] W. C. Ao, S.-M. Cheng, and K.-C. Chen, "Phase transition diagram for underlay heterogeneous cognitive radio networks," in *Global Telecommunications Conference (GLOBECOM 2010)*, dec. 2010, pp. 1 –6. (Cited on page 71.)

[104] ——, "Connectivity of multiple cooperative cognitive radio ad hoc networks," *IEEE Journal on Selected Areas in Communications*, vol. 30, no. 2, pp. 263 –270, february 2012. (Cited on page 71.)

[105] L. Fu, L. Qian, X. Tian, H. Tang, N. Liu, G. Zhang, and X. Wang, "Percolation degree of secondary users in cognitive networks," *IEEE Journal on Selected Areas in Communications*, 2012. (Cited on page 71.)

[106] T. Jing, X. Chen, Y. Huo, and X. Cheng, "Achievable transmission capacity of cognitive mesh networks with different media access control," in *Proceedings of IEEE INFOCOM*. IEEE, 2012, pp. 1764–1772. (Cited on page 71.)

[107] B. Blaszczyszyn, P. Muhlethaler, and S. Banaouas, "Coexistence of radio networks using aloha," in *IFIP Wireless Days Conference*, 2010. (Cited on page 71.)

[108] S. Zaidi, M. Ghogho, D. McLernon, and A. Swami, "Achievable spatial throughput in multi-antenna cognitive underlay networks with multi-hop relaying," *IEEE Journal on Selected Areas in Communications*, vol. PP, no. 99, pp. 1–16, 2013. (Cited on page 71.)

[109] D. Stoyan, W. Kendall, J. Mecke, and L. Ruschendorf, *Stochastic geometry and its applications.* Wiley New York, 1987, vol. 2. (Cited on pages 72, 74, 75, and 103.)

[110] H. Kobayashi, Y. Onozato, and D. Huynh, "An approximate method for design and analysis of an aloha system," *IEEE Transactions on Communications*, vol. 25, no. 1, pp. 148–157, 1977. (Cited on page 91.)

[111] M. Haenggi, "Outage, local throughput, and capacity of random wireless networks," *IEEE Transactions on Wireless Communications*, vol. 8, no. 8, pp. 4350–4359, 2009. (Cited on pages 92 and 156.)

[112] X. Hong, C. Wang, and J. Thompson, "Interference modeling of cognitive radio networks," in *IEEE Vehicular Technology Conference, VTC Spring*, 2008, pp. 1851–1855. (Cited on pages 113, 116, 154, and 174.)

[113] J. Lee, S. Lim, J. Andrews, and D. Hong, "Achievable Transmission Capacity of Secondary System in Cognitive Radio Networks," in *IEEE International Conference on Communications*, 2010. (Cited on pages 113 and 136.)

[114] S. A. R. Zaidi, D. McLernon, and M. Ghogho, "Transmission capacity analysis of cognitive radio networks under coexistence constraints," in *IEEE International Workshop on Signal Processing Advances for Wireless Communications.*, 2010. (Cited on pages 113 and 136.)

[115] M. Hanif and P. Smith, "On the statistics of cognitive radio capacity in shadowing and fast fading environments," *IEEE Transactions on Wireless Communications*, vol. 9, no. 2, pp. 844–852, 2010. (Cited on page 113.)

[116] S. Zaidi, D. McLernon, and M. Ghogho, "Quantifying the primary's guard zone under cognitive user's routing and medium access," *IEEE Communications Letters*, vol. 16, no. 3, pp. 288–291, 2012. (Cited on page 115.)

[117] R. Ganti and M. Haenggi, "Spatial analysis of opportunistic downlink relaying in a two-Hop cellular system," *Arxiv preprint arXiv:0911.2948*, 2009. (Cited on page 115.)

[118] J. Ma, G. Li, and B. Juang, "Signal processing in cognitive radio," *Proceedings of the IEEE*, vol. 97, no. 5, pp. 805–823, 2009. (Cited on page 116.)

[119] C. Cordeiro, K. Challapali, D. Birru, S. Shankar *et al.*, "IEEE 802.22: an introduction to the first wireless standard based on cognitive radios," *Journal of communications*, vol. 1, no. 1, pp. 38–47, 2006. (Cited on page 116.)

[120] S. Kay, *Fundamentals of Statistical Signal Processing, Volume 2: Detection Theory.* Prentice Hall PTR, 1998. (Cited on pages 117, 118, and 176.)

[121] F. Andrews, "Two 50% probabilities," *The Journal of the Acoustical Society of America*, vol. 57, p. 245, 1975. (Cited on pages 118, 120, and 177.)

[122] I. Gradshteun, I. Ryzhik, A. Jeffrey, and D. Zwillinger, *Table of integrals, series and products.* Academic press, 2007. (Cited on pages 127 and 150.)

[123] S. A. R. Zaidi, D. McLernon, and M. Ghogho, "Outage probability analysis of cognitive radio networks under self-coexistence constraint," in *44th Annual Conference on Information Sciences and Systems (CISS)*, 2010. (Cited on pages 133, 173, and 174.)

[124] T. C. Clancy, "Formalizing the interference temperature model," *Wireless Communications and Mobile Computing*, vol. 7, no. 9, pp. 1077–1086, 2007. (Cited on page 154.)

[125] S. A. R. Zaidi, D. McLernon, and M. Ghogho, "Outage probability analysis of cognitive radio networks under self-coexistence constraint," *CISS, Princeton, NJ, USA.*, 2010. (Cited on pages 159, 160, and 163.)

[126] S. Weber, J. Andrews, and N. Jindal, "A tutorial on transmission capacity," *IEEE Transaction on Communications, submitted, available at: arxiv. org/abs/0809.0016.* (Cited on pages 160, 163, 165, and 181.)

[127] H. Inaltekin and S. Wicker, "The behavior of unbounded path-loss models and the effect of singularity on computed network interference," in *4th Annual IEEE Communications Society Conference on Sensor, Mesh and Ad Hoc Communications and Networks*, 2007, pp. 431–440. (Cited on page 163.)

[128] D. Cabric, A. Tkachenko, and R. Brodersen, "Spectrum sensing measurements of pilot, energy, and collaborative detection," in *Military Communications Conference*, 2006, pp. 1–7. (Cited on page 177.)

[129] W. Gautschi, "The incomplete gamma functions since tricomi," in *In Tricomi's Ideas and Contemporary Applied Mathematics, Atti dei Convegni Lincei, n. 147, Accademia Nazionale dei Lincei.* Citeseer, 1998. (Cited on page 180.)

[130] M. Holland, "Optimizing physical layer parameters for wireless sensor networks," Ph.D. dissertation, Citeseer, 2007. (Cited on pages 192, 193, 197, 201, 204, 206, and 233.)

[131] S. Cui, A. Goldsmith, and A. Bahai, "Energy-constrained modulation optimization," *IEEE Transactions on Wireless Communications*, vol. 4, no. 5, pp. 2349–2360, 2005. (Cited on pages 192, 193, 195, 196, 197, 204, 206, 207, 229, and 233.)

[132] A. Goldsmith and S. Wicker, "Design challenges for energy-constrained ad hoc wireless networks," *IEEE Wireless Communications*, vol. 9, no. 4, pp. 8–27, 2002. (Cited on pages 193, 195, and 196.)

[133] L. Feeney and M. Nilsson, "Investigating the energy consumption of a wireless network interface in an ad hoc networking environment," in *Twentieth Annual Joint Conference of the IEEE Computer and Communications Societies*, vol. 3. IEEE, 2001, pp. 1548–1557. (Cited on pages 193, 195, and 196.)

[134] M. Gursoy, D. Qiao, and S. Velipasalar, "Analysis of energy efficiency in fading channels under QoS constraints," *IEEE Transactions on Wireless Communications*, vol. 8, no. 8, pp. 4252–4263, 2009. (Cited on pages 193 and 198.)

[135] R. Madan, S. Cui, S. Lal, and A. Goldsmith, "Cross-layer design for lifetime maximization in interference-limited wireless sensor networks," *IEEE Transactions on Wireless Communications*, vol. 5, no. 11, pp. 3142–3152, 2006. (Cited on pages 194 and 196.)

[136] R. Madan, S. Cui, S. Lall, and A. Goldsmith, "Modeling and optimization of transmission schemes in energy-constrained wireless sensor networks," *IEEE/ACM Transactions on Networking (TON)*, vol. 15, no. 6, pp. 1359–1372, 2007. (Cited on pages 194 and 196.)

[137] S. Mukherjee, D. Avidor, and K. Hartman, "Connectivity, power, and energy in a multihop cellular-packet system," *IEEE Transactions on Vehicular Technology*, vol. 56, no. 2, pp. 818–836, 2007. (Cited on pages 193 and 198.)

[138] S. Mukherjee and D. Avidor, "Connectivity and transmit-energy considerations between any pair of nodes in a wireless ad hoc network subject to fading," *IEEE Transactions on Vehicular Technology*, vol. 57, no. 2, pp. 1226–1242, 2008. (Cited on pages 193, 198, and 201.)

[139] D. Qiao, M. Gursoy, and S. Velipasalar, "The impact of QoS constraints on the energy efficiency of fixed-rate wireless transmissions," *IEEE Transactions on Wireless Communications*, vol. 8, no. 12, pp. 5957–5969, 2009. (Cited on page 198.)

[140] E. Shih, S. Cho, N. Ickes, R. Min, A. Sinha, A. Wang, and A. Chandrakasan, "Physical layer driven protocol and algorithm design for energy-efficient wireless sensor networks," in *Proceedings of the 7th Annual International Conference on Mobile Computing and Networking*. ACM, 2001, pp. 272–287. (Cited on pages 193, 195, 196, 197, and 236.)

[141] L. Tong, Q. Zhao, and S. Adireddy, "Sensor networks with mobile agents," in *IEEE Military Communications Conference*, vol. 1. IEEE, 2004, pp. 688–693. (Cited on page 197.)

[142] L. Zhang and B. Soong, "Energy efficiency analysis of channel aware geographic-informed forwarding (cagif) for wireless sensor networks," *IEEE Transactions on Wireless Communications*, vol. 7, no. 6, pp. 2033–2038, 2008. (Cited on pages 193, 194, 198, 201, 209, 220, and 225.)

[143] Q. Zhao and L. Tong, "Energy efficiency of large-scale wireless networks: proactive versus reactive networking," *IEEE Journal on Selected Areas in Communications*, vol. 23, no. 5, pp. 1100–1112, 2005. (Cited on pages 193, 197, 209, and 211.)

[144] M. Zorzi and R. Rao, "Geographic random forwarding (GeRaF) for ad hoc and sensor networks: energy and latency performance," *IEEE Transactions on Mobile Computing*, pp. 349–365, 2003. (Cited on page 198.)

[145] ——, "Energy-efficient forwarding for ad hoc and sensor networks in the presence of fading," in *IEEE International Conference on Communications*, vol. 7. IEEE, 2004, pp. 3784–3789. (Cited on pages 193, 198, 201, 209, 211, and 225.)

[146] C. Yu, B. Lee, and H. Yong Youn, "Energy efficient routing protocols for mobile ad hoc networks," *Wireless communications and mobile computing*, vol. 3, no. 8, pp. 959–973, 2003. (Cited on pages 193 and 198.)

[147] S. Weber, N. Jindal, R. Ganti, and M. Haenggi, "Longest edge routing on the spatial Aloha graph," in *Global Telecommunications Conference*. IEEE, 2008, pp. 1–5. (Cited on pages 193 and 198.)

[148] Z. Zhang, G. Mao, and B. Anderson, "On the effective energy consumption in wireless sensor networks," in *2010 IEEE Wireless Communica-*

tions and Networking Conference (WCNC). IEEE, 2010, pp. 1–6. (Cited on pages 193, 198, and 201.)

[149] X. Ta, G. Mao, and B. Anderson, "On the probability of k-hop connection in wireless sensor networks," *IEEE Communications Letters*, vol. 11, no. 8, pp. 662–664, 2007. (Cited on pages 194, 198, and 211.)

[150] D. Chen, J. Deng, and P. Varshney, "On the forwarding area of contention-based geographic forwarding for ad hoc and sensor networks," in *Proc. SECON*, 2005, pp. 130–141. (Cited on pages 193, 194, 201, 209, 211, 220, and 225.)

[151] M. Haenggi, "On routing in random rayleigh fading networks," *IEEE Transactions on Wireless Communications*, vol. 4, no. 4, pp. 1553–1562, 2005. (Cited on pages 193, 197, 198, and 200.)

[152] C. Bettstetter and J. Eberspacher, "Hop distances in homogeneous ad hoc networks," in *The 57th Vehicular Technology Conference,VTC-Spring. IEEE Semiannual*, vol. 4. IEEE, 2003, pp. 2286–2290. (Cited on pages 193 and 198.)

[153] T. He, J. Stankovic, C. Lu, and T. Abdelzaher, "A spatiotemporal communication protocol for wireless sensor networks," *IEEE Transactions on Parallel and Distributed Systems*, pp. 995–1006, 2005. (Cited on pages 193 and 220.)

[154] M. Haenggi and R. K. Ganti, "Interference in large wireless networks," *Foundations and Trends in Networking*, vol. 3, no. 2, pp. 127–248, 2008, available at http://www.nd.edu/~mhaenggi/pubs/now.pdf. (Cited on pages 193, 197, and 214.)

[155] J. Chen, K. Sivalingam, P. Agrawal, and S. Kishore, "A comparison of MAC protocols for wireless local networks based on battery power consumption," in *Seventeenth Annual Joint Conference of the IEEE Computer and Communications Societies. Proceedings.*, vol. 1. IEEE, 2002, pp. 150–157. (Cited on pages 197 and 201.)

[156] R. Jurdak, C. Lopes, and P. Baldi, "A survey, classification and comparative analysis of medium access control protocols for ad hoc networks," *IEEE Communications Surveys & Tutorials*, vol. 6, no. 1, pp. 2–16, 2009. (Cited on page 197.)

[157] I. Demirkol, C. Ersoy, and F. Alagoz, "MAC protocols for wireless sensor networks: a survey," *IEEE Communications Magazine*, vol. 44, no. 4, pp. 115–121, 2006. (Cited on page 197.)

[158] M. Haenggi and D. Puccinelli, "Routing in ad hoc networks: a case for long hops," *IEEE Communications Magazine*, vol. 43, no. 10, pp. 93–101, 2005. (Cited on page 198.)

[159] S. De, A. Caruso, T. Chaira, and S. Chessa, "Bounds on hop distance in greedy routing approach in wireless ad hoc networks," *International Journal of Wireless and Mobile Computing*, vol. 1, no. 2, pp. 131–140, 2006. (Cited on page 198.)

[160] J. Kuo and W. Liao, "Hop count distribution of multihop paths in wireless networks with arbitrary node density: Modeling and its applications," *IEEE Transactions on Vehicular Technology*, vol. 56, no. 4, pp. 2321–2331, 2007. (Cited on page 211.)

[161] M. Er, B. Wang, and H. Lim, "K-hop statistics in wireless sensor networks," in *5th International Conference on Intelligent Sensors, Sensor Networks and Information Processing (ISSNIP)*. IEEE, 2010, pp. 469–474. (Cited on pages 198 and 201.)

[162] R. Hekmat and P. Van Mieghem, "Degree distribution and hopcount in wireless ad-hoc networks," in *Proceeding of the 11th IEEE International Conference on Networks (ICON 2003), Sydney, Australia*, pp. 603–609. (Cited on page 198.)

[163] D. Stoyan, W. Kendall, J. Mecke, and L. Ruschendorf, *Stochastic geometry and its applications*. Wiley Chichester, 1995. (Cited on pages 199, 206, 212, and 213.)

[164] T. Instrument, *Recommended solutions for softwared defined radio*. TI, 2010, available at http://focus.ti.com/docs/solution/folders/print/357.html. (Cited on page 204.)

[165] A. Behzad, *Wireless LAN radios: system definition to transistor design*. Wiley-IEEE Press, 2007. (Cited on pages 204 and 205.)

[166] Q. Gu, *RF system design of transceivers for wireless communications*. Springer Verlag, 2005. (Cited on page 205.)

[167] T. Instrument, *TMS3206412 power consumption summary*. TI, 2010, available at http://focus.ti.com/dsp/docs/litabsmultiplefilelist.tsp?sectionId=3&tabId=409&literatureNumber=spra967e&docCategoryId=1&familyId=132. (Cited on pages 205 and 207.)

[168] R. Alini, A. Baschirotto, and R. Castello, "Tunable BiCMOS continuous-time filter for high-frequency applications," *IEEE Journal of Solid-State Circuits*, vol. 27, no. 12, pp. 1905–1915, 2002. (Cited on page 207.)

[169] F. Dulger, E. Sanchez-Sinencio, and J. Silva-Martinez, "A 1.3-V 5-mW fully integrated tunable bandpass filter at 2.1 GHz in 0.35-μm CMOS," *IEEE Journal of Solid-State Circuits*, vol. 38, no. 6, pp. 918–928, 2003. (Cited on page 207.)

[170] D. Li and Y. Tsividis, "A 1.9 GHz Si active LC filter with on-chip automatic tuning," in *IEEE International Solid-State Circuits Conference, Digest of Technical Papers. ISSCC.* IEEE, 2002, pp. 368–369. (Cited on page 207.)

[171] V. Aparin, E. Zeisel, and P. Gazzerro, "Highly linear SiGe BiCMOS LNA and mixer for cellular CDMA/AMPS applications," in *IEEE Radio Frequency Integrated Circuits (RFIC) Symposium.* IEEE, 2002, pp. 129–132. (Cited on page 207.)

[172] S. Otaka, T. Yamaji, R. Fujimoto, C. Takahashi, and H. Tanimoto, "A low local input 1.9 GHz Si-bipolar quadrature modulator with no adjustment," *IEEE Journal of Solid-State Circuits*, vol. 31, no. 1, pp. 30–37, 2002. (Cited on page 207.)

[173] M. Kovacevic and M. Madihian, "GSM and DCS SiGe BiCMOS mixer ICs with wide LO power range," in *IEEE MTT-S International Microwave Symposium Digest*, vol. 2. IEEE, 2003, pp. 1299–1302. (Cited on page 207.)

[174] S. Otaka, G. Takemura, and H. Tanimoto, "A low-power low-noise accurate linear-in-dB variable-gain amplifier with 500-MHz bandwidth," *IEEE Journal of Solid-State Circuits*, vol. 35, no. 12, pp. 1942–1948, 2002. (Cited on page 207.)

[175] T. Instrument, *8 channel wideband digital down converter with front end AGC.* TI, 2010, available at http://focus.ti.com/docs/prod/folders/print/gc5018.html. (Cited on page 207.)

[176] ——, *Programmable 4-PLL VCXO Clock Synthesizer with 2.5V or 3.3V LVCMOS Outputs.* TI, 2010, available at http://focus.ti.com/docs/prod/folders/print/cdce949.html. (Cited on page 207.)

[177] ——, *16-bit Ultra-Low-Power Microcontroller, 8kB Flash, 256B RAM, 10 bit ADC, 1 USART .* TI, 2010, available at http://focus.ti.com/docs/prod/folders/print/msp430f1232.html. (Cited on page 207.)

[178] D. Curd, "Power consumption in 65 nm FPGAs," *Xilinx White Paper WP246*, 2006. (Cited on page 207.)

[179] R. Ganti and M. Haenggi, "Dynamic connectivity and packet propagation delay in ALOHA wireless networks," in *Conference Record of*

the Forty-First Asilomar Conference on Signals, Systems and Computers. IEEE, 2008, pp. 143–147. (Cited on page 208.)

[180] S. Kotz and S. Nadarajah, *Extreme value distributions: theory and applications.* World Scientific Publishing Company, 2000. (Cited on page 219.)

[181] K. Cooray, "Generalized Gumbel distribution," *Journal of Applied Statistics*, vol. 37, no. 1, pp. 171–179, 2010. (Cited on page 219.)

[182] F. Rossi, M. Fiorentino, and P. Versace, "Two-component extreme value distribution for flood frequency analysis," *Water Resources Research*, vol. 20, no. 7, pp. 847–856, 1984. (Cited on page 219.)

[183] M. Shadlen, "Implications for psychometric function,chronometric function, and Weber's law," in *CNS NYU Technical Report*, 2004, pp. 1–24, available at www.cns.nyu.edu/csh04/Handouts/Wald_Identity.pdf. (Cited on page 224.)

[184] V. Fakour and H. Azarnoush, "A note on strong law of large numbers," *Journal of Iranian Statistical Society*, 2005. (Cited on page 224.)

[185] L. Gradshteyn and L. Ryzhik, "Table of integrals, series, and products." (Cited on page 266.)

COLOPHON

This document was typeset using the typographical look-and-feel classicthesis developed by André Miede. The style was inspired by Robert Bringhurst's seminal book on typography *"The Elements of Typographic Style"*. classicthesis is available for both LaTeX and LyX:

http://code.google.com/p/classicthesis/

Happy users of classicthesis usually send a real postcard to the author, a collection of postcards received so far is featured at:

http://postcards.miede.de/

Final Version as of January 7, 2014 (classicthesis version 4.1).

3G CSI DFS NN DIP FUE BS CRN CR DSA D2D M2M MF ED MAC MAP CGF MGF MRC MRT MIMO NAIP OP SIR SNR SINR SPPP HPPP PPP MPPP RSF UCF HPF LTE